

FOCUSED FLUID CONDUITS
IN THE SOUTHERN VIKING GRABEN
AND THEIR IMPLICATIONS FOR
THE SLEIPNER CO₂ STORAGE PROJECT

Dissertation
zur Erlangung des Doktorgrades
der Mathematisch-Naturwissenschaftlichen Fakultät
der Christian-Albrechts-Universität zu Kiel

vorgelegt von
Jens Karstens

Kiel, 2015

Erster Gutachter:.....Prof. Dr. Christian Berndt
Zweiter Gutachter:.....Prof. Dr. Ingo Grevemeyer
Tag der mündlichen Prüfung:.....04. Juni. 2015
Zum Druck genehmigt am:.....

.....
Der Dekan

ERKLÄRUNG

Hiermit erkläre ich, dass ich die vorliegende Doktorarbeit mit dem Titel „Focused fluid conduits in the Southern Viking Graben and their implications for the Sleipner CO₂ storage project“ selbstständig und ohne Zuhilfenahme unerlaubter Hilfsmittel angefertigt habe. Meine Doktorarbeit stellt, abgesehen von der Beratung durch meine Betreuer, nach Inhalt und Form meine eigene Arbeit dar. Der Anteil von Koautoren an von mir verfassten und in dieser Arbeit integrierten Manuskripten, sowie mein Anteil an von Dritten verfassten Manuskripten sind kenntlich gemacht. Diese Arbeit wurde weder in dieser noch in einer ähnlichen Form an einer anderen Abteilung oder Hochschule im Rahmen eines Prüfungsverfahrens vorgelegt, veröffentlicht oder zur Veröffentlichung vorgelegt. Ich versichere, dass diese Arbeit unter Einhaltung der Regeln guter wissenschaftlicher Praxis der Deutschen Forschungsgemeinschaft entstanden ist.

Kiel, den 16. April 2015

Jens Karstens

SUMMARY

Focused fluid flow in marine sediments affects the evolution of sedimentary basins by altering the integrity of sealing caprocks and by transferring fluids as well as pressure. The formation of focused fluid conduits initiates, when the pore pressure within a reservoir exceeds the seal's resistance against fracture or capillary failure. In seismic data, focused fluid conduits manifest as vertical zones of anomalous seismic amplitudes, which are known as seismic chimneys or pipes. The understanding of focused fluid flow manifestations is of great importance for hydrocarbon exploration because these structures may act as indicators for hydrocarbon reservoirs and sub-seafloor operations, as they may pose a hazard to drilling operations and influence the long-term efficiency sub-seabed storage of CO₂.

The geological storage of CO₂ known as carbon capture and storage (CCS) is a key technology for the mitigation of climate sensitive greenhouse gas emissions recommended by the Intergovernmental Panel on Climate Change. Marine saline aquifers are a favorable storage option, because such systems have virtually infinite capacity, no influence on ground water production and bear the least conflict potential with the public. However, the success of CCS as a climate change mitigation technology depends on its public acceptance and builds on a reliable and transparent risk assessment, which is studied by the interdisciplinary, international ECO₂ project. The project's main aims are to investigate the likelihood of leakage from marine CO₂ storage sites and its potential effect on marine ecosystems, to develop monitoring strategies, and to define best environmental practice guidelines for implementing and managing storage sites.

Within this framework, my PhD thesis concentrates on the investigation of focused fluid conduits in the Southern Viking Graben and their implications for the Sleipner CO₂ storage project, where CO₂ is injected into a ~850 meter deep saline aquifer known as the Utsira Formation. My studies are based on the interpretation of 3D and time-lapse 4D seismic data covering more than 2000 km² of the Southern Viking Graben, numerical fluid flow simulation, and field geological observations.

My thesis builds on a detailed description of the fluid flow system in the Sleipner area, which is characterized by the interplay between deep hydrocarbon reservoirs, the Utsira Formation and the overlying strata hosting various fluid flow features. The key elements of seal-bypassing fluid flow in the strata overlying the Utsira Formation are several hundreds of meters-wide chimney structures. The study area hosts at least 46 of these focused fluid conduits, which are categorized based on their seismic appearance into three types (A, B and C). Type-A-chimney shows similarities to "blowout pipes", which are known from different sedimentary basins around the world and generally associated with rapid expulsion of fluids. Type B is very similar to large "gas chimney" structures, which have been identified above several leaking hydrocarbon reservoirs and which are interpreted as gas filled fracture networks crosscutting a low permeable seal. Type-C-chimneys cause seismic disturbances in bands of up to 6 km length and correlate with overlying tunnel valleys.

The formation of focused fluid conduits requires high pore overpressure. The analysis of the Sleipner palaeo fluid flow system indicates that there may be a link between chimney formation and the last glacial cycle. Building on this, we present a novel hypothesis, which predicts that undrained fluid flow systems could produce significant overpressure as a result of the interplay between loading and unloading during a glacial cycle and resulting gas compression and sediment compaction.

The closest chimney structures with a probable connection to the Utsira Formation are 7 km away from the Sleipner CO₂ injection point. We have evaluated the propensity of leakage along these structures by performing numerical modeling of the CO₂ plume evolution with the multiphase fluid flow simulator DuMu^x. The simulations revealed that it is not likely that the modeled CO₂ plume will ever reach the chimney structures. Additionally, it is unlikely that the injection of CO₂ itself may cause the formation of chimney structures at Sleipner.

Although seismic pipes and chimneys are very common features in seismic data and their interpretation as focused fluid flow conduits is well-established, only little is known about the underlying geological processes and how these link up with their seismic image. The comparison of field analogues of focused fluid conduits from the Colorado Plateau (USA) and seismic chimneys revealed that specific seismic signatures correlate well with certain field-based examples. The integration of field geological observations may help to improve seismic interpretations of chimney structures and fluid flow systems in general.

The importance of focused fluid flow conduits for the evolution of sedimentary basins is not sufficiently addressed yet. The results of this thesis highlight the relevance of focused fluid flow conduits for long-term integrity of sub-seabed storage of CO₂ operations and that focused fluid flow conduits have to be considered for site selection of storage projects. A deeper understanding of focused fluid flow will help to understand the flux of fluids from the geosphere into the hydro- and atmosphere as well as geological and climatic processes of the past and future.

ZUSAMMENFASSUNG

Fokussierter Fluidfluss in marinen Sedimenten beeinflusst die Entwicklung von Sedimentbecken nachhaltig, indem er die Permeabilität von zuvor undurchlässigen Schichten erhöht und so den Transport von Fluiden als auch den Transfer von Drücken ermöglicht. Fokussierte Fluidflussstrukturen entstehen, wenn der Porendruck innerhalb eines Reservoirs die Widerstandsfähigkeit einer Deckschicht gegen Bruch- oder Kapillarversagen übersteigt. Fokussierte Fluidflussstrukturen zeigen sich in seismischen Daten als Zonen mit gestörter Amplitudensignatur, welche als seismische Chimneys oder Pipes bezeichnet werden. Das Verständnis fokussierter Fluidflussstrukturen ist von großer Bedeutung für industrielle Anwendungen unter dem Meeresboden, weil diese als Indikator für Kohlenwasserstoffreservoirs dienen, aber auch ein Sicherheitsrisiko für Bohrungen darstellen und die Langzeiteffizienz von CO₂-Speicherstätten unter dem Meeresgrund beeinflussen könnten.

Die geologische Speicherung von CO₂, die als „Carbon Capture and Storage“, kurz CCS, bekannt ist, stellt für das „Intergovernmental Panel on Climate Change“ eine Schlüsseltechnologie für die Verringerung von Treibhausgasemissionen dar. Die Nutzung mariner saliner Aquifere ist eine bevorzugte Speicheroption, weil solche Systeme nahezu unerschöpfliche Speicherkapazitäten aufweisen, keinen Einfluss auf die Grundwasserproduktion haben und nur ein geringes Konfliktpotential mit der Öffentlichkeit bergen. Der Erfolg von CCS als Technologie die Folgen des Klimawandels abzumildern, hängt von der öffentlichen Akzeptanz gegenüber dieser Technologie ab und muss auf einer belastbaren und vertrauenswürdigen Risikoabschätzung beruhen. Eine solche wird vom EOR-Projekt, dessen Hauptziele die Abschätzung der Wahrscheinlichkeiten von CO₂-Leckagen, sowie deren Einfluss auf marine Ökosysteme, als auch die Entwicklung von Überwachungsstrategien und das Erstellen von Richtlinien für die Implementierung und die Organisation von Speicherstätten sind, vorangetrieben.

Meine Doktorarbeit richtet den Blick auf die Untersuchung von fokussierten Fluidflussstrukturen im Südlichen Viking-Graben und deren Einfluss auf die Sleipner CO₂-Speicherstätte, bei welcher CO₂ in die Utsira Formation, einen salinen Aquifer in einer Tiefe von 850 Meter unterhalb des Meeresbodens, injiziert wird. Die Arbeit beruht auf der Interpretation 3D- und 4D-seismischer Daten, die mehr als 2000 km² des Südlichen Viking-Grabens abdecken, numerischen Fluidflusssimulationen und feldgeologischen Beobachtungen.

Die Grundlage meiner Arbeit ist eine detaillierte Beschreibung des Fluidflusssystems im Sleipner-Gebiet, welches durch ein Zusammenspiel tiefer Kohlenwasserstoffreservoirs, der Utsira Formation als temporäre Kohlenwasserstoffspeicherformation und deren durch fokussierten Fluidfluss gekennzeichnetes Deckgestein. Das Schlüsselement des Fluidflusses sind große Chimney-Strukturen, die das Deckgestein der Utsira Formation durchstoßen. Das Untersuchungsgebiet beherbergt mindestens 46 dieser Strukturen, die auf Grund ihrer seismischen Erscheinung in drei Typen (A, B und C) unterteilt werden können. Typ-A-Chimneys ähneln Blowout-Strukturen, welche aus verschiedenen Sedimentbecken weltweit bekannt sind, und können mit dem schnellen Ausstoß von Fluiden erklärt werden. Typ B ähnelt stark Fluidflussstrukturen, die oberhalb von undichten Kohlenwasserstoffreservoirs identifiziert worden sind und im Allgemeinen als mit Gas gefüllte Brüche in niedrig permeablen Sedimenten interpretiert werden. Typ-C-Chimneys erzeugen bis zu 6 km lange Bänder gestörter seismischer Amplitude und ihre Lage korreliert mit glazialen Tunneltälern, von denen es im Untersuchungsgebiet sehr viele gibt.

Die Entstehung fokussierter Fluidflussstrukturen setzt hohe Porenüberdrucke voraus und die Untersuchung des Paläofluidsystems des Südlichen Viking-Grabens deutet darauf hin, dass ein Zusammenhang zwischen Chimney-Entstehung, Überdruck und dem letzten glazialen Zyklus besteht. Darauf aufbauend präsentiert diese Arbeit eine neue Hypothese zur Entstehung fokussierter Fluidflussstrukturen als Resultat von Belastung und Entlastung während eines glazialen Zyklus. Diese Hypothese sagt voraus, dass ein hydraulisch abgeschlossenes Fluidflusssystem signifikante Überdrucke, die auf einem Zusammenspiel von Gaskompression und Sedimentkompaktion beruhen, produzieren kann.

Manche Chimney-Strukturen weisen augenscheinlich eine Verbindung mit der Utsira Formation auf und sind gerade einmal 7 km vom Sleipner CO₂-Injektionspunkt entfernt. Die Wahrscheinlichkeit für eine Leckage von CO₂ entlang dieser Chimney-Strukturen wurde durch numerische Simulationen mit dem Fluidflusssimulator DuMu^x evaluiert. Die Simulationen zeigten, dass es nicht wahrscheinlich ist, dass das CO₂ jemals die Chimney-Strukturen erreichen wird. Auch ist es unwahrscheinlich die CO₂-Speicherung bei Sleipner selbst zur Formation neuer Chimney-Strukturen führen kann.

Obwohl seismische Chimneys und Pipes sehr häufig in seismischen Daten identifiziert werden und ihre Interpretation als fokussierte Fluidflusstrukturen etabliert ist, weiß man doch nur sehr wenig über die sie zugrundeliegenden geologische Prozesse und wie diese die seismische Abbildung beeinflussen. Der Vergleich feldgeologischer Analogien von fokussierten Fluidflusstrukturen im Colorado Plateau (USA) und seismischen Chimneys zeigt, dass bestimmte seismische Signaturen mit Feldbeobachtungen von Sandinjektionen, Sedimentverflüssigungen und Bruchnetzwerken korrelierbar sein könnten.

Die Ergebnisse meiner Doktorarbeit verdeutlichen die Relevanz von fokussierten Fluidflusstrukturen für die Speicherung von CO₂ unter dem Meeresboden. Fokussierte Fluidflusstrukturen müssen bei der Standortwahl von CO₂-Speicherstätten berücksichtigt werden. Die Wichtigkeit von fokussierten Fluidflusstrukturen für die Entwicklung von Sedimentbecken ist noch nicht ausreichend gewürdigt und ein tiefergehendes Verständnis dieser Strukturen ist notwendig, um die mit dem Fluss von Fluiden von der Geosphäre in die Hydro- und Atmosphäre verbundenen geologischen und klimatischen Prozesse in der Vergangenheit und in der Zukunft besser zu verstehen.

ACKNOWLEDGEMENTS

In the beginning, I would like to thank Christian Berndt for being the main supervisor of my PhD studies during the last four years. Christian, you have always supported me on a professional level as well as on a personal and you have taught me way too many things to list here. You have encouraged me to question existing knowledge and to develop my own ideas and hypotheses. After the cruises to the Okinawa Trough and to Poland got canceled or failed, it was only your encouragement that prevented me from quitting my PhD. When my mother became seriously ill in beginning of 2013 and I needed my energy and time for more important things than my thesis, you provided me all the freedom and support I required that time. I will always be grateful for this. Thank you, Christian!

I would like to thank Ingo Grevemeyer for being my co-supervisor during my PhD. Ingo, you had always an open ear for me and many times you gave me helpful advise. Your opinions and thoughts on topics regarding my thesis and my career planning were very valuable. Thank you, Ingo!

In addition, I would like to thank Sebastian Krastel-Gudegast and Christian Dullo for agreeing to be members of my examination board.

I would like to thank GEOMAR and the ECO2 project for financing my PhD studies. During the meetings of the ECO2 project, I had the chance to meet many researchers from different research fields and institutes and to build a broad scientific network, which I can build on in the future. Special thanks for their support within the ECO2 project go to Klaus Wallmann, Matthias Haeckel, Stefan Bünz and Anja Reitz.

I would like to thank the ECO2 project and the GEOMAR for giving me the possibility to present the progress of my work at various internal project meetings and workshops as well as at international conferences including the ECORD Summer school in Bremen (2011), the 12th International Conference of Gas in Marine Sediments (GIMS) 2014 in Taipei and at the fall meeting of the American Geophysical Union 2014 in San Francisco. In April 2014, I had the great opportunity to study field analogues of focused fluid conduits during a fieldtrip to the Colorado Plateau, which allowed me to approach my scientific subject from a field geological perspective. The 3D and 4D seismic datasets, which I analyzed during my thesis, were provided for the ECO2 project by the Norwegian Petroleum Directorate and Statoil ASA. I would like to thank them for their permission to interpret the data and to publish my results. The seismic analysis has been carried out with the software packages Kingdom Suite by IHS, OpendTect by dGB and Petrel by Schlumberger. I thank them for granting access to their software through educational licenses.

I would like to thank the entire Geodynamics group for the nice atmosphere and the many great experiences I have made during cruises and back home in the office. I had the great privilege to be involved in different projects, scientific publications, which were related to my PhD or not during the last years. I would like to thank Waqas Ahmed, Melanie Darcis and Holger Class for conducting the numerical simulations, which formed a solid base for one of the presented manuscripts.

My special thank goes to Lisa Vielstädte, who saw the potential of integrating my seismic interpretations into her studies on leaking wells. This work resulted in the two manuscripts, which I could contribute to as a co-author and which are integrated into this thesis as well. These studies added an additional component to my thesis and broadened its impact. Thank you very much, Lisa!

I would like to thank Sudipta Sarkar for proofreading parts of this thesis as well as for many intense and enlightening discussions. Many thanks go to Gareth Crutchley for proofreading the introduction of this thesis as well as many other texts I have written in the beginning of my PhD and for being a great friend even being on the other side of world. I would like to thank Florian Wolf for spending his holydays for supporting me during my fieldtrip to the Colorado Plateau and being a close friend from day one at university.

One of the highlights of my PhD studies was the Young Scientist Event, which Lisa Vielstädte, Dirk Schroller and I organized with the financial support of ECO2 and the Graduiertenzentrum of the Christian-Albrechts-Universität. Those days on Lipari and Salina gave me the required energy for the last year of my studies. Thank you, Lisa and Dirk!

Special thanks go to Ines Dumke and Stefanie Koch, who have somehow managed to share an office with me over three years. Thank you for the nice conversations, the good working climate and for tolerating the chaos on my desks.

Finally, I want to thank my friends and my family for supporting me on my long way to the doctorate. The last years were the most exciting, but also the most difficult and saddest of my life. Thank you for being there for me and helping me on my way.

I would like to thank my family for always supporting and encouraging me to follow my dreams and to never give up. Without your support, I would have never come to this point. The last years have been difficult, but I think we have grown as a family and are even closer together than we had already been before. Thank you!

Content

Erklärung	i
Summary	ii
Zusammenfassung	iv
Acknowledgements	vi
CHAPTER 1: INTRODUCTION	1
1.1. Motivation	2
1.2. Global Warming	2
1.3. The role of methane in marine sediments on the global carbon cycle	4
1.4. Fluid flow in marine sediments	5
1.4.1. Controls of focused fluid flow	5
1.4.2. Focused fluid flow manifestations at the seafloor	6
1.4.3. Focused fluid flow manifestations in hydro-acoustic and seismic data	8
1.4.3.1. Gas accumulations and gas hydrates in seismic data	8
1.4.3.2. Seismic chimneys and pipes	9
1.4.3.3. Seismic image of sediment mobilizations	10
1.5. Carbon capture and storage	11
1.5.1. The Sleipner CO ₂ storage project	12
1.5.2. Geotechnical incidents with relevance for CCS	15
1.5.3. The ECO2 project	16
1.6. The influence of focused fluid flow on hydrocarbon exploration and wellbore activities	16
1.7. Aims of the thesis	17
1.8. Introduction of the chapters	18
References	20
CHAPTER 2: SEISMIC CHIMNEYS IN THE SOUTHERN VIKING GRABEN – IMPLICATIONS FOR PALAEO FLUID MIGRATION AND OVERPRESSURE EVOLUTION	27
2.1. Abstract	28
2.2. Introduction	28
2.3. Geological background	29
2.4. Data and methods	32
2.5. Results	32
2.5.1. Bright spots – Shallow gas pockets	32
2.5.1. Vertical seismic anomalies	34
2.5.1.1. Type-A-anomalies	34

2.5.1.2.	Type-B-anomalies	34
2.5.1.3.	Type-C-anomalies	34
2.5.2.	Subsurface sediment mobilization	38
2.6.	Discussion	39
2.6.1.	Fluid flow overview	39
2.6.2.	Imaging artifact or geological feature	39
2.6.3.	The nature of type-A-anomalies	40
2.6.4.	The nature of type-B-anomalies	41
2.6.5.	The nature of type-C-anomalies	42
2.6.6.	Seismic chimneys and their implications for the evolution of the fluid flow system	42
2.7.	Conclusions	46
	Acknowledgements	47
	References	48

CHAPTER 3: THE GLACIAL METHANE PUMP: OVERPRESSURE AND FOCUSED FLUID FLOW DUE TO GAS COMPRESSION COMPENSATED SEDIMENT COMPACTION		53
3.1.	Introductory paragraph	54
3.2.	Letter	54
3.3.	Methods	58
	References	60

CHAPTER 4: THE IMPACT OF CHIMNEY STRUCTURES ON CO ₂ STORAGE AT SLEIPNER: EVALUATION OF NUMERICAL FLUID FLOW SIMULATIONS BASED ON TIME-LAPSE SEISMIC DATA		63
4.1.	Abstract	64
4.1.	Introduction	64
4.2.	Geological background	65
4.2.1.	Study area and the local stratigraphy	65
4.3.	Data and methods	66
4.3.1.	Seismic and well data	66
4.3.2.	Seismic observations	67
4.3.2.	Modeling	68
4.3.2.1.	Model building	68
4.3.2.2.	Modeling objectives	69
4.3.2.3.	Model setup in DuMu ^x	69
4.4.	Results	71
4.4.1.	Reservoir parameterization by history matching	71
4.4.2.	Long-term plume evolution simulation	73
4.4.3.	Leakage at the seafloor	74
4.5.	Discussion	76

4.5.1.	Evaluation of models and simulations	76
4.5.1.1.	Simplifications and limitations	76
4.5.1.2.	Implications of hydraulic properties of the Utsira Formation	76
4.5.2.	Hydraulic properties of chimney structures	77
4.5.3.	Chimney formation as the result of CO ₂ storage	78
4.5.4.	Propensity of CO ₂ leakage along chimney structures at Sleipner	79
4.6.	Conclusions	80
	Acknowledgements	80
	References	81

CHAPTER 5: INSIGHTS INTO FOCUSED FLUID CONDUIT FORMATION FROM COMPARING SEISMIC CHIMNEYS AND PIPES WITH FIELD OBSERVATIONS OF FLUID FLOW MANIFESTATIONS IN THE COLORADO PLATEAU		85
5.1.	Introduction	86
5.2.	Focused fluid conduits in seismic data	86
5.3.	Field geological observations	88
5.3.1.	Sand injections in the Kodachrome basin	88
5.3.2.	Fluidized sands at Last Chance Bay and Warm Creek Bay, Lake Powell	89
5.3.3.	Fractured mound at Cookie jar Butte, Lake Powell	91
5.4.	Correlation of seismic and field geological observations	92
5.5.	Conclusions	93
	References	94

CHAPTER 6: QUANTIFICATION OF METHANE EMISSIONS AT ABANDONED GAS WELLS IN THE CENTRAL NORTH SEA		97
6.1.	Abstract	98
6.2.	Introduction	98
6.2.1.	Study area	99
6.3.	Methodology	101
6.3.1.	Sediment and gas sampling	101
6.3.2.	Video based quantification of gas emissions	102
6.3.2.1.	Gas flow measurements	102
6.3.2.2.	Bubble size spectra	103
6.3.2.3.	Gas bubble dissolution model	103
6.4.	Results	105
6.4.1.	Gas composition and isotopic signatures	105
6.4.2.	Leakage site characteristics	106
6.4.2.1.	The Nature of Surface Sediments	106
6.4.2.2.	The Nature of Methane Seepage	106
6.4.3.	Seabed methane emissions	108

6.4.5.	Contribution to atmospheric methane	111
6.5.	Discussion	111
6.5.1.	Gas origin	111
6.5.2.	The nature of gas migration along an abandoned well	112
6.5.3.	Geological control of leakage	113
6.5.4.	Methane emissions in a North Sea context	115
6.5.5.	Methane contribution to the atmosphere	116
6.6.	Conclusions	117
	Acknowledgements	117
	References	118
Chapter 7: GREATER FOCUS NEEDED ON BIOGENIC METHANE LEAKAGE FROM OIL AND GAS WELLS IN THE NORTH SEA		125
7.1.	Introductory paragraph	126
7.2.	Letter	126
7.4.	Methods summary	132
	References	134
CHAPTER 8: SYNTHESIS, RECOMMENDATIONS AND OUTLOOK		137
8.1.	Summary of main results	138
8.1.1.	The evolution of the fluid flow system in the Southern Viking Graben	138
8.1.2.	The formation of large-scale focused fluid conduits in the Southern Viking Graben	139
8.1.3.	The impact of chimney structures on the Sleipner CO ₂ storage operation	140
8.1.4.	Implications of shallow fluid flow on wellbore activities	140
8.2.	Recommendations for site selection of future sub-seabed CO ₂ storage operations	141
8.3.	Outlook on planned projects and recommendations for future research	142
APPENDIX		145
A.1	List of research articles published in the period of my PhD	146
A.2	List of presentations during my PhD	150
A.3.	Appendix of Quantification of methane emissions at abandoned gas wells in the Central North Sea	151
A.4.	Supplementary methods for “Greater focus needed on biogenic methane leakage from oil and gas wells in the North Sea“	152
A.5.	Curriculum Vitae	167

CHAPTER 1: INTRODUCTION



Soft sediment deformation, White Pocket, Vermillion Cliffs, Arizona, USA

1.1. MOTIVATION

The migration of fluids in marine sediments is an important geological process in the marine environment and has influences on hydrocarbon resources, benthic and sub-seafloor ecosystems, natural and exploration-related geohazards, the carbon cycle and Earth's climate. The biogenic and thermogenic formation of hydrocarbons in sedimentary basins creates fossil fuel reservoirs, which have profound implications for energy production and economic growth. The migration of fluids at hydrothermal vents and cold seeps are the foundation of chemosynthetic biological communities, which may represent the oldest microbial ecosystems on Earth (Martin et al., 2008). The emission of greenhouse gases, such as carbon dioxide and methane from the production and burning of hydrocarbons has a direct influence on global warming, which will be one of the major challenges for the global community in the next decades to centuries (IPCC, 2013).

Natural fluid flow has a direct impact on geotechnical operations both on and beneath the seafloor, including exploration and exploitation of resources as well as in sub-seafloor storage activities. A lack of understanding of shallow fluid flow systems has resulted in numerous operational and life-threatening hazards (e.g. the North Sea blowout in 1990) causing the uncontrolled release of hydrocarbons. Focused fluid flow manifestations are often sourced from deep hydrocarbon reservoirs and may therefore be used as indicators for hydrocarbon prospects, while the release of fluids on the other hand may destroy seal integrity and drain promising reservoirs (Heggland, 1998, 2005; Løseth et al., 2009). Seal integrity also plays an important role for the sub-seabed storage of carbon dioxide, which is a key technology for the mitigation of greenhouse gas emissions. The injection of carbon dioxide into marine saline aquifers or depleted hydrocarbon reservoirs may have the potential to reduce emissions to amounts that limit the expected global temperature increase to 2°C (Metz et al., 2005; IEA, 2012). However, most marine sedimentary basins are densely populated with shallow fluid flow manifestations and the influence of such natural focused fluid flow on the long-term performance of storage operations is only poorly constrained. Sub-seabed exploration, exploitation and storage activities have left a multitude of wellbores on the continental shelves worldwide. These structures connect deep fluid flow systems with the seafloor and represent focused weakness zones in the sealing overburden of fluid reservoirs.

Many of the several hundred thousand wells on the continental shelves show integrity issues resulting in the leakage of hydrocarbons (Vignes et al., 2006; 2011). The interaction between abandoned wells and shallow fluid flow systems often results in the seepage of methane, whose quantity and impact on methane budgets requires integrated investigations. As the flux of methane from shallow reservoirs into the hydrosphere has an important role in the global carbon cycle and may affect the ongoing process of global warming, it is of significant importance to understand the subsurface focused fluid flow systems. A detailed understanding is also required for the utilization of sub-seafloor resources and the implementation of large-scale geological storage operations of greenhouse gases.

1.2. GLOBAL WARMING

Global warming and climate change have been in the focus of scientific research in the last decades, and since 1988 the climate science community is organized as the Intergovernmental Panel on Climate Change (IPCC). The IPCC's main aims are to inform society and policy makers about the connection between anthropogenic greenhouse gas release and global warming as well as giving advice for strategies to mitigate the consequences of climate change. Non-anthropogenic climate factors on time scales of thousands to several millions of years are orbital processes controlling the amount of solar radiation reaching the Earth, tectonic processes controlling the area and distribution of landmasses and volcanism (Crowley, 2000; Zachos, 2001). The removal of these non-anthropogenic influences from the temperature trend of the last thousand years reveals a pronounced warming for the 20th century, which correlates with the predicted effect of greenhouse gas

forcing (Crowley, 2000). The atmospheric concentrations of the greenhouse gases carbon dioxide, methane and nitrous oxide have all significantly increased since pre-industrial time (Fig. 1.1) and their concentrations exceed those concentrations reconstructed from ice core records dating back 800,000 years (IPCC, 2013).

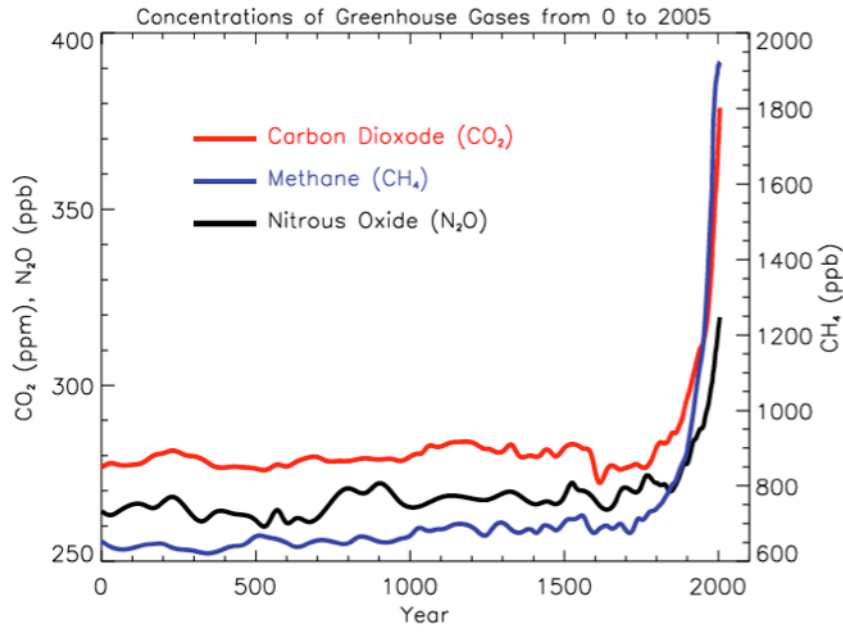


Fig.1.1: Atmospheric concentration of carbon dioxide (CO₂), methane (CH₄) and nitrous oxide (N₂O) over the past 2000 years (Solomon et al., 2007, Chapter 2).

Over the past decades, the anthropogenic link to global warming has been unequivocally established by 97% of all climate-change related scientific studies (Cook et al., 2013). The ongoing global warming has already manifested itself by an increase of surface and upper ocean temperatures, partial melting of the Greenland and Antarctic ice sheets and an average sea-level rise of ~20 cm during the last century (IPCC, 2013). Continuing greenhouse gas emissions will cause further temperature increase with severe and irreversible impact on surface temperatures, water cycles and ocean currents, and will have a direct feedback on the Arctic ice cover, global sea-level and precipitation (IPCC, 2013). According to the IPCC (2013), the warming of the global climate system is “unequivocal” and the IPCC claims that a significant reduction of greenhouse gas emissions, most importantly of CO₂, is necessary to limit global warming to a tolerable amount of 2°C. The emissions of CO₂ are of special interest, because it remains in the atmosphere over hundreds (to thousands) of years (IPCC, 2013). To achieve the 2°C goal, global energy production and consumption have to be reduced, so that the concentration of CO₂ within the atmosphere will not exceed 450 ppm according to the World Energy Organization (IEA; 2012). This 450 ppm scenario requires a combination of different strategies and technologies to significantly reduce CO₂ emissions including improvements in energy efficiency, the usage of less CO₂ intensive energy sources like nuclear power, renewable energy sources and biofuels as well as the development of carbon capture and storage (CCS) projects (IEA, 2012). CCS has the potential to reduce CO₂ emissions by 2 to 3 Gt/a (17% of the total reduction potential by 2035; IEA, 2012). However, CCS cannot be the solution for reducing CO₂ emissions to a tolerable amount, but it may provide time for the development and implementation of more sustainable energy sources.

1.3. THE ROLE OF METHANE IN MARINE SEDIMENTS ON THE GLOBAL CARBON CYCLE

The formation of methane and other hydrocarbons by microbial degradation and thermogenic breakdown of organic matter in marine sediments is a key element of the global carbon cycle (Judd et al., 2002). The global methane release to the atmosphere is about 600 Mt per year, where 18% (or 110 Mt) of the released methane consists of ^{14}C -depleted carbon that can be attributed to fossil methane from hydrocarbon exploitation and natural seepage (Kvenevolden and Rogers, 2005; IPCC, 2013). The release of methane from marine sediments into the water column is a common process and global flux estimates are 6 – 65 Mt per year (Hovland et al., 1993). The amount of methane that ultimately reaches the atmosphere and becomes a concern for global warming has been estimated to be 6.6 – 19.5 Mt per year for marine sediments (Judd et al., 2002) and 45 Mt per year for all natural geological sources. However, recent analysis of specific seeps (e.g. offshore Svalbard) shows that the amount of methane from seafloor seepage reaching the atmosphere is limited (Fisher et al., 2011).

The far more significant mechanism for transporting carbon from marine sediments into the atmosphere is the global exploitation of oil, gas (combined 25 Mt per year) and coal (40 Mt per year) reservoirs (Kvenevolden and Rogers, 2005). Most of the global hydrocarbon resources were formed within marine sediments by the thermogenic cracking of kerogens, which are the remains of organic matter that make up to 2% of sedimentary rocks (Judd and Hovland, 2007). When kerogen-bearing source rocks get buried due to basin subsidence and ongoing sedimentation, they reach temperature and pressure conditions that initiate their maturation to dry gas, wet gas, condensates and crude oil (Judd and Hovland, 2007). The maturity of hydrocarbons is controlled by the duration of their exposure to certain temperature conditions. There are two ways to form thermogenic methane: either by exposing hydrocarbons to temperatures beyond the “oil window”, or during the upward migration of hydrocarbons by the breaking down of complex hydrocarbon molecules into simpler molecules and ultimately into methane (Judd and Hovland, 2007). However, methane released at most seafloor seeps is microbial in origin, formed by the degradation of organic matter by methanogenic archaea (Judd and Hovland, 2007). The biochemical processes leading to the formation of methane are acetate fermentation and CO_2 reduction and are promoted by anoxic conditions, high sedimentation rates, low temperatures and limited availability of sulfate (Katz, 2011).

A large portion of marine methane is bound in gas hydrates, which are mainly found in water depths greater than 300 m and bottom water temperatures less than 2°C (Kvenevolden, 1995). Gas hydrates are ice-like compounds, in which gas molecules, primarily methane, are hosted within crystal lattices made up of ice molecules (Kvenevolden, 1995). Estimates of the global gas hydrate reserves have varied over the last decades reaching from 2,000 to 4,000,000 Gt of carbon (Kvenevolden, 1988) over 500 to 2500 Gt (Milkov, 2004) to 4.18 to 995 Gt (Burwicz et al., 2011) and ~550 Gt (Piñero et al., 2013).

The impact of methane from marine sediments on the global carbon cycle is determined by complex coupled fluxes between the geosphere, the biosphere, the hydrosphere and the atmosphere (Judd and Hovland, 2007). For example, the influence of gas hydrate dissociation on global climate and the stability of submarine slopes has been the focus of much scientific research during the last decades (Vogt und Jung, 2002; Kennett et al., 2005; Bünz et al., 2003; Mienert et al., 2005; Berndt et al., 2009). The global sea-level drop during glacial periods in the Quaternary (120 m during the last glacial maximum) is believed to have caused shoaling of the gas hydrate stability zone (GHSZ), a process with the potential to generate overpressured gas from the dissociating hydrates that could have destabilized continental slopes and contributed to landslides (Judd and Hovland, 2007). Another potential mechanism for destabilizing gas hydrates and thereby influencing continental slope stability is ocean warming (Vogt und Jung, 2002). The dissociation of gas hydrates is also a favored explanation for the formation of focused fluid conduits in glacially affected marine sediments (Forsberg et al., 2007).

The most prominent climatic extreme event with a correlation between methane concentration in the atmos-

phere and the global temperature is the Paleocene- Eocene thermal maximum (PETM; Zachos, 2001). The PETM marks a prominent warming signal in the global temperature curve, which is based on $\delta^{18}\text{O}$ record obtained from marine sediment cores and is unique to the last 65 million years (Zachos, 2001). $\delta^{13}\text{C}$ measurements indicate that the PETM correlates with a sudden and massive release of light carbon, indicating that it may be explained by the release of methane from hydrates, pore water venting, turbidite oxidation, or metamorphism of marine sediments as the result of volcanic intrusions (Zachos et al, 2001; Higgins and Schrag, 2006). The global warming associated with the massive release of carbon makes the PETM the best historic equivalent for present-day global warming.

1.4. FLUID FLOW IN MARINE SEDIMENTS

1.4.1. CONTROLS OF FOCUSED FLUID FLOW

Fluid flow in marine sediments is driven by different hydrodynamic potentials, which are equilibrated by diffuse fluid discharge through the connected pore space (Bjørlykke, 2010). The resistance of a fluid system against equilibrating a pressure gradient ($\text{grad}(P)$) through diffuse (Darcy) flow for a given fluid viscosity (μ) is defined by its permeability (k), and is described by the Darcy equation (Bjørlykke, 2010):

$$F = \text{grad}(P) * k / \mu \quad (\text{Eq. 1.1})$$

The most important requirement for diffuse and focused fluid flow is the availability of unbound fluids, which can be either water or hydrocarbons. In the marine environment, water may be sourced by groundwater flow of meteoric fresh water from onshore, burial of seawater during sedimentation, dehydration of minerals, hydrothermal venting from volcanic activity, or compaction of sediments (Berndt, 2005; Bjørlykke, 2010). The biogenic and thermogenic generation of hydrocarbons in marine sediments contribute additional fluid phases.

Diffusive fluid flow through the pore space is oriented perpendicular to isopotential lines in homogeneous porous media, but is strongly influenced by the distribution of permeability barriers (Bjørlykke, 2010). The permeability (k) of sediments generally correlates with the grain size (d) of the matrix material and this relationship can be described by the following equation (c is a constant varying between 1.11 and 2.05; Shepherd, 1989):

$$k = cd^2 \quad (\text{Eq. 1.2})$$

Permeability barriers inhibit the discharge of fluids and may result in accumulations of pore overpressures. A lithological unit with permeability low enough to impede or retard the flow of fluids to the surface is defined as a seal (Cartwright et al., 2007). Seals have the potential to accumulate overpressures in the pore space of underlying sediments. The generation of pore overpressure is a common process in sedimentary basins, and according to Osbourne and Swarbrick (1997), it can be attributed to (1) increased compressive stress and reduction of pore volume, (2) changes in the fluid volume due to diagenesis or hydrocarbon generation and (3) fluid migration due to different hydraulic heads, osmosis or buoyancy.

The formation of focused fluid conduits initiates when the pore overpressure exceeds the permeable barrier's resistance against capillary or fracture failure (Clayton and Hay, 1994). The creation of fractures in response to pore fluid overpressure is called hydrofracturing (for water) or pneumatic fracturing (for gas), and occurs when the pore pressure is higher than the combined least principal stress and tensile strength of the sediment (Hubbert and Willis, 1957). A capillary failure initiates when a non-wetting phase (e.g. gas) enters the pore space of a low-permeability, fine-grained sediment as the result of exceeding its capillary entry pressure (Clayton and Hay, 1994). Both processes correspond to a rapid loss of the sealing potential, which leads to the focused discharge of overpressured fluids.

1.4.2. FOCUSED FLUID FLOW MANIFESTATIONS AT THE SEAFLOOR

Focused fluid flow manifests itself at the seafloor in numerous ways, including the development of biological communities, carbonates, pockmarks, mud and asphalt volcanoes, seafloor fractures and gas hydrates (Judd and Hovland, 2007). The occurrence of specific features depends on the venting fluids, the seepage rate and the physical conditions at the seafloor. Perhaps the most widely known fluid flow manifestations are black smokers, whose discovery during dives with the submersible Alvin in 1977 at the East Pacific Rise in a depth of 2500 m was a scientific sensation (Spiess et al., 1980; Macdonald et al., 1980). The discovery of extremophile biological communities including tube worms, clams and crabs, which build on chemosynthetic bacteria and withstand temperatures around 380°C, changed our perspective on the origin of life on Earth (Baross and Hoffman, 1985).

At the same time, bacterial mats associated with hydrocarbon seepage were discovered in Santa Barbara Channel offshore California (Fig. 1.2a; Spiess and Davies, 1979) and in 1985 deep sea trawling in the Gulf of Mexico recovered tube worms comparable to those found at hydrothermal vents (Kennicut et al., 1985). This finding initiated an intense study of seepage related biologic communities at cold seeps, which build on chemosynthetic, methane-oxidating, symbiotic bacteria (Kennicut et al., 1988). Ever since, chemosynthetic cold seep communities have been identified around the world at vent sites including Hydrate Ridge offshore Oregon, the Laurantian Fan, at several mud volcanoes and even in deep sea trenches (Hovland and Judd, 2007). The consumption of methane due to sulphate reduction coupled anaerobic oxidation of methane by archaea and bacteria leads to the precipitation of authigenic carbonates (Hovland 1987; Boetius et al., 2000). Methane-derived authigenic carbonates (MDAC) are clear indicators for fluid flow and form crusts, concretions and small chimneys, which have been identified all around the world (Fig. 1.5b; Hovland 1987; Boetius et al., 2000; Judd and Hovland, 2007; Magalhães et al., 2012).

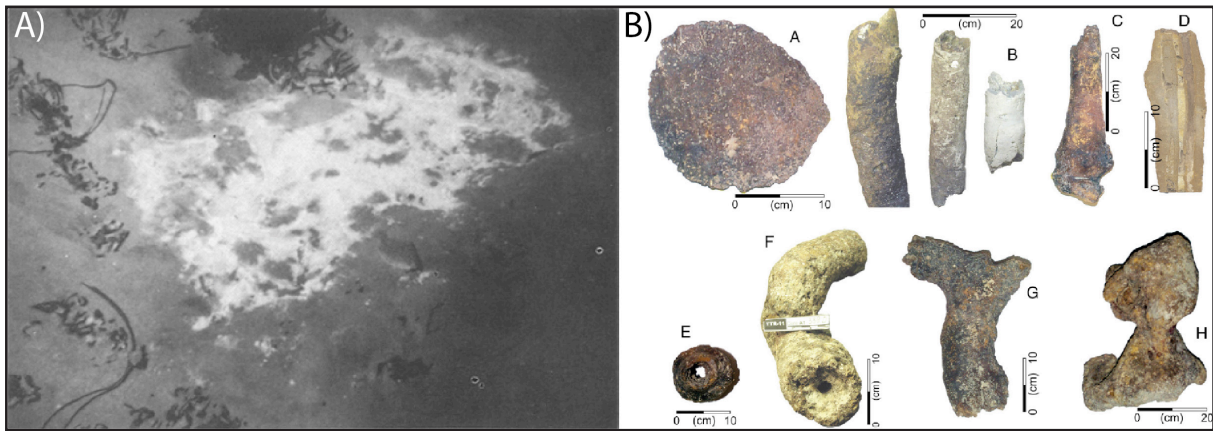


Fig. 1.2: A) Bacterial mats in the Santa Barbara Channel offshore California (Spiess and Davies, 1979). B) Methane-derived authigenic carbonates from the Gulf of Cadiz (Magalhães et al., 2012)

Bacterial mats and MDAC are generally associated with steady, prolonged seepage, but the release of fluids at the seafloor can also occur more explosively with much higher flow rates, which cause the mobilization of seafloor substrate resulting in the formation of crater-like depressions known as pockmarks (Judd and Hovland, 2007). The term pockmark was introduced in a study by King and MacLean in 1970, who reported cone-like depressions on the Scotian shelf. Since then, pockmarks have been identified by sidescan-sonar, seismic and echosounder surveys around the world (Judd and Hovland, 2007). The morphology and size of pockmarks are very diverse and it is possible to differentiate between circular to elliptical pockmarks, elongated and asymmetric pockmarks, merged composite pockmarks, pockmark strings, small unit pockmarks forming around a larger centric pockmark, and giant pockmarks (Fig. 1.3; Judd and Hovland, 2007). There are several observations of MDAC found in pockmarks (Judd and Hovland, 2007, Andresen, 2012), which indicate that

a continuous, less rapid vertical fluid flow may persist after the expulsive formation of a pockmark.

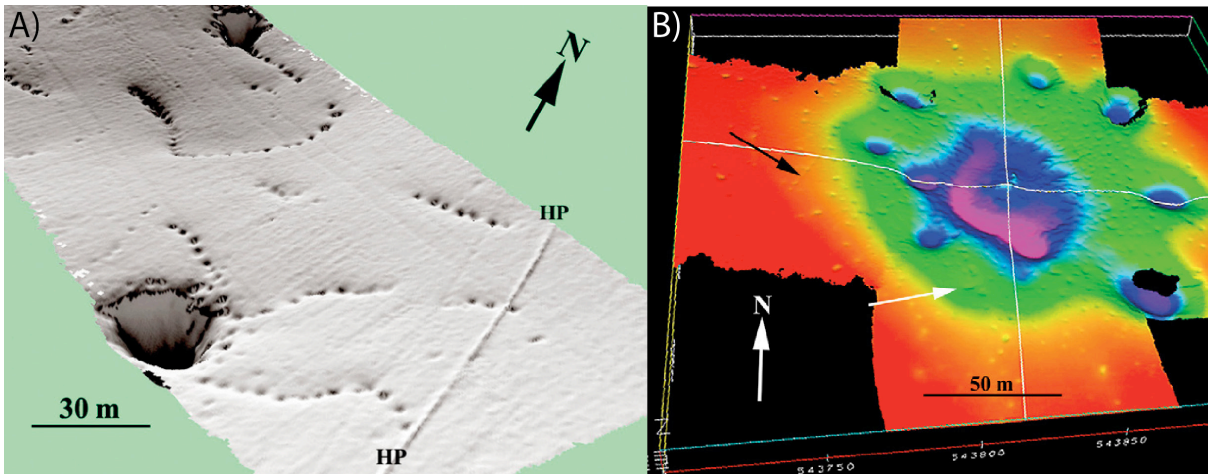


Fig.1.3: A) Two pockmarks with several unit-pockmark strings. B) Parent pockmark in the center of seven satellite pockmarks surrounded by numerous unit-pockmarks (Hovland et al., 2010).

Several other seafloor fluid flow manifestations exist, including mud volcanoes (Kopf, 2002), asphalt volcanoes (MacDonald et al., 2004) or the recently described seafloor fracture just 25 km north of Sleipner (Pedersen, et al., 2013). The so-called Hugin-fracture is about 3 km long and was discovered using AUV-mounted high-resolution synthetic aperture sonar by the University in Bergen within the framework of the ECO2 project in 2011 (Fig. 1.4; ECO2, 2014). The structure was not visible in 3D seismic data or in the conventional multi-beam bathymetry data (ECO2, 2014), which highlights the potential of discovering new types of seafloor fluid flow manifestations with advancing technology.

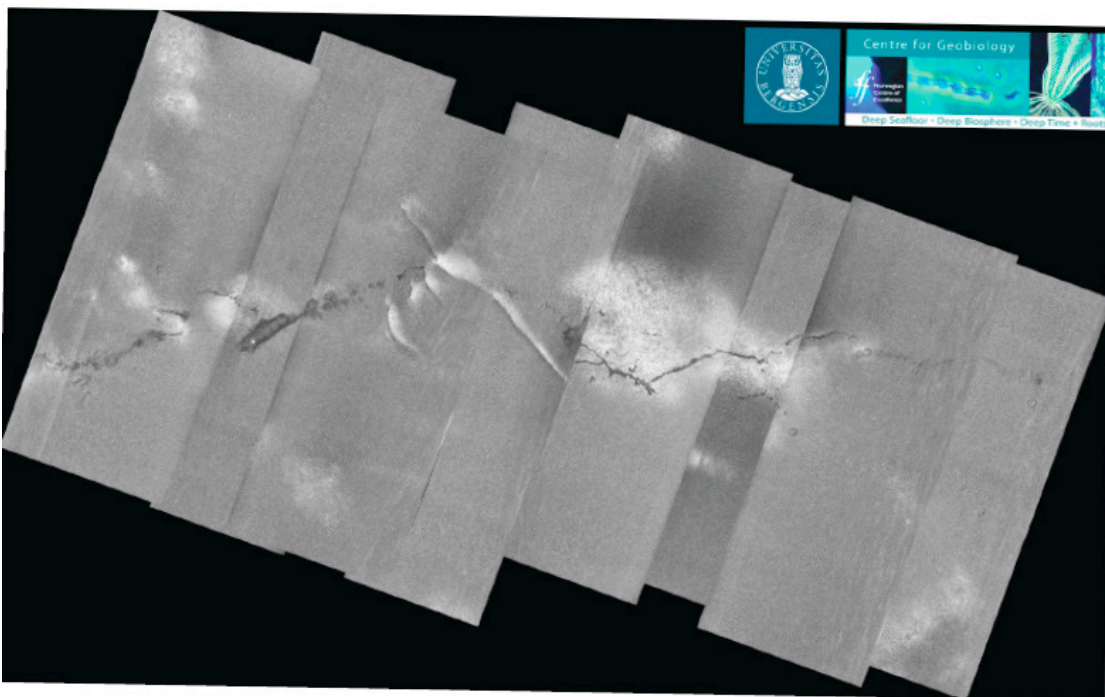


Fig.1.4: HISAS sidescan sonar mosaic showing the Hugin Fracture north of the Sleipner CO₂ storage site (ECO2, 2014).

1.4.3. FOCUSED FLUID FLOW MANIFESTATIONS IN HYDRO-ACOUSTIC AND SEISMIC DATA

Hydro-acoustic and seismic data can reveal pathways of migrating fluids in marine sediments, especially gas, because a small fraction of free gas in the pore space has a strong influence on velocities and attenuation of seismic waves travelling through marine sediments (White, 1975). This effect causes significant changes of the bulk modulus of sediments, leading to a disturbed seismic appearance, as well as amplitude and velocity anomalies (Granli et al., 1999). Seismic anomalies associated with subsurface fluid flow and gas accumulations have been summarized by Løseth et al. (2009) and include:

- Bright spots and zones with increased seismic amplitude
- Dim spots and zones with decreased seismic amplitudes
- Phase reversals
- Changes in the continuity of seismic reflections
- Structurally deformed seismic reflections, e.g. mounds and depressions
- Push-down or pull-up of seismic reflections caused by changes in the seismic velocity
- Non-lithological reflections, e.g. flat spots and bottom simulating reflections (BSRs)

These anomalies may be associated with various focused fluid flow manifestations, including gas accumulations, vertical/sub vertical fluid conduits, sediment deformation processes (e.g. sediment mobilization, polygonal faulting) and gas hydrates. The understanding of focused fluid flow gained tremendous momentum with the advent of 3D seismic technology (Cartwright and Huuse, 2005). 3D seismic datasets collected by the industry for exploration purposes provide the possibility to seismically analyze large areas in high resolution (e.g. spatial resolutions often higher than 15 m). Industrial 3D seismic datasets have been used to reveal the nature of geological structures within sedimentary basins, which had previously not even been recognized (e.g. Cartwright and Huuse, 2005). New technology for recording and processing conventional 3D seismic data, the availability of powerful interpretation workstations, calculation of 3D seismic attributes and the usage of ultra-high resolution 3D seismic systems (e.g. P-cable) are further advancing our understanding of subsurface geology and fluid flow.

1.4.3.1. GAS ACCUMULATIONS AND GAS HYDRATES IN SEISMIC DATA

In seismic data, gas accumulations commonly manifest themselves as bright spots accompanied by a phase reversal of the seismic reflection at the top of the gas pocket (Fig. 1.5a). In settings where pressure and temperature conditions allow the formation of gas hydrates, bottom-simulating reflections (BSRs; Fig. 1.5b) are another indicator for the presence of gas. BSRs mimic the seafloor topography in depths of up to 1000 mbsf, have a reversed polarity compared to the seafloor reflection and indicate the base of the gas hydrate stability zone (Kvenvolden, 1988; Hyndman and Spence, 1992). BSRs are the result of accumulation of free gas below the gas hydrate layer (Hyndman and Spence, 1992).

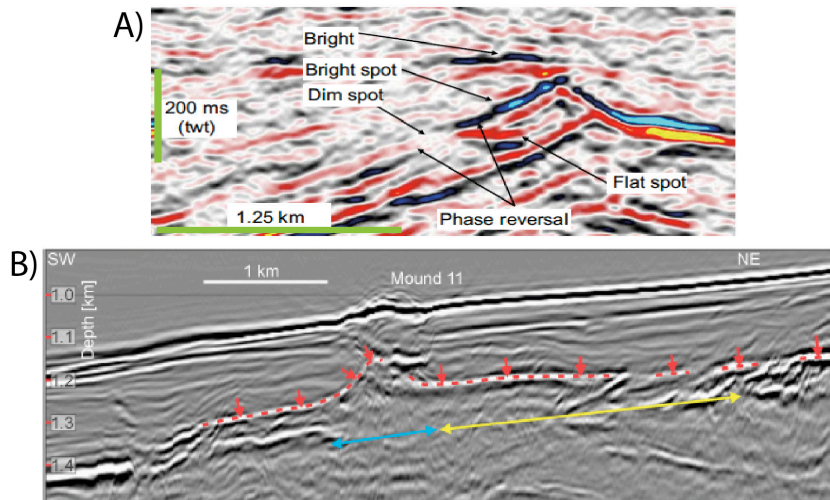


Fig.1.5: A) Different gas associated seismic anomalies (Løseth et al., 2009). B) Seismic profile showing a bottom-simulating reflection (red arrows) affected by fluid flow (Crutchley et al., 2014).

1.4.3.2. SEISMIC CHIMNEYS AND PIPES

Gas accumulations may be formed in-situ or have migrated laterally within a highly permeable layer, but in many cases gas originates from greater depths and migrates vertically via focused fluid conduits, (sections 1.4 and 1.4.1). The seismic image of vertical, strata crosscutting, focused fluid conduits are generally labeled as seismic pipes or chimneys (Fig. 1.6; Cartwright et al., 2007, Løseth et al., 2009, Andresen, 2012). The term seismic chimney or gas chimney originally described dimmed or wiped-out zones in seismic data, which have been identified above several hydrocarbon fields in the North Sea, e.g. Ekofisk (Hovland and Sommerville, 1985), Hild (Lønøy et al., 1986) and Tommeliten (Granli et al., 1999). Some of these features represent a direct connection from deep reservoirs to the seafloor and feed active seafloor seeps (Ekofisk; Hovland and Sommerville, 1985; Tommeliten; Schneider von Deimling et al., et al., 2011). Such “classical gas chimneys” may have diameters of several km (e.g. Tommeliten; Løseth et al., 2009), which distinguishes them from another type of vertical seismic anomalies known as seismic pipes. Seismic pipes have been described in the Nyegga area, offshore Norway (Fig. 1.6b; Mienert et al., 1998). While the term chimney was originally used for very wide structures and the term pipe for comparably narrow structures, the terminology of fluid flow-associated vertical seismic anomalies has become somewhat arbitrary over time and both terms are nowadays used interchangeably for similar structures. This becomes obvious when comparing the three most recent fluid flow overview publications by Cartwright et al. (2007), Løseth et al. (2009), and Andresen (2012). However, all authors agree on associating vertically oriented seismic anomalies with fluid conduits, which are part of seal bypass systems (Cartwright et al., 2007), hydrocarbon leakage systems (Løseth et al. 2009) or hydrocarbon plumbing systems (Andresen, 2012).

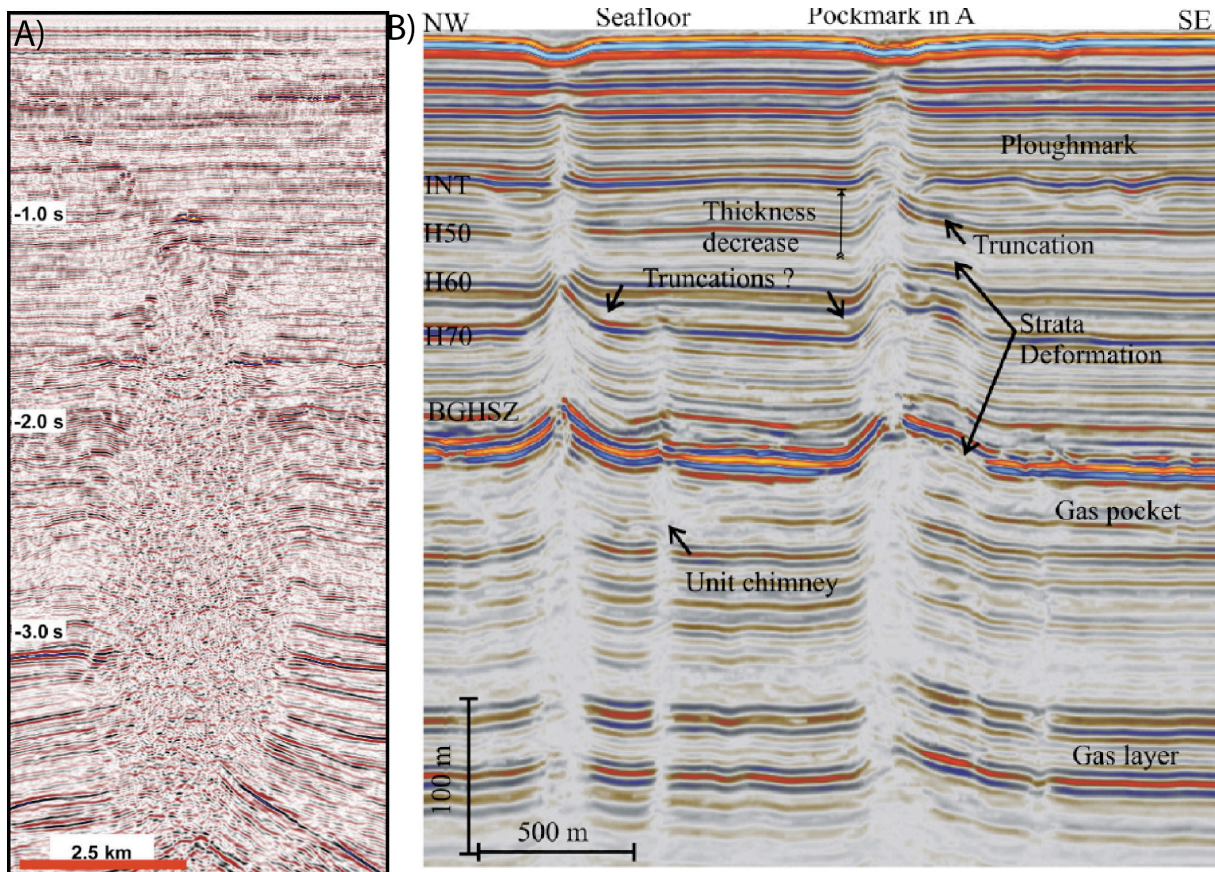


Fig. 1.6: A) Seismic chimneys above the Tommeliten field (Løseth et al., 2009). B) Seismic pipes described by Mienert et al. (1998) from a study by Plaza-Faverola et al., (2011).

1.4.3.3. SEISMIC IMAGE OF SEDIMENT MOBILIZATIONS

In some cases, seismic chimneys and pipes show evidence for deforming or mobilizing sediments (Fig. 1.6b). The mobilization of sediments may occur within coarse-grained sediments resulting in sand injectites (Hurst et al., 2011) as well as in fine-grained clay-rich sediments, where it sources mud diapirism and volcanism (Kopf, 2002). The formation of sand injections is generally associated with rapid fluid discharge or strong seismicity and affects fluid flow over long time-scales (Hurst, et al., 2011). The North Sea basin hosts numerous sub-seafloor sand mobilizations and some of these structures have volumes of up to 10 km³ (Fig. 1.7; Løseth et al., 2012). The injection of sands may deform overlying sediments by forced folding for several hundred meters (Cartwright et al., 2008).

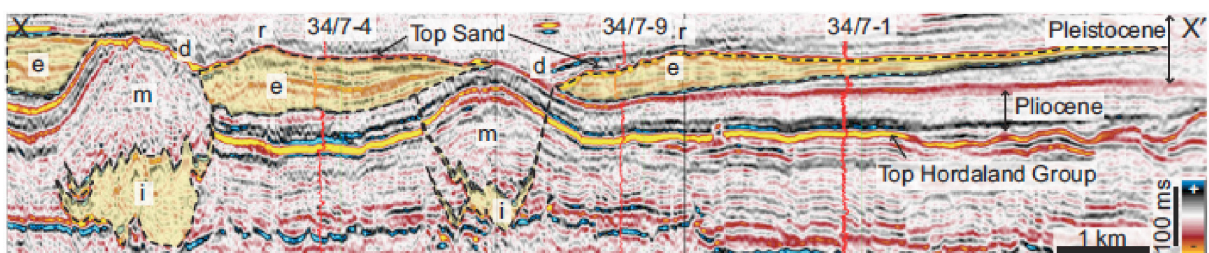


Fig. 1.7: Large-scale sand bodies including large-scale sand intrusions (i) and extrusions (e) from Løseth et al., 2014.

1.5. CARBON CAPTURE AND STORAGE

Carbon capture and storage (CCS) is a technology aiming to reduce the emission of CO₂ from fossil fuel power plants and oil and gas production by transporting and storing it safely in geological formations (Gibbins and Chalmer, 2008). By November 2014, thirteen CCS projects were in the stage of operation, including Sleipner and Snøhvit in Norway, In Salah in Algeria, Century Plant, Shute Creek and five more in the United States, Boundary Dam in Canada and Lula Oil Field in Brazil (Global CCS Institute, 2014). 42 CCS projects are in the planning or evaluation phase, mainly in China, the United States and the United Kingdom (Global CCS Institute, 2014). Most operating CCS projects have the purpose of enhanced oil recovery, whereas only the Statoil-operated projects Sleipner, Snøhvit and In Salah are dedicated for the geological storage of CO₂ (Global CCS Institute, 2014).

The sequestration of CO₂ can be applied from waste-gas or natural gas production by wet scrubbing with aqueous amine solutions or prior consumption by applying physical solvents to gasified fossil fuels (Gibbins and Chalmer, 2008). In the case of Sleipner, the wellstream is transported via pipelines to the Sleipner platform, where gas, condensates and water are separated within an inlet separator and the gas is then sent to a gas scrubber, filter coalescers and absorbers for CO₂ removal using amines (Korbøl and Kaddour, 1995).

Several geological formations have the potential for storing CO₂, for example, saline aquifers, depleted oil and gas reservoirs, and coal seams, as well as only locally relevant geological formations, such as basalts, oil or gas rich shales, salt caverns and abandoned mines (Metz et al., 2005). Depleted oil and gas reservoirs and saline aquifers are the most favored storage formations and all 17 operating CO₂ storage operations make use of these storage opportunities (Global CCS Institute, 2014). The storage of CO₂ within depleted oil and gas reservoirs makes use of fluid traps, which safely store hydrocarbons over millions of years and which have been studied in great detail prior to and during hydrocarbon exploitation (Metz et al., 2005). However, the storage capacity of those reservoirs is comparably small and hydrocarbon exploitation may have affected the integrity of the sealing layers, which may not support the broad usage of this storage solution (Metz et al., 2005). A more feasible option is the injection of CO₂ during hydrocarbon exploitation for enhanced oil and gas recovery, which allows an increase in the oil recovery by 13% on average (Fig. 1.9a; Metz et al., 2005). However, it is arguable to understand enhanced hydrocarbon recovery as an action or the mitigation of CO₂ emissions, because 50% to 67% of the injected CO₂ returns back with produced oil and needs to be re-injected (Metz et al., 2005) and CO₂ is used to produce fossil fuels.

Saline aquifers, which are deep, highly permeable formations containing large quantities of brines that are not usable for human consumption or agriculture (Metz et al., 2005), may represent the most favorable geological storage opportunity for CO₂. Saline aquifers have the highest global storage potential for CO₂ (Fig. 1.9b; Michael et al., 2010). All three CO₂ storage dedicated CCS operations (Sleipner, Snøhvit and In Salah) make use of saline aquifers. Sleipner, Snøhvit and In Salah have an estimate combined storage capacity of 60 Mt and the combined peak injection rate of all three operations was about 3Mt/a (Michael et al., 2010). To put this number into perspective, the recently constructed coal power plant Moorburg, in Hamburg, will have an estimated CO₂ production of 8.7 Mt/a (Vattenfall, web link in reference list). Therefore it would be necessary to operate nine Sleipner-sized CO₂ storage operations to store the total CO₂ emissions of only one modern coal power plant. If CCS is to be an efficient tool to reduce CO₂ emissions on a global scale, it is necessary to significantly increase injection rates and total storage volumes of future operations, which appears only realistic for CCS projects using saline aquifers as storage formations (Michael et al., 2010).

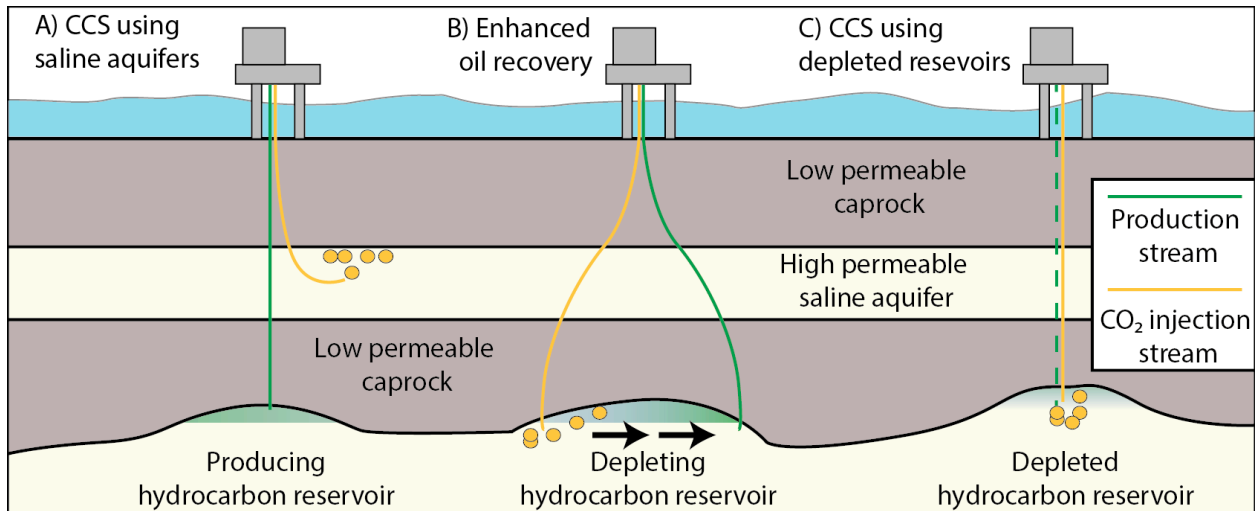


Fig. 1.9: Illustration of CO₂ storage concepts: A) the storage of CO₂ into a saline aquifer at Sleipner, B) enhanced oil recovery using CO₂ and C) Storage of CO₂ in a depleted hydrocarbon reservoir.

1.5.1. THE SLEIPNER CO₂ STORAGE PROJECT

The Sleipner area is located in the Southern Viking Graben, which is the northeastern branch of the Late Jurassic to Early Cretaceous North Sea rift system hosting several highly productive hydrocarbon fields (Ziegler et al., 1992; Gautier, 2005; Fig. 1.10a). The Sleipner CO₂ storage project is part of the Sleipner field development, which was proposed in 1986 and initiated with development of the Sleipner East field in 1993 and Sleipner West in 1996 (Kongsjorden et al., 1998). The Sleipner field had an estimated extractable gas reserve of 173 billion m³ and 98 million m³ of condensates (Kongsjorden et al., 1998). The gas produced at Sleipner Vest is partly used for enhancing condensate production at Sleipner Øst field (Fig. 1.10b; Kongsjorden et al., 1998). The gas produced at Sleipner Vest has a CO₂ content of 4 - 9.5% and needs treatment to fulfill the customer's requirements of a maximum of 2.5% CO₂ (Fig. 1.11; Korbøl and Kaddour, 1995; Kongsjorden et al., 1998). The CO₂ removal is achieved by absorption in an amine tower at a dedicated treatment module (Sleipner T; Kongsjorden et al., 1998).

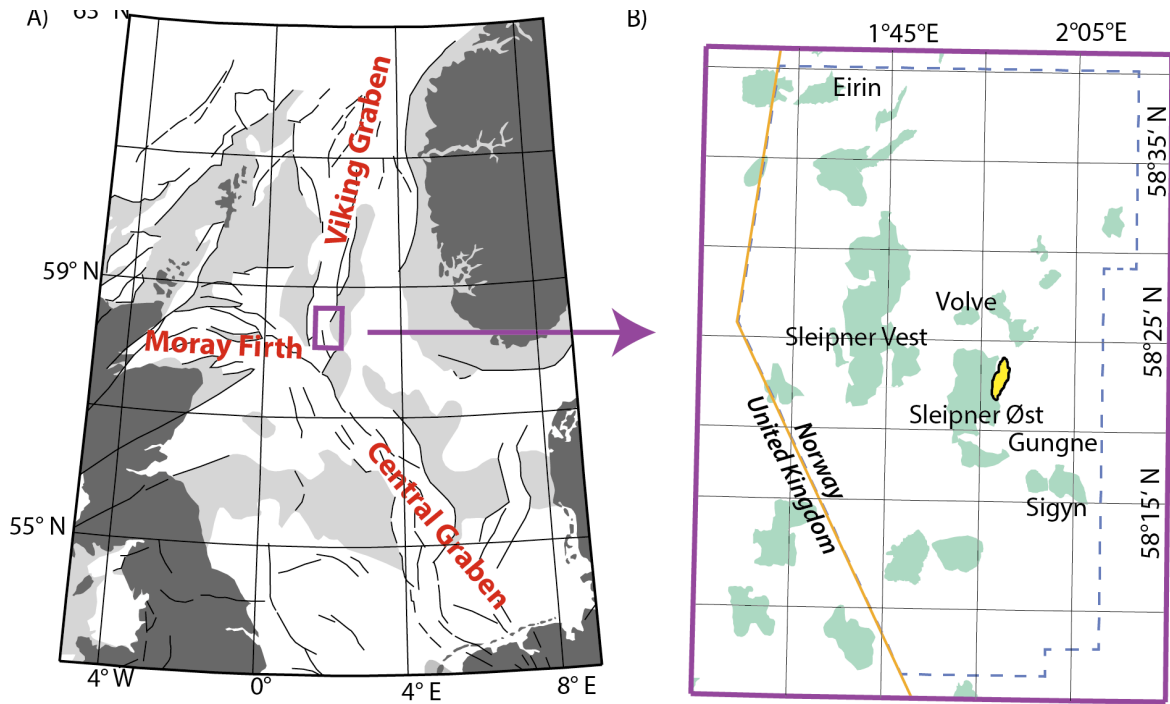


Fig.1.10: A) Map of the North Sea. B) The Sleipner are in the Southern Viking Graben with major hydrocarbon fields (green) and the Sleipner CO₂ plume (yellow).

This complex procedure was implemented to avoid the release of CO₂ into the atmosphere in order to not increase Norway's CO₂ emissions further, and to avoid payment of a CO₂ tax of 55 US\$/t (today 65 US\$/t; Kongsjorden et al., 1998; Cavanagh and Haszeldine, 2014). The sequestered CO₂ is injected at a depth of 1012 mbsf into the Utsira Formation, which is an 850 mbsf saline aquifer with a thickness of 250 m at Sleipner (Arts et al., 2008). The Utsira Formation extends about 450 km N-S and 90 km E-W and has a potential storage capacity of 16 billion tons (Halland et al., 2011). The Utsira Formation is overlain by the Nordland Formation, which is supposed to act as a 200 – 300 m thick, impermeable seal prohibiting the escape of CO₂ from the storage formation (Arts et al., 2008).

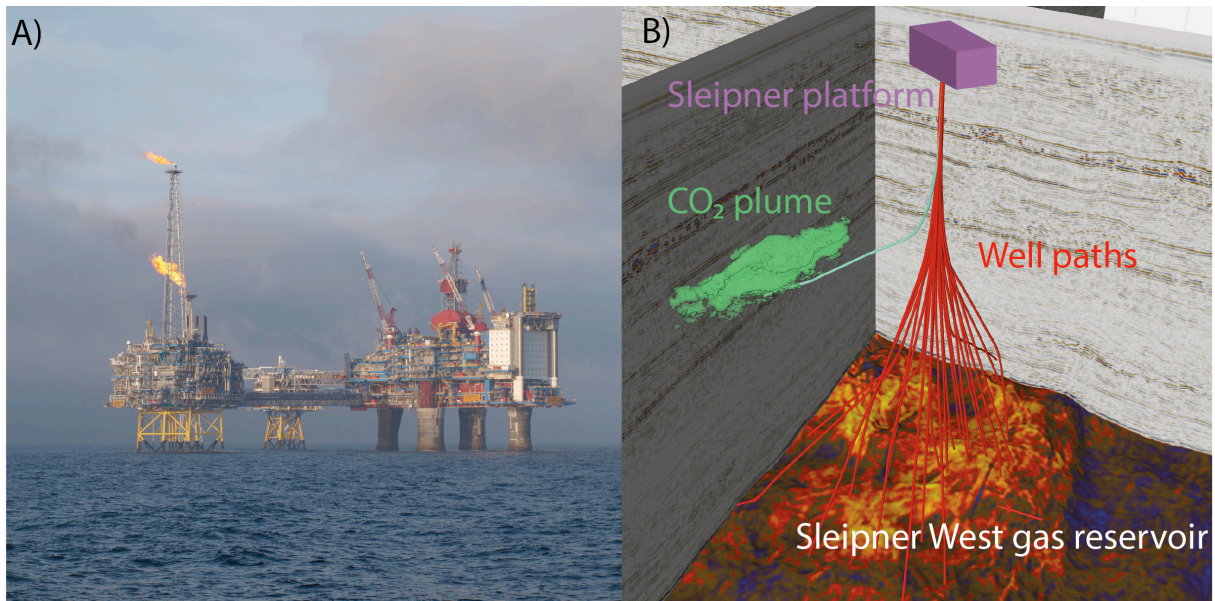


Fig. 1.11: A) Sleipner platform in the North Sea. B) 3D view on the well paths for gas production (red) and CO₂ injection (green), the CO₂ plume at Sleipner

The local stratigraphy has been extensively investigated by several studies and the following summary is taken from Chapter 3.3: The Southern Viking Graben formed in late Jurassic to Early Cretaceous times as a branch of the North Sea failed rift system (Ziegler et al., 1992). Post-rift subsidence and uplift of the surrounding landmasses led to the deposition of prograding deltaic sequences into the deepened North Sea Basin from the Shetland Platform and West Norway in Oligocene and Miocene time (Eidvin et al., 2014). During the Late Miocene, the paleogeographic setting remained stable for a period of 8 Ma and a large eastward-prograding, deltaic system deposited the 250 – 300 m thick Utsira Formation in a high energy, shelf environment (Galloway, 2001; 2002; Eidvin and Rundberg, 2007; Eidvin, et al., 2014). The Utsira sand is intersected by thin, low permeability and apparently fractured mudstone layers, which have a strong impact on the evolution of the CO₂ plume (Chadwick et al., 2009; Cavanagh and Haszeldine, 2014). The main Utsira sand body is covered by a >5 m thick mudstone layer, which separates it from another sand layer hosting the shallow-most layer of the CO₂ plume (Cavanagh, 2013). The Utsira Formation consists of poorly cemented, fine-to-medium grained, moderately sorted sand, which is mainly composed of angular to rounded quartz grains with minor K-feldspars, plagioclase, calcite, coarse to gravel-sized shell fragments and only little clay-grade material (Audigane et al., 2007). The Utsira Formation has excellent reservoir properties characterized by a porosity of 35 – 40% and a permeability of 1000 – 3000 mD (Chadwick, et al., 2004).

The Utsira Formation is directly overlain by the Nordland Shales, which form the Quaternary section with a thickness of more than 800 m in the Sleipner area. The boundary between Utsira Formation and Nordland Shales marks the beginning of glacially influenced sediments in the SVG (Ottesen et al., 2014), which is characterized by the deposition of the 50 – 150 m-thick Shale Drape, which consists of grey mudstones with high clay content in the Sleipner area (Chadwick et al., 2004; Gregersen and Johannessen, 2007). Rock physical property tests on a Nordland Shale sample from the Sleipner area revealed a capillary entry pressure of 1.6 – 1.9 MPa, a permeability of 4×10^{-10} mD perpendicular and 10^{-9} mD parallel to bedding (Harrington et al., 2009). A complex of prograding clinofolds sourced by distal-fluvial and fluvial-glacial sources overlies this unit (Ottesen et al., 2014; Gregersen and Johannessen, 2007). The Quaternary succession is divided by an unconformity (Ottesen et al., 2014), which marks the base of glacially reworked sediments of Pleistocene age that are characterized by frequent tunnel valley incisions (Huuse and Lykke-Andersen, 2000; Lonergan et al., 2006).

1.5.2. GEOTECHNICAL INCIDENTS WITH RELEVANCE FOR CCS

The most crucial requirement for the long-term efficiency of a CO₂ storage operation is the integrity of the caprock. The injection of fluids and the associated increase of pressure within a storage formation have the potential to breach a caprock, which became obvious by two fluid injection related geotechnical incidents at Tordis (Norwegian North Sea) in 2008 (Eidvin and Øverland, 2009) and at In Salah (onshore Algeria) between 2004 and 2011 (White et al., 2014). Potential seal integrity problems at In Salah were discovered after the cessation of injection by analyzing seismic data, interferometric synthetic aperture radar data and wellbore measurements (White et al., 2014). The data indicated that CO₂ leaked into the lower seal from the formation, where it was supposed to be contained, indicating hydrofracturing or the reactivation of pre-existing faults or fractures (White et al., 2014). Time-lapse 4D seismic data revealed two northeast-southwest trending features on the horizon map from the lower caprock, which are most likely associated with the leakage of CO₂ (Fig 1.12a; White et al., 2014).

The Tordis incident was detected by the discovery of an oil slick in the vicinity of the Tordis field. At Tordis, oil is produced by subsea installations with an increasing water cut, which is separated by an on-site installation from the wellstream (Eidvin and Øverland, 2009). The separated water and sand were supposed to be injected at a depth of 1km into a sandstone formation, which was believed to represent the Utsira Formation (Eidvin and Øverland, 2009). The injection was stopped after approximately 1100 barrels of oil leaked at the seafloor forming a 30 - 40 m diameter crater on the seabed (Fig. 1.12b; Eidvin and Øverland, 2009). This incident raised concerns about the operational safety at the Sleipner site due to apparent failure of its storage system, which was believed to be also used for the CO₂ injection. However, later investigations revealed that the wastewater injection mistakenly targeted a sandy glacial deposit with poorer hydraulic properties than the Utsira Formation (Eidvin and Øverland, 2009). Nevertheless, this incident emphasizes the importance of detailed site surveying prior to CO₂ injection.

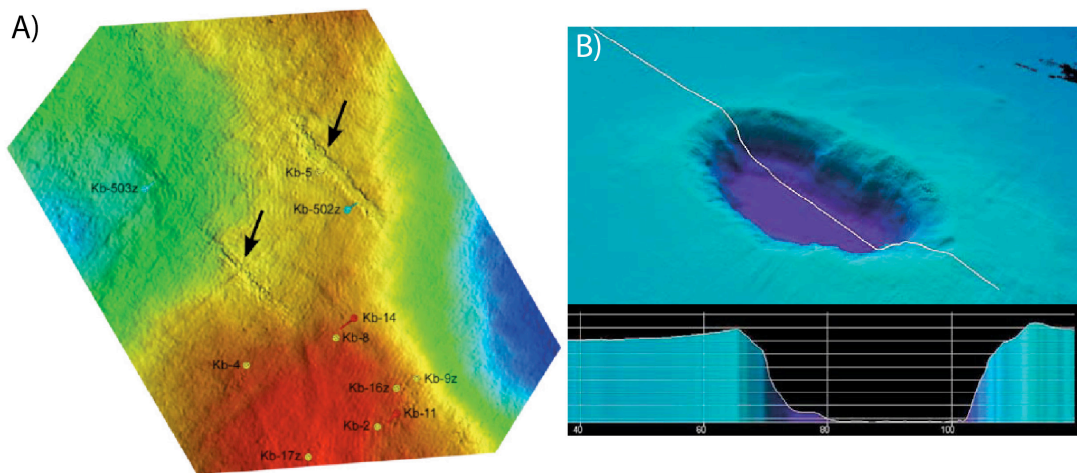


Fig.1.12: A) Map of a seismic horizon above the In Salah storage Formation from 2009. Black arrows indicate seal fracturing associated anomalies (White et al., 2014). B) Seafloor crater at Tordis (Eidvin and Øverland, 2009)

1.5.3. THE ECO2 PROJECT

The evaluation of comparable CO₂ storage related incidents is the main motivation of the ECO2 project, which is a European Commission funded, international, interdisciplinary project. The ECO2 project studies natural (volcanic) CO₂ seeps at Panarea, Jan Mayen and Salt dome Juist as field equivalents for leakage events, as well as planned and operating CO₂ storage projects including B3 field (Poland), Snøhvit and Sleipner.

The ECO2 project consists of six scientific work packages and four crosscutting themes. Work package 1 deals with the architecture and integrity of the sedimentary cover at storage sites. The main purpose of this work package is the assessment and evaluation of potential leakage scenarios for the currently operational storage sites Sleipner and Snøhvit. Work package 2 is about fluid and gas fluxes across the seabed at storage sites and natural CO₂ seeps. The main objectives are the development of effective leakage tracers, leakage quantification methods, the assessment strategies of toxic metal mobilization and numerical models.

The topic of work package 3 is the fate of CO₂ and other gases emitted at the seabed. The main purpose of this work package is the assessment of CO₂ transport mechanisms and leakage in the water column as well as the development of risk assessment simulations and best practices for baseline surveys. Work package 4 deals with the impact of leakage on benthic organisms and the marine ecosystems". This work package aims to quantify the consequences of CO₂ leakage on marine organisms and their ability for adoption of elevated CO₂ levels as well as the identification of biologic leakage indicators.

Work package 5 purposes are risk assessment, economics, legal studies and policy stakeholder dialogue". The main objectives are to assess the environmental risks associated with CCS, potential costs for monitoring and potential interventions, review the legal framework of CCS. Furthermore, it is this work package's task to communicate the findings of ECO2 to stakeholders. Work package 6: is about public perception assessment. This work package investigates the terminology of CCS, public perception and provides guidance for communication between stakeholders and the public.

The crosscutting themes include the development of monitoring techniques and strategies (CCT1), interfacing of the numerical models of the different work packages (CCT2), international collaboration (CCT3) and the development of a framework for best environmental practices in the management of offshore CCS (CCT4). My PhD studies were conducted within the framework of work package 1, but I also contributed to work package 2, CCT2 and CCT4.

1.6. THE INFLUENCE OF FOCUSED FLUID FLOW ON HYDROCARBON EXPLORATION AND WELLBORE ACTIVITIES

Shallow focused fluid flow systems strongly influence the safety and success of exploration wellbore activities because gas accumulations, especially when undetected, bear high risks for hydrocarbon production (Hovland and Sommerville, 1985). Several drilling accidents may at least partly be related to an insufficient understanding of shallow fluid flow systems (e.g. the 22/4b blowout in the North Sea, 1990).

In addition, focused fluid flow may influence hydrocarbon exploration by seismically masking underlying prospects. For example, seismic chimneys above the Tommeliten Alpha field cause pronounced seismic disturbance, which prohibit imaging the faulted dome structure of the reservoir (Granli et al., 1999). Similar gas chimneys have been identified above numerous hydrocarbon reservoirs including Ekofisk (Hovland and Sommerville, 1985) Hild (Lønøy et al., 1986), in block 5604/26 in the Danish sector of the North Sea (Heggland, 1998), the Gulf of Mexico, Nigeria and the Capian Sea (Heggland, 2005). The correlation between seismic chimneys and hydrocarbon prospects has two important implications for hydrocarbon exploration: (1) Seismic chimneys and other focused fluid flow manifestations may be used as indicators for the presence

of deep hydrocarbon reservoirs and (2) seismic chimneys as seal-bypassing fluid conduits may explain several dry reservoirs (Heggland, 2005).

The exploration of hydrocarbons has resulted in more than 15,000 wells in the North Sea (Chapter 7). 18% of all active and 38% of all temporarily abandoned wells in Norwegian waters show integrity problems (Vignes et al., 2006; 2011). The impact of the associated methane release on the carbon budgets of the North Sea and other hydrocarbon provinces has not been constrained yet. The release of methane from wells is generally attributed to ongoing hydrocarbon migration from deep reservoirs to the surface (Gasda et al., 2004; Vignes et al., 2006, Davies et al., 2014). However, the origin of the gas leaking from abandoned wells is poorly understood and the leakage of shallow biogenic gas rather than deep thermogenic gas would have important implications for the geological storage of CO₂. Wells penetrating CO₂ storage formations have been recognized as potential leakage pathways (Nordbotten et al., 2005).

1.7. AIMS OF THE THESIS

This thesis deals with the impact of focused fluid flow systems in marine sediments on sub-seafloor storage and exploration activities and is based on the interpretation of 3D and 4D time-lapse seismic data, numerical fluid flow simulations, as well as field geological observations. The analyzed seismic data cover more than 2000 km² of the Southern Viking Graben in the Norwegian sector of the North Sea and the field geological observations are from different outcrops in the Colorado Plateau (Utah, USA). Some of the findings and their implications are site specific, while others may be globally useful for sedimentary basins in general. Within this thesis, I seek to provide new insights for the following questions:

- How did the fluid flow system in the Southern Viking Graben evolve?
- What caused the formation of focused fluid conduits in the North Sea Basin?
- Is it possible to constrain the nature of chimney structures by correlating specific seismic features of with field geological observations?
- What are the risks associated with focused fluid conduits in the overburden of sub-seafloor CO₂ storage sites?
- What are the implications of shallow fluid flow systems for wellbore activities?

1.8. INTRODUCTION OF THE CHAPTERS

This thesis consists of eight chapters including an introduction, six manuscripts dealing with different aspects of focused fluid flow within the framework of the ECO2 project and a concluding chapter. I authored four of the presented manuscripts and contributed relevant inputs to the other two manuscripts. The manuscripts have been published, submitted or are planned to be submitted to peer-review journals and are detailed below.

Chapter 2 deals with the reconstruction of the palaeo fluid flow system in the Southern Viking Graben. This reconstruction enables the identification of focused fluid flow manifestations including gas accumulations, sediment mobilizations as well as chimney and pipe structures in 3D seismic data. The presence of three different types of vertical fluid flow conduits highlights the diversity of focused fluid flow patterns within a comparably small study area. In order to constrain formation parameters such as timing, migrating fluids, duration of fluid flow activity and flow dynamics, it was necessary to analyze the nature of each fluid conduit based on its seismic appearance. Additionally, it was necessary to study the interaction of these structures with the local stratigraphy and glacial bedforms as well as the correlation with deep hydrocarbon reservoirs to understand the formation processes of the focused fluid flow conduits. Chapter 2 is published as “Karstens, J., and Berndt, C., 2015. Seismic chimneys in the Southern Viking Graben – Implications for palaeo fluid migration and overpressure evolution” in the journal *Earth and Planetary Science Letters*. I carried out seismic analysis, prepared the illustrations, and wrote the first draft of the manuscript. Discussions with Christian Berndt improved it for publication.

Chapter 3 focuses on the investigation of the formation process of the observed chimney structures. The analysis of fluid flow system revealed that the chimneys crosscut the shallowest glacial sediments and glacial tunnel valleys, which indicates a relatively recent formation age. This points towards a correlation between focused fluid conduit formation and glacial dynamics. However, there has been no convincing mechanism that links the generation of high pore overpressure within highly permeable, gas-bearing sedimentary layers with loading and unloading by growing and retreating ice sheets. We introduce a novel process for predicting generation of high overpressure, which is the result of undrained compaction facilitated by gas compression. Chapter 3 has been submitted as “Karstens, J., and Berndt, C. The glacial methane pump: Overpressure and focused fluid flow due to gas compression compensated sediment compaction” to *Nature Geoscience*. The idea for this paper and the development of the presented mechanism for the generation of overpressure are the result of long and intense conversations with Christian Berndt and based on the findings presented in chapter 2. I am responsible for the figures and the writing of the manuscript. Christian Berndt helped me in revising and improving the quality of the manuscript.

In **chapter 4**, I evaluate the risks of CO₂ leakage along fluid conduits as part of natural fluid flow systems, which has not been done before. Such an evaluation must build on detailed understanding of the natural fluid flow system allowing the creation of geological models for fluid flow simulations. Within the framework of the ECO2 project, we have performed numerical simulations of multi-phase fluid flow. These simulations are the basis for assessing hydraulic properties of the Utsira Formation and evaluating the permeability of chimney structures. Long-term simulations over a modelling period of 200 years were used to evaluate leakage scenarios. Chapter 4 is submitted as “Karstens, J., Ahmed, W., Berndt, C., and Class, H. The impact of chimney structures on CO₂ storage at Sleipner: Evaluation of numerical fluid flow simulations based on time-lapse seismic data” to the journal *Geochemistry, Geophysics, Geosystems*. I am responsible for the development of the geological models, modeling objectives and the evaluation of modeling results as well as the creation of figures and the writing of the manuscript. Waqas Ahmed has implemented and executed the simulations. Christian Berndt and Holger Class helped in revising and improving the manuscript.

Chapter 5 deals with the comparison of field geological and seismic observations of focused fluid conduits. The seismic analysis in the Southern Viking Graben has revealed that it is possible to differentiate between different types of seismic chimneys based on specific seismic signatures (e.g. upward bended, downward bended reflection and zones with chaotic seismic amplitudes). This chapter aims to correlate these seismic signatures with field analogues of sand injections, sediment fluidizations and fracture networks. Chapter 5 is an extended version of the talk “Karstens, J., and Berndt, C. 2014. Insights into focused fluid conduit formation from comparing seismic chimneys and pipes with field observations of fluid flow manifestations in the Colorado Plateau”, which I presented at the Fall Meeting of the American Geophysical Union in December 2014. I am responsible for the figures and the writing of the presentation. Christian Berndt helped me in revising and improving the quality of the presentation.

Chapters 6 is written by Lisa Vielstädte and is based on the geochemical and video-based analysis of bubble streams from leaking, abandoned wells in the Sleipner area revealing methane release rates that are comparable to those known from natural seeps. A combined geochemical and geophysical analysis reveals that the leaking gas is of shallow, microbial origin and only a small fraction (< 2%) reaches directly to the atmosphere. Chapter 5 is submitted as “Vielstädte, L., Karstens, J., Haeckel, M., Schmidt, M., Liebetrau, V., Reimann, S., McGinnis, D.F., Linke, P., and Wallmann, K. Quantification of methane emissions at abandoned gas wells in the Central North Sea” to the Journal of Marine and Petroleum Geology. My contribution to this chapter is the analysis of seismic data in the vicinity of the three analyzed abandoned wells, the part of the discussion, which correlates leakage rates and shallow fluid flow manifestations, and the creation of figures 6.2 and 6.5 presented in the manuscript.

Chapter 7 is written by Lisa Vielstädte and uses the findings of chapter 7 to extrapolate methane emissions from leaking wells on a North Sea scale. This extrapolation reveals that methane emission from leaking wells may be in an order of 19 (± 10) kt per year, which has an impact on the methane budget of the North Sea. This chapter will be submitted to Nature as: “Vielstädte, L., Haeckel, M., Karstens, J., Linke, P., Schmidt, M., Steinle, L., and Wallmann, K. Greater focus needed on biogenic methane leakage from oil and gas wells in the North Sea”. My contribution to this chapter is the analysis of seismic data in the direct vicinity of the well path of 55 wells and the creation of figure 7.1.

Chapter 8 summarizes the results from the previous chapters and draws integrated conclusions for site selection of sub-seabed CCS operations. Further, I provide recommendations for future fluid flow and CCS related studies and give an outlook on already planned follow-up research activities.

REFERENCES

- Andresen, K.J., 2012. Fluid flow features in hydrocarbon plumbing systems: What do they tell us about the basin evolution? *Marine Geology* 1–20. doi:10.1016/j.margeo.2012.07.006
- Arts, R.J., Chadwick, R.A., Eiken, O., Thibeau, S., Nooner, S., Lamont-Doherty Geological Observatory of Columbia University, 2008. Ten years' experience of monitoring CO₂ injection in the Utsira Sand at Sleipner, offshore Norway.
- Audigane, P., Gaus, I., Czernichowski-Lauriol, I., Pruess, K., Xu, T., 2007. Two-dimensional reactive transport modeling of CO₂ injection in a saline aquifer at the Sleipner site, North Sea. *American Journal of Science* 307, 974–1008. doi:10.2475/07.2007.02
- Baross, J.A., Hoffman, S.E., 1985. Submarine hydrothermal vents and associated gradient environments as sites for the origin and evolution of life. *Origins of Life and Evolution of the Biosphere* 15, 327–345. doi:10.1007/BF01808177
- Berndt, C., 2005. Focused fluid flow in passive continental margins. *Philosophical Transactions of the Royal Society A: Mathematical, Physical and Engineering Sciences* 363, 2855–2871. doi:10.1098/rsta.2005.1666
- Berndt, C., Brune, S., Nisbet, E., Zschau, J., Sobolev, S.V., 2009. Tsunami modeling of a submarine landslide in the Fram Strait. *Geochem. Geophys. Geosyst.* 10, n/a–n/a. doi:10.1029/2008GC002292
- Bjørlykke, K., 2010. *Petroleum Geoscience: From sedimentary environments to rock physics*. Berlin, Heidelberg: Springer Berlin Heidelberg. doi:10.1007/978-3-642-02332-3
- Boetius, A., Ravensschlag, K., Schubert, C.J., Rickert, D., 2000. A marine microbial consortium apparently mediating anaerobic oxidation of methane. *Nature* 407, 623–626. doi:10.1038/35036572
- Bünz, S., Mienert, J., Berndt, C., 2003. Geological controls on the Storegga gas-hydrate system of the mid-Norwegian continental margin. *Earth and Planetary Science Letters* 209, 291–307. doi:10.1016/S0012-821X(03)00097-9
- Burwicz, E.B., Rüpke, L.H., Wallmann, K., 2011. Estimation of the global amount of submarine gas hydrates formed via microbial methane formation based on numerical reaction-transport modeling and a novel parameterization of Holocene sedimentation. *Geochimica et Cosmochimica Acta* 75, 4562–4576. doi:10.1016/j.gca.2011.05.029
- Cartwright, J.A., Huuse, M., Aplin, A., 2007. Seal bypass systems. *Bulletin* 91, 1141–1166. doi:10.1306/04090705181
- Cartwright, J.A., Huuse, M., 2005. 3D seismic technology: the geological 'Hubble'. *Basin research* 17, 1–20. doi:10.1111/j.1365-2117.2005.00252.x
- Cartwright, J.A., James, D., Huuse, M., Vetel, W., Hurst, A., 2008. The geometry and emplacement of conical sandstone intrusions. *Journal of Structural Geology* 30, 854–867. doi:10.1016/j.jsg.2008.03.012
- Cavanagh, A., 2013. Benchmark Calibration and Prediction of the Sleipner CO₂ Plume from 2006 to 2012. *Energy Procedia* 37, 3529–3545. doi:10.1016/j.egypro.2013.06.246
- Cavanagh, A.J., Haszeldine, R.S., 2014. The Sleipner storage site: Capillary flow modelling of a layered plume requires fractured shale barriers within the Utsira Formation. *International Journal of Greenhouse Gas Control* 21, 101–112. doi:10.1016/j.ijggc.2013.11.017
- Chadwick, R. A. (2012). Reflections on storage site monitoring. *Greenhouse Gases: Science and Technology*,

2(4), 219–222. doi:10.1002/ghg.1297

Chadwick, R.A., Noy, D., Arts, R.J., Eiken, O., 2009. Latest time-lapse seismic data from Sleipner yield new insights into CO₂ plume development. *Energy Procedia* 1, 2103–2110. doi:10.1016/j.egypro.2009.01.274

Chadwick, R.A., Zweigel, P., Gregersen, U., Kirby, G.A., Holloway, S., Johannessen, P.N., 2004. Geological reservoir characterization of a CO₂ storage site: The Utsira Sand, Sleipner, northern North Sea. *Energy* 29, 1371–1381. doi:10.1016/j.energy.2004.03.071

Clayton, C.J., Hay, S.J., 1994. Migration mechanisms from accumulation to surface. *Bulletin of the Geological Society of Denmark* 41, 12–23.

Cook, J., Nuccitelli, D., Green, S. A., Richardson, M., Winkler, B., Painting, R., et al., 2013. Quantifying the consensus on anthropogenic global warming in the scientific literature. *Environmental Research Letters*, 8(2), 024024. doi:10.1088/1748-9326/8/2/024024

Crowley, T.J., 2000. Causes of Climate Change Over the Past 1000 Years. *Science* 289, 270–277. doi:10.1126/science.289.5477.270

Crutchley, G.J., Klaeschen, D., Planert, L., Bialas, J., 2014. The impact of fluid advection on gas hydrate stability: Investigations at sites of methane seepage offshore Costa Rica. *Earth and Planetary Science Letters*.

Davies, R.J., et al., 2014. Oil and gas wells and their integrity: Implications for shale and unconventional resource exploitation. *Mar. Petrol. Geol.* 56, 239-154.

ECO2, 2014. WP1 result summary report relevant for “Environmental Best Practice”. ECO2 Deliverable, D1.2 . , 32 pp.

Eidvin, T., Riis, F., Rasmussen, E.S., 2014. Marine and Petroleum Geology. *Marine and Petroleum Geology* 56, 184–221. doi:10.1016/j.marpetgeo.2014.04.006

Eidvin, T., Rundberg, Y., 2007. Post-Eocene strata of the southern Viking Graben, northern North Sea; integrated biostratigraphic, strontium isotopic and lithostratigraphic study. *Norwegian Journal of Geology* 87, 391–450.

Eidvin, T., Øverland, J.A., 2009. Faulty geology halts project. *Norwegian Continental Shelf*.

Fisher, R.E., Sriskantharajah, S., Lowry, D., Lanoisellé, M., Fowler, C.M.R., James, R.H., Hermansen, O., Lund Myhre, C., Stohl, A., Greinert, J., Nisbet-Jones, P.B.R., Mienert, J., Nisbet, E.G., 2011. Arctic methane sources: Isotopic evidence for atmospheric inputs. *Geophys. Res. Lett.* 38, n/a–n/a. doi:10.1029/2011GL049319

Forsberg, C.F., Planke, S.F., Tjelta, T.I., Svano, G.F., Strout, J.M., Svensen, H.F., 2007. Formation of pockmarks in the Norwegian channel. *Offshore site investigation and geotechnics, Confronting New Challenges and Sharing Knowledge*.

Galloway, W.E., 2001. Seismic expressions of deep-shelf depositional and erosional morphologies, Miocene Utsira Formation, North Sea Basin. *Marine Geophysical Research* 22, 309–321.

Galloway, W.E., 2002. Paleogeographic setting and depositional architecture of a sand-dominated shelf depositional system, Miocene Utsira Formation, North Sea Basin. *Journal of Sedimentary Research* 72, 476–490.

Gasda, S.E., Bachu, S., Celia, M.A., 2004. Spatial characterization of the location of potentially leaky wells penetrating a deep saline aquifer in a mature sedimentary basin. *Environmental Geology* 46, 707-720

- Gautier, D.L., 2005. Kimmeridgian Shales Total Petroleum System of the North Sea Graben Province: U.S. Geological Survey Bulletin 2204-C, 24 pp.
- Global CCS Institute, 2014. The Global Status of CCS: 2014, Melbourne, Australia. 199 pp.
- Gibbins, J., Chalmers, H., 2008. Carbon capture and storage. *Energy Policy* 36, 4317–4322. doi:10.1016/j.enpol.2008.09.058
- Granli, J.R., Arntsen, B., Sollid, A., Hilde, E., 1999. Imaging through gas-filled sediments using marine shear-wave data. *Geophysics* 64, 668–677.
- Gregersen, U., Johannessen, P.N., 2007. Distribution of the Neogene Utsira Sand and the succeeding deposits in the Viking Graben area, North Sea. *Marine and Petroleum Geology* 24, 591–606. doi:10.1016/j.marpetgeo.2007.04.006
- Halland, E.K., Tjelta Johansen, W., Riis, F., 2011. CO₂ storage Atlas Norwegian North Sea 1–72.
- Harrington, J.F., Noy, D.J., Horseman, S.T., Birchall, D.J., 2009. Laboratory study of gas and water flow in the Nordland Shale, Sleipner, North Sea.
- Heggland, R., 1998. Gas seepage as an indicator of deeper prospective reservoirs. A study based on exploration 3D seismic data. *Marine and Petroleum Geology* 15, 1–9.
- Heggland, R., 2005. Using gas chimneys in seal integrity analysis: A discussion based on case histories. doi:10.1306/1060767H23170
- Higgins, J.A., Schrag, D.P., 2006. Beyond methane: Towards a theory for the Paleocene–Eocene Thermal Maximum. *Earth and Planetary Science Letters* 245, 523–537. doi:10.1016/j.epsl.2006.03.009
- Hovland, M., 1987. Methane-related carbonate cements in pockmarks of the North Sea. *Journal of Sedimentary Petrology* 1–12.
- Hovland, M., Heggland, R., De Vries, M.H., Tjelta, T.I., 2010. Unit-pockmarks and their potential significance for predicting fluid flow. *Marine and Petroleum Geology* 27, 1190–1199. doi:10.1016/j.marpetgeo.2010.02.005
- Hovland, M., Judd, A.G., Burke, R.A., 1993. The global flux of methane from shallow submarine sediments. *Chemosphere* 26, 559–578.
- Hovland, M., Sommerville, J.H., 1985. Characteristics of two natural gas seepages in the North Sea. *Marine and Petroleum Geology* 2, 319–326.
- Hurst, A., Scott, A., Vigorito, M., 2011. Physical characteristics of sand injectites. *Earth Science Reviews* 106, 215–246. doi:10.1016/j.earscirev.2011.02.004
- Huuse, M., Lykke Andersen, H., 2000. Overdeepened Quaternary valleys in the eastern Danish North Sea: morphology and origin. *Quaternary Science Reviews* 19, 1233–1253.
- Hyndman, R.D., Spence, G.D., 1992. A seismic study of methane hydrate marine bottom simulating reflectors. *Journal of Geophysical Research: Solid Earth* (1978–2012) 97, 6683–6698. doi:10.1029/92JB00234
- IEA, 2012. World Energy Outlook 2012, World Energy Outlook, World Energy Outlook. OECD Publishing. doi:10.1787/weo-2012-en
- IPCC, 2013. Summary for Policymakers in Climate Change 2013: The Physical Science Basis, Contribution of

Working Group I to the Fifth Assessment Report of Intergovernmental Panel on Climate Change.

Judd, A., Hovland, M., 2007. Seabed fluid flow: the impact on geology, biology and the marine environment. Cambridge University Press, Cambridge. doi:10.1017/cbo9780511535918

Judd, A.G., Hovland, M., Dimitrov, L.I., Gil, S.G., Jukes, V., 2002. The geological methane budget at Continental Margins and its influence on climate change. *Geofluids* 2, 109–126. doi:10.1046/j.1468-8123.2002.00027.x

Katz, B.J., 2011. Microbial Processes and Natural Gas Accumulations. *The Open Geology Journal* 5, 75–83. doi:10.2174/1874262901105010075

Kennett, J.P., 2000. Carbon Isotopic Evidence for Methane Hydrate Instability During Quaternary Interstadials. *Science* 288, 128–133. doi:10.1126/science.288.5463.128

Kennett, J.P., Cannariato, K.G., Hendy, I.L., Behl, R.J., Behl, R.J., 2005. Methane Hydrates in Quaternary Climate Change: The Clathrate Gun Hypothesis. American Geophysical Union. doi:10.1002/9781118665138.ch0

Kennicutt, M., Brooks, J., Bidigare, R., 1988. Hydrocarbon Seep Communities: Four Years of Study. *Oceanography* 1, 44–45. doi:10.5670/oceanog.1988.11

Kennicutt, M.C., Brooks, J.M., Bidigare, R.R., Fay, R.R., 1985. Vent-type taxa in a hydrocarbon seep region on the Louisiana slope. *Nature* 317, 351–353. doi:10.1038/317351a0

King, L.H., Maclean, B., 1970. Pockmarks on the Scotian Shelf. *Geol Soc America Bull* 81, 3141. doi:10.1130/0016-7606(1970)81[3141:potss]2.0.co;2

Kongsjorden, H., Kårstad, O., Torp, T.A., 1998. Saline aquifer storage of carbon dioxide in the Sleipner project. *Waste Management* 17, 303–308. doi:10.1016/s0956-053x(97)10037-x

Kopf, A.J., 2002. Significance of mud volcanism. *Rev. Geophys.* 40, 1005–2–52. doi:10.1029/2000RG000093

Korbøl, R., Kaddour, A., 1995. Sleipner vest CO₂ disposal-injection of removed CO₂ into the Utsira Formation. *Energy Conversion and Management* 36, 509–512.

Kvenvolden, K.A., 1988. Methane hydrate — A major reservoir of carbon in the shallow geosphere? *Chemical Geology* 71, 41–51. doi:10.1016/0009-2541(88)90104-0

Kvenvolden, K.A., 1995. A review of the geochemistry of methane in natural gas hydrate. *Organic Geochemistry* 23, 997–1008. doi:10.1016/0146-6380(96)00002-2

Kvenvolden, K.A., Rogers, B.W., 2005. Gaia's breath—global methane exhalations. *Marine and Petroleum Geology* 22, 579–590. doi:10.1016/j.marpetgeo.2004.08.004

Løseth, H., Gading, M., Wensaas, L., 2009. Hydrocarbon leakage interpreted on seismic data. *Marine and Petroleum Geology* 26, 1304–1319. doi:10.1016/j.marpetgeo.2008.09.008

Løseth, H., Rodrigues, N., Cobbold, P.R., 2012. World's largest extrusive body of sand? *Geology* 40, 467–470. doi:10.1130/G33117.1

Lonergan, L., Maidment, S.C.R., Collier, J.S., 2006. Pleistocene subglacial tunnel valleys in the central North Sea basin: 3-D morphology and evolution. *J. Quaternary Sci.* 21, 891–903. doi:10.1002/jqs.1015

Lønøy, A., Akselsen, J., Ronning, K., 1986. Diagenesis of a deeply buried sandstone reservoir; Hild Field,

northern North Sea. *Clay Minerals* 21, 497–511.

Hubbert, M.K., Willis, D.G., 1957. Mechanic of hydraulic fracturing. *Transactions of Society of Petroleum Engineers of AIME*, 1957, v. 210, p. 153-168.

MacDonald, I.R., 2004. Asphalt Volcanism and Chemosynthetic Life in the Campeche Knolls, Gulf of Mexico. *Science* 304, 999–1002. doi:10.1126/science.1097154

Macdonald, K.C., Becker, K., Spiess, F.N., 1980. Hydrothermal heat flux of the “black smoker” vents on the East Pacific Rise. *Earth and Planetary ...* 48, 1–7. doi:10.1016/0012-821x(80)90163-6

Magalhães, V.H., Pinheiro, L.M., Ivanov, M.K., Kozlova, E., Blinova, V., Kolganova, J., Vasconcelos, C., McKenzie, J.A., Bernasconi, S.M., Kopf, A.J., Díaz-del-Río, V., González, F.J., Somoza, L., 2012. Formation processes of methane-derived authigenic carbonates from the Gulf of Cadiz. *Sedimentary Geology* 243-244, 155–168. doi:10.1016/j.sedgeo.2011.10.013

Martin, W., Baross, J., Kelley, D., Russell, M.J., 2008. Hydrothermal vents and the origin of life. *Nat Rev Micro*. doi:10.1038/nrmicro1991

Metz, B., Davidson, O., De Coninck, H.C., Loos, M., 2005. IPCC special report on carbon dioxide capture and storage. Prepared by Working Group III of the Intergovernmental Panel on Climate Change. IPCC.

Michael, K., Golab, A., Shulakova, V., Ennis-King, J., Allinson, G., Sharma, S., Aiken, T., 2010. Geological storage of CO₂ in saline aquifers: A review of the experience from existing storage operations. *International Journal of Greenhouse Gas Control* 4, 659–667. doi:10.1016/j.ijggc.2009.12.011

Mienert, J., Posewang, J., Baumann, M., 1998. Gas hydrates along the northeastern Atlantic margin: possible hydrate-bound margin instabilities and possible release of methane. *Geological Society, London, Special Publications* 137, 275–291. doi:10.1144/GSL.SP.1998.137.01.22

Mienert, J., Vanneste, M., Bünz, S., Andreassen, K., Hafliðason, H., Sejrup, H.P., 2005. Ocean warming and gas hydrate stability on the mid-Norwegian margin at the Storegga Slide. *Marine and Petroleum Geology* 22, 233–244. doi:10.1016/j.marpetgeo.2004.10.018

Milkov, A.V., 2004. Global estimates of hydrate-bound gas in marine sediments: how much is really out there? *Earth Science Reviews* 66, 183–197. doi:10.1016/j.earscirev.2003.11.002

Nordbotten, J.M., Celia, M.A., Bachu, S., Dahle, H.K., 2005. Semianalytical Solution for CO₂ Leakage through an Abandoned Well. *Environ. Sci. Technol.* 39, 602–611. doi:10.1021/es035338i

Osborne, M.J., Swarbrick, R.E., 1997. Mechanisms for generating overpressure in sedimentary basins; a re-evaluation. *Bulletin* 81, 1023–1041.

Ottesen, D., Dowdeswell, J.A., Bugge, T., 2014. Morphology, sedimentary infill and depositional environments of the Early Quaternary North Sea Basin (56°N–62°N). *Marine and Petroleum Geology* 56, 123–146. doi:10.1016/j.marpetgeo.2014.04.007

Pedersen, R. B., Blomberg, A., Landschulze, K., Baumberger, T., Økland, I., Reigstad, L., Gracias, N., Mørkved, P. T., Stensland, A., Lilley, M. D., Thorseth, I. H., 2013. American Geophysical Union, Fall Meeting 2013, abstract #OS11E-03

Piñero, E., Marquardt, M., Hensen, C., Haeckel, M., Wallmann, K., 2013. Estimation of the global inventory of methane hydrates in marine sediments using transfer functions. *Biogeosciences* 10, 959–975. doi:10.5194/bg-10-959-2013

- Plaza-Faverola, A., Bünz, S., Mienert, J., 2011. Repeated fluid expulsion through sub-seabed chimneys offshore Norway in response to glacial cycles. *Earth and Planetary Science Letters* 305, 297–308. doi:10.1016/j.epsl.2011.03.001
- Schneider von Deimling, J., Rehder, G., Greinert, J., McGinnis, D.F., Boetius, A., Linke, P., 2011. Continental Shelf Research. *Continental Shelf Research* 31, 867–878. doi:10.1016/j.csr.2011.02.012
- Shepherd, R.G., 1989. Correlations of Permeability and Grain Size. *Groundwater*, 27(5), 633–638. doi:10.1111/j.1745-6584.1989.tb00476.x
- Solomon, S., Qin, D., Manning, M., Chen, Z., 2007. Climate change 2007: the physical science basis. Contribution of working group I to the fourth assessment report of the intergovernmental panel on climate change. doi:10.4324/9781849770804
- Spies, R.B., Davis, P.H., 1979. The infaunal benthos of a natural oil seep in the Santa Barbara channel. *Marine Biology* 50, 227–237. doi:10.1007/bf00394204
- Spiess, F.N., Macdonald, K.C., Atwater, T., Ballard, R., Carranza, A., Cordoba, D., Cox, C., Garcia, V.M.D., Francheteau, J., Guerrero, J., Hawkins, J., Haymon, R., Hessler, R., Juteau, T., Kastner, M., Larson, R., Luyendyk, B., Macdougall, J.D., Miller, S., Normark, W., Orcutt, J., Rangin, C., 1980. East Pacific Rise: Hot Springs and Geophysical Experiments. *Science* 207, 1421–1433. doi:10.1126/science.207.4438.1421
- Vattenfall. Moorburg power plant – Facts and figures. http://corporate.vattenfall.de/globalassets/deutschland/geschaeftsfelder/erzeugung/neubauprojekte/moorburg_und_fischtreppe/faktenblatt_moorburg_en.pdf
- Vogt, P.R., Jung, W.Y., 2002. Holocene mass wasting on upper non-Polar continental slopes—due to post-Glacial ocean warming and hydrate dissociation? *Geophys. Res. Lett.* doi:10.1029/2001GL013488
- Vignes, B., Andreassen, J., Tønning, S.A., 2006. PSA Well Integrity Survey, Phase 1 summary report. Petroleum Authority.
- Vignes, B., 2011. Contribution to Well Integrity and Increased Focus on Well Barriers from a Life Cycle Aspect (PhD thesis). University of Stavanger.
- White, J.E., 1975. Computed seismic speeds and attenuation in rocks with partial gas saturation. *Geophysics* 40, 224–232.
- White, J.A., Chiaromonte, L., Ezzedine, S., Foxall, W., Hao, Y., Ramirez, A., McNab, W., 2014. Geomechanical behavior of the reservoir and caprock system at the In Salah CO₂ storage project. *Proceedings of the National Academy of Sciences* 111, 8747–8752. doi:10.1073/pnas.1316465111
- Zachos, J., 2001. Trends, Rhythms, and Aberrations in Global Climate 65 Ma to Present. *Science* 292, 686–693. doi:10.1126/science.1059412
- Ziegler, P.A., 1992. North Sea rift system. *Tectonophysics* 208, 55–75.

CHAPTER 2: SEISMIC CHIMNEYS IN THE SOUTHERN VIKING GRABEN – IMPLICATIONS FOR PALAEO FLUID MIGRATION AND OVERPRESSURE EVOLUTION

Karstens, J., and Berndt, C.



Soft sediment deformation, White Pocket, Vermilion Cliffs, Arizona, USA

2.1. ABSTRACT

Detailed understanding of natural fluid migration systems is essential to minimize risks during hydrocarbon exploration and to evaluate the long-term efficiency of the subsurface storage of wastewater and gas from hydrocarbon production as well as CO₂. The Southern Viking Graben (SVG) hosts numerous focused fluid flow structures in the shallow (< 1000 m) subsurface. The seismic expressions of vertical fluid conduits are variously known as seismic chimneys or pipes. Seismic pipes are known to form large clusters. Seismic chimneys have so far been described as solitary structures. Here, we show that the study area in the SVG hosts more than 46 large-scale vertical chimney structures, which can be divided in three categories implying different formation processes. Our analysis reveals that seal-weakening, formation-wide overpressure and the presence of free gas are required to initiate the formation of vertical fluid conduits in the SVG. The presence of numerous vertical fluid conduits implies inter-stratigraphic hydraulic connectivity, which significantly affects the migration of fluids in the subsurface. Chimney structures are important for understanding the transfer of pore pressure anomalies to the shallow parts of the basin.

2.2. INTRODUCTION

The Southern Viking Graben (SVG) is one of the most productive hydrocarbon provinces in the North Sea. It hosts several major hydrocarbon fields charged by Jurassic source rocks (Justwan and Dahl, 2005). In many cases, the upward migration of hydrocarbons is not limited to the path from the source rocks to the reservoir, but it continues to shallower stratigraphic levels (Cartwright et al., 2007; Løseth et al., 2009). Sub-seafloor fluid migration manifests itself in a large variety of seismically detectable features, such as vertical fluid conduits, sediment mobilization, pockmarks and gas accumulations (Cartwright et al., 2007; Løseth et al. 2009). Seismic chimneys and pipes are vertical seismic anomalies interpreted as focused fluid flow structures, which hydraulically connect deeper stratigraphic layers with the overburden (Berndt, 2005; Løseth et al., 2009; Cartwright et al. 2007). Their formation is generally believed to be controlled by overpressure-induced hydrofracturing of an impermeable cap rock (Løseth et al., 2009; Cartwright et al. 2007). The activity of vertical fluid conduits can be limited to blowout-like events, e.g. resulting in pipe structures offshore Nigeria (Løseth et al., 2011) or Norway (Bünz, 2003), or fluid flow may be continuous and long-lasting, e.g. the chimney structures above the leaking hydrocarbon reservoirs Ekofisk (Hovland and Sommerville, 1985) and Tommeliten (Granli et al., 1999; Arntsen et al. 2007). The terms seismic chimney and pipe are used interchangeably in the literature. Following Andresen (2012), we use the term pipe-like for strictly columnar anomalies associated with stacks of increased or dimmed amplitudes and chimneys-like for anomalies with much larger dimensions, complex shape and internal architecture as well as chaotic amplitude distribution.

The understanding of shallow fluid flow systems has always been important for offshore hydrocarbon exploration, because gas accumulations in shallow sediments, especially when undetected, bear high risks for drilling. The study area hosts the longest operating offshore CO₂ storage project at Sleipner, where CO₂ is injected into the Utsira formation, a saline aquifer, at a depth of ~1012 m (Arts et al., 2008). This CO₂ is a byproduct of natural gas production at Sleipner (Korbøl and Kaddour, 1995) and its injection is an alternative to releasing it to the atmosphere. Research on the Sleipner CO₂ storage has mainly focused on the CO₂ migration within the storage formation (e.g. Chadwick et al, 2009, Arts et al., 2008), while natural fluid manifestations in the overburden of the Utsira Formation including the presence of shallow gas accumulations, mud volcanoes, seafloor craters and vertical fluid migration pathways have only been reported briefly by Heggland (1997) and by Nicoll (2011).

Analysis of 3D seismic data is the most effective method for the large-scale investigation of subsurface fluid flow systems, but the interpretation of fluid flow structures, in particular when vertically oriented, must include careful consideration of seismic imaging phenomena and the influence of seismic processing. Effects like

blanking beneath gas accumulations, migration artifacts due to near surface velocity anomalies or bad seismic traces may lead to spurious interpretation of vertical conduits. The first objective of this paper is to investigate if there is evidence for widespread focused fluid migration in the SVG. To achieve this we have compiled an inventory of shallow fluid flow manifestations in the SVG using 3D seismic data, which will extend and update the work of Hegglund (1997). The second objective is to determine hydraulic connections between different stratigraphic levels by analyzing the interaction of different fluid flow manifestations. The main focus is on vertical focused fluid flow conduits, whose seismic expressions are known as chimneys and pipes (Cartwright et al., 2007; Løseth et al., 2009). Our third objective is to constrain the formation processes for focused fluid conduits, i.e. when did they develop, how long have they been active, were they active continuously or episodically, and if they transport aqueous fluids or gaseous fluids.

2.3. GEOLOGICAL BACKGROUND

The study area is located in the SVG, which is part of a Late Jurassic to Early Cretaceous failed rift system forming the North Sea Basin (Fig. 2.1; Ziegler et al., 1992; Gautier, 2005). Rifting led to the rapid deposition of the up to 3000 m thick, organic carbon-rich Kimmeridgian shales under anoxic conditions, which represent the main source rock interval for the entire North Sea Basin (Gautier, 2005). Post-rift subsidence due to gradual cooling allowed the deposition of more than 2500 m thick post-rift (Fig. 2.2) initiating the generation of oil due to thermal maturation in Neogene to Holocene times in the Viking Graben (Gautier, 2005). The study area hosts several large hydrocarbon reservoirs including Eirin, Gungne, Sigyn, Sleipner Øst, Sleipner Vest and Volve (Fig. 2.1).

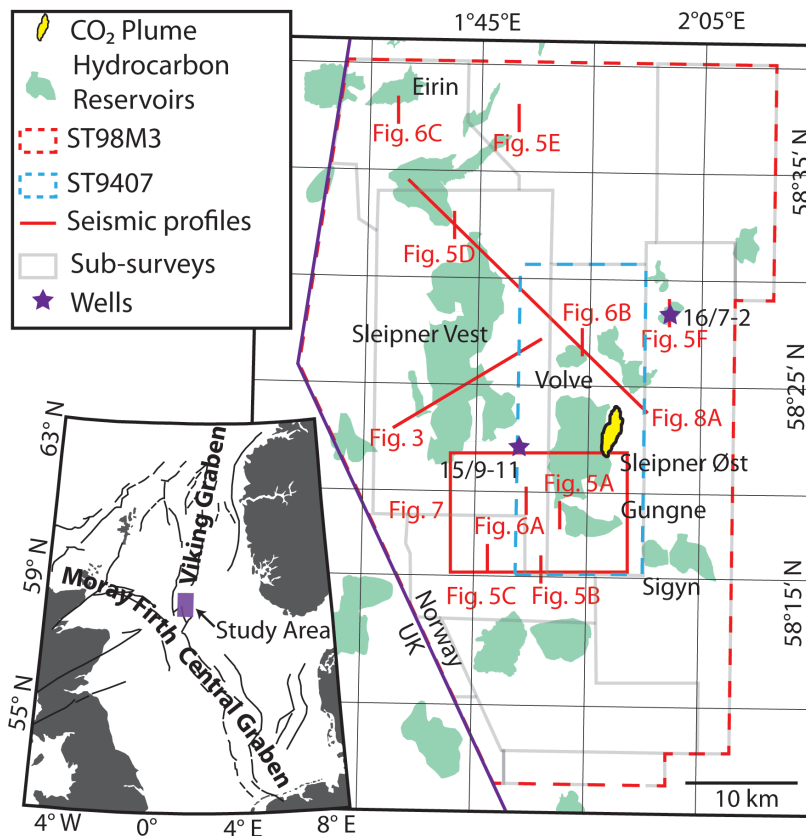


Fig. 2.1: Map of the study area showing the extent of the 3D seismic survey (ST98M3; dashed red line), seismic profiles (Fig. 2.3, 2.5, 2.6 and 2.7a; red lines), extents of sub-surveys (grey lines), location of extracted seismic profiles presented in this paper (solid blue lines), deep hydrocarbon reservoirs (green), Sleipner CO₂ plume (2006; yellow), wells (purple stars) and border between Norway and UK (solid black line). Lower left Corner: Regional map of the North Sea Basin showing: location of the study area (purple box), major faults (black lines, simplified after Brennand et al., 1998).

The Cenozoic sequence of the SVG includes the Hordaland and the Nordland formations and is well-constrained by an integrated bio-stratigraphic, seismo-stratigraphic, litho-stratigraphic and geochemical analysis performed by Eidvin and Rundberg (2007) and summarized in the following paragraphs. The pre-Eocene sedimentary succession of the SVG is controlled by gravity flow deposition during the Paleocene and subsidence of the SVG relative to the uplifted Utsira High during the Eocene (Eidvin and Rundberg, 2007). The base of the Nordland Group consists of brownish mudstones intersected by thin sand beds and were deposited under outer neritic conditions (Eidvin and Rundberg, 2007).

The Utsira Formation was deposited in a highly energetic sandy shelf shoal environment sourced by denudation of the uplifted North Sea basin margins (Galloway, 2001; 2002; Gregersen et al., 2007). The paleogeographic setting has been stable for a period of 8 Ma facilitating the deposition of a 100 to 300 m-thick sand body (Galloway, 2001; 2002), which is intersected by thin layers of shale (Cavanagh and Haszeldine, 2014). The base of the Utsira Formation is strongly deformed by remobilized sediments as the result of sand intruding into mudstones at the top of the Hordaland Group (Rodriguez et al. 2009; Løseth et al. 2012).

The transition from a shallow marine Middle Miocene to Early Pliocene deposition environment to a deeper marine environment in the Late Pliocene can be recognized in the well data (Fig. 2.2b; Gregersen et al., 1997). At well-site 15/9-11, the top of the Utsira Formation is overlain by a stack of 8 m-thick mudstones, an 11 m-thick unit of sands and the Late Pliocene depositional sequence (Fig. 2.2b; Gregersen et al., 1997). The top and the base of the thin sand layer directly above the Utsira Formation cannot be resolved by exploration-type seismic data, but plays an important role in the shallow fluid flow system and we will refer to this unit as the sand wedge. The Late Pliocene depositional sequence and the overlying Pleistocene section consist of sands and mudstones (Fig. 2.2a; Eidvin and Rundberg, 2007), which are known as the Nordland Shales. Rock physical examinations of Nordland Shales samples revealed an intrinsic permeability of 4×10^{-7} D perpendicular and 10^{-6} D parallel to the bedding (Harrington et al., 2009), which effectively inhibits fluid migration by diffusion even over long time scales.

During Pleistocene time, the study area was highly affected by glaciations causing strong erosion and reworking of surface sediments in the North Sea Basin (Sejrup et al., 2000). Glacial activity can still be documented by iceberg plough marks and streamlined bedforms (Graham et al, 2007) as well as tunnel valleys (Fig. 2.2a, seismic section), which were generated by melt water flow underneath retreating ice sheets (Lonergan et al, 2006).

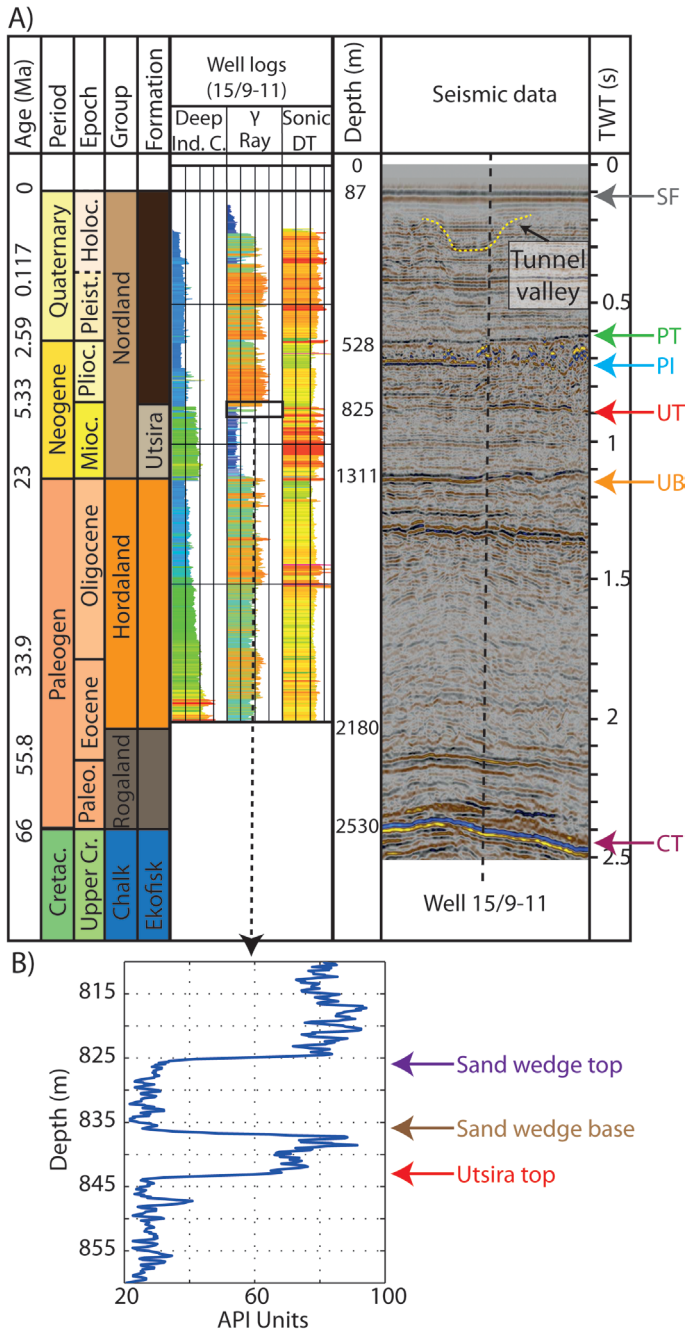


Fig. 2.2: A) Stratigraphy of the study area based on well 15/9-11 showing the chronostratigraphy in the study area (according to International Commission on Stratigraphy; Holoc. = Holocene, Pleist. = Pleistocene, Paleo. = Paleocene, Moch. = Miocene, Plioc. = Pliocene, Cretac. = Cretaceous, Upper Cr. = Upper Cretaceous), well-logs of Deep inductive conductivity, Gamma-ray, Sonic-DT, black box marking zoom-in presented in B), seismic section with well position and colored arrows marking seismic reflections corresponding to important stratigraphic boundaries (SF = Seafloor; PT = Pliocene top, PI = Pliocene intra, UT = Utsira top, UB = Utsira base, CT = Cretaceous top). B) Zoom-in of the Gamma-ray log between 810 and 860 m. The high API values between 835 and 845 indicate a shale or mudstone layer interbedded between the Utsira Formation and the sand wedge.

2.4. DATA AND METHODS

This study is mainly based on the analysis of the three-dimensional (3D) seismic data set ST98M3, which is the result of merging seven independently acquired and processed 3D volumes. Detailed information regarding processing parameters of the specific subsets are not available, while the processing sequence for merging the data included resampling, filtering, phase rotation and amplitude adjustments. The final 3D seismic cube shows positive acoustic impedance contrasts as positive amplitude (blue) followed by negative amplitude (yellow). The bin-size is 12.5 m and the vertical resolution is ~10 m (dominant frequency 45 Hz, seismic velocity of ~ 1800 m/s). The dataset extends 62 km from North to South and 46 km East to West covering an area of more than 2,000 km². In addition, we used a second 3D seismic dataset (ST9407; Fig. 2.1) with better shallow data quality to investigate the relationship of tunnel valleys and fluid flow structures.

The 3D seismic data analysis included tracking of horizons corresponding to important stratigraphic boundaries and the interpretation of amplitude anomalies on cross-sections as well as time- and horizon maps. In order to highlight amplitude anomalies within specific stratigraphic units, we calculated the minimal (most negative) amplitude distribution within different stratigraphic units between interpreted seismic horizons. The lower boundary of the Upper Pliocene section and the sand wedge do not correspond to continuously traceable seismic reflections. For mapping amplitude anomalies, we calculated the minimum amplitude 1) between the top Utsira and the base Utsira horizons for the Utsira Formation, 2) along the top Pliocene horizon and within a time window beneath the top Pliocene horizon (10 ms and 150 ms downshifted) for the Upper Pliocene and 3) within a time window above the top Utsira horizon (10 ms and 100 ms upshifted) for the sand wedge.

2.5. RESULTS

2.5.1. BRIGHT SPOTS – SHALLOW GAS POCKETS

While bright spots are present throughout the analyzed dataset, their abundance is significantly increased in specific stratigraphic intervals. These layers are the top of Utsira Formation, the sand wedge and within the Upper Pliocene, which are characterized by high sand content (Figs. 2.2 and 2.3). The bright spots at the top of the Utsira Formation are mainly limited to the northwestern part of our study area (Fig. 2.4). The bright spots at the top of the Utsira Formation show a reversed polarity (compared to the seafloor reflection), strongly increased amplitudes compared to the background, sharp boundaries (Fig. 2.3) and their distribution is limited to local topographic heights. These observations suggest that the bright spots at the top of the Utsira Formation represent gas accumulations.

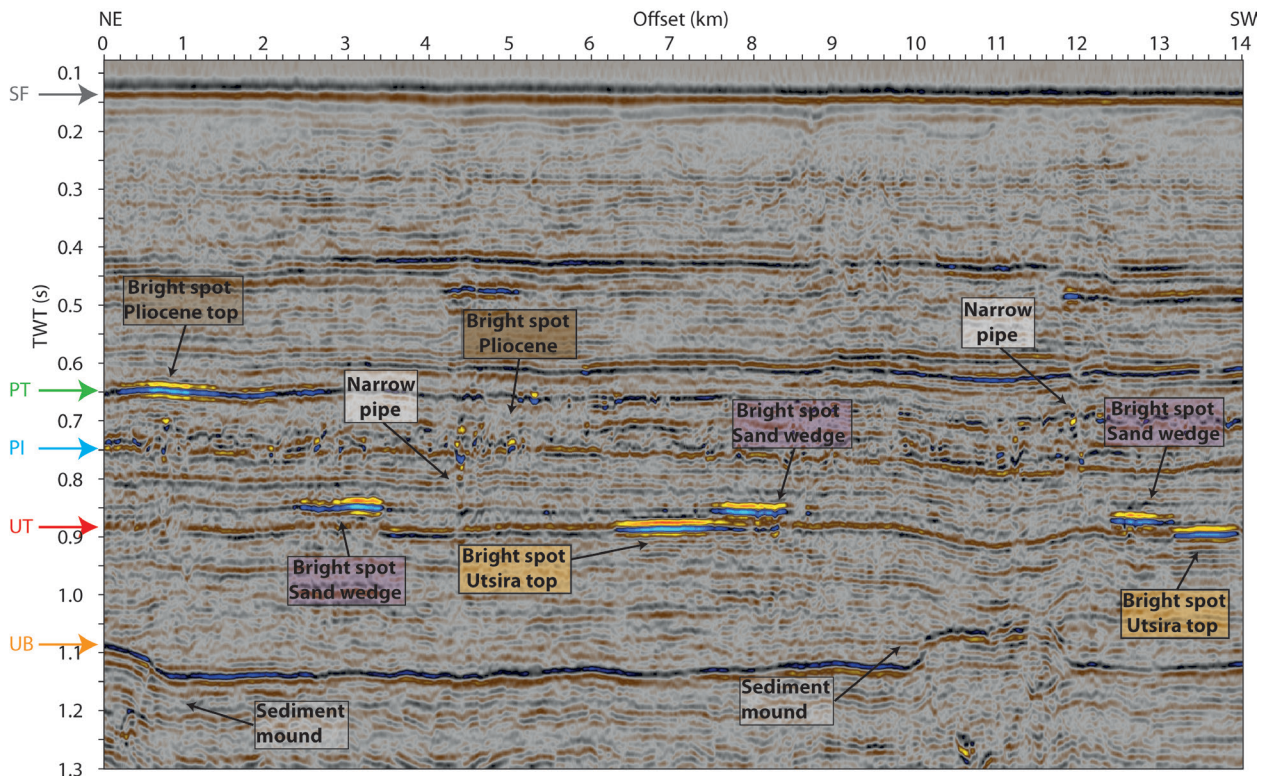


Fig. 2.3: Seismic profile showing fluid flow associated seismic features including narrow pipes, sediment mounds caused by sand injections and bright spots beneath the top of the Utsira Formation (green colored boxes), within the sand wedge (red colored boxes) and within and beneath the top of the Pliocene section (blue colored boxes). Colored arrows mark seismic reflections corresponding to important stratigraphic boundaries (SF = Seafloor, PT = Pliocene top, PI = Pliocene intra, UT = Utsira top, UB = Utsira base).

The seismic signature as well as the distribution of bright spots within the sand wedge is similar to those beneath the top of the Utsira Formation, whereas the number of bright spots is significantly higher within the sand wedge (Fig. 2.4). Figure 2.3 shows two examples for bright spots of the two stratigraphic layers occurring in direct proximity. The locations of the overlying (sand wedge) bright spots coincide in one case with the sharp boundary and in the other case with a gradual dimming of the deeper (Utsira Formation) bright spots.

There are two categories of bright spots within the Pliocene section. The first category is present at the top of the Pliocene section. They share the properties of those beneath the top of the Utsira Formation and within the sand wedge. The second category of bright spots occurs within the Upper Pliocene section (between the top Pliocene and the intra Pliocene reflections), shows a patchy, chaotic seismic signature and in some places coincides with narrow pipe-like structures (Fig. 2.3). These pipes may indicate a hydraulic connection between the Upper Pliocene and deeper sections. The spatial distribution of Pliocene bright spots is dominated by elongated bands formed by bright spots beneath the top reflection and a multiplicity of small patchy, randomly distributed deeper seated Upper Pliocene bright spots (Fig. 2.4).

2.5.1. VERTICAL SEISMIC ANOMALIES

Narrow pipe structures are mostly limited to the Pliocene section, where such features are abundant (Fig. 2.3). The vast majority terminates beneath the top Pliocene reflection and has no connection to shallower stratigraphic levels. We focus our analysis on those vertical seismic anomalies, which can be traced further up. These features have a more complex seismic signature and (in most cases) much larger extents compared to the Pliocene pipes. Based on their seismic character, we are able to distinguish between three categories of vertical seismic anomalies.

2.5.1.1. TYPE-A-ANOMALIES

Type-A-anomalies are prominent vertical seismic features characterized by two or more reversed-phase, high-amplitude reflections between 50 and 500 ms beneath the seafloor reflection (Fig. 2.5a-c). The depth of the bright spots is variable and does not appear to correlate with specific stratigraphic layers. The seismic character between the bright spots is chaotic with partly reduced seismic amplitudes. Seismic reflections of stratigraphic boundaries crosscut by type-A-anomalies are either dimmed or slightly bended downward, whereas an upward buckling of the reflections occurs directly next to the anomalies (Fig. 2.5a, b). Most type-A-anomalies terminate close to the seafloor or even affect the seafloor reflection (Fig. 2.5a-c). The amplitude anomalies associated with type-A-anomalies can be traced as deep as the top Pliocene or the top of the Utsira Formation, thus the height of the sedimentary column affected by type-A-anomalies varies between 550 and 800 ms. In total, we have identified 21 type-A anomalies. Six have diameters of 300 to 600 m, while the remaining nine anomalies have diameters of less than 300 m. With a decreasing diameter, the seismic signature of type-A-anomalies becomes similar to the Pliocene pipes.

2.5.1.2. TYPE-B-ANOMALIES

Type-B- anomalies form a second, less obvious group of large scale vertical seismic features in the study area and are characterized by a chaotic seismic character, caused by a multitude of small, patchy bright spots and dimmed and disturbed seismic reflections (Fig. 2.5 d-f). The cross-section of type-B-anomalies is more irregular than columnar and the boundaries to the unaffected background geology are diffuse. Many type-B-anomalies coincide with amplitude anomalies of the seafloor reflection indicating a very shallow upper termination. Type-B-anomalies can be traced for ~500 to 650 ms TWT. The features terminate at the top of the Pliocene section or at the top of the Utsira Formation (Fig. 2.5 d-f). The typical width of type-B- anomalies varies between 300 and 500 m, but in some instances it exceeds 1000 m. The study area hosts at least 22 type-B-anomalies mostly in the northern part of the study area (Fig. 2.4).

2.5.1.3. TYPE-C-ANOMALIES

The identified type-C-anomalies differ significantly from concentric type-A- and type-B-anomalies as they form elongated, up to 6 km long, slightly meandering bands (Fig. 2.4, 2.6c and 2.7). Type-C-anomalies have a complex internal structure. The middle section is characterized by a narrow ~50 to 200 m-wide central vent, which causes bending and dimming of reflections and is accompanied by bright spots. The seismic character of type-C-anomalies is variable along their path. The three identified type-C-anomalies root at different stratigraphic layers. C01 can be traced as deep as the top of the Utsira Formation and C03 as deep as the top of the Pliocene section. Both show a spatial correlation with funnel-shaped reflections of overlying tunnel valleys, which will be discussed in more detail in section 5.2 (Fig. 2.6c).

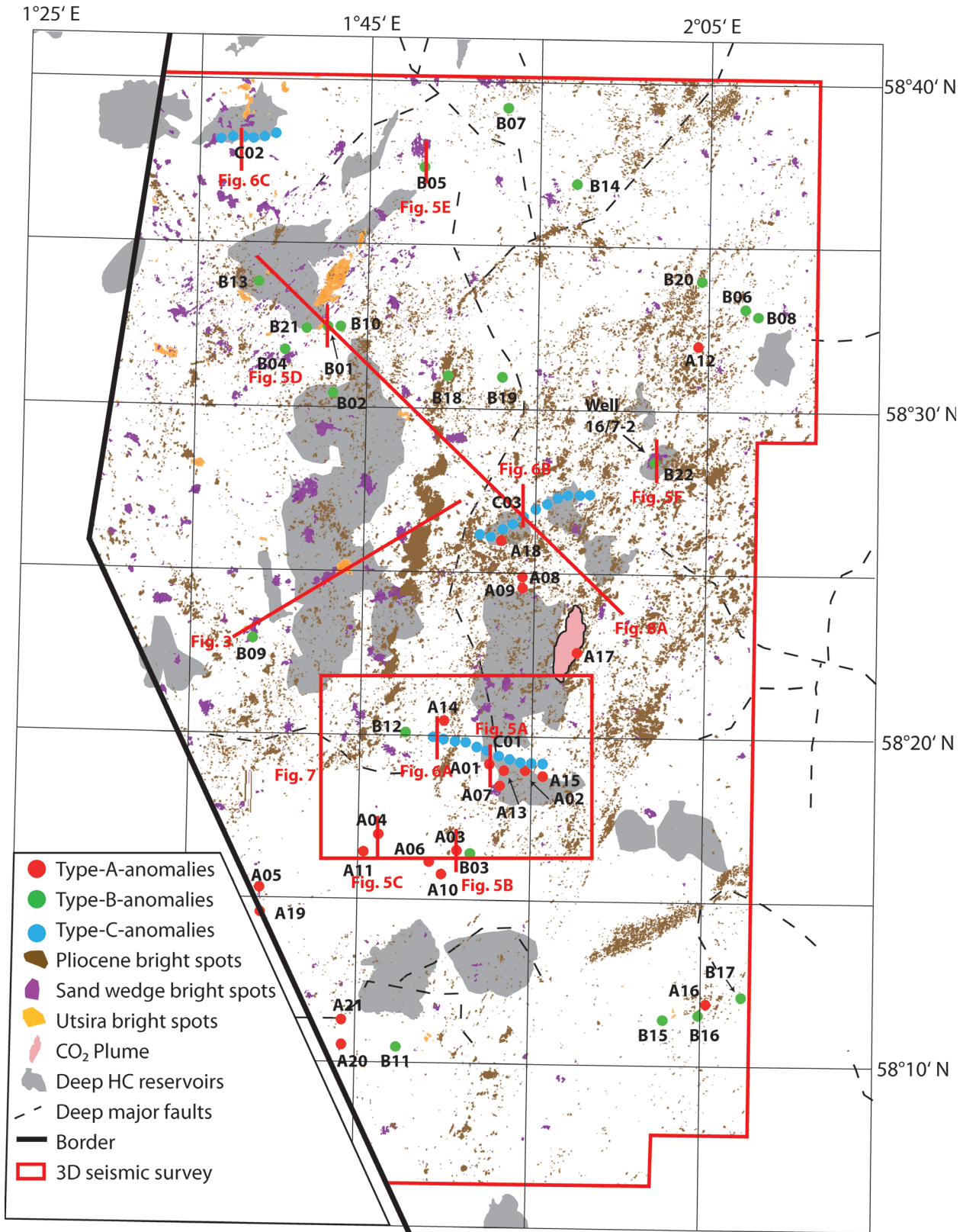


Fig. 2.4: Map of the study area showing the location of fluid flow manifestations and seismic profiles (Fig. 2.3, 2.5, 2.6 and 2.7a; red lines): bright spots beneath the top of the Utsira Formation (pale green), within the sand wedge (pale red), beneath the top Pliocene (pale blue), type-A-anomalies (red dots), type-B-anomalies (green dots), type-C-anomalies (red dots), CO₂-plume (rose), deep hydrocarbon reservoirs (grey), deep faults (black lines).

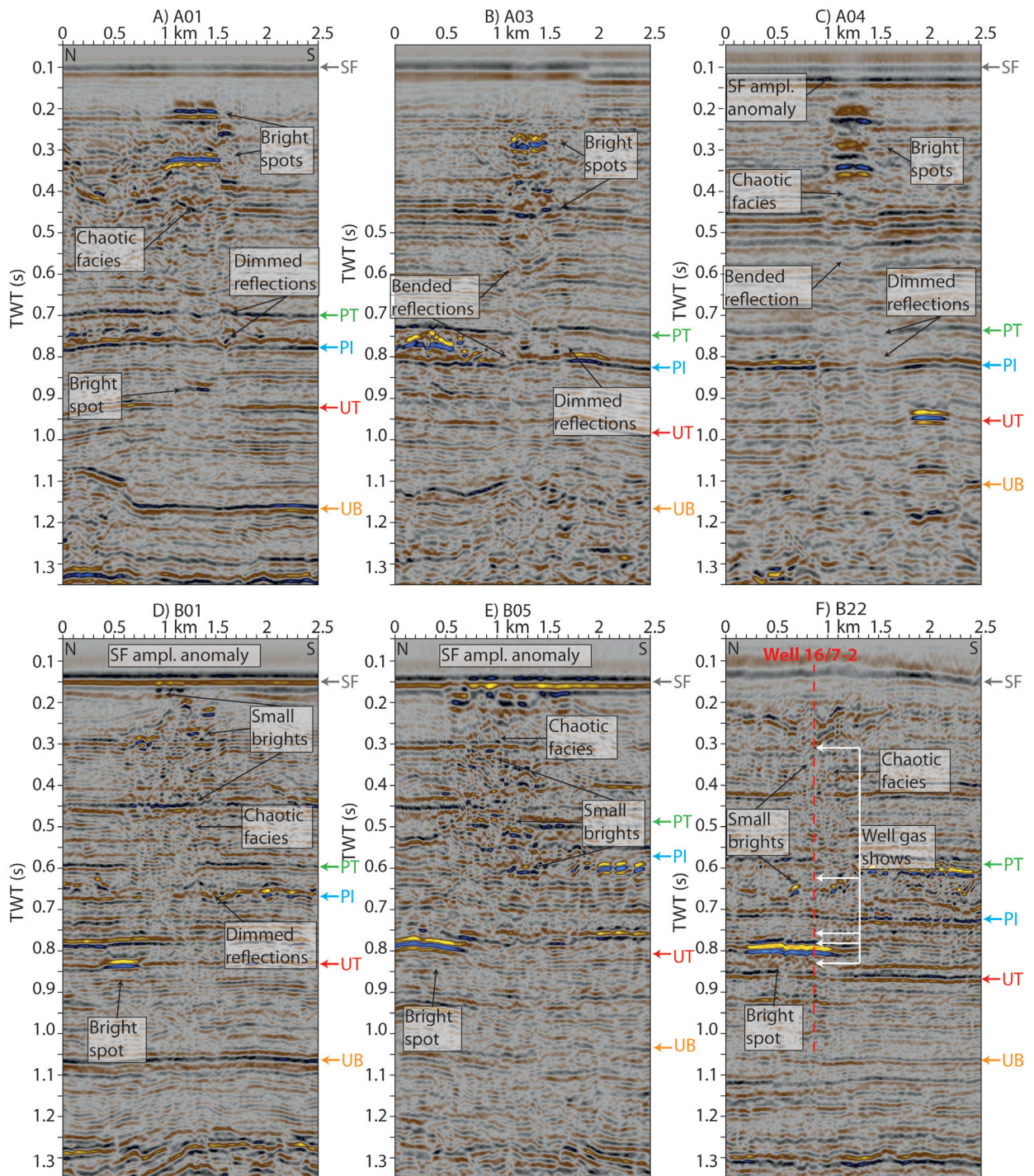


Fig. 2.5: A, B, C). Seismic profile showing vertical seismic anomalies with columnar signature (Type-A). Colored arrows mark seismic reflections corresponding to important stratigraphic boundaries (SF = Seafloor, PT = Pliocene top, PI = Pliocene intra, UT = Utsira top, UB = Utsira base). D, E, F) Seismic profile showing vertical seismic anomalies with chaotic seismic signature (Type-B). Colored arrows mark seismic reflections corresponding to important stratigraphic boundaries (SF = Seafloor, PT = Pliocene top, PI = Pliocene intra, UT = Utsira top, UB = Utsira base). Gas readings for well 16/7-2 based on Horvig (1982).

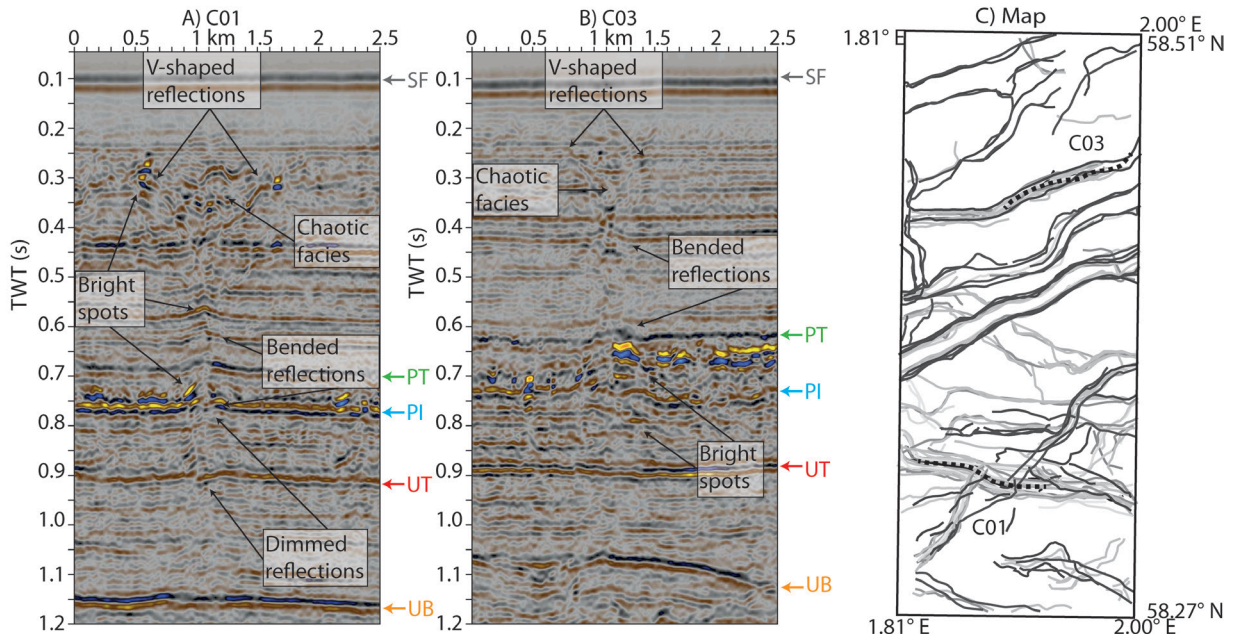


Fig. 2.6: A, B) Seismic profile crossing elongated, sediment-deforming chimneys (Type-C). Colored arrows mark seismic reflections corresponding to important stratigraphic boundaries (SF = Seafloor, PT = Pliocene top, PI = Pliocene intra, UT = Utsira top, UB = Utsira base). C) Map showing correlation between tunnel valleys and chimneys C01 and C03. Colored lines mark the boundary of the tunnel valleys derived from time slices between

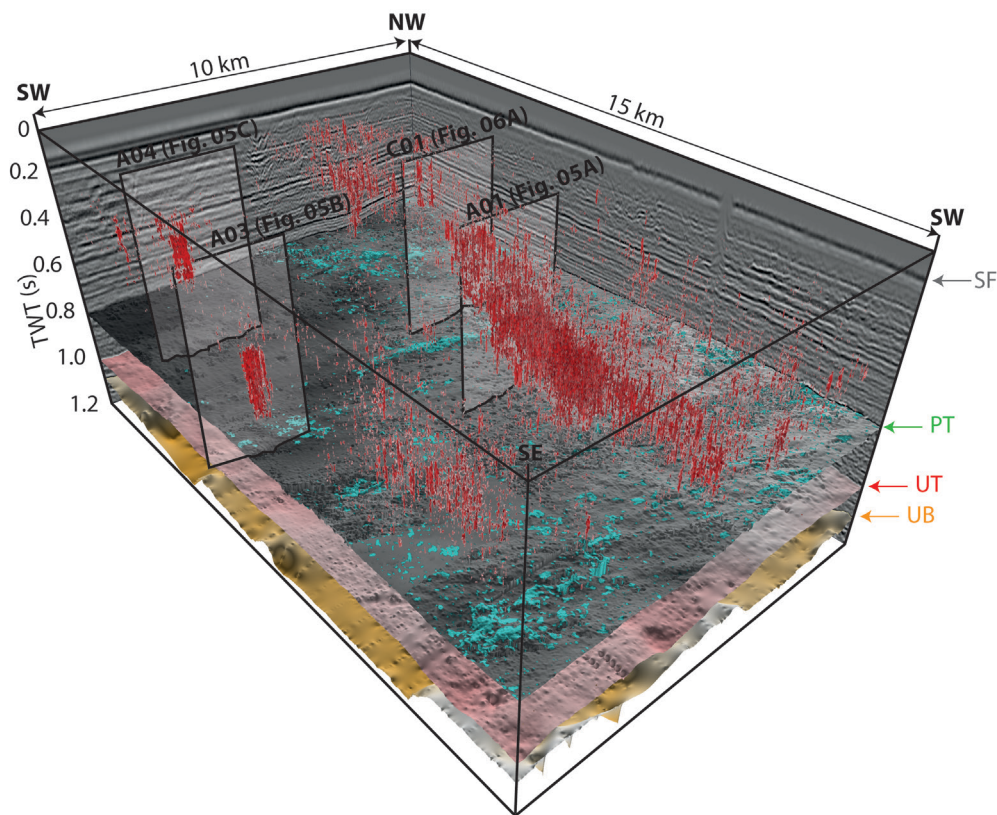


Fig. 2.7: 3D view of a semitransparent chimney cube calculated with OpendTect highlighting the vertical seismic anomalies and the main seismic horizons (SF = Seafloor, PT = Pliocene top, UT = Utsira top, UB = Utsira base,). The top Pliocene horizon shows the location of bright spots in the Upper Pliocene section

2.5.2. SUBSURFACE SEDIMENT MOBILIZATION

The base of the Utsira Formation is highly disturbed by the mobilization of underlying Oligocene mudstones (Figs. 2.2 and 2.8), which form mounds, elongated ridges and complex shaped structures with diameters ranging from one to tens of km (Fig. 2.8b). Huuse (2008), Rodriguez et al. (2009) and Løseth et al. (2012) interpret these structures as the result of fluidized sand injection within the Hordaland Group.

The well-developed seismic reflection marking the boundary between the Utsira Formation and the underlying Hordaland Group is not present on top of some mud diapirs (Fig. 2.8a), which may indicate reworking and mixing of both facies. The structural deformation related to the injection of sands within the Hordaland Group affects the overlying sediment column as shallow as the top of the Pliocene reflection. The primary layering within the Hordaland mudstone section in areas unaffected by mobilization is strongly disturbed within the mounds.

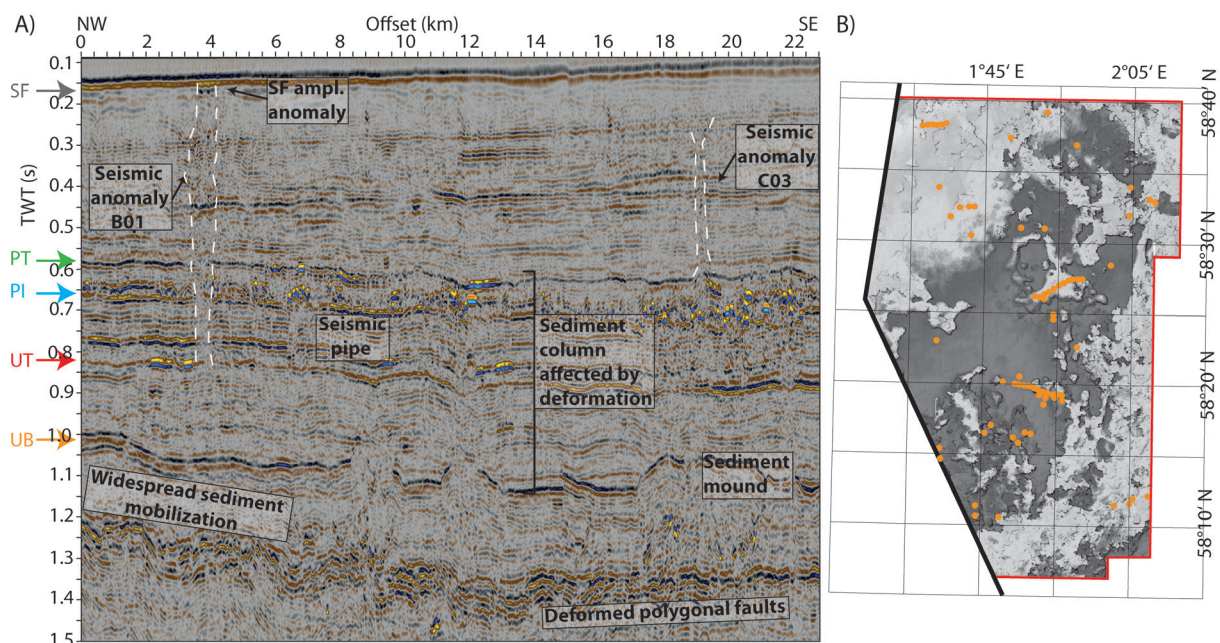


Fig. 2.8: A) Seismic profile showing sediment mounds caused by sand injections, deformed sediments, bright spots and seismic chimneys. Colored arrows mark seismic reflections corresponding to important stratigraphic boundaries (SF = Seafloor, PT = Pliocene top, PI = Pliocene intra, UT = Utsira top, UB = Utsira base). B) Map of the study area showing the base of the Utsira Formation (greyscale; time-structure; dark grey = deeper) and the location of seismic chimneys and sediment mounds caused by sand injections at that stratigraphic level (seismic chimneys = orange).

2.6. DISCUSSION

2.6.1. FLUID FLOW OVERVIEW

3D seismic interpretation revealed a multitude of vertical seismic anomalies in the shallow (> 1000 m) subsurface. The shallow fluid flow system is controlled by three sandy layers (Utsira Formation, sand wedge and the Upper Pliocene section), which host the majority of shallow gas accumulations and are separated by impermeable layers of shale or mudstones (Fig. 2.2). The three sandy layers have been (or possibly may still be) hydraulically connected as indicated by pipe-like seismic anomalies linking bright spots at different stratigraphic levels (Fig. 2.3). The most prominent features are large scale (500 – 800 m long, and 100 to 1000 m wide) seismic anomalies, which are crosscutting the Nordland shales (Figs. 2.5 and 2.6). Comparable seismic anomalies, with either pipe- or chimney-like seismic signatures, have been recognized around the world and are generally associated with vertical fluid flow (e.g. Berndt, 2005; Cartwright et al., 2007; Løseth et al., 2009; Andresen, 2012; Gay et al., 2012). Therefore, we suggest that the interpreted seismic anomalies also represent fluid conduits between deep stratigraphic units and the shallow subsurface or even seafloor. Based on our interpretations, 46 large-scale vertical seismic anomalies are present in the study area. Large scale chimney-like anomalies have so far been described as solitary structures (Gay et al., 2012), in many cases above leaking deep reservoirs (Hovland and Sommerville, 1985; Granli et al., 1999).

2.6.2. IMAGING ARTIFACT OR GEOLOGICAL FEATURE

The presence of three different, seismically distinct types of vertical seismic anomalies is the most important observation. Each type can be identified in different subsets of the merged dataset, while several subsets host different types of anomalies at once. Thus, this distinction is not skewed by different seismic recording or processing parameters of specific sub-surveys. The sub-surveys of the analyzed seismic dataset were acquired and processed primarily to image deep hydrocarbon reservoirs. The applied processing procedures have not been optimized to image the upper-most 400 ms TWT resulting in rather poor data quality of the section of interest to our interpretation. This complicates the analysis of vertical seismic anomalies (chimneys), which are defined by their disturbed seismic character, and to differentiate these structures from imaging artifacts.

For type-A-anomalies, the presence of stacked bright spots arranged in a strictly columnar shape, which have an irregular spacing between them and vary in width, cannot be explained by imaging artifacts beneath shallow gas pockets because internal multiples would be periodic and amplitudes should constantly decay with depth.

Several type-B-anomalies show seafloor anomalies indicating the presence of very shallow gas, which may suggest interpreting these structures as artifacts due to bad imaging. However, the seafloor anomalies differ in size and location from the underlying type-B-structures, which show a depth-varying shape and several internal high amplitude anomalies, which would not be expected for acoustic blanking beneath a shallow gas accumulation. Therefore, it appears more likely that type-B-anomalies are real gas-related geological structures like the ones discussed by Arntsen et al. (2007) rather than seismic artifacts beneath shallow gas pockets.

The probability that type-C-anomalies are seismic artifacts is much higher. The analysis of the 3D seismic cube ST9407 revealed that anomalies C01 and C03 are located directly beneath two tunnel valleys (Fig. 2.6c). It has been shown that tunnel valley infill with high seismic velocity is capable of causing vertical seismic artifacts characterized by upward-bending reflections and poor imaging, if these velocity heterogeneities are not attributed during processing (Armstrong et al., 2001; Kristensen and Huuse, 2012).

However, the presence of small bright spots within type-C-structures, the not perfectly vertical, but laterally varying path and their termination at the top of stratigraphic layers with the potential of accumulating over-pressured fluids cannot be convincingly explained by a seismic artifact. Also, the fact that the seismic anoma-

lies occur only under distinct sections of two tunnel valleys while they are absent beneath all others would require very heterogeneous infill for these tunnel valleys if the anomalies were just seismic artifacts (Fig. 2.6c).

The location of tunnel valleys is primarily controlled by ice sheet dynamics, but there are indications that tunnel valley formation may also be controlled by the presence of weakness zones, e.g. faults, which represent zones with higher erosional potential than the unaffected sediments (Huuse and Lykke-Andersen, 2000). For the Western Baltic Sea, Al Hseinat and Hübscher (2014) have reported a pronounced upward bending of seismic reflectors beneath a tunnel valley and could relate this effect to faulting and fluid flow, while being able to rule out a seismic velocity effect. The Hugin fracture, an elongated vertical fluid structure, has recently been discovered in the SVG (~10 km north of Chimney C-02; Pedersen et al, 2013). Although its width of ~10 m is much narrower than the observed type-C-anomalies and a connection to stratigraphic layers deeper than 200 m has been ruled out, it is proof for the presence for elongated vertical fluid escape structures in the SVG. Comparable fluid escape structures may have acted as weakness zones during the latest period of tunnel valley formation resulting in the observed correlation. Since we do not have access to pre-stack seismic data for reprocessing of the data, we are not able to establish conclusively if the type-C structures are real. While the upper part (down to 0.6 s) may be explained by a velocity effect, it is hard to explain the anomalous configuration of deep reflections including bending, brightening or dimming (Fig. 2.6) by the influence of a shallow high-velocity anomaly on seismic imaging considering that such an effect should decay with depth (away from the velocity anomaly) as these are long-offset data. Fig. 2.6. shows the complex patterns of up-bending underneath the type-C-anomalies, which are not easily reconciled with an origin by velocity pull-up. Nevertheless, we would like to stress that the possibility remains that the type-C-anomalies are artifacts caused by complex seismic wave propagation.

2.6.3. THE NATURE OF TYPE-A-ANOMALIES

Type-A-anomalies are the most obvious seismic features in the study area due to their pronounced stack of two or more internal bright spots and their columnar shape. Their seismic character is similar to pipe structures offshore Nigeria (Løseth et al., 2011) or Norway (Bünz et al., 2003), which are believed to have formed as blowouts as the result of over-pressured reservoirs. The identified type-A-anomalies root in sealed, gas-carrying sandy layers, which have the potential to come under high overpressure and subsequent fluid expulsion. If this well-established explanation for pipe-formation is valid for the narrower conduits (e.g. offshore Nigeria and Norway), it appears to be a likely explanation for the larger type-A-anomalies as well. Many type-A-anomalies host significant amounts of gas indicated by strong internal bright spots that do not coincide with prominent stratigraphic boundaries. This may be evidence for secondary permeability barriers within the conduit, which may have formed after fluid expulsion terminated and fluidized matrix material consolidated within the chimney. Downward-bended reflections at the sites of large type-A-chimneys may support this explanation, although a velocity push-down cannot be ruled out (Fig. 2.5a-c). Post-expulsion plugging of pipes by mobilized sediments is known from onshore outcrops on Rhodes (Løseth et al., 2011). Plugging of pipe structures may be caused by secondary mineralization or by compaction of the sediments after gas migration has finished.

Alternatively, it is possible that the observed anomalies represent a stack of gas bearing sand layers, which would have in this case been charged by the migration of gas from the deep to shallower stratigraphic levels along seal-bypassing fractures and would also represent focused fluid conduits. However, the buckling of reflections suggests a displacement of sediments, which favors a pipe-like formation including development of fractures. These explanations do not exclude each other, but differ in the degree of matrix mobilization.

Most type-A-anomalies cluster in the central part of the study area (Fig. 2.4). The majority is located at the edge or in the vicinity of underlying deep hydrocarbon reservoirs, which may have been the source for the involved fluids. Such a correlation is in agreement with observations that Fichler et al. (2005) made for shal-

low crater structure north of our study area. Assuming type-A-anomalies represent the remnants of focused fluid release events, the depth of the shallowest large bright spot may help to determine the formation time of type-A-anomalies. Their depth ranges from 200 ms below the seafloor to directly below the seafloor (Fig. 2.5a-c) indicating that type-A-chimneys have formed at different times during the Late Pleistocene and Holocene. However, there are no indications for geologically very recent events, such as pockmarks or gas plumes in the water column. While the absence of craters at the seafloor and in the shallow subsurface indicates that type-A's formation dynamic are not the result of explosive blowout events (e.g. Tordis) or proposed by Løseth et al. (2011) for the Nigerian pipe structures, the bending of reflections and the sharp edges of type-A point towards a comparably fast and not diffusive formation.

In conclusion, type-A-anomalies may represent exceptionally large gas pipes, which were formed by more rapidly ascending gas than the Type B structures discussed below. It is likely that after pore pressure bleed-off at the end of the formation of such a feature, the mobilized shales plugged the conduit and terminated fluid flow.

2.6.4. THE NATURE OF TYPE-B-ANOMALIES

The chaotic seismic character of type-B-anomalies is very similar to those of much larger chimney structures, which have been identified above apparently leaking hydrocarbon reservoirs in the North Sea, e.g. Ekofisk (Hovland and Sommerville, 1985) and Tommeliten (Granli et al., 1999; Arntsen et al. 2007).

Well data penetrating such chimney structures revealed an increased gas content and reduced seismic velocities compared to the unaffected surrounding rocks (Løseth et al., 2009). These observations were confirmed by a shear wave experiment indicating high gas-saturation within a chimney structure at Tommeliten (Granli et al., 1999). This kind of chimney is interpreted to be caused by gas saturated fractures within a low permeable cap rock (Løseth et al., 2009). The type-B-anomalies in our study area have smaller dimensions compared to the chimney-structures above leaking hydrocarbon reservoirs, but their overall seismic character including the irregular shape and the chaotic internal is strikingly similar (Fig. 2.5d-f).

These observations are in good agreement with high gas-readings in different sections between 242 and 750 mbsf for the abundant production well 16/7-2, which penetrates the zone of disturbed seismic character of anomaly B-22 (Fig. 2.5f: Horvig, 1982). A comparison of seafloor gas flux measurements at wells 16/7-2, 15/9-13 and 16/4-2 support this interpretation. Wells 15/9-13 and 16/4-2 show no chimney-like seismic signature and release 1 t/a and 3.8 t/a, respectively, while the measurements at well 16/7-2 revealed gas emission of 18.2 t/a (Vielstädte et al., 2014). Gas emissions at well 16/2 are of the same magnitude as the 26 t/a measured above the gas chimney at Tommeliten (Schneider von Deimling et al., 2011). This indicates that the availability of mobile gas from the surrounding sediments is higher at well 16/7-2 than the background.

Bauer and Fichler (2002) reported that a chimney structure with a seismic expression comparable to type-B-anomalies is associated with a negative free-air anomaly in high-resolution gravity data. The gravimetric observations could be reproduced by forward modelling of the seismic chimney as a negative density anomaly, which may partly be explained by the presence of free gas.

Most of the type-B-anomalies can be traced from as deep as the Utsira Formation up to the seafloor or the very shallow subsurface indicated by amplitude anomalies of the seafloor reflection (Fig. 2.5d, e). In several cases, the anomalies root in the direct vicinity of bright spots at the top of the Utsira Formation (Fig. 2.5d-f). This observation is valid especially for the most pronounced type-B-anomalies cluster in the north-west, which spatially coincides with large underlying bright spots (Fig. 2.4).

Type-B-anomalies form three clusters in the Northwest, the Northeast and in the South of the study area (Fig. 2.4). The northern clusters are located in the vicinity of underlying hydrocarbon reservoirs, but such a correla-

tion cannot be established for the southern cluster. The seismic amplitude anomalies at the seafloor reflection above several of the type-B-anomalies suggest a young, possibly Holocene (11.7 ka to recent), formation age. The seismic data cannot resolve if the type-B-anomalies have been formed by a single event, in multiple activity phases or as the result of a continuous long-term process that has been ongoing for thousands or millions of years. The seismic reflectors affected by type-B-anomalies are not deformed (Fig. 2.5d-f), ruling out major displacement of matrix material. This suggests that the formation has been less focused in comparison to type-A-anomalies and that gas is the dominating fluid for this type of conduit. However, the direct proximity of type-B-anomalies and gas accumulations suggests seal-breaching due to a build-up of overpressure as a likely reason for their formation, which will be discussed in detail in section 5.6.

2.6.5. THE NATURE OF TYPE-C-ANOMALIES

Interpreting type-C-anomalies as real geological structures would have important implications for the understanding of the shallow fluid flow system, but is not conclusively confirmable by the available data. The most important observation regarding type-C-anomalies is their elongated shape (Fig. 2.6 and 7) following the trend of tunnel valleys. This observation may suggest that type-C-anomalies are the result of poor imaging due to a seismic velocity anomaly, which has been described for other tunnel valleys in the North Sea (Armstrong et al., 2001; Kristensen and Huuse, 2012). However, bright spots far below the tunnel valleys, the not strictly vertical path of the seismic disturbance and seismic anomalies at deep reflections (as deep as the top of the Utsira Formation, Fig. 2.6a) point towards a geological origin of type-C-anomalies although this cannot be proven with the available data. There are examples for aligned fluid flow-associated features, such as seismic pipes (Løseth et al., 2011), pockmarks (Pinet et al., 2009; Andresen et al., 2011), and seafloor fractures (Pedersen et al., 2013). Stacks of upward-bended seismic reflections (Fig. 2.6) are comparable with observations from seismic pipe structures (Bünz et al., 2003; Løseth et al., 2011), which may indicate rapid emplacement, if they are real. However, as discussed above the observed deflection of seismic reflections may be due to imaging problems.

Due to their generally weak contrast to the background, especially in the upper section, it is hard to define an upper limit for type-C-anomalies. In case of a geological origin, the possible correlation with tunnel valley formation may indicate a Late Pleistocene formation unless the tunnel valleys have formed at locations that were weakened by the formation of type-C-anomalies. Type-C-anomalies may represent elongated fluid conduits, which are the result of overpressure-driven, focused fluid flow leading to the displacement and/or liquefaction of a sandy reservoir matrix; although there is a real possibility type-C-anomalies represent seismic artifacts.

2.6.6. SEISMIC CHIMNEYS AND THEIR IMPLICATIONS FOR THE EVOLUTION OF THE FLUID FLOW SYSTEM

The presence of vertical seismic anomalies, which we interpret as the seismic image of fluid conduits, demonstrates that migrating fluids have by-passed the Nordland Shales in geological times. This process was not uniform as indicated by the presence of three types of seismic anomalies. Their different seismic signatures highlight formation parameters, which only become obvious by a comparative analysis (Tab. 2.1).

Tab. 2.1: Formation parameter of fluid conduits associated with vertical seismic anomalies

	Type A	Type B	Type C
Number	21	22	3
Shape	Circular, aligned	circular	Elongate, continuous
Migrating fluids	Gas, water, sediment	Gas	Water, sediment, gas
Formation character	More rapid	Less rapid	Potentially rapid
Min formation age	Holocene	Holocene or recent	Late Pleistocene
Max formation age	Late Pleistocene	Early Pleistocene	Pleistocene
Evidence for ongoing activity	Ambiguous	Yes	No

Bright spots below and within these seismic anomalies indicate that gas plays a role in the formation of these geological structures. In most cases, chimneys or pipes are attributed to hydrofracturing of an impermeable cap rock (Berndt et al., 2005; Cartwright et al., 2007; Løseth et al., 2009). In most publications, hydrofracturing is used as a synonym of seal-breaching, which can however be attributed to either capillary or fracture failure (Clayton and Hay, 1994). Fracture failure corresponds to hydrofracturing, which occurs if the pore pressure exceeds the combined least principal stress and tensile strength of the sediment (Hubbert and Willis, 1957). Capillary failure occurs, when pore pressure overcomes the capillary resistance to flow (Clayton and Hay, 1999) and gas as a non-wetting phase is introduced to the pore space leading to rapid loss of sealing capability and thereby rapid fluid release (Cathles et al., 2010). Both seal failing mechanism rely on the build-up of high pore overpressure, which requires the presence of mobile fluids and a highly permeable reservoir facilitating fluid migration as well as a cap rock with a low permeability, which inhibits the reduction of pore pressure via diffuse flow. The buoyancy of free gas causes a local pressure increase on the sealing cap rock, which may result in rapid fluid expulsion if the pore pressure in the reservoir overcomes the capillary entry pressure (Cathles et al., 2007; 2010). The amount of pressure increase directly depends on the column height of the gas pocket. By knowing the capillary entry pressure of a rock, it is possible to calculate the height of the gas column required to cause seal-breaching. Rock physical tests on a Nordland Shale sample revealed a capillary entry pressure of 3 MPa for Nitrogen, which can be transferred to other gases using the following equation (Harrington et al., 2009):

$$P_{wm} = P_{wn} \cdot \gamma_{wc} / \gamma_{wn} \quad , \quad (\text{Eq. 2.1})$$

where P_{wm} is the capillary pressure between Methane and water, P_{wn} is the capillary pressure between nitrogen and water (3 MPa) and γ_{wn} is the interfacial tension coefficient for nitrogen and water (72.8×10^{-3} N/m; Harrington et al., 2009). γ_{wc} is the interfacial tension coefficient for Methane and water at 8.5 MPa and 48°C ($\sim 62 \times 10^{-3}$ N/m; Khosharay et al., 2013), which represents the pressure and temperature condition at the top of the Utsira Formation (Alnes et al., 2010). According to this equation, the capillary entry pressure for methane P_{wm} entering the Nordland Shales should be around 2.55 MPa under Utsira Formation conditions. This can be translated to a corresponding gas column height necessary to initiate seal-breaching (Harrington et al., 2009):

$$H_{hf} = P_{wm} / (g \cdot (\rho_w - \rho_{CH_4})) \quad , \quad (\text{Eq. 2.2})$$

where H_{hf} represents the gas column height required for hydrofracturing, P_{wm} is the capillary entry pressure between methane and water (2.55 MPa), g is gravitational acceleration (9.81 m/s^2), ρ_w is density of the formation water (1025 kg/m^3 ; Harrington et al., 2009) and ρ_{CH_4} is density of methane (55 kg/m^3 ; calculated values for 8 to 9 MPa and 50°C vary between 52.6 and 59.4 kg/m^3 ; Pieperbeck et al., 1991).

According to this calculation a methane gas column height of ~268 m (more than the Utsira thickness) would be necessary to initiate capillary entry of the gaseous phase and thereby a seal failure. Such a high gas column is unrealistic considering the high permeability in the Utsira formation, which would facilitate widespread gas distribution. Therefore, it is not plausible that gas buoyancy on its own is sufficient to have caused seal-breaching of the Nordland Shales and additional processes need to be considered for explaining the formation of the 46 identified seal by-passing fluid conduits.

Formation pressure increase

While the buoyancy effect of a gas pocket is limited to the interface between its top and the cap rock, there are processes capable of causing formation-wide overpressures, e.g. increased compressive stress and changes of pore-fluid or matrix volume area (Osborne & Swarbrick, 1997). The difference between formation pressure and hydrostatic pressure would simply add on the pressure effect caused by gas buoyancy and thereby reduce the gas column height required for seal-breaching. Monitoring of the wellhead pressure of the Sleipner CO₂ injection well suggested close to hydrostatic formation pressure within the Utsira Formation at present (Chadwick et al., 2012). Following our interpretations, this observation may be explained by understanding the chimney-like anomalies as pressure valves, which would have released potentially pre-existing overpressure. Pressure conditions may have been significantly different in the past. A possible process for the formation of overpressure in the study area may be the sand injection controlled intrusion of mobilized sediments at the base of the Utsira Formation. In some areas, the mobilized sediments have displaced significant amounts of the Utsira sand causing volumetric changes and most likely fluid migration (Fig. 2.8).

Another possible process for the generation of overpressure may be loading and unloading by the Fennoscandian ice sheet during the last glacial cycle. The thickness of the ice sheet in the Southern Viking Graben cannot be conclusively reconstructed, but modeling suggests a maximum thickness of 1500 m (Siegert et al., 2001) to 2000 m (Kleman et al., 2013) for the last glacial maximum. Such loading could have triggered the expulsion of pore-fluids due to compaction and de-watering of clay minerals resulting in overpressure (Osborne & Swarbrick, 1997). Another possible explanation is the disability of mudstones to return to hydrostatic pressure condition after glacial loading, which has been proposed for thin mud layers within the Utsira Formation by Cavanagh and Haszeldine (2014). The young formation age (Pleistocene to Holocene) of most of the identified chimney-like anomalies may point to a link between their formation and loading by ice.

Seal weakening due to deformation

While the reconstruction of palaeo pressure conditions based on seismic data is difficult, the seismic data still show evidence for structural deformation, which may imply a seal weakening. The Utsira Formation is heavily deformed by intruding sediments, which affect about two thirds of the formation in the study area (Fig. 2.8b). Comparing the topography of the base of the Utsira formation with the spatial distribution of the vertical seismic anomalies reveals that the vast majority (44 of 46; Fig. 2.8b) of these features is located in areas, which were affected by underlying sediment mobilization. The intruding sediments have a clearly visible imprint on the morphology of the cap rock until about 200 m above the top of the Utsira Formation (Fig. 2.8a).

This deformation may locally decrease the tensile strength of the cap rock and thereby significantly reduce its resistance against hydrofracturing. The comparison of the location of each type of seismic chimney and the extent of deformation reveals an interesting relationship. Assuming that deformation is equivalent to seal weakening, areas with widespread basal deformation are expected to be more affected by weakening than areas, where deformation is limited to distinct sediment mobilizations. Type-B-anomalies are found in areas with widespread basal deformation of the Utsira formation (Fig. 2.8), while type-A-anomalies are located in

the vicinity of steep and rather distinct mound structures surrounded by unaffected sediments. Therefore, we suggest that the cap rock above type-B-anomalies is weakened and seal-breaching may initiate at much lower overpressure than the estimated 3 MPa facilitating the generation of a diffuse fracture networks.

Deep hydrocarbon leakage

The main contribution of deep hydrocarbon reservoirs to the fluid flow system is leaking gas, which represents the key element for the understanding of the fluid flow system. Gas may migrate both in dissolved and free form and it will cause changes to the buoyancy of the fluids when coming out of solution. The presence of narrow pipe structures in the Upper Pliocene section indicates that the bright spots in the Upper Pliocene section and the sand wedge have been charged with gas, which previously accumulated in the Utsira Formation (Fig. 2.3 and 2.8). The sandy Utsira Formation itself is unlikely to be the primary source of gas and was probably charged by deeper sources. The sediment mounds formed by the injection of liquefied sand represent efficient entries for gas that leaked from deep hydrocarbon reservoirs over long time scales (Fig. 2.9). The Hordaland mudstones are highly affected by polygonal faults, which may have facilitated upward migration of fluids during their formation. It is likely that a large fraction of the shallow gas has originally been kept within the Utsira Formation and that more gas has been released from the sediments via fluid conduits. In addition to the above-described buoyancy effect, the gas would have caused overpressure just by occupying pore space within the water-saturated aquifer. However, this effect has probably been minor considering the large dimension of the Utsira Formation and the high compressibility of gas.

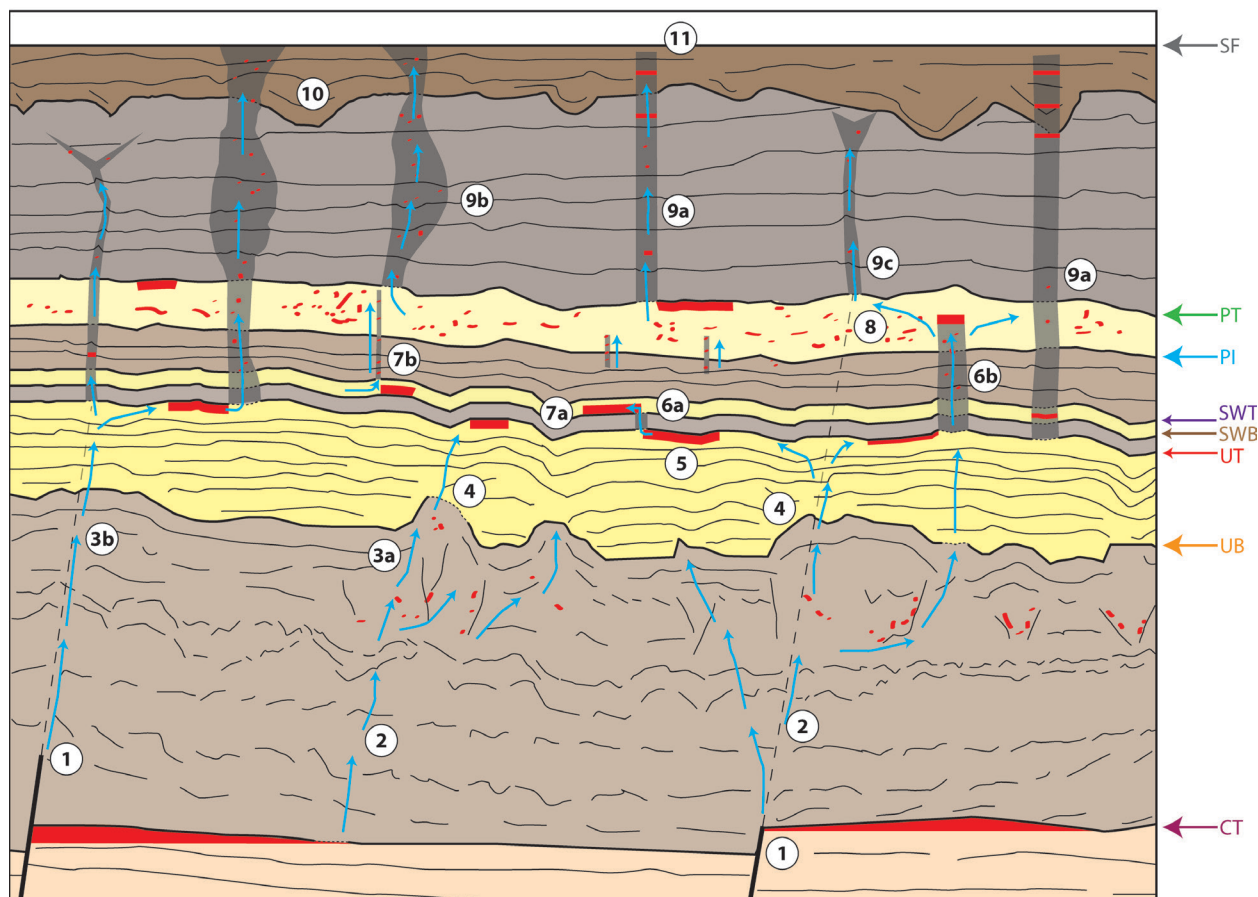


Fig. 2.9: Sketch of the local fluid flow system illustrating the different stages of fluid migration: 1) Fluids leaking from deep hydrocarbon reservoirs; 2) fluids pass through the Hordaland mudstones via polygonal faults; 3) fluids cause mud liquefaction forming a) mud diapirs and b) wide-spread mobilizations; 4) fluids enter the Utsira Formation and 5) accumulate at its top; 6) gas migrate from the Utsira Formation towards shallower depth (a) sand wedge or b) Upper Pliocene section) using hydrofracturing related pipes; 7) gas a) accumulate within the sand wedge or b) create pipes and migrate into the Upper Pliocene section; 8) fluids accumulate within and at the top of the Upper Pliocene section; 9) high overpressure leads to the formation of hydrofracturing related a) type-A-chimneys, b) type-B-chimneys and c) type-C-chimneys a) at the top of the Utsira Formation and at the top Pliocene, which continue to shallower depth; 10) chimneys cross-cut buried tunnel-valleys; 11) in some cases chimneys reach the seafloor causing the release of fluids to the water column. Colored arrows mark seismic reflections corresponding to important stratigraphic boundaries (SF = Seafloor, PT = Pliocene top, PI = Pliocene intra, UT = Utsira top, UB = Utsira base, CT = Cretaceous top).

2.7. CONCLUSIONS

The study area in the Southern Viking Graben hosts a complex fluid flow system, which can be divided into a shallow and a deep subsystem with the Utsira Formation representing the boundary between both subsystems (Fig. 2.9). Leaking fluids from deep hydrocarbon reservoirs seem to have entered the Utsira formation via underlying sediment mounds formed by the injection of liquefied sand. These fluids accumulated at the top the Utsira Formation causing overpressure. The overlying Nordland Shales prohibited migration further upward due to their low permeability. Additional pressure increase due to continuing gas accumulation from deep sources, loading by the Fennoscandian ice sheet, as well as seal weakening due to deformation by mobilized mud and deep faults must have caused seal-breaching of the Nordland Shales. This evolution is still well documented by seismic data by bright spots within the sand wedge and the Upper Pliocene section, which are connected to the Utsira Formation by narrow pipe structures.

The most prominent seismic remnants of this process are large-scale chimney-like seismic anomalies, which can be divided into three sub-types (Figs. 2.5, 2.6 and 2.9). Type-A is believed to represent the seismic image of large-scale pipe-structures, which have formed due to comparably rapid fluid expulsion. The seismic image of type-B-anomalies suggests the presence of slowly-developed, gas-filled fracture networks. Type-C-anomalies form up to 6 km-long, linear structures and correlate with overlying tunnel valleys. While there is a real possibility that at least the upper section of Type-C-anomalies is the result of poor imaging due to velocity heterogeneities in the tunnel valley infill, a number of observations point towards a fluid flow-related geological origin of these structures. The detailed analysis of seismic chimneys has been shown to be an effective tool for the reconstruction of palaeo fluid flow processes and our findings may help to predict the response of the present-day system to natural changes or anthropogenic interactions.

Inter-stratigraphic fluid flow along chimney structures represents an efficient pressure transfer process. The creation of chimneys by hydrofracturing implies the transfer of overpressure to shallower depth. This process may have repercussions for other fields of geological research. For example, overpressure at shallow depth may reduce slope stability and cause landslides. It may also control the location of benthic ecosystems as it focuses the advection of methane to the seafloor. Pre-existing fluid conduits may inhibit accumulation of overpressure within a chimney-connected reservoir affecting subsurface storage of wastewater and CO₂.

ACKNOWLEDGEMENTS

We thank Statoil ASA for permission to use the 3D seismic data. The research leading to these results has received funding from the European Community's Seventh Framework Programme [FP7/2007-2013] under grant agreement n° 265847. We would like to thank Mads Huuse, Henrik Svensen, three anonymous reviewers for their insightful comments, which helped to improve the quality of this study.

REFERENCES

- Alnes, H., Eiken, O., Nooner, S., Sasagawa, G., Stenvold, T., Zumberge, M., 2011. Results from Sleipner gravity monitoring: Updated density and temperature distribution of the CO₂ plume. *Energy Procedia* 4, 5504–5511.
- Andresen, K.J., Huuse, M., Schødt, N.H., Clausen, L.F., Seidler, L., 2011. Hydrocarbon plumbing systems of salt minibasins offshore Angola revealed by three-dimensional seismic analysis. *AAPG Bulletin* 95, 1039–1065.
- Andresen, K.J., 2012. Fluid flow features in hydrocarbon plumbing systems: What do they tell us about the basin evolution? *Marine Geology*, 1–20.
- Armstrong, T., McAteer, J., Connolly, P., 2001. Removal of overburden velocity anomaly effects for depth conversion. *Geophysical Prospecting* 49, 79–99.
- Arntsen, B., Wensaas, L., Løseth, H., Hermanrud, C., 2007. Seismic modeling of gas chimneys. *Geophysics* 72, 251–259.
- Arts, R., Chadwick, R.A., Eiken, O., Thibeau, S., Nooner, S., 2008. Ten years' experience of monitoring CO₂ injection in the Utsira sand at Sleipner, offshore Norway. *First Break* 26, 65–72.
- Bauer, C., Fichler, C., 2002. Quaternary lithology and shallow gas from high resolution gravity and seismic data in the central North Sea. *Petroleum Geoscience* 8, 229–236.
- Berndt, C., 2005. Focused fluid flow in passive continental margins. *Philosophical Transactions of the Royal Society A: Mathematical, Physical and Engineering Sciences* 363, 2855–2871.
- Brennand, T. P., van Hoorn, B., James, K. H. and Glennie, K. W., 1998. Historical Review of North Sea Exploration, in *Petroleum Geology of the North Sea: Basic Concepts and Recent Advances*, Fourth Edition (ed. K. W. Glennie), 1–41.
- Bünz, S., Mienert, J., Berndt, C., 2003. Geological controls on the Storegga gas-hydrate system of the mid-Norwegian continental margin. *Earth and Planetary Science Letters* 209, 291–307.
- Cartwright, J., Huuse, M., Aplin, A., 2007. Seal bypass systems. *AAPG Bulletin* 91, 1141–1166.
- Cathles, L. M., 2007. Changes in sub-water table fluid flow at the end of the Proterozoic and its implications for gas pulsars and MVT lead-zinc deposits. *Geofluids*, 7(2), 209–226.
- Cathles, L.M., Su, Z., Chen, D., 2010. The physics of gas chimney and pockmark formation, with implications for assessment of seafloor hazards and gas sequestration. *Marine and Petroleum Geology* 27, 82–91.
- Cavanagh, A.J., Haszeldine, R.S., 2014. The Sleipner storage site: Capillary flow modelling of a layered plume requires fractured shale barriers within the Utsira Formation. *International Journal of Greenhouse Gas Control* 21, 101–112.
- Chadwick, R.A., Noy, D., Arts, R., Eiken, O., 2009. Latest time-lapse seismic data from Sleipner yield new insights into CO₂ plume development. *Energy Procedia* 1, 2103–2110.
- Chadwick, R.A., Williams, G.A., Williams, J.D.O., Noy, D.J., 2012. Measuring pressure performance of a large saline aquifer during industrial-scale CO₂ injection: The Utsira Sand, Norwegian North Sea. *International Journal of Greenhouse Gas Control* 10, 374–388.
- Clayton, C.J., Hay, S.J., 1994. Gas migration mechanisms from accumulation to surface. *Bulletin of the Geo-*

logical Society of Denmark 41, 12-23.

Eidvin, T., Rundberg, Y., 2007. Post-Eocene strata of the southern Viking Graben, northern North Sea; integrated biostratigraphic, strontium isotopic and lithostratigraphic study. *Norwegian Journal of Geology* 87, 391–450.

Fichler, C., Henriksen, S., Rueslaatten, H., Hovland, M., 2005. North Sea Quaternary morphology from seismic and magnetic data: indications for gas hydrates during glaciation? *Petroleum Geoscience* 11 (4), 331-337.

Galloway, W.E., 2001. Seismic expressions of deep-shelf depositional and erosional morphologies, Miocene Utsira Formation, North Sea Basin. *Marine Geophysical Research* 22, 309–321.

Galloway, W.E., 2002. Paleogeographic setting and depositional architecture of a sand-dominated shelf depositional system, Miocene Utsira Formation, North Sea Basin. *Journal of Sedimentary Research* 72, 476–490.

Gautier, D.L., 2005. Kimmeridgian Shales Total Petroleum System of the North Sea Graben Province: U.S. Geological Survey Bulletin 2204-C, 24 p.

Gay, A., Mourgues, R., Berndt, C., Bureau, D., Planke, S., Laurent, D., Gautier, S., Lauer, C., Loggia, D., 2012. Anatomy of a fluid pipe in the Norway Basin: Initiation, propagation and 3D shape. *Marine Geology* 1–14.

Graham, A., Lonergan, L., Stoker, M., 2007. Evidence for Late Pleistocene ice stream activity in the Witch Ground Basin, central North Sea, from 3D seismic reflection data. *Quaternary Science Reviews* 26, 627–643.

Granli, J.R., Arntsen, B., Sollid, A., Hilde, E., 1999. Imaging through gas-filled sediments using marine shear-wave data. *Geophysics* 64, 668–677.

Gregersen, U., Johannessen, P.N., 2007. Distribution of the Neogene Utsira Sand and the succeeding deposits in the Viking Graben area, North Sea. *Marine and Petroleum Geology* 24, 591–606.

Gregersen, U., Sorensen, J.C., Michelsen, O., 1997. Stratigraphy and Facies Distribution in the Utsira Formation and the Pliocene Sequences in the Northern North Sea.

Harrington, J.F., Noy, D.J., Horseman, S.T., Birchall, D.J., Chadwick, R.A., 2009. Laboratory study of gas and water flow in the Nordland Shale, Sleipner, North Sea. Carbon dioxide sequestration in geological media—State of the Science: AAPG Studies 59.

Heggland, R., 1997. Detection of gas migration from a deep source by the use of exploration 3D seismic data. *Marine Geology* 137, 41–47.

Horvig, S., 1982. WDSS 40 01 16 7 2: Geological Completion Report Well 16/7-2. Esso Exploration and production Norway Inc.

Hovland, M., Sommerville, J.H., 1985. Characteristics of two natural gas seepages in the North Sea. *Marine and Petroleum Geology* 2, 319–326.

Hseinat, Al, M., Hübscher, C., 2014. Ice-load induced tectonics controlled tunnel valley evolution - instances from the southwestern Baltic Sea. *Quaternary Science Reviews* 97, 121–135. doi:10.1016/j.quascirev.2014.05.011

Hubbert, M.K., Willis, D.G., 1957. Mechanic of hydraulic fracturing. *Transactions of Society of Petroleum Engineers of AIME*, 1957, v. 210, p. 153-168.

Huuse, M., Lykke-Andersen, H., 2000. Overdeepened Quaternary valleys in the eastern Danish North Sea: morphology and origin. *Quaternary Science Reviews* 19, 1233–1253.

- Huuse, M., 2008. Sandstone intrusions: Implications for exploration and production: *World Oil* 229, 87-91.
- Jackson, C., Stoddart, D., 2005. Temporal constraints on the growth and decay of large-scale mobilized mud masses and implications for fluid flow mapping in sedimentary basins. *Terra Nova* 17, 580–585.
- Justwan, H., Dahl, B., 2005. Quantitative hydrocarbon potential mapping and organofacies study in the Greater Balder Area, Norwegian North Sea 6, 1317–1329.
- Khosharay, S., Varaminian, F., 2013. Modeling interfacial tension of $(\text{CH}_4+\text{N}_2)+\text{H}_2\text{O}$ and $(\text{N}_2+\text{CO}_2)+\text{H}_2\text{O}$ systems using linear gradient theory. *Korean J. Chem. Eng.* 30, 724–732.
- Kleman, J., Fastook, J., Ebert, K., Nilsson, J., Caballero, R., 2013. Pre-LGM Northern Hemisphere ice sheet topography. *Clim. Past* 9, 2365–2378.
- Korbøl, R., Kaddour, A., 1995. Sleipner vest CO_2 disposal-injection of removed CO_2 into the Utsira Formation. *Energy Conversion and Management* 36, 509–512.
- Kristensen, T.B., Huuse, M., 2012. Multistage erosion and infill of buried Pleistocene tunnel valleys and associated seismic velocity effects. Geological Society, London, Special Publications 368, 159–172. doi:10.1144/SP368.15
- Loneragan, L., Maidment, S.C.R., Collier, J.S., 2006. Pleistocene subglacial tunnel valleys in the central North Sea basin: 3-D morphology and evolution. *J. Quaternary Sci.* 21, 891–903.
- Løseth, H., Wensaas, L., Arntsen, B., Hovland, M., 2003. Gas and fluid injection triggering shallow mud mobilization in the Hordaland Group, North Sea. Geological Society, London, Special Publications 216, 139–157.
- Løseth, H., Gading, M., Wensaas, L., 2009. Hydrocarbon leakage interpreted on seismic data. *Marine and Petroleum Geology* 26, 1304–1319.
- Løseth, H., Wensaas, L., Arntsen, B., Hanken, N.-M., Basire, C., Graue, K., 2011. 1000 m long gas blow-out pipes. *Marine and Petroleum Geology* 28, 1047–1060.
- Løseth, H., Rodrigues, N., Cobbold, P.R., 2012. World's largest extrusive body of sand? *Geology* 40, 467–470. doi:10.1130/G33117.1
- Nicoll, D.G., 2011. Evaluation of the Nordland Group overburden as an effective seal for the Sleipner CO_2 storage site (offshore Norway) using analytical and stochastic modelling techniques. PhD Thesis, School of Geosciences, University of Edinburgh, 383 pages
- Osborne, M.J., Swarbrick, R.E., 1997. Mechanisms for generating overpressure in sedimentary basins; a re-evaluation. *AAPG Bulletin* 81, 1023–1041.
- Pedersen, R. B., Blomberg, A., Landschulze, K., Baumberger, T., Økland, I., Reigstad, L., Gracias, N., Mørkved, P. T., Stensland, A., Lilley, M. D., Thorseth, I. H., 2013. American Geophysical Union, Fall Meeting 2013, abstract #OS11E-03
- Pieperbeck, N., Kleinrahm, R., Wagner, W., Jaeschke, M., 1991. Results of (pressure, density, temperature) measurements on methane and on nitrogen in the temperature range from 273.15 K to 323.15 K at pressures up to 12 MPa using a new apparatus for accurate gas-density measurements. *The Journal of Chemical Thermodynamics* 23, 175–194
- Pinet, N., Duchesne, M., Lavoie, D., 2009. Linking a linear pockmark train with a buried Palaeozoic structure: a case study from the St. Lawrence Estuary. *Geo-Marine Letters* 30, 517–522.

Rodrigues, N., Cobbold, P.R., Loseth, H., 2009. Physical modelling of sand injectites. *Tectonophysics* 474, 610–632. doi:10.1016/j.tecto.2009.04.032

Schneider von Deimling, J., Rehder, G., Greinert, J., McGinnis, D.F., Boetius, A., Linke, P., 2011. Quantification of seep-related methane gas emissions at Tommeliten, North Sea. *Continental Shelf Res.* 31, 867-878.

Sejrup, H.P., Larsen, E., Landvik, J., King, E.L., Hafliðason, H., Nesje, A., 2000. Quaternary glaciations in southern Fennoscandia: evidence from southwestern Norway and the northern North Sea region. *Quaternary Science Reviews* 19, 667–685.

Siegert, M.J., Dowdeswell, J.A., Hald, M., Svendsen, J.-I., 2001. Modelling the Eurasian Ice Sheet through a full (Weichselian) glacial cycle. *Global and Planetary Change* 31, 367–385.

Vielstädte, L., Karstens, J., Haeckel, M., Schmidt, M., Linke, P., Reimann, S., Liebetrau, V., Wallmann, K., 2014: Anthropogenic Methane Emissions from Abandoned Oil and Gas Wells in the North Sea- How much Methane is Leaking into the Ocean and finally into the Atmosphere?. 12th Gas in marine sediments conference (GIMS 12), Taipei, 2014.

CHAPTER 3: THE GLACIAL METHANE PUMP: OVERPRESSURE AND FOCUSED FLUID FLOW DUE TO GAS COMPRESSION COMPENSATED SEDIMENT COMPACTION

Karstens, J., and Berndt, C.



Vertical fluid conduit, Lake Powell, Utah, USA

3.1. INTRODUCTORY PARAGRAPH

Focused fluid flow in sedimentary basins is primarily controlled by the presence of mobile fluids and permeability barriers prohibiting the equilibration of pore pressure through diffusion. The North Sea and Barents Sea basins host a multitude of focused fluid flow manifestations, which show evidence that they have formed after the last phase of glaciation. However, so far the correlation between deglaciation and fluid conduit formation has not been explained convincingly. Here we present a novel explanation for the formation of focused fluid conduits that is consistent with rock samples and seismic data from the Southern Viking Graben. The compressibility difference between rocks and free gas and small amounts of compaction during glacial loading can account for high over pressure when ice loading ceases. This process is independent of the thickness of the affected sand body or its burial depth. It can explain the formation of pockmarks and seafloor seepage as well as large-scale chimney structures above hydrocarbon reservoirs, and should be taken into account when such structures are used as proxies for past carbon release from the geosphere into the climate system. Furthermore, the process may transfer overpressure from the deep to shallow layers, where it can influence the stability of continental slopes.

3.2. LETTER

Global hydrocarbon prospection has revealed numerous focused fluid flow-related geological structures including free gas accumulations, pipe or chimney structures as well as pockmarks and seeps at the seafloor (Judd and Hovland, 2007; Løseth et al, 2009). Many of these features can be directly related to hydrocarbon leakage from deep reservoirs. Large chimney structures have been identified above several hydrocarbon reservoirs (e.g. Tommeliten; Granli et al, 1999), where they represent a pathway for fluids that source ongoing seafloor seepage. Therefore, hydrocarbon emanating cold seeps have been used as an indicator for the presence of deeper reservoirs, while seepage itself offers an explanation for dry wellbores in otherwise promising reservoirs. However, most gas accumulations close to the seafloor have been charged by biogenic methane production within the uppermost kilometer of sediments (Judd and Hovland, 2007). Depending on the substrate, the seeping fluid and the seepage rate, focused fluid flow manifests itself either in crater-like pockmarks, bacterial mats, or carbonate deposits at the seafloor (Judd and Hovland, 2007).

Gas migration in marine sediments is governed by contrasts in pore pressure and sediment permeability. The formation of vertical focused fluid flow conduits, e.g. pipes and chimneys (Fig. 1), can generally be attributed to the seal-bypassing release of fluids due to either a (hydro)-fracture or capillary failure of the seal (Clayton and Hay, 1994). Hydrofracturing initiates, when the pore pressure exceeds the tensile strength of the overlying rocks (Hubbert and Willis, 1957), while a capillary failure develops, when pore pressure reaches the capillary entry pressure (Cathles et al., 2010). The capillary entry pressure is a measure of the resistance of the pore space against the entry of fluids and if this threshold is overcome, the seal rapidly loses its sealing capability (Cathles et al., 2010). Permeability barriers prohibit pressure equilibration and thereby facilitate the build-up of overpressure, which is defined here as the difference between pore pressure and hydrostatic pressure. The buoyancy of free gas itself is a source for local, caprock-directed overpressure, which depends on the height of the gas column. Beside this gas-intrinsic permeability-overpressure relation, there are several other processes capable of generating overpressure in sedimentary basins, e.g. increased compressive stress by tectonic forces or loading, changes in the volume of pore fluids or the matrix and fluid migration, which can affect each other (Osborne and Swarbrick, 1997).

The Southern Viking Graben in the Central North Sea Basin hosts a multitude of focused fluid flow manifestations (Karstens and Berndt, 2015). The local stratigraphy is characterized by alternating mudstone and sandstone sequences including the sand-rich Utsira Formation, which is an approximately 850 m deep buried, up to 250 m thick, extensive, highly porous and permeable saline aquifer (Arts et al, 2008). The overlying strata of the Utsira Formation consist of almost impermeable mudstones. Rock physical tests of samples of

the overlying Nordland Formation yielded a capillary entrance pressure of 2.55 MPa for methane (Karstens and Berndt, 2015; Harrington et al., 2009). These mudstones are covered by glacial sediments (Karstens and Berndt, 2015). Subglacial tunnel valleys overprinted these sediments during the last glacial period (Lonergan et al., 2006), when the Southern Viking Graben was covered by several hundred meters of ice (Kleman et al., 2013). The Utsira Formation is the origin of several large (more than 500 m in diameter) chimney structures which crosscut the mudstone caprock as well as the glacial sediment cover and almost reach the present-day seafloor (Fig. 3.1). In terms of timing, this stratigraphic relationship puts the maximum formation age of the chimney structures to the end of glaciation in Late Pleistocene. Many chimneys root in the direct vicinity of gas accumulations. Although a relationship between these gas accumulations and the fluid conduit formation appears obvious, the buoyancy of gas itself is not sufficient to result in an overpressure of 2.55 MPa as this equals to the buoyancy of a ~270 m high gas column (Karstens and Berndt, 2015; Harrington et al., 2009), which cannot be observed in any of the abundant reflection seismic data.

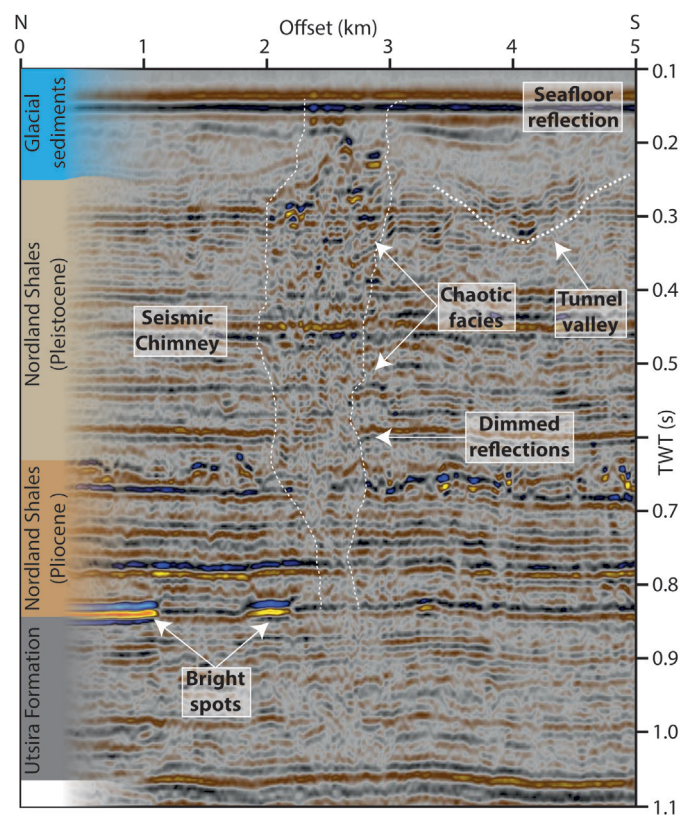


Fig. 3.1: Seismic profile showing chimneys with chaotic seismic signature, bright spots, the position of glacial tunnel valleys and the basic stratigraphy

Therefore, additional processes related to glacial loading and unloading are required to explain the generation of overpressure, which needs to be sufficient for breaching the caprock. The expulsion of water from shale either in response to compaction or due to their inability to return to hydrostatic pressure conditions after glacial loading, as proposed by Cavanagh and Hazeldine (2014), may be valid for overpressure generation within impermeable layers, but cannot be applied to highly permeable, sandy units of regional extent. Intrusion of mud mounds at the base of the Utsira Formation caused its structural deformation. However, onlap relationships onto the deformed strata show that this process must have terminated long before the formation time of the chimneys indicated by the termination of folding of seismic horizon younger than the Late Pliocene (Fig. 3.1). Therefore it cannot be the reason for overpressure generation. There is also no evidence for expulsion of additional brine or hydrocarbons from deeper reservoirs correlating with the last glacial period. Therefore, there is no evidence for any conventional process that may explain the timing and the large overpressure

required for breaching the caprock at the time of chimney formation.

The occurrence of free gas accumulations at the top of the Utsira Formation (Fig. 3.1) points to a different mechanism for the generation of significant amounts of overpressure. We propose that the formation of chimney structures is the direct response of free gas compression and decompression during a cycle of loading and unloading. Loading of a water-saturated highly porous and permeable sediment layer results in a non-reversible reduction of the pore space by compaction associated with the discharge of pore water. If a water saturated system cannot expel pore-fluids, an increasing compressive stress would cause an increase in pore pressure leading to pore-fluid compression. In case of full saturation (no gas in the pore space), the associated volume reduction due to pore fluid compression would be minor due to the high bulk modulus (low compressibility) of water, which directly controls the bulk modulus of the saturated porous system K_{sat} .

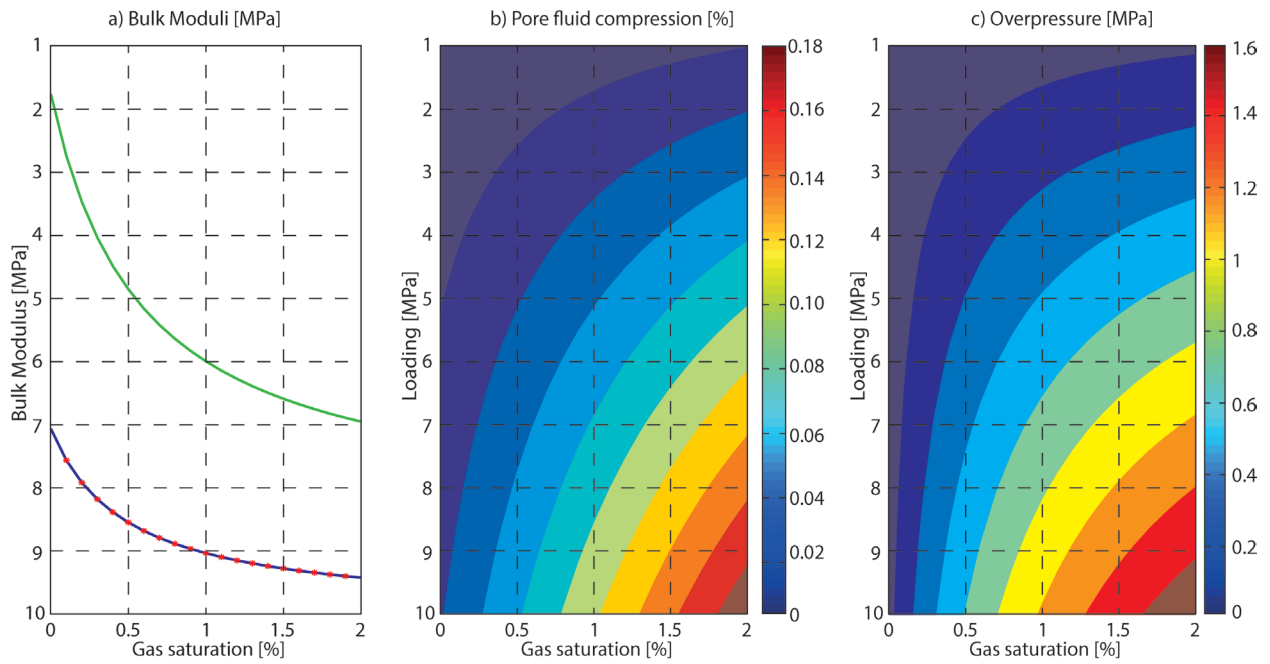


Fig. 3.2: A) Diagram showing the relation of the bulk modulus in relation to gas saturation. B) Diagram showing the relation of pore fluid compression in relation to gas saturation for an ambient pressure of 1, 5 and 10 MPa. C) Overpressure as the result of gas-compression compensated compaction (GCCC).

However, the system's bulk modulus changes considerably in the presence of free gas (Methods, Fig. 3.2a). Even a small fraction of gas in the pore-fluid has a strong influence on the bulk modulus of the pore fluid K_{fl} and potential pore-volume reduction due to compression (Fig. 3.2a,b). Under the same pressure conditions, the potential compression of the pore fluid itself would be much greater than the compression of the entire system due to its significantly higher compressibility. This implies that the volume reduction of the system is smaller than the theoretical volume reduction of the pore fluid under the same pressure conditions implying a relative underpressure of the pore fluids (p). This results in a pressure difference between pore fluid and the total stress (σ) applied to the system, which is defined as effective stress (Terzaghi, 1923):

$$\sigma' = \sigma - p \quad (\text{Eq. 3.1})$$

Assuming that the sediments are not over-consolidated, the system will equilibrate the effective stress by compaction (Fig. 3.3). The system has the ability to reduce pore-space by compaction without removing pore-fluids. The amount of compaction (C) is the difference between potential pore fluid compression weighted by the system's porosity (σ) and the compression of the saturated system and can be quantified:

$$C = \Phi \sigma / K_{fl} - \sigma / K_{sat} \quad (\text{Eq. 3.2})$$

If loading is temporary and the system is closed, subsequent unloading would lead to expansion of the compressed material including the gas. Due to compaction the reduction of pore space is irreversible and the gas cannot expand to its previous volume, which implies that the pore fluid preserves the acquired increased pressure, when the system is not able to expel pore fluids quickly (Fig. 3.3). We call this process gas-compression compensated compaction (GCCC). The amount of overpressure as the result of GCCC can be quantified as the product of the pore fluid's bulk modulus and the volume loss due to compaction (Fig. 2c):

$$P_{\text{GCCC}} = C \cdot K_{\text{fl}} \quad (\text{Eq. 3.3})$$

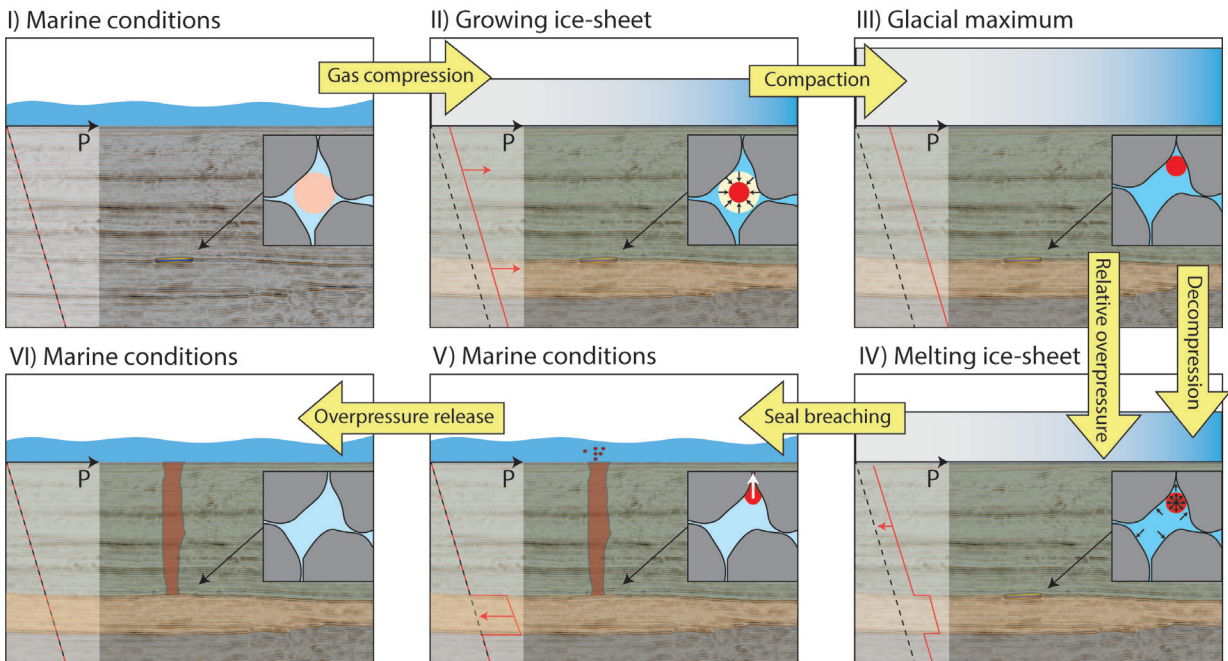


Fig. 3.3: Concept of overpressure generation and chimney formation as the result of GCCC during a glacial cycle. I) Marine conditions: the pressure-depth profile (red line) shows no pressure anomalies and the system is under hydrostatic pressure conditions (dashed line). II) Growing ice-sheet: The pressure within the sedimentary column increases equally in all three sedimentary units (green: caprock consisting of low permeable mudstones, orange: reservoir consisting of high permeable sand layer; brown: low permeable mudstone). Gas within the pore space of the sand layer requires less space under the increased pressure conditions. III) Glacial maximum: The pressure in the sedimentary column reaches its maximum and the systems uses its potential for pore space reduction due to the gas compression for compaction. IV) Melting ice-sheet: The pressure within the caprock moves back towards hydrostatic pressure condition, while the gas in the sand layer tends to return to its original volume, which is not possible due to the inelastic deformation of compaction. Consequently, it retains its volume and thereby the accumulated pressure leading to a pressure contrast between reservoir and caprock. V) Marine conditions: the pore pressure difference at the boundary between caprock and reservoir reaches a maximum and exceeds the caprock's resistance against capillary or fracture failure and forms a focused fluid flow conduit, which discharges overpressured fluids from the reservoir. VI) Marine conditions: the overpressure within the reservoir has bled off and the sedimentary column has returned to hydrostatic pressure conditions.

The concept of overpressure generation due to GCCC is independent of burial depth, thickness formation thickness, or extent of the compacted layer, but requires sediments with the potential to consolidate and sufficient capillary sealing to prevent diffusive equilibration of overpressure. These requirements are fulfilled at a regional scale for deep saline aquifers as well as on a much smaller scale for near surface sand lenses underneath glacial tills. The key requirement for this process is the presence of free gas. Figure 2 shows that the influence of gas saturation on the system's bulk modulus, compression and the resulting overpressure due to GCCC is exponential for saturations between 0 and 2%. Even 0.1% gas saturation of the pore space and loading of 0.9 MPa, which is equivalent to an ice sheet height of 100 m, may result in overpressure of ~0.028 MPa. Such overpressure is comparable to the effect of an 11 m-high gas column. An ice sheet height

of 1000 m and a gas saturation of 0.5% have the potential to generate ~0.73 MPa. Both parameters appear realistic for the Southern Viking Graben considering the strong glacial imprint and the multitude of fluid flow manifestations and we propose that this process offers an elegant explanation both for the development of seismic chimney structures rooted in the Utsira Formation as well as for the development of pockmarks in other glacial settings (Fig. 3.3).

The process has to be taken into account when incorporating the formation of fluid migration structures in global climate modeling. In particular claims of large-scale methane release (Forsberg et al., 2007; Hornbach et al., 2012) from the seafloor that may impact climate should be re-evaluated. For example, pockmark formation near the Troll Field was interpreted as a result of sub-glacial gas hydrate dissociation when the North Sea ice-sheet melted. Considering the basin-wide presence of post-glacial fluid flow manifestations (Judd and Hovland, 2007) this formation mechanism would require the existence of widespread gas hydrate occurrence and implies substantial liberation of methane at the end of the last glaciations for which there is no geochemical evidence from ice cores (Petit et al., 1999). In contrast, GCCC is possible at comparably low gas saturations and is not limited to shallow depths, thus reconciling the geological and geochemical observations.

The concept should also be considered in hazard assessment of submarine slope failures. Abrupt removal of large portions of the sedimentary overburden during a submarine slope failure may be an even more effective mechanism for pressure release on previously compacted gas saturated rocks in the shallow subsurface than the gradual melting of ice sheets and may lead to the formation of fluid pathways. Some of the biggest known landslides (Bünz et al., 2005, Yang et al., 2013) are underlain by numerous pipe structures and their shallow termination depth is consistent with them having formed during sliding due to GCCC. Rapid formation of such pathways would connect gas-rich regions in the subsurface, e.g. at the base of the hydrate stability zone (Hornbach et al., 2004), with the shallow sedimentary strata and may lead to fast increase of pore pressure within permeable beds that may serve as slide planes. The frequent occurrence of gas hydrate indicators near submarine slope failures (Booth et al., 1994; Skarke et al., 2014) have led to speculation that gas hydrate dissociation due to changes in the temperature and/or pressure conditions may cause slope failures (Mienert et al., 1998; Sultan et al., 1998). However, so far no conclusive evidence of this process has been found. GCCC offers an alternative explanation for the spatial relationship between gas hydrate indicators and large slope failures as it may explain why hydrates promote sliding on large areas rather than causing slope failures.

3.3. METHODS

Overpressure quantification. The amount of overpressure caused by GCCC is controlled by pore space reduction as the result of compaction of the gaseous phase C and the bulk modulus of the pore fluid K_{fl} . The bulk modulus is the inverse of the compressibility of a material and represents the relation between volume reduction and applied pressure. The bulk modulus of a saturated porous medium can be quantified using Gassmann's equation (Mavko et al., 2009):

$$K_{sat} = K_m \cdot (K_{dry} / (K_m - K_{dry}) + K_{fl} / (\Phi \cdot (K_m - K_{fl}))) / (1 + K_{dry} / (K_m - K_{dry}) + K_{fl} / (\Phi \cdot (K_m - K_{fl}))) \quad (\text{Eq. 3.4.})$$

where Φ is the porosity, K_{sat} is the bulk modulus of the fluid saturated sediment, K_m is the bulk modulus of a sand grain, K_{dry} is the bulk modulus of the sediment matrix frame. The bulk modulus of the pore fluid can be calculated using Biot's formula (Mavko et al., 2009):

$$K_{fl} = 1 / ((1 - S_g) / K_w + S_g / K_g) \quad (\text{Eq. 3.5.})$$

where K_w and K_g are the bulk moduli of water and gas and S_g is the gas saturation. The parameter values used for our calculation are listed in table 3.1.

Tab. 3.1: parameter used for overpressure calculation

Parameter for Utsira Formation (10 MPa, 37°C)	Value	Reference
Bulk modulus of a sand grain K_m	40*109 MPa	Carcione et al., 2006
Bulk modulus of the matrix frame K_{dry}	1.37*109 MPa	Carcione et al., 2006
Bulk modulus of the brine (water) K_w	2.61*109 MPa	Carcione et al., 2006
Bulk modulus of methane (gas) K_g	1.27*107 MPa	Carcione et al., 2006
Porosity Φ	37%	Arts et al., 2008
Compaction parameter k	0.0266 MPa ⁻¹	Hantschel and Kauerauf, 2009

The relative volume change by compression for a given specimen is defined as the quotient of total stress (σ) and the bulk modulus (K)

$$V/V_0 = \sigma / K \quad (\text{Eq. 3.6})$$

The potential compaction (C) can be quantified by subtracting the potential compression of the system from the potential compression of the pore fluid weighted by the volume fraction of the pore filling defined as the porosity (Φ):

$$C = \Phi * \sigma / K_{fl} - \sigma / K_{sat} \quad (\text{Eq. 3.2})$$

If the system would have the potential to release fluids (drained conditions), the amount of compaction could be quantified by simple empiric solutions such as Athy's Law (Hantschel and Kauerauf, 2009):

$$\Phi = \Phi_0 * \exp(-k * \sigma') \quad (\text{Eq. 3.7})$$

where Φ_0 is porosity before applying an effective stress σ' and k is the compaction parameter. Given a total stress of 1 MPa and a gas saturation of 0.1%, the system would compact by ~2.6% under drained conditions and 0.014% applying GCCC. Therefore, we assume that the system would utilize the pore space clearance by GCCC completely for compaction.

The compression of the gaseous phase has direct influence on the volumetric gas saturation (S_g) and the porosity (Φ) and thereby on the bulk moduli of the pore fluid (K_{fl}) and the porous system K_{sat} . The differences are however negligible (Fig 2a). In conclusion, only the loading P and the gas saturation S_g control the amount of GCCC related overpressure and can be quantified by multiplying the estimated the compression of the gaseous phase C_g and the bulk modulus of the system pore fluid K_{fl} :

$$P_{GCCC} = C_g * K_{fl} \quad (\text{Eq. 3.1})$$

REFERENCES

- Arts, R., Chadwick, R.A., Eiken, O., Thibeau, S., Nooner, S., Lamont-Doherty Geological Observatory of Columbia University, 2008. Ten years' experience of monitoring CO₂ injection in the Utsira sand at Sleipner, offshore Norway.
- Booth, J. S., Winters, W. J., & Dillon, W. P. (1994). Circumstantial Evidence of Gas Hydrate and Slope Failure Associations on the United-States Atlantic Continental-Margin. *International Conference on Natural Gas Hydrates*, 715(1), 487–489. doi:10.1111/j.1749-6632.1994.tb38863.xREF22
- Bünz, S., Mienert, J., Bryn, P., Berg, K., 2005. Fluid flow impact on slope failure from 3D seismic data: a case study in the Storegga Slide. *Basin research* 17(1), 109–122. doi:10.1111/j.1365-2117.2005.00256.x
- st, J. M., Picotti, S., Gei, D., & Rossi, G., 200). Physics and Seismic Modeling for Monitoring CO₂ Storage. *Pure and Applied Geophysics*, 163(1), 175–207. doi:10.1007/s00024-005-0002-1
- Cathles, L.M., Su, Z., Chen, D., 2010. The physics of gas chimney and pockmark formation, with implications for assessment of seafloor hazards and gas sequestration. *Marine and Petroleum Geology* 27, 82–91.
- Cavanagh, A.J., Haszeldine, R.S., 2014. *International Journal of Greenhouse Gas Control*. *International Journal of Greenhouse Gas Control* 21, 101–112. doi:10.1016/j.ijggc.2013.11.0171.
- Clayton, C.J., Hay, S.J., 1994. Gas migration mechanisms from accumulation to surface. *Bulletin of the Geological Society of Denmark* 41, 12-23.
- Forsberg, C. F., Plank, S. F., Tjelta, T. I., Svano, G. F., Strout, J. M., & Svensen, H. F. (2007). Formation of pockmarks in the Norwegian Channel. *Proceedings of the 6th International Offshore Site Investigation and Geotechnics Conference; Confronting New Challenges and Sharing Knowledge*. 11–13 September 2007, London, UK.
- Granli, J.R., Arntsen, B., Sollid, A., Hilde, E., 1999. Imaging through gas-filled sediments using marine shear-wave data. *Geophysics* 64, 668–677.
- Hantschel, T., Kauerauf, A.I., 2009. *Fundamentals of Basin and Petroleum Systems Modeling*. Springer-Verlag Berlin Heidelberg. doi:10.1007/978-3-540-72318-9
- Harrington, J.F., Noy, D.J., Horseman, S.T., Birchall, D.J., Chadwick, R.A., 2009. Laboratory study of gas and water flow in the Nordland Shale, Sleipner, North Sea. *Carbon dioxide sequestration in geological media—State of the Science: AAPG Studies* 59.
- Hornbach, M. J., Bangs, N. L., & Berndt, C., 2012. Detecting hydrate and fluid flow from bottom simulating reflector depth anomalies. *Geology*, 40(3), 227–230. doi:10.1130/G32635.1
- Hornbach, M. J., Saffer, D. M., & Holbrook, W. S. (2004). Critically pressured free-gas reservoirs below gas-hydrate provinces. *Nature*, 427(6970), 142–144. doi:10.1038/nature02172
- Hubbert, M.K., Willis, D.G., 1957. Mechanic of hydraulic fracturing. *Transactions of Society of Petroleum Engineers of AIME*, 1957, v. 210, p. 153-168.
- Judd, A.G., Hovland, H., 2007. *Seabed fluid flow - Impact on Geology, Biology, and the Marine Environment*. Cambridge University Press, Cambridge.
- Karstens, J., Berndt, C., in review. Seismic chimneys in the Southern Viking Graben – Implications for palaeo fluid migration and overpressure evolution. *Earth and Planetary Science Letters*

- Kleman, J., Fastook, J., Ebert, K., Nilsson, J., Caballero, R., 2013. Pre-LGM Northern Hemisphere ice sheet topography. *Clim. Past* 9, 2365–2378.
- Lonergan, L., Maidment, S.C.R., Collier, J.S., 2006. Pleistocene subglacial tunnel valleys in the central North Sea basin: 3-D morphology and evolution. *J. Quaternary Sci.* 21, 891–903.
- Løseth, H., Gading, M., Wensaas, L., 2009. Hydrocarbon leakage interpreted on seismic data. *Marine and Petroleum Geology* 26, 1304–1319.
- Mavko, G., Mukerji, T. Dvorkin, J., 2009. *The rock physics handbook: Tools for seismic analysis of porous media.* Cambridge University Press, Cambridge.
- Mienert, J. Posewang, M. Baumann, 1998. Gas hydrates along the northeastern Atlantic margin: possible hydrate-bound margin instabilities and possible release of methane Geological Society, London, Special Publications, 137:275-291, doi:10.1144/GSL.SP.1998.137.01.22 REF24
- Osborne, M.J., Swarbrick, R.E., 1997. Mechanisms for generating overpressure in sedimentary basins; a re-evaluation. *Bulletin* 81, 1023–1041.
- Petit, J. R., Jouzel, J., Raynaud, D., Barkov, N. I., Barnola, J. M., Basile, I., et al., 1999. Climate and atmospheric history of the past 420,000 years from the Vostok ice core, Antarctica. *Nature*, 399(6735), 429–436. doi:10.1038/20859
- Skarke, A., Ruppel, C., Kodis, M., Brothers, D., & Lobecker, E., 2014. Widespread methane leakage from the sea floor on the northern US Atlantic margin. *Nature Geoscience*, 7(9), 657–661. doi:10.1038/ngeo2232
- Sultan, N., Cochonat, P., Foucher, J. P., & Mienert, J. (2004). Effect of gas hydrates melting on seafloor slope instability. *Marine Geology*, 213(1-4), 379–401. doi:10.1016/j.margeo.2004.10.015
- Terzaghi, K., 1923. Die Berechnung der Durchlässigkeitsziffer des Tones im Verlauf der hydrodynamischen Spannungserscheinungen. *Szber Akademie Wissenschaft, Vienna, Math–naturwissenschaft Klasse IIa* , (132):125–138.
- Yang, J., Davies, R. J., & Huuse, M., 2013. Gas migration below gas hydrates controlled by mass transport complexes, offshore Mauritania. *Marine and Petroleum Geology*, 48(C), 366–378. doi:10.1016/j.marpet-geo.2013.09.003

CHAPTER 4: THE IMPACT OF CHIMNEY STRUCTURES ON THE CO₂ STORAGE AT SLEIPNER: EVALUATION OF NUMERICAL FLUID FLOW SIMULATIONS BASED ON TIME-LAPSE SEISMIC DATA

Karstens, J., Ahmed, W., Berndt, C., and Class, H.



Sleipner CO₂ treatment and injection platform, Norwegian North Sea

4.1. ABSTRACT

The integrity of the overburden above a storage reservoir is the most crucial parameter for the long-term performance of the geological storage of CO₂. The CO₂ storage operation at In Salah (Algeria) shows strong indication for hydrofracturing of caprock as the result of the injection of supercritical CO₂. These observations may raise questions about the storage safety of other CO₂ storage operations like Sleipner. Time-lapse seismic monitoring shows that the injection activity at Sleipner has not fractured the caprock and no CO₂ has left the Utsira Formation. However, large chimney structures 7 km from the injection point indicate that the caprock has been breached in the geological past. Here, we show seismically constrained numerical simulations that evaluate the influence of chimney structures on the long-term performance of the CO₂ storage operation at Sleipner. The simulation could reproduce the anisotropic permeability field in the Utsira Formation. Our long-term simulations reveal that CO₂ will not reach the existing chimney structures assuming a realistic injection duration of 30 years. In order to understand the interaction of the CO₂ plume and chimney structures, we continue numerically injection for 200 years. In such a scenario the CO₂ requires between 92 and 140 years to migrate through the chimneys to the seafloor and that a comparably low chimney permeability of 10 mD may result in leakage. Our results highlight that the reconstruction of the plaeo fluid flow system and the identification of focused fluid conduits is of great importance for the assessment of CO₂ storage sites.

4.1. INTRODUCTION

The geological storage of CO₂ is a key technology for the mitigation of climate gas emissions recommended by the IPCC (2013). By beginning of 2015, thirteen industrial scale carbon capture and storage (CCS) facilities are operating (Global CCS institute, 2014). Most of these operations use CO₂ for enhanced oil recovery, while only the storage operations at In Salah (Algeria), Snøhvit and Sleipner (both Norway) are actually dedicated to the geological storage of CO₂, which, at these fields, is a byproduct of natural gas production (Global CCS institute, 2014).

In 1996, Statoil initiated the Sleipner CO₂ storage operation and the injection of CO₂ as the response to the Norwegian state tax on offshore petroleum industry emissions (Cavanagh and Haszeldine, 2014). The project's storage target is to inject 20 Mt (Chadwick et al, 2004), which will be achieved in 2020 assuming a continuous injection with the current rate of 0.9 Mt/yr (Cavanagh and Haszeldine, 2014). The injected CO₂ is the byproduct of natural gas production from the Sleipner Vest fields, where the natural CO₂ content is about 4 – 9,5% (Korbøl and Kaddour, 1995). The gas is transported via pipelines to the Sleipner T platform, where the CO₂ gets sequestered, compressed and re-injected into the Utsira Formation at about 1012 m depth (Korbøl and Kaddour, 1995; Arts et al., 2008). The Utsira Formation is a saline aquifer extending about 450 km N-S and 90 km E-W and has a potential storage capacity of 16 billion tons (Halland et al., 2011).

The most crucial factor for the long-term efficiency of a geological storage reservoir is the integrity of the sealing caprock and there are two geotechnical incidents with special importance for the storage of CO₂ within saline aquifers, these occurred at the Tordis Field (Norwegian North Sea) in 2008 and at the In Salah (Algeria) CO₂ storage site between 2004 and 2011 respectively. The Tordis incident was discovered by oil slicks on the sea surface, which could be related to a 20 m-wide seafloor crater in the vicinity of the seafloor installations of the Tordis oil production site (Eidvin and Øverland, 2009). Wastewater from oil production was originally supposed to be injected in the Utsira Formation, but due to interpretation ambiguities the injection targeted glacial sediments of the Nordland Group, which have poor reservoir quality resulting in the hydrofracturing of the overlying sediments (Eidvin and Øverland, 2009). The fact that the injection did not target the Utsira Formation and that it was water and not hypercritical CO₂ that was injected at Tordis has to be taken into account when comparing the injection activities at Sleipner and Tordis. However, it is a proof that it is possible to breach the Nordland Group sediments, which represent the seal of the Sleipner CO₂ storage operation. The

potential overburden integrity problems at In Salah were detected after injection stopped in 2011 by seismic, interferometric synthetic aperture radar and wellbore observations, which indicated hydrofracturing of the lower seal above the storage formation (White et al., 2014).

There are no reports of any comparable incidents or other technical problems for the CO₂ storage operation at Sleipner. The publicly available time-lapse seismic dataset (pre injection till 2008) does not show any evidence for CO₂ leakage from the Utsira Formation (Arts et al., 2008; Boait et al., 2012; Chadwick et al., 2009; 2012; 2014). However, there are several natural, seal-crosscutting, fluid conduits known as seismic chimneys in the study area, which have already been noted by Heggland in 1997. An extensive fluid flow analysis of the greater Sleipner area in the Southern Viking Graben (SVG) revealed the presence of 46 vertical seismic anomalies, which most likely represent the seismic image of focused fluid conduits (Karstens and Berndt, 2015). These structures are as proximal as 7 km to the CO₂ injection point and have not been integrated in publicly available risk assessment.

The overall aim of this paper is to evaluate the relevance of large chimney structures on the long-term storage safety at Sleipner and sub-seafloor CO₂ storage projects in general. The first objective is to evaluate the poorly understood hydraulic properties of chimney structures, and is based on information about the hydraulic properties from literature as well as multiphase fluid flow simulation performed with the DuMux code (Flemisch et al., 2011).

The second objective is to assess, when and under which conditions CO₂ will reach potential fluid pathways and ultimately the seafloor. For this purpose, we extract the CO₂ plume from the Sleipner time-lapse seismic dataset and use this information to perform an iterative history matching between CO₂ migration simulations and the CO₂ plume evolution for estimating the hydraulic properties of the Utsira Formation. These results are then used to extrapolate the CO₂ plume evolution for 200 years of CO₂ storage at Sleipner for an injection period of 30 years (realistic case) and for 200 years. The 200 years injection time aims at forcing the CO₂ to reach the chimney structures in order to study their interaction and to obtain more generalized information. Our final objective is to investigate the possibility of creating chimney-like blowout structures due to CO₂ injection at Sleipner.

4.2. GEOLOGICAL BACKGROUND

4.2.1. STUDY AREA AND THE LOCAL STRATIGRAPHY

The Sleipner area is located in the Southern Viking Graben (SVG), which is one of the most productive hydrocarbon provinces in the North Sea Basin. The SVG formed in late Jurassic to Early Cretaceous times as a branch of the North Sea failed rift system (Ziegler et al., 1992). Post-rift subsidence and uplift of the surrounding landmasses led to the deposition of prograding deltaic sequences into the deepened North Sea Basin from the Shetland Platform and West Norway in Oligocene and Miocene time (Eidvin et al., 2014). During the Late Miocene, the palaeogeographic setting remained stable for a period of 8 Ma and a large eastward-prograding system deposited the 250 – 300 m thick Utsira Formation in a high energy, shelf environment (Galloway, 2001; 2002; Eidvin and Rundberg, 2007; Eidvin, et al., 2014). The Utsira sand is intersected by thin, low permeable and apparently fractured mudstone layers, which have a strong impact of the evolution of the CO₂ plume (Chadwick et al., 2009; Cavanagh and Haszeldine, 2014). The main Utsira sand body is covered by a >5m thick mudstone layer, which separates it from another sand layer hosting the shallow-most layer of the CO₂ plume (Cavanagh, 2013). The Utsira Formation consists of poorly cemented, fine-to-medium grained, moderately sorted sand, which is mainly composed of angular to rounded quartz grains with minor K-feldspars, plagioclase, calcite, coarse to gravel-sized shell fragments and only little clay-grade material (Audigane et al., 2007). The Utsira Formation has excellent reservoir properties characterized by a porosity of 35 – 40% and a permeability of 1000 – 3000 mD (Chadwick, et al., 2004).

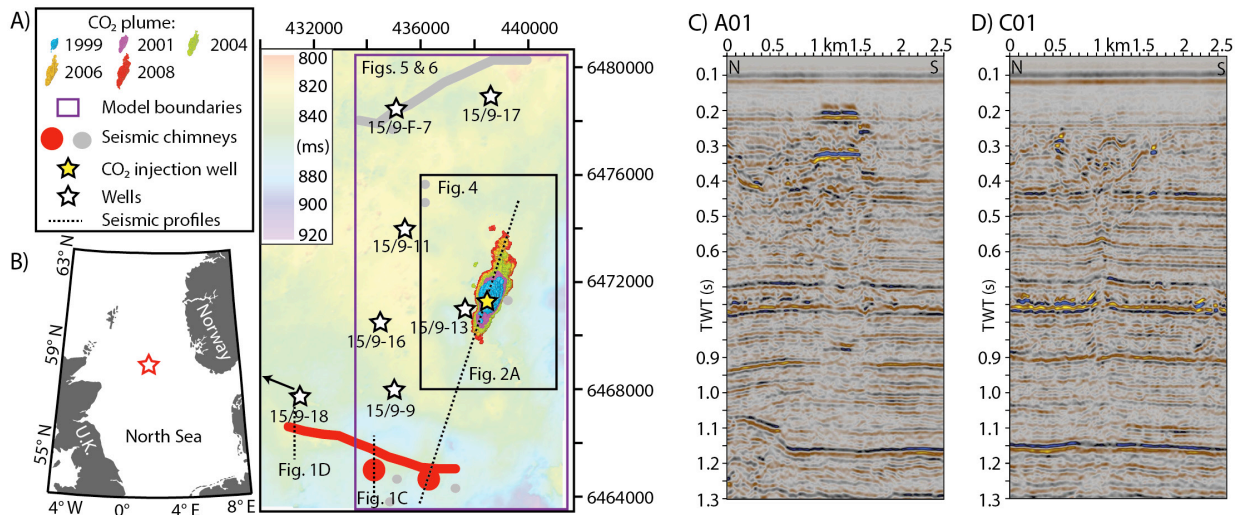


Fig. 4.1: A) Map of the study area showing the extent of the model boundaries (purple), seismic chimneys (red: with connection to the Utsira Formation; grey: without connection to the Utsira Formation; based on Karstens and Berndt, 2015), wells (white stars), the CO₂ injection point (yellow star), the growing CO₂ plume and seismic profiles shown in this study (black dashed lines). B) Overview map of the North Sea showing the location of the study area. C) Seismic profile showing chimney A01. D) Seismic profile showing chimney C01.

The Utsira Formation is directly overlain by the Nordland Shales, which form the Quaternary section with a thickness of more than 800 m in the Sleipner area. The boundary between Utsira Formation and Nordland Shales marks the beginning of glacially influenced sediments in the SVG (Ottesen et al., 2014), which is characterized by the deposition of the 50 – 150 m-thick Shale Drape, which consists of grey mudstones with high clay content in the Sleipner area (Chadwick et al., 2004; Gregersen and Johannessen, 2007). Rock physical tests on a Nordland Shale sample from the Sleipner area revealed a capillary entry pressure of 1.6 – 1.9 MPa for CO₂, a permeability of 4×10^{-10} mD perpendicular and 10^{-9} mD parallel to bedding (Harrington et al., 2009). A complex of prograding clinofolds sourced by distal-fluvial and fluvial-glacial sources overlies this unit (Ottesen et al., 2014; Gregersen and Johannessen, 2007). The Quaternary succession is divided by an unconformity (Ottesen et al., 2014), which marks the base of glacially reworked sediments of Pleistocene age that are characterized by frequent tunnel valley incisions (Huuse and Lykke-Andersen, 2000; Lonergan et al., 2006).

4.3. DATA AND METHODS

4.3.1. SEISMIC AND WELL DATA

Our fluid flow simulations base on seismic interpretation of the regional industry 3D seismic cube ST98M3 and the Sleipner time-lapse benchmark dataset provided by Statoil for scientific usage (Fig. 4.1). ST98M3 was used for interpreting the most important seismic horizons and mapping seismic chimneys as potential fluid flow conduits.

The time-lapse 4D seismic data set includes 3D seismic cubes from prior injection, 1999 (3 years after injection started), 2001, 2004, 2006 and 2008 and was used to constrain the evolution of the plume shape with time. For this purpose, we calculated the difference between the 3D seismic amplitude distributions of the different time-steps and the pre-injection vintage and thereby extracted the 3D shape of the CO₂ plume (Fig. 4.1). This information is particularly important for ground-truthing the plume dynamics of our simulations and thereby testing the hydraulic parameterization of the model.

For our analysis, we had access to well paths and well check-shots of 6 local wells (15/09-9, 15/09-11,

15/09-13, 15/09-15, 15/09-16, and 15/09-17). This information was used to compile an averaged time-depth correlation for the local stratigraphy (Fig. 4.3b), which was used to convert the seismic data including the interpreted horizons from time into depth domain.

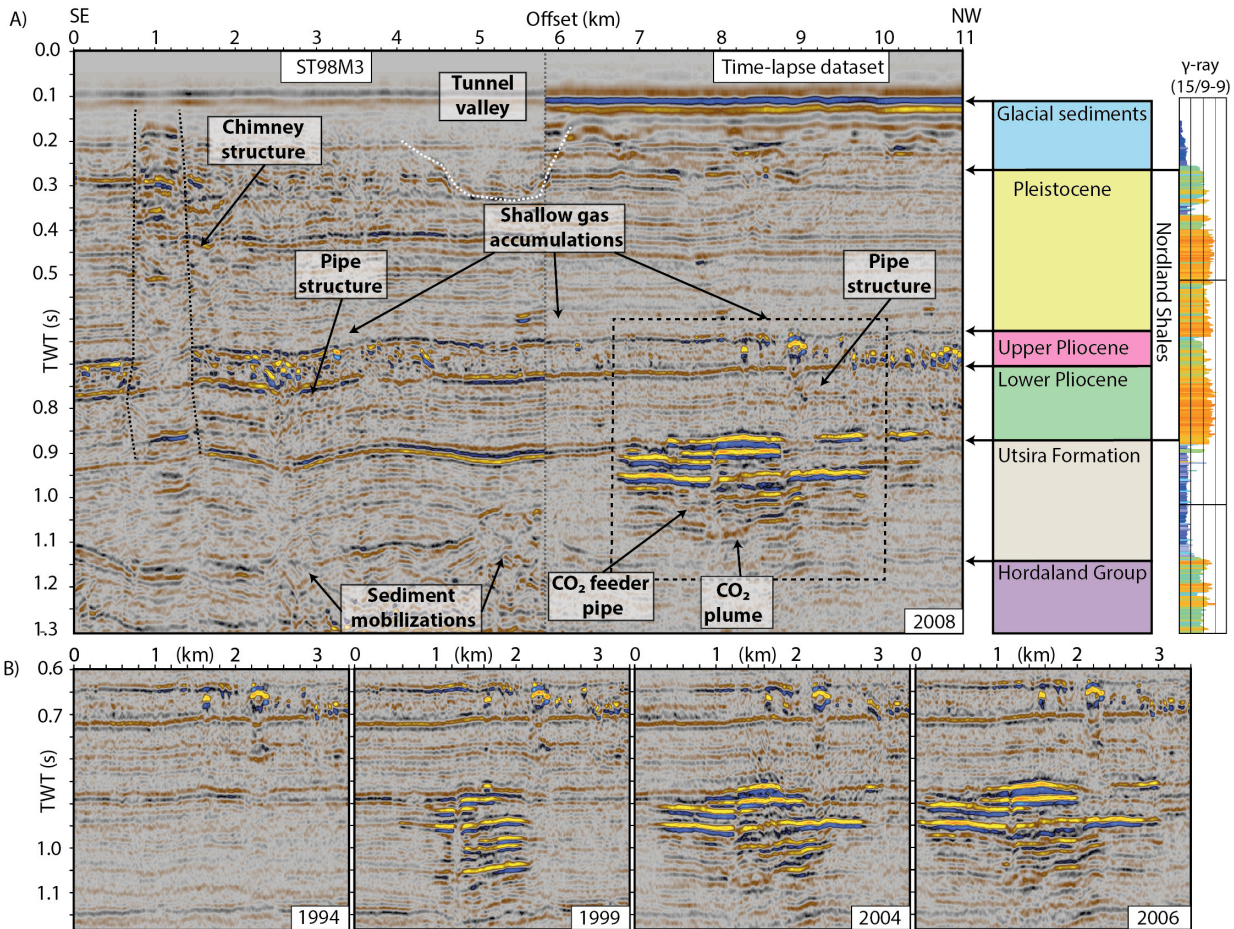


Fig. 4.2: A) Seismic profile showing the CO₂ plume from 2008, a chimney structure and other fluid flow associated seismic features; the seismic profile was merged from ST98M3 (left side) and the Sleipner time-lapse dataset (right side). B) Stratigraphy of the study area with gamma-ray log from well 15/9-9. C) Seismic profiles from the Sleipner time-lapse dataset showing the area highlighted by the dashed box in A) from 1994, 1999, 2004 and 2006.

4.3.2. SEISMIC OBSERVATIONS

The Sleipner area hosts a multitude of fluid flow manifestations including gas accumulation, sediment mobilizations, narrow pipe structures and large chimney structures (Fig. 4.1 and 4.2; Heggland, 1997; Nicoll, 2011; Karstens and Berndt, 2015). The interaction of CO₂ with these existing shallow fluid flow structures constrains the long-term performance of the storage operation and is monitored by the time—lapse seismic experiment. There are several small pipe structures with overlying bright spots in the direct vicinity of the injection site (Fig. 4.1 and 4.2), which show no seismically detectable changes with ongoing injection. This indicates that the naturally trapped gas did not migrate (at least detectably) and that CO₂ has not infiltrated these pipe structures. Therefore, we consider these pipe structures as not connected to the CO₂ injection system or impermeable and did not integrate them as conduits in our models. The large chimney structures are not covered by the time-lapse data and it is not possible to evaluate their response to the injection activity. These structures have a far more complex internal architecture and it is possible to differentiate between two types of chimney structures. Type A is interpreted to represent large gas pipes, which formed as result of over-

pressure and partly mobilized the cross-cut sediments, while type C may represent elongated fluid conduits including the displacement or liquefaction of reservoir matrix (Karstens and Berndt, 2015).

4.3.2. MODELING

4.3.2.1. MODEL BUILDING

Based on the seismic observations, we decided which fluid flow related features have to be considered in the geological models. We did not include the small pipe structures and focused on the large chimney structures, which show evidence for having a direct connection to the Utsira Formation. The interpretation of type A is comparably robust, while it is not possible to exclude that type C only represents seismic artifacts (Karstens and Berndt, 2015). To address this, we have performed both simulations including and excluding type C. The geological models were based on the seismic dataset ST98M3 and created using Petrel. The first step was to interpret the seismic horizons, which correspond to the boundaries between the most important sedimentary units (Fig. 4.2) including the seafloor, the base of the glacially deformed sediments (base of tunnel valleys), the top Pliocene, a prominent Intra-Pliocene reflection and the top and the base of the Utsira Formation. The boundaries of the sand and shale wedges were seismically not traceable and were added as artificial horizons by upward shifting copies of the top Utsira reflection by 10 and 20 m. These seismic horizons were converted from time to depth domain using an averaged time-depth relationship obtained from well check-shots (Fig. 4.3b). The depth-converted horizons were used to create the model grid with a grid-cell size of 50 m x 50 m and the model zones using Petrel. The cell-size was limited by the maximum number of nodes of the DuMux code (at this time one million) and the requirements of the model to cover the injection site, the seismic chimneys as well as a sufficiently large area around to model the plume evolution. The model zones were subdivided into layers and populated with values for porosity, lateral and vertical permeability applying a Gaussian value distribution (Tab. 4.1). The chimney structures were integrated as cylindrical structures extending from the top of the Utsira reflection to the base of the glacial sediments and their shapes were defined by polygons. The hydraulic parameters assigned to these structures are listed in Tab. 4.1. Finally, all zones and the chimneys were populated with an index parameter, which was later used for adding additional parameters and scaling properties in the DuMux code (Tab. 4.1).

Tab. 4.1: Model zones and parameters

Zone	Model	Porosity	Permeability	Permeability
		(%)	lateral (mD)	vertical (mD)
Glacial sediments	II, III	10.5 ± 1.875	600	120
Pleistocene	II, III	0	0	0
Upper Pliocene	II, III	3.5 ± 0.625	200	40
Lower Pliocene	II, III	0	0	0
Sand wedge	II, III	35 ± 6.25	2000	400
Shale wedge	I - III	0	0	0
Utsira Formation	I - III	35 ± 6.25	2000	400 -2000
Chimneys	II, III	35 ± 6.25	10 - 2000	10 - 2000

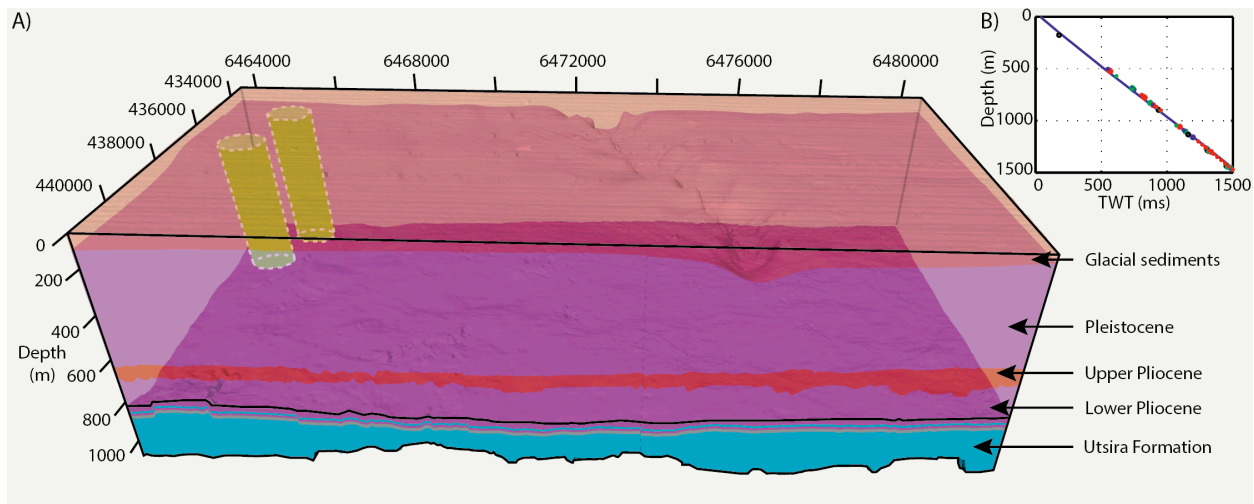


Fig. 4.3.: A) The geological models used for the simulations. B) Time-depth chart used for conversion.

4.3.2.2. MODELING OBJECTIVES

We created different sub-models for specific simulation objectives, which all were based on the previously described setup and parameterization (Fig. 4.3). The first modeling objective was the determination of the permeability field of the model by iterative history matching with the seismically derived CO₂ plume extents. For this purpose, we created Model I, which only includes the Utsira Formation and the shale wedge. The second objective was to model the plume evolution over a period of 200 years for an injection duration of 30 and 200 years without the potential influence of the chimney structure. For this purpose, it is - again - not necessary to include the entire overburden, and we could continue using Model I. The third modeling objective was to analyze the influence of chimney structures and to simulate the leakage of CO₂ along these conduits. Models II and III cover the same area as Model I, but include the entire overburden. Model III includes type-A and type-C-chimneys, while Model IV only includes type-A chimneys.

4.3.2.3. MODEL SETUP IN DUMUX

The fluid flow simulations were performed with the numerical simulator DuMux (Flemisch et al., 2011), which was designed specifically for flow and transport of multiple fluids through porous media and is based on DUNE (Distributed and Unified Numerics Environment; Bastian et al., 2008). The DuMux module applied for this study uses a fully implicit two-phase flow model with the water pressure and the CO₂ saturation as primary unknowns. The spatial discretisation of the balance equations (formulated on the Darcy scale) is done with the BOX method, which is a subdomain collocation method on a dual-mesh approach that has linear Finite-Elements shape function and piece-wise constant weighting functions, thus providing a mass-conservative Finite-Volume-like scheme. A Newton-Raphson method with adaptive time-stepping according to the convergence behaviour is applied to handle non-linearities. The geological model grids were imported into DuMux preserving the model geometry defined in Petrel. For the initial conditions and the boundary conditions, a hydrostatic pressure distribution based on a seafloor depth of 80 m and a fully brine saturated pore space are assigned. Top and bottom boundary were considered as no-flow boundary, and a temperature gradient of 31.7°C/km (Alnes et al., 2011) was applied for calculating the pressure and temperature dependent densities. Brooks-Corey relationships to calculate the capillary pressure with an entry pressure of 4 kPa for the Utsira Formation and 1.7 MPa for the overburden (Cavanagh and Haszeldine, 2014) were used. The most relevant model parameters are listed in Table 4.2.

Tab. 4.2: Background model parameters

Parameter	Value	Reference
Injection rate	1 Mt/a	
Injection depth	1012 m	Sing et al., 2010
Seafloor depth	80 m	
Seafloor temperature	3.4 °C	Alnes et al., 2011
Thermal gradient	31.7 °C/km	Alnes et al., 2011
Capillary entry pressure (Utsira Formation)	4 KPa	Chadwick et al., 2012
Capillary entry pressure (caprock)	1.7 MPa	Harrington et al., 2009
Swr	0.11	Sing et al., 2010
Snr	0.21	Sing et al., 2010

Tab. 4.3: Model list

Simulation	Model	KN-S (D)	KE-W (D)	KV (D)	PDA (°)	Injection duration (a)	Simulation duration (a)
A1	I	2	2	0.4	0	30	30
A2	I	2	1	0.4	0	30	30
A3	I	2	0.4	0.4	0	30	30
A4	I	2	0.2	0.4	0	30	30
A5	I	2	0.1	0.4	0	30	30
A6	I	2	0.2	0.4	15	30	30
A7	I	2	0.2	0.4	30	30	30
A8	I	6	0.6	0.4	30	30	30
A9	I	2	0.2	2	30	30	30
B1	I	2	0.2	2	30	30	200
B2	I	2	0.2	2	30	200	200
C1	II	2	0.2	2	30	200	200
C2	II	2	0.2	2	30	200	200
C3	II	2	0.2	2	30	200	200
C4	III	2	0.2	2	30	200	200
C5	III	2	0.2	2	30	200	200
C6	III	2	0.2	2	30	200	200
C7	III	2	0.2	2	30	200	200
C8	III	2	0.2	2	30	200	200
C9	III	2	0.2	2	30	200	200

4.4. RESULTS

4.4.1. RESERVOIR PARAMETERIZATION BY HISTORY MATCHING

In order to find the best parameters to reproduce the hydraulic properties of the Utsira Formation by history matching, we performed fifteen simulations. Their results are shown in Figure 4.4. These simulations have been iteratively changed in order to reproduce the results from the time-lapse seismic data. The simulations reveal that the Utsira Formation has a pronounced lateral permeability anisotropy. The best fit for the seismically-determined plume shape could be achieved by using a scaling factor KEW of 0.1 for the East-West direction and KNS of 1 for the North-South direction considering a background permeability of 2000 mD laterally and 400 mD vertically (Tab. 4.3; Fig. 4.4c). In the time-lapse seismic data, the plume spreads not perfectly in N-S direction, which is partly controlled by the topography of the top of the Utsira Formation (Fig. 1) and could be simulated by a declination of the permeability anisotropy from N-S of 30° (Fig. 4.4f).

While the plume shape could be reproduced successfully, the extent of the plume with time (the spreading velocity) could not be reproduced accurately. We increased the lateral background permeability by a factor of three, which had no significant impact (Fig. 4.4g). Therefore, we continued using 2000 mD as the lateral background permeability and increased the vertical permeability, which puts the flow of CO₂ to the top of the Utsira Formation (Fig. 4.4h). By using a vertical permeability of 2000 mD, we achieved good agreement with seismic observations of the plume evolution with time. Based on this, we continued using a vertical and horizontal permeability of 2000 mD, a lateral permeability anisotropy of 10:1 with an anisotropy declination angle of 30° for all following simulations as hydraulic reservoir parameters.

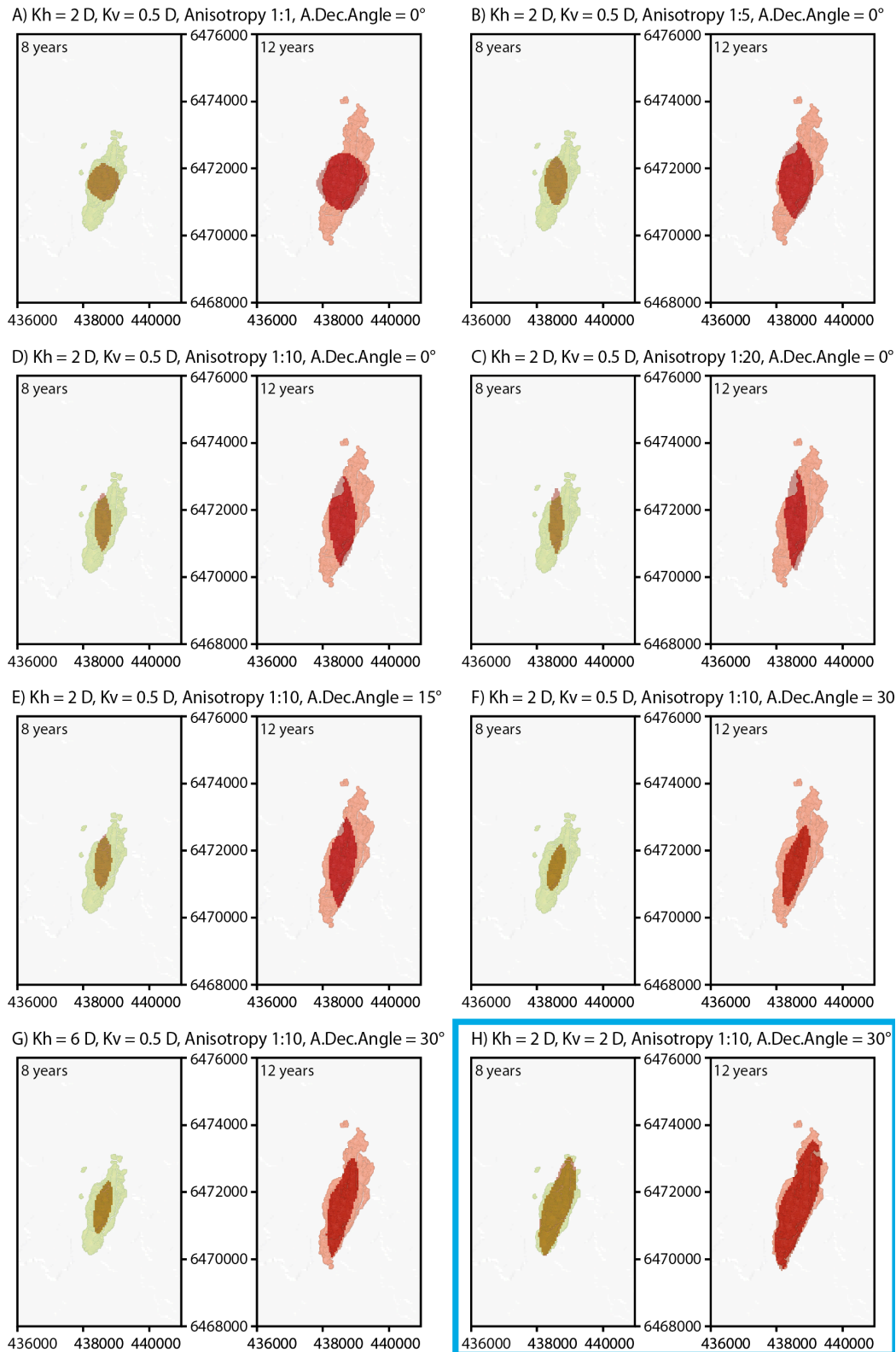


Fig. 4.4: Results of the history matching showing the seismically derived plume after 8 years (green plume), after 12 years (light red) and the simulated plume (dark red) using different values for horizontal permeability (KES and KNS), vertical permeability (KV) and permeability anisotropy declination angle: A) $KES=2000$ mD, $KNS=2000$ mD, $KV=500$ mD, $PDA=0^\circ$. B) $KES=500$ mD, $KNS=2000$ mD, $KV=500$ mD, $PDA=0^\circ$. C) $KES=200$ mD, $KNS=2000$ mD, $KV=500$ mD, $PDA=0^\circ$. D) $KES=100$ mD, $KNS=2000$ mD, $KV=400$ mD, $PDA=0^\circ$. E) $KES=200$ mD, $KNS=2000$ mD, $KV=400$ mD, $PDA=15^\circ$. F) $KES=200$ mD, $KNS=2000$ mD, $KV=400$ mD, $PDA=30^\circ$. G) $KES=600$ mD, $KNS=6000$ mD, $KV=400$ mD, $PDA=30^\circ$. H) $KES=200$ mD, $KNS=2000$ mD, $KV=2000$ mD, $PDA=30^\circ$.

4.4.2. LONG-TERM PLUME EVOLUTION SIMULATION

Based on the results of the history matching, we used Models I, II and III to evaluate the long-term evolution of the CO₂ plume. The migration of the CO₂ plume is primarily buoyancy-driven, resulting in an upward-flow of CO₂ towards the top of the Utsira Formation, where it gets deflected and then starts to migrate laterally (Fig. 4.5b). The lateral plume migration is similar in all long-term (200 years) simulations (Fig. 4.5c-e) and CO₂ continues to spread in NNE and SSW direction, which corresponds to the declination angle of the permeability anisotropy axis and topographic lows of the top of the Utsira Formation (Fig. 4.5d). The influence of both effects becomes obvious comparing the plume extent east and west of the spreading axis. The plume spreads much further on the western side, which is due to the influence of topography. Because the topography to the west of the axis is comparably flat, the CO₂ spreading is NNE-SSW directed, which is the result of the permeability anisotropy. Simulation B1 shows that the CO₂ continues spreading for the entire simulation duration of 200 years after stopping injection at 30 years (Fig. 4.5b). After 50 years, the CO₂ migration is mainly controlled by the topography of the top of the Utsira Formation and CO₂ fills the topographic highs, which leads to the irregular shape of the southern part of the plume. The plume growth is generally faster in north direction, which can be attributed to a slight southwards dip of the Utsira Formation (Fig. 4.2).

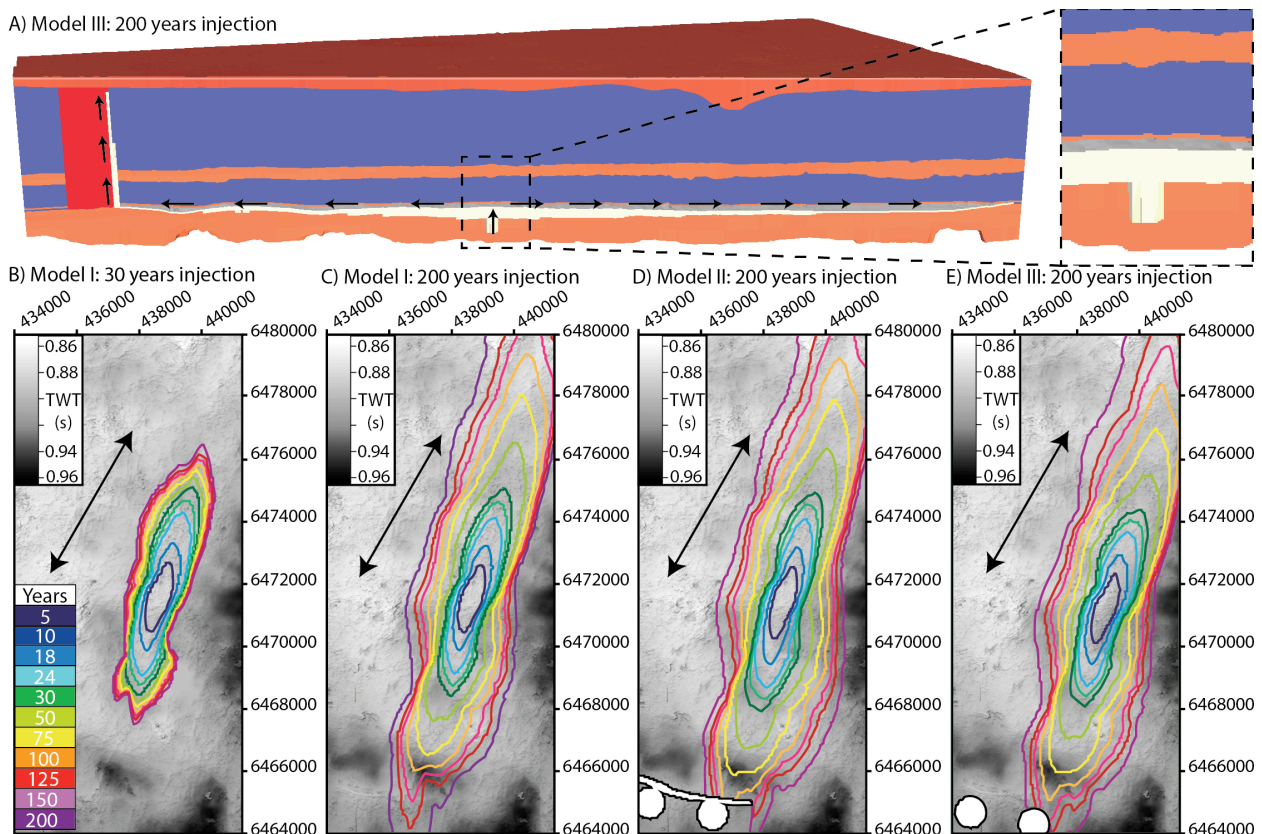


Fig. 4.5: A) Vertical profile cutting through Model III showing the migration of CO₂ (white) through the Utsira Formation and chimney A01. B) Plume evolution in Model I for an injection duration of 30 years and a simulation length of 200 years; black arrow indicate the permeability anisotropy. C) Plume evolution in Model I for a injection duration of 200 years and a simulation length of 200 years; black arrow indicate the permeability anisotropy. D) Plume evolution in Model II for a injection duration of 200 years and a simulation length of 200 years; black arrow indicate the permeability anisotropy. E) Plume evolution in Model III for a injection duration of 200 years and a simulation length of 200 years; black arrow indicates the permeability anisotropy.

The plume shapes of simulations B2 and C1 fit well with B1 for the first 30 years. While the plume growth after 30 years significantly decelerates for B1, the growth preserves its velocity for the simulations with ongoing injection. The influence of minor permeability heterogeneities due to the Gaussian value distribution, which was independently applied during model building, become obvious, when comparing B2 and C1. The plume evolution for the period between 30 and 100 years shows differences, while their overall trends are similar. The presence of chimney structures in C1 and C2 influences the plume evolution after 100 years in the near-field of the vertical conduits, but appears not to change the overall flow pattern.

Comparison of the simulations C1 and C2, which use exactly the same permeability field, reveals a high reproducibility of the simulations (Fig. 4.5d, e). Figure 4.6 shows the simulation results of C1 and C2 in three dimensions and in plan view. The plume shapes as well as the CO₂ saturations are very similar and only differ in the near-field of the chimney structures. The CO₂ saturation has its highest values within the chimney structures, which can most likely be attributed to the high permeability of 2000 mD facilitating the entry of CO₂.

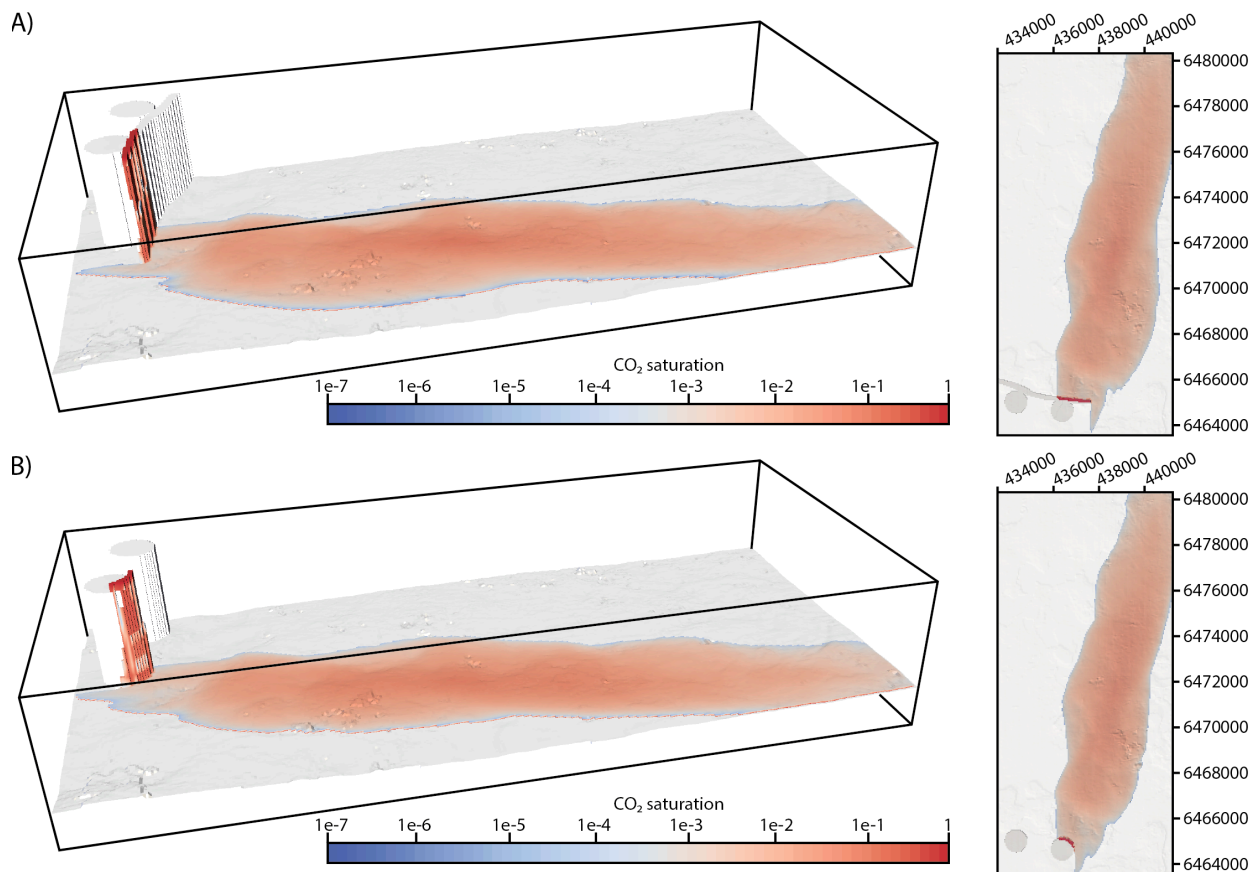


Fig. 4.6: A) 3D view of long-term simulation using Model III after 200 years of CO₂ injection. B) 3D view on long-term simulation using Model IV after 200 years of CO₂ injection.

4.4.3. LEAKAGE AT THE SEAFLOOR

By continuing CO₂ injection for 200 years, it is possible to force the CO₂ to interact with the chimney structures. The simulations reveal that CO₂ will use the chimneys as pathways towards shallower depth and enter the glacial sediments, which are located at the top of the chimney structures in our model. Since the glacial sediments are considered to be highly permeable, the CO₂ continues to rise and ultimately reaches the seafloor. The seafloor CO₂ flow rates for the entire simulation duration of models C1 to C9 are plotted in Figure 4.7. The simulations C1 to C3, which consider type-A and type-C-chimneys, show correlation between

permeability and the rate and onset of leakage (Fig. 4.7a). The type-C-chimney is closer to the spreading CO₂ plume than type-A and CO₂ reaches the type-C-chimney structure earlier at about 80 years. Depending on the chimney permeability, the CO₂ requires at least 12 years to reach the surface even using an extremely high permeability of 2000 mD. For 100 mD, the migration time through the chimney is about 35 years. The slope of the leakage curves is very similar for all three permeability values indicating that the chimney permeability only influences the onset of leakage and not the leakage rate evolution.

In simulations C4 to C9 only type-A-chimneys are implemented and the CO₂ uses the eastern chimney for leakage (Fig. 4.6b). The leakage curves show again a correlation between permeability and leakage onset and similar leakage curve slopes for different chimney permeability values. However, the difference between the leakage onset for 100 mD and 200 mD of C5 and C6 is significantly smaller compared with simulations C2 and C3. Simulations C7, C8 and C9 show that even comparably low chimney permeability values of 10 mD result in surface leakage and that the leakage curves are similar to high permeability simulations.

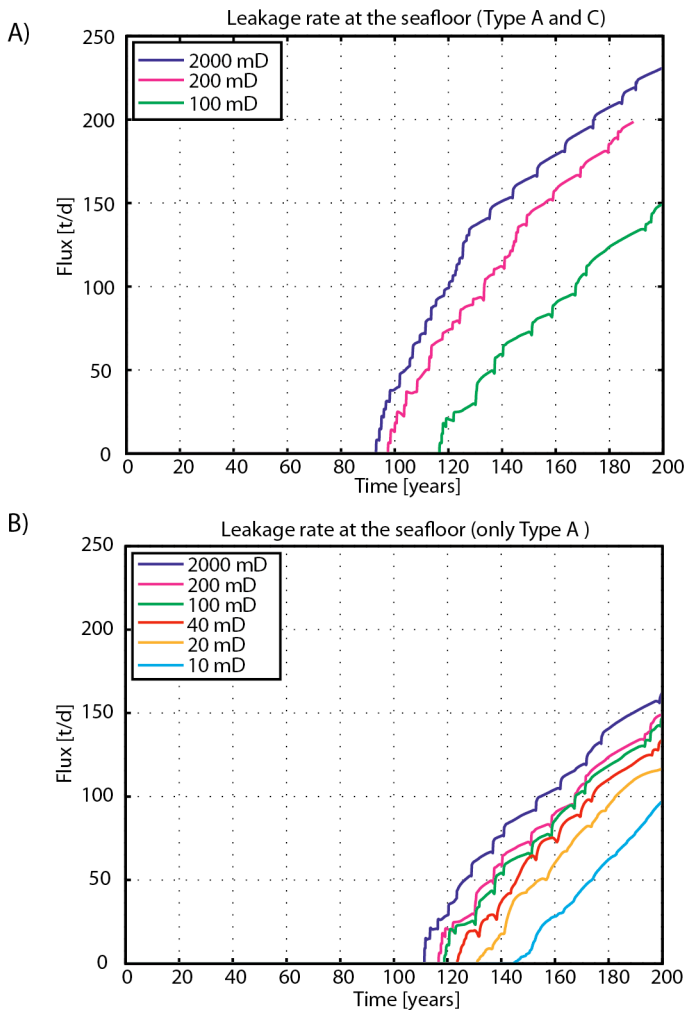


Fig. 7: A) CO₂ leakage rate at the surface for different chimney permeability values for Model II (type-A and type-C-chimneys). B) CO₂ leakage rate at the surface for different chimney permeability values for Model III (type-A-chimneys).

4.5. DISCUSSION

4.5.1. EVALUATION OF MODELS AND SIMULATIONS

4.5.1.1. SIMPLIFICATIONS AND LIMITATIONS

In contrast to other published simulations of the evolution of the Sleipner CO₂ plume (Chawick and Noy, 2010; Cavanagh, 2013; Zhang et al., 2014, Zhu et al., 2015), our main aims were (i) to analyze the process of leakage along existing chimney structures and (ii) to find the limits of its propensity. For this purpose, our model had to cover the most relevant chimney structures, the injection site itself and a sufficiently large area around. These requirements and the limited computational resources resulted in a comparably coarse (50 m x 50 m) lateral grid size and a limited number of model layers. As a result, the models could not implement the internal shale layers of Utsira Formation, which represent significant permeability barriers. However, the time-lapse seismic monitoring has revealed the formation of a pipe structure (Chadwick et al., 2010), which crosscuts the shale layers. It further showed that the CO₂ flow focuses on the upper layers of the Utsira Formation. The bulk hydraulic properties within the uppermost sand layers could be successfully reproduced by history matching and are in good agreement with parameters in literature.

Our history matching attempts and the leakage simulations build only on the variation of the permeability field, while other factors such as porosity, capillary entry pressure, reservoir pressure variation, fluid viscosity or temperature were not varied. The permeability field itself included four degrees including, the vertical permeability, the horizontal bulk permeability, the horizontal permeability anisotropy and its declination angle. This focus on permeability was possible, because most other parameters were already well determined by previous studies. Our simulations did neither include the dissolution of CO₂ in the brine nor did we implement other physical or chemical processes, which would change the viscosity of the CO₂. Therefore, we would like to stress that our simulations represent simplified “worst case” end members within a complex parameter space. Prediction of realistic leakage rates would require models that include these processes and it would require more knowledge about the actual permeability of the fluid pathways, which are not available to us at present. We perceive distribution of permeability and distinct geologic features as the main parameters of influence for leakage, and – accordingly – uncertainty reduction should have its primary focus on these, see also in Walter et al. (2012) and Class et al. (2009).

The Viking Graben is the site of a wide range of hydrocarbon exploration and production activities. Some use the Utsira Formation as a water source for enhanced hydrocarbon recovery (e.g. Volve field, Norwegian Petroleum Directorate) or as a storage formation for waste-water (Tordis; Eidvin and Øverland, 2009). The formation water production at Volve takes place only ~ 7.5 km from the Sleipner CO₂ injection site and is likely to influence the pressure field in the Utsira Formation. However, it is not reported, whether or not the Volve and Sleipner operations affect each other and if so, how large this effect is. Due to the absence of direct measurements, our simulations do not include the effects of nearby exploration activities or pressure variations in general.

4.5.1.2. IMPLICATIONS OF HYDRAULIC PROPERTIES OF THE UTSIRA FORMATION

Taking all these limitations and simplifications into account, our simulations were successful in reproducing the plume growth for the first twelve years of CO₂ injection and the chosen permeability field could reproduce the bulk permeability parameters of the Utsira Formation. The growth of the CO₂ plume documented by the time-lapse seismic experiment and the numerical simulations reveal a pronounced lateral permeability anisotropy, which appears to have a similarly strong influence on the CO₂ migration as the topography of the top of the Utsira Formation. By using an isotropic permeability field, it is not possible to reproduce the observed CO₂ plume (Fig. 4a). Other groups before us made similar observations and the permeability anisotropy was

previously attributed to uncertainties of the top Utsira horizon topography (Chadwick and Noy 2010; Zhu et al., 2015) or an additional plume internal fluid conduit (Zhang, et al., 2014; Zhu et al., 2015). There is no evidence for each of the explanations in the time-lapse seismic data. We interpret the permeability anisotropy as the result of the depositional system in which the Utsira sands have been emplaced.

The Utsira Formation was deposited during the Middle to Late Miocene, when the North Sea was a shallow shelf sea with water depths of 100 m to 200 m in the Viking Trough and connection to the North Atlantic via the Viking Street (Galloway, 2001; 2002). The large eastward-prograding, deltaic system, which deposited the Utsira sands, was influenced by periodic sea-level changes that deposited intersecting mudstone layers, which correspond to calmer depositional conditions (Gregersen and Johannessen, 2007). Such sea-level fluctuation will have caused coast parallel, prograding deposition of sand beds mainly sourced by the Shetland High in the east. Considering such a stratigraphic architecture, the permeability anisotropy is most likely the result of bedding-parallel flow within generally highly permeable sand layers. The history matching shows good agreement with the plume spread direction for an anisotropy declination angle of 30° from North. This correlates well with the orientation of the southern section of the Utsira Formation (Gregersen and Johannessen, 2007), which is controlled by the orientation of the rift axis of the SVG.

History matching revealed that the reconstruction of the plume evolution from time-lapse seismic data requires a comparably high vertical permeability. This is in good agreement with observed development of a pipe structure, which crosscuts the shale layers and is apparent in the time-lapse seismic data (Fig. 2.). A vertical permeability of 2000 mD allows an unhindered, buoyancy-controlled upward migration from the injection point, which is likely the case for the Sleipner CO₂ plume after the formation of the internal feeder pipe structure.

4.5.2. HYDRAULIC PROPERTIES OF CHIMNEY STRUCTURES

Chimney structures are interpreted as the seismic expression of focused fluid flow conduits that bypass an impermeable seal (Cartwright et al., 2007; Løseth et al, 2009, Karstens and Berndt, 2015). There are no direct measurements for the permeability of focused fluid conduits during their formation or for the short- and long-term permeability evolution after the active discharge of fluids. There are indications that at least some conduits may have lost their high permeability after the fluid discharge had stopped and become plugged and inactive (e.g. offshore Namibia; Løseth et al., 2011). Other conduits remain active and the venting of fluids appears to be a continuous process (e.g. Tommeliten; Schneider von Deimling et al., 2011).

There is a multitude of factors, which may control, why one vent site shuts down after a single, rapid fluid release event and others remain active including the evolution of overpressure, the long-term availability of mobile fluids, or the seals ability for closing the conduit by mineralization or consolidation of mobilized sediments. However, the most important control is the nature of the conduit itself. Although the focused fluid conduits have a very similar appearance in seismic data, they may represent fundamentally different geological structures, such as fracture networks (Granli et al., 1999; Arntsen et al. 2007), sediment injections (Hurst et al., 2011) or blowout pipes (Bünz et al., 2003; Løseth et al., 2011).

These different types of conduits are likely having different implications on the long-term evolution of their hydraulic properties (Karstens and Berndt, 2015). However, the hydraulic properties, especially the long-term permeability of focused fluid conduits, are only poorly determined by direct measurement and an evaluation of the permeability of chimney structures has to rely on indirect observations. The narrow pipe structures above the CO₂ plume offer a first indicator for the permeability of focused fluid conduits in the model area. These structures show no changes in the time-lapse seismic data, which indicates that no CO₂ has entered these structures implying very low permeability. As mentioned before, we simulated models including and

excluding the type-C-anomaly in the south, because it cannot be excluded that this structure represents an imaging artifact. If this structure has a geological origin, the internal upward-bended reflections indicate a rapid emplacement comparable to the formation of pipe structures (Bünz et al., 2003; Løseth et al., 2011; Karstens and Berndt, 2015), which may indicate a low long-term permeability for this type of structure as well.

The formation of type-A-chimneys most likely occurred comparably rapid indicated by bended reflection and sharp edges (Karstens and Berndt, 2015). In contrast to the narrow pipe structures and type-C, there are indications that their formation involved the fluidization of matrix material, which sank back in the conduit after overpressure was released and plugged the conduit indicated by downward-bended reflections and internal bright spots (Karstens and Berndt, 2015). The bright spots are of special interest, because they indicate that gas can (or could) enter the chimney structure, but is hindered to reach the seafloor due to internal flow barriers. In post-stack seismic data, it is not possible to quantify the amount of gas causing the bright spot, which may be an indicator for the minimal resistance against breaching of the internal barriers. Post-expulsion plugging may have reduced the permeability of the upper section of the conduit significantly, while no flow barriers are visible in the lower section of the chimney. Therefore, we suggest it is likely that gas (methane and CO₂) could enter this structure reactivating the conduit. Comparing both types of chimney structures, the reactivation and leakage appears more realistic for type A.

Figure 4.7 shows that even a comparably low chimney permeability of 10 mD is sufficient to facilitate leakage of CO₂ from a storage reservoir. Based on post-stack seismic data, it is impossible to determine the permeability of a chimney structure and only direct measurements by wellbores would allow estimation of its effective permeability. However, there are no observations, which would exclude a chimney permeability of 10 mD (or even higher) and the flow of CO₂ along reactivated chimney structures is a potential leakage scenario.

Our models integrate the chimney structures as homogenous, high permeable, cylindrical elements. Such a simplification may be valid for freshly emplaced sand injections, but appears unrealistic for fracture networks or plugged blowout pipes. Therefore, we would like to state clearly that the simulated conduits represent end members and the fluid pathways within large-scale fluid conduits are probably far more complex, but as yet completely unconstrained. The simulated leakage rate evolutions are very similar using very different chimney permeability values and only the onset of leakage appears to be affected by the chimney permeability. This observation may be surprising, because the amount of CO₂ entering the structures should depend on the conduit's permeability. However, the large dimensions of the modeled fluid conduits enable them to absorb all arriving CO₂ even for comparably low permeability values. These observations would be different for narrower chimney structures. The simulated leakage rates of 100 to 250 t/d are several magnitudes higher than leakage rates from natural seep sites (e.g. Tommeliten, North Sea: ~0.07 t/d; Schneider von Deimling et al., 2011), but in the same range as those measured at man-made blowout sites (e.g. 22/4b site in the North Sea: ~68.5 t/d more than 20 years after the blowout occurred; Leifer et al., submitted). We expect leakage rates of reactivated chimneys to be rather in the order of natural seepage sites than those of blowout sites.

4.5.3. CHIMNEY FORMATION AS THE RESULT OF CO₂ STORAGE

The formation of focused fluid conduits such as chimneys is mainly controlled by pore overpressure and initiates, when the pore pressure exceeds the seal resistance against capillary or fracture failure (Hubbert and Willis, 1957, Clayton and Hay, 1999; Cathles et al., 2010). Rock physical experiments revealed that the Nordland Shales have capillary entry pressure of 1.6 to 1.9 MPa for CO₂ (Harrington et al., 2009), which represents the threshold for breaching the seal above the Utsira Formation. Of course the strength of a seal depends on its weakest part (Cartwright et al., 2007) and it is possible that there are some pre-existing weakness zones where these measurements are not representative. However, there are no indications that the CO₂ injection has caused a significant increase of the pore pressure (<0.1 MPa) of the Utsira Formation, which may

be explained by its excellent reservoir quality and enormous extent (Chadwick et al, 2012). The injected CO₂ is lighter than the formation brine implying an upward-directed buoyancy force, which may be sufficient for breaching the seal, when the CO₂ column height exceeds 150 m.

On the other hand, the CO₂ feeder pipe structure cross-cutting the thin shale layers within the Utsira Formation, which is visible in the time-lapse seismic data (Fig. 2), proves that the hydraulic breaching of low permeability barriers by CO₂ is possible and actually occurred at Sleipner. Cavanagh and Haszeldine (2014) could show that failure threshold pressure for the shale layers must be around 0.05 MPa, which is more than thirty times lower than the values derived by Harrington et al. (2009). Such low permeability values for shales can be explained only by previous fracturing of the shale layers and potentially of the caprock as well (Cavanagh and Haszeldine 2014).

The potential of creating chimney structures by breaching the caprock above the Sleipner CO₂ storage site depends on its resistance against breaching, which is significantly different for apparently fractured (shale layers) and unfractured (specimen used for rock physical tests) material. Considering a uniformly strong (or weak) seal, we would expect the fracturing of the seal directly to occur above the CO₂ feeder pipe structures, because the focusing of the CO₂ at this point. There is no indication in the seismic data that the stress related to the CO₂ upward-flow has caused any breaching of the seal so far and there is no reason that the strain should increase in the future, while the seal's resistance against capillary or fracture failure should be constant.

Therefore, it appears unlikely that the storage of CO₂ at Sleipner may create chimney structures, because rock physical tests have revealed a high bulk resistance against breaching and possible weakness zones would have been already activated, which can be excluded by the seismic data (at least until 2008, when the last of the repeat surveys available to us was acquired). Nevertheless, the effect of undetected weakness zones further away from the injection point cannot be constrained and the presence of large “natural” chimney structures in the study area prove the potential of breaching and bypassing the entire seal by focused fluid conduits.

4.5.4. PROPENSITY OF CO₂ LEAKAGE ALONG CHIMNEY STRUCTURES AT SLEIPNER

The propensity of CO₂ migration along chimney structures depends on the likelihood of the reactivation of existing chimney structures by migrating CO₂ and the formation of new chimney structures as a direct result of the injection of CO₂. Both scenarios are potential leakage scenarios for the geological storage of CO₂ and the events at In Salah and Tordis have shown that the reservoir's response to the injection of fluids is sometimes unpredictable and technically challenging (Eidvin and Øverland, 2009; White et al., 2014). However, the propensity of both leakage scenarios appears to be small at Sleipner. The creation of chimneys by the injection of CO₂ requires pore overpressures that are many times higher than the expected, measured and modeled values. Although, it is not sure, if the rather conservative values determined by rock physical tests are representative for the entire seal. However, the fact that no seal-crosscutting chimney has been formed so far is a very strong argument against this scenario, but does not provide any guarantee.

The possibility that CO₂ will reach the existing chimneys structures is much easier to control by monitoring and can be influenced by the operation itself and was constrained by our models. The simulation using an injection duration of 30 years shows that no CO₂ will reach the chimney structures within the next 200 years. This simulation even neglects dissolution of CO₂, which would further reduce the plume growth and most likely its final size. Only by continuing CO₂ injection with a constant injection rate over an unrealistic long time could leakage of CO₂ along existing chimney structures be induced. However, it may be possible that the ongoing storage operation may reactivate existing chimney structures. In this case injection may induce the release of water and potentially methane from shallow strata at the seafloor, but not release of CO₂.

4.6. CONCLUSIONS

The study area hosts a multitude of large-scale chimney structures with apparent connection to the Utsira Formation, which are located as close as 7 km to the injection point of CO₂ at Sleipner East. The growth of the CO₂ plume is monitored by time-lapse seismic experiments; its extension was used to find estimates for the permeability field of the Utsira Formation by iterative history matching using the numerical fluid flow simulator DuMux. The growing CO₂ plume shows a pronounced elliptical shape, which is the result of the topography of the top Utsira horizon and a lateral permeability anisotropy of 10:1 between N-S and E-W. The anisotropy is oriented NNE – SSW (with a declination of 30° from N), which may have been controlled by the orientation of the depositional system of the Utsira Formation and roughly corresponds to the spreading axis of the Viking Graben. Furthermore, history matching could show that the CO₂ plume internal feeder pipe facilitates a fast upward migration of CO₂ from the injection point to the top of the Utsira Formation.

Our long-term simulations show that CO₂ will never reach the existing chimney structures assuming the present-day injection rate and planned operation duration. These simulations have to be considered as conservative as they do not implement the dissolution of CO₂. Only after continuing injecting CO₂ for more than 90 years, CO₂ would reach the chimney structures and ultimately the seafloor. It is not possible to determine the chimney permeability based on seismic observation or numerical simulation results. The simulated peak leakage rates are several magnitudes higher than leakage rates observed at natural seep sites and of the same order of magnitude as those estimated for blowout sites in the North Sea. As these are the results of worst-case scenarios, the probability of such leakage is indeed very low. However, estimation of realistic leakage rates would require much more detailed information on the geological model, i.e. primarily the permeability field and geologic structures, and – if the latter is available - more sophisticated modeling approaches including the chemical reactions between CO₂ and the host rock. The minor pore pressure increase by the injection of CO₂ and rock physical tests on a caprock mudstone sample suggests that the formation of injection-related seal-crosscutting chimney structures as the result of CO₂ at Sleipner is very unlikely. The leakage of CO₂ along chimney structures (pre-existing or man-made) is a relevant leakage scenario, but its propensity is low at Sleipner. However, our study highlights the importance of detailed site surveys for future CCS sites and that the understanding of the palaeo fluid flow system is just as important as determining the reservoir and seal quality for evaluating CO₂ storage site. In general, we would recommend avoiding areas with pronounced palaeo fluid flow, especially chimney structures, to ensure an optimal long-term performance of the injection and storage operation. If this is not possible, it is crucial to determine the hydraulic properties of focused fluid conduits in order to allow a reliable leakage risk assessment.

ACKNOWLEDGEMENTS

We would like to thank Statoil Petroleum AS, ExxonMobil Exploration & Production Norway AS, and Total E&P Norge AS for making the Sleipner time-lapse dataset available. Furthermore, we would like to thank Statoil Petroleum AS and the Norwegian Petroleum Directorate for providing access to the 3D seismic dataset ST98M3 and the several wellbore data. This study was funded within the framework of the ECO2 project by the European Community's Seventh Framework Programme [FP7/2007-2013] under grant agreement n° 265847.

REFERENCES

- Alnes, H., Eiken, O., Nooner, S., Sasagawa, G., Stenvold, T., & Zumberge, M. (2011). Results from Sleipner gravity monitoring: Updated density and temperature distribution of the CO₂ plume. *Energy Procedia*, 4, 5504–5511.
- Arntsen, B., Wensaas, L., Loeseth, H., & Hermanrud, C. (2007). Seismic modeling of gas chimneys. *Geophysics*, 72(5), SM251–SM259. doi:10.1190/1.2749570
- Arts, R. J., Chadwick, R. A., Eiken, O., Thibeau, S., Nooner, S., Lamont-Doherty Geological Observatory of Columbia University. (2008). Ten years' experience of monitoring CO₂ injection in the Utsira Sand at Sleipner, offshore Norway.
- Audigane, P., Gaus, I., Czernichowski-Lauriol, I., Pruess, K., & Xu, T. (2007). Two-dimensional reactive transport modeling of CO₂ injection in a saline aquifer at the Sleipner site, North Sea. *American Journal of Science*, 307(7), 974–1008. doi:10.2475/07.2007.02
- Audigane, P., Gaus, I., Pruess, K., & Xu, T. (2006). A long term 2D vertical modelling study of CO₂ Storage at Sleipner (North Sea) using TOUGHREACT, 17, 2006.
- Bastian, P., Blatt, M., Dedner, A., Engwer, C., Klöfkor, R., Kornhuber, R., Ohlberger, M., & Sander, O. (2008). A Generic Grid Interface for Parallel and Adaptive Scientific Computing. Part II: Implementation and Tests in DUNE. *Computing*, 82(2-3), pp. 121-138.
- Boait, F. C., White, N. J., Bickle, M. J., Chadwick, R. A., Neufeld, J. A., & Huppert, H. E. (2012). Spatial and temporal evolution of injected CO₂ at the Sleipner Field, North Sea. *Journal of Geophysical Research: Solid Earth* (1978–2012), 117(B3). doi:10.1029/2011JB008603
- Bünz, S., Mienert, J., & Berndt, C. (2003). Geological controls on the Storegga gas-hydrate system of the mid-Norwegian continental margin. *Earth and Planetary Science Letters*, 209(3-4), 291–307. doi:10.1016/S0012-821X(03)00097-9
- Cartwright, J. A., Huuse, M., & Aplin, A. (2007). Seal bypass systems. *AAPG Bulletin*, 91(8), 1141–1166. doi:10.1306/04090705181
- Cathles, L. M., Su, Z., & Chen, D. (2010). The physics of gas chimney and pockmark formation, with implications for assessment of seafloor hazards and gas sequestration. *Marine and Petroleum Geology*, 27(1), 82–91. doi:10.1016/j.marpetgeo.2009.09.010
- Cavanagh, A. J., & Haszeldine, R. S. (2014). The Sleipner storage site: Capillary flow modeling of a layered CO₂ plume requires fractured shale barriers within the Utsira Formation. *International Journal of Greenhouse Gas ...* doi:10.1016/j.ijggc.2013.11.017
- Chadwick, R. A. (2012). Reflections on storage site monitoring. *Greenhouse Gases: Science and Technology*, 2(4), 219–222. doi:10.1002/ghg.1297
- Chadwick, R. A., Marchant, B. P., & Williams, G. A. (2014). CO₂ storage monitoring: leakage detection and measurement in subsurface volumes from 3D seismic data at Sleipner. *Energy Procedia*, 63, 4224–4239. doi:10.1016/j.egypro.2014.11.458
- Chadwick, R. A., Noy, D., Arts, R. J., & Eiken, O. (2009). Latest time-lapse seismic data from Sleipner yield new insights into CO₂ plume development. *Energy Procedia*, 1(1), 2103–2110. doi:10.1016/j.egypro.2009.01.274

- Chadwick, R. A., Zweigel, P., Gregersen, U., Kirby, G. A., Holloway, S., & Johannessen, P. N. (2004). Geological reservoir characterization of a CO₂ storage site: The Utsira Sand, Sleipner, northern North Sea. *Energy*, 29(9-10), 1371–1381. doi:10.1016/j.energy.2004.03.071
- Class, H., Ebigbo, A., Helmig, R., Dahle, H.K., Nordbotten, J.M., Celia, M.A., Audigane, P., Darcis, M., Ennis-King, J., Fan, Y., Flemisch, B., Gasda, S.E., Jin, M., Krug, S., Labregere, D., Naderi Beni, A., Pawar, R.J., Sbai, A., Thomas, S.G., Trenty, L., Wei, L. (2009). A benchmark study on problems related to CO₂ storage in geologic formations: Summary and discussion of the results. *Computational Geosciences* 13, 4, 409-434. doi:10.1007/s10596-009-9146-x
- Deimling, von, J. S., Rehder, G., Greinert, J., McGinnis, D. F., Boetius, A., & Linke, P. (2011). Continental Shelf Research. *Continental Shelf Research*, 31(7-8), 867–878. doi:10.1016/j.csr.2011.02.012
- Eidvin, T., & Rundberg, Y. (2007). Post-Eocene strata of the southern Viking Graben, northern North Sea; integrated biostratigraphic, strontium isotopic and lithostratigraphic study. *Norwegian Journal of Geology*, 87, 391–450.
- Eidvin, T., & Øverland, J.A., (2009). Faulty geology halts project. *Norwegian Continental Shelf*, no. 2, 35-36.
- Eidvin, T., Riis, F., & Rasmussen, E. S. (2014). Marine and Petroleum Geology. *Marine and Petroleum Geology*, 56(c), 184–221. doi:10.1016/j.marpetgeo.2014.04.006
- Flemisch, B., Darcis, M., Erbertseder, K., Faigle, B., Lauser, A., Mosthaf, K., Müthing, S., Nuske, P., Tatomir, A., Wolff, M., & R. Helmig. (2011). DUMUX: DUNE for multi-{phase, component, scale, physics, ...} flow and transport in porous media. *Advances in Water Resources* 34, 9, 1102-1112
- Galloway, W. E. (2001). Seismic expressions of deep-shelf depositional and erosional morphologies, Miocene Utsira Formation, North Sea Basin. *Marine Geophysical Research*, 22(5), 309–321.
- Galloway, W. E. (2002). Paleogeographic setting and depositional architecture of a sand-dominated shelf depositional system, Miocene Utsira Formation, North Sea Basin. *Journal of Sedimentary Research*, 72(4), 476–490.
- Granli, J. R., Arntsen, B., Sollid, A., & Hilde, E. (1999). Imaging through gas-filled sediments using marine shear-wave data. *Geophysics*, 64(3), 668–677.
- Gregersen, U., & Johannessen, P. N. (2007). Distribution of the Neogene Utsira Sand and the succeeding deposits in the Viking Graben area, North Sea. *Marine and Petroleum Geology*, 24(10), 591–606. doi:10.1016/j.marpetgeo.2007.04.006
- Halland, E. K., Tjelta Johansen, W., & Riis, F. (2011). CO₂ storage Atlas Norwegian North Sea, 1–72.
- Harrington, J. F., Noy, D. J., Horseman, S. T., & Birchall, D. J. (2009). Laboratory study of gas and water flow in the Nordland Shale, Sleipner, North Sea.
- Hay, C. J. C. S. J., Clayton, C. J., & Hay, S. J. (1994). Gas migration mechanisms from accumulation to surface. *Bulletin of the Geological Society of Denmark*.
- Heggland, R. (1997). Detection of gas migration from a deep source by the use of exploration 3D seismic data. *Marine Geology*, 137(1), 41–47.
- Hubbert, M.K., Willis, D.G., 1957. Mechanic of hydraulic fracturing. *Transactions of Society of Petroleum Engineers of AIME*, 1957, v. 210, p. 153-168.

- Hurst, A., Scott, A., & Vigorito, M. (2011). Physical characteristics of sand injectites. *Earth-Science Reviews*, 106(3-4), 215–246. doi:10.1016/j.earscirev.2011.02.004
- Huuse, M., & Lykke Andersen, H. (2000). Overdeepened Quaternary valleys in the eastern Danish North Sea: morphology and origin. *Quaternary Science Reviews*, 19(12), 1233–1253.
- IPCC. (2005). *Carbon Dioxide Capture and Storage*. Cambridge University Press.
- Karstens, J., & Berndt, C. (2015). Seismic chimneys in the Southern Viking Graben – Implications for palaeo fluid migration and overpressure evolution. *Earth and Planetary Science Letters*, 412(0), 88–100. doi:http://dx.doi.org/10.1016/j.epsl.2014.12.017
- Korbøl, R., & Kaddour, A. (1995). Sleipner vest CO₂ disposal-injection of removed CO₂ into the Utsira Formation. *Energy Conversion and Management*, 36(6), 509–512.
- Leifer, I., Solomon, E., Schneider von Deimling, J., Rehder, G., Coffin, R., & Linke, P. (submitted). The Fate of Bubbles in a Large, Intense Megaplume for Stratified and Unstratified Water: Numerical Simulations of 22/4b Expedition Field Data. *Journal of Marine and Petroleum Geology*
- Løseth, H., Gading, M., & Wensaas, L. (2009). Hydrocarbon leakage interpreted on seismic data. *Marine and Petroleum Geology*, 26(7), 1304–1319. doi:10.1016/j.marpetgeo.2008.09.008
- Løseth, H., Wensaas, L., Arntsen, B., Hanken, N.-M., Basire, C., & Graue, K. (2011). 1000 m long gas blow-out pipes. *Marine and Petroleum Geology*, 28(5), 1047–1060. doi:10.1016/j.marpetgeo.2010.10.001
- Lonergan, L., Maidment, S. C. R., & Collier, J. S. (2006). Pleistocene subglacial tunnel valleys in the central North Sea basin: 3-D morphology and evolution. *Journal of Quaternary Science*, 21(8), 891–903. doi:10.1002/jqs.1015
- Nicoll, G. D. (2011, November 25). Evaluation of the Nordland Group overburden as an effective seal for the Sleipner CO₂ storage site (offshore Norway) using analytical and stochastic modelling techniques. Heriot-Watt University.
- Singh, V. P., Cavanagh, A., Hansen, H., Nazarian, B., Iding, M., Ringrose, P. S. (2010). Reservoir Modeling of CO₂ Plume Behavior Calibrated Against Monitoring Data From Sleipner, Norway. Presented at the SPE Annual Technical Conference and Exhibition, Society of Petroleum Engineers. doi:10.2118/134891-ms
- Walter, L., Binning, P.J., Oladyshkin, S., Flemisch, B., H. Class (2012). Brine migration resulting from CO₂ injection into saline aquifers - An approach to risk estimation including various levels of uncertainty. *International Journal of Greenhouse Gas Control* 9. 495-506.
- White, J. A., Chiamonte, L., Ezzedine, S., Foxall, W., Hao, Y., Ramirez, A., & McNab, W. (2014). Geomechanical behavior of the reservoir and caprock system at the In Salah CO₂ storage project. *Proceedings of the National Academy of Sciences*, 111(24), 8747–8752. doi:10.1073/pnas.1316465111
- Ziegler, P. A. (1992). European Cenozoic rift system. *Tectonophysics*, 208(1), 91–111.

CHAPTER 5: INSIGHTS INTO FOCUSED FLUID CONDUIT FORMATION FROM COMPARING SEISMIC CHIMNEYS AND PIPES WITH FIELD OBSERVATIONS OF FLUID FLOW MANIFESTATIONS IN THE COLORADO PLATEAU

Karstens, J., and Berndt, C.



Sand injection pipe, Kodachrome Basin, Utah, USA

5.1. INTRODUCTION

The understanding of focused fluid flow in sedimentary basins builds on field geological observations and the interpretation of reflection seismic data, where fluid conduits manifest as anomalous amplitude patterns known as seismic chimneys or pipes. Seismic data is the most effective method for the analysis of entire fluid flow systems by constraining subsurface geometries, fluid accumulations and permeability barriers, but seismic data cannot provide information about the internal architecture, interaction with the bedrock and flow processes due to its coarse resolution. Field geological investigations of fluid conduit outcrops are capable of filling observation gaps on a sub-seismic scale and help constrain formation dynamics as well as hydraulic properties of fluid conduits and the bedrock. Although it is obvious that both approaches complement each other, the approach of integrating seismic data analysis and field observations in the study of fluid flow phenomena is still in its infancy.

Here we show that it is possible to correlate specific amplitude patterns of seismic chimneys with field observation of focused fluid conduits from the Colorado Plateau. The migrating fluids (gas, water, fluidized sediment) and their formation dynamics, which can be associated with different types of conduits (fractures, fluidizations, injections), result in distinguishable seismic signatures. These constraints improve the qualitative interpretation of seismic chimneys and pipes by adding information about migration and formation characteristics. A further integration of field geological and seismic investigation of focused fluid flow structures may help to quantify their hydraulic properties and how these evolve with time, which has important implications for the hydrocarbon prospection and the subsurface storage of wastewater and CO₂.

5.2. FOCUSED FLUID CONDUITS IN SEISMIC DATA

Focused fluid conduits manifest in seismic data as anomalous amplitude signatures including brightening or dimming, deformation and changes of the continuity of seismic reflections (Cartwright et al., 2007; Løseth et al., 2009; Andresen 2012). The amplitude effects can be attributed to the presence of free gas in the pore space, which significantly influences the velocities and attenuation of seismic waves (White, 1975). Velocity variations may also cause up-bending and down-bending of seismic reflections, which needs to be considered, when interpreting structural deformations associated with focused fluid conduits.

The term seismic chimney was originally used to describe zones with chaotic, dimmed or wiped-out seismic amplitudes, which have been identified above several hydrocarbon fields in the North Sea, e.g. Tommeliten (Løseth et al., 2009). Such “classical gas chimneys” may have diameters of several km (e.g. Tommeliten; Fig. 1E; Løseth et al., 2009), which distinguishes them from another type of vertical seismic anomalies known as seismic pipes. The term pipe is normally used for narrower, more distinct, vertical seismic anomalies. Prominent examples for pipe structures are those described for the Nyegga area, offshore Norway (Fig. 1B; Plaza-Faverola et al., 2011).

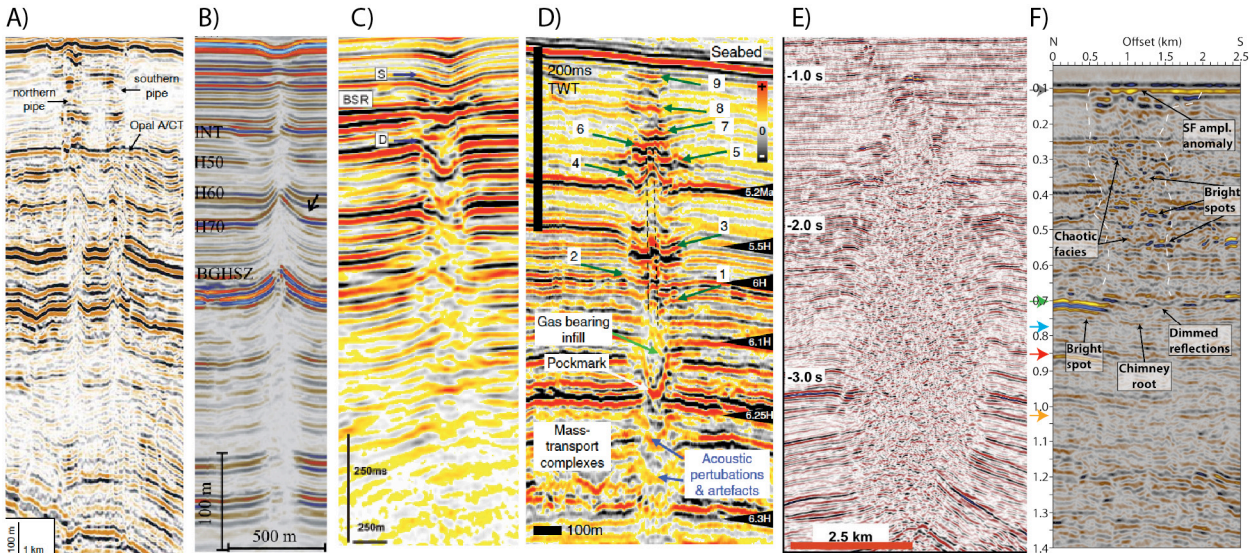
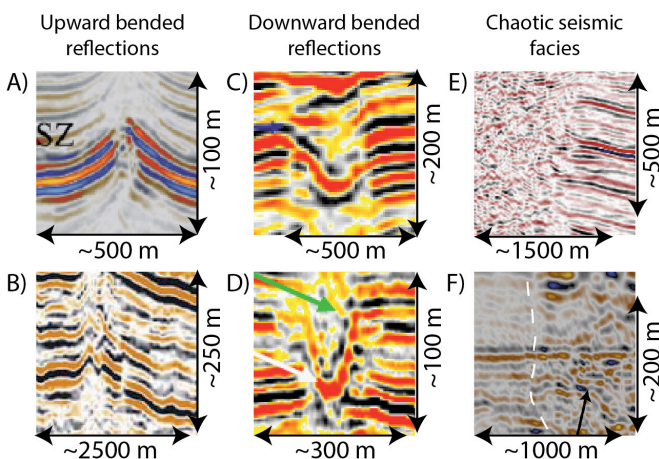


Fig. 1: Focused fluid conduit from A) Gjallar Ridge, Norwegian Sea (Dumke et al., 2014), B) Nyegga, Norwegian North Sea (Plaza-Faverola et al., 2011), C) offshore Namibia (Moss et al., 2010), D) offshore Angola (Ho et al., 2012), E) Tommeliten, Norwegian North Sea (Loeseth et al., 2009) and F) Southern Viking Graben, Norwegian North Sea (Karstens and Berndt, 2015).

The comparison of different seismic chimneys and pipes from literature reveals that focused fluid conduits in seismic data may show very different seismic appearances, while it is possible to categorize them by specific seismic characteristics including (Fig. 5.1 and 5.2):

- Up-bended and/or broken reflections
- Down-bended reflections
- Zones with chaotic seismic appearance

These signatures can be identified in seismic datasets from different geological settings. In some cases, it is even possible to differentiate between different types of chimneys within one dataset (Karstens and Berndt, 2015). There are indications that some seismic anomalies could be caused by different acquisition systems or processing routines, but there is strong evidence that seismic anomalies associated with fluid flow can be the result of different underlying geological processes.



Typical seismic signatures associated with fluid flow showing up- reflections, down-bended reflections and zones with chaotic seismic signature from A) Plaza-Faverola et al., 2011, B) Dumke et al., 2014, C) Moss et al., 2010, D) Ho et al., 2012, E) Løseth et al., 2009 and F) Karstens and Berndt, 2015. The vertical scale of D, E and F is calculated by assuming a seismic velocity of 2,000 m/s.

5.3. FIELD GEOLOGICAL OBSERVATIONS

The Colorado Plateau is a lifted sedimentary basin in the Southwest United States and hosts a multitude of focused fluid conduits exposed at numerous outcrops (Netoff et al., 2001; Huuse et al., 2005; Ross et al., 2014). Several of these outcrops are located at the border between Utah and Arizona (Fig. 3) and the presented examples are found in Jurassic sediments of the Navajo, Carmel and Entrada Formations, which were deposited in shallow marine to arid palaeo-environments (Netoff et al., 2001; Ross et al., 2014). The presented field analogues of focused fluid conduits are from the Kodachrome Basin and three sites at the north shore of lake Powell including Warm Creek Bay, Cookie Jar Butte and Last Chance Bay (Fig. 5.3).

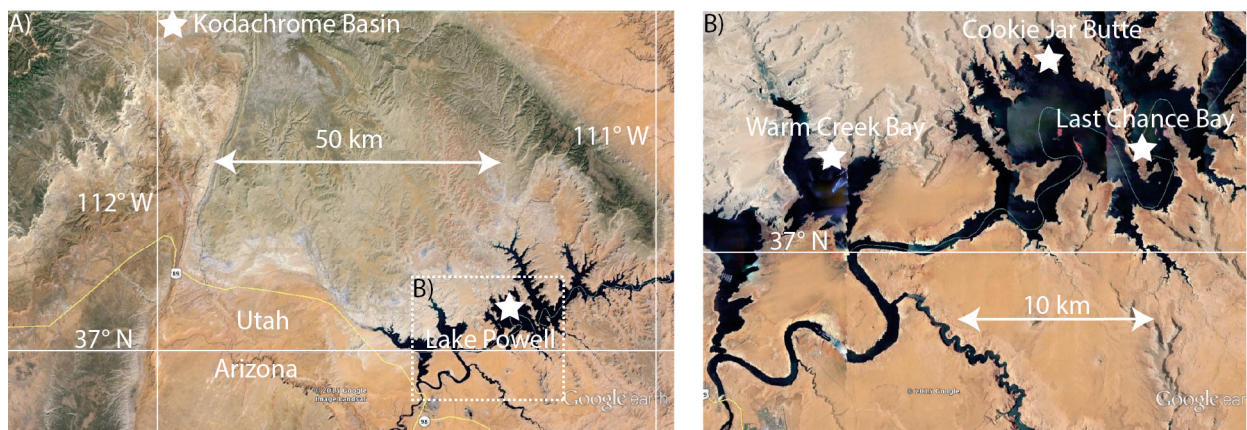


Fig. 5.3: A) Map showing the locations of the presented field analogues. B) Detailed map of Lake Powell showing the locations of the visited outcrops.

5.3.1. SAND INJECTIONS IN THE KODACHROME BASIN

The Kodachrome Basin hosts several sandstone intrusions, which primarily occur in the Carmel and Entrada formations (Fig. 4a; Ross et al., 2014). The sandstone pipes intruded the aeolian and coastal sands (Netoff et al., 2001; Huuse et al., 2005; Ross et al., 2014) and they consist of either homogeneous pipe rock (completely fluidized sands), cobble and pebble conglomerates, or a mixture of pipe rock and conglomerates including clasts of host rock (Ross et al., 2014). The pipe structures at Kodachrome Basin have diameters of up to 15 meter, but most pipes are not wider than 7 meters.

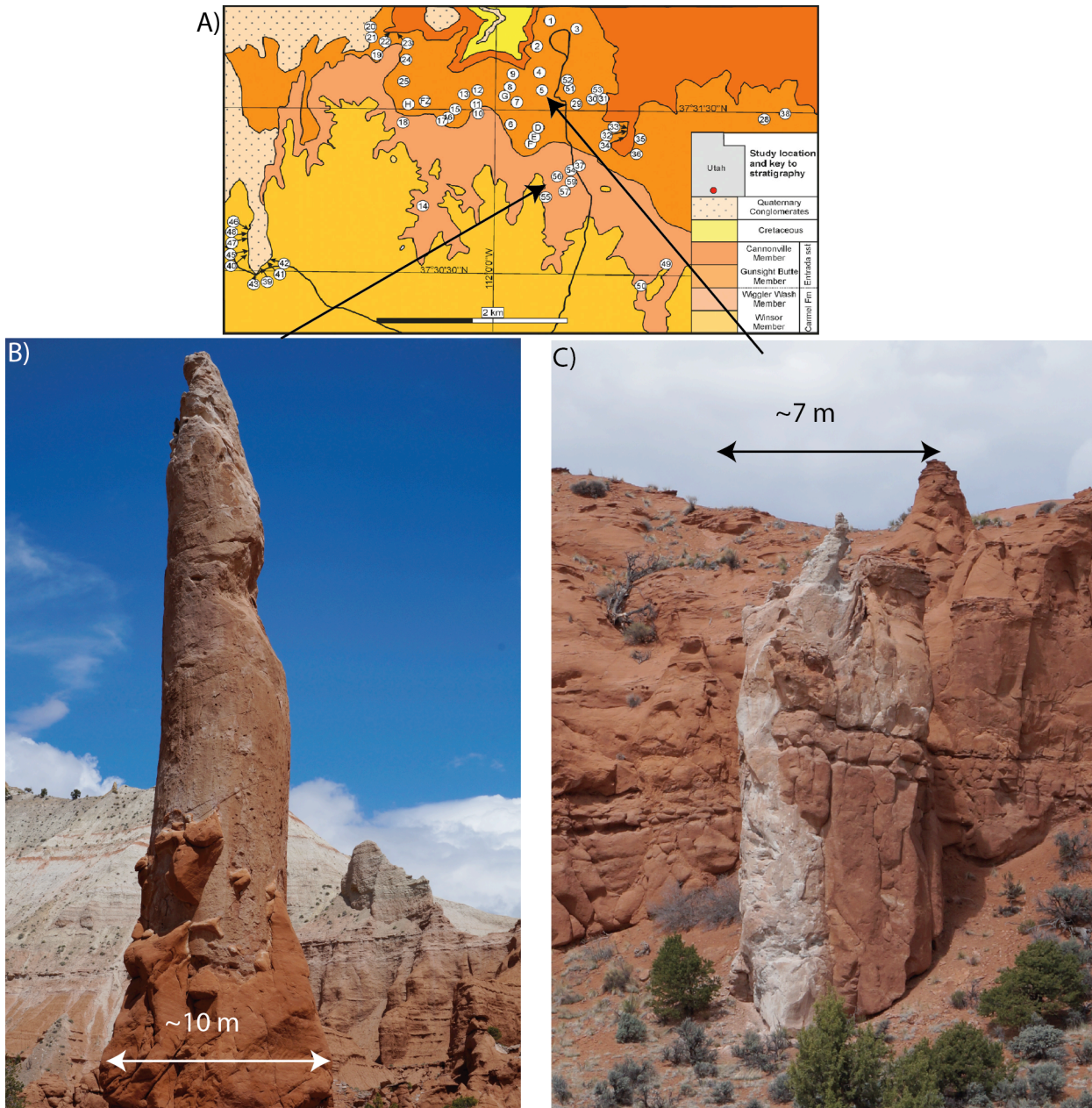


Fig. 5.4.: A) Overview map of the Kodachrome Basin showing the sand injection pipe locations (Ross et al., 2014). B) Sand injection pipe hosting clasts of bedrock. C) Sand injection pipe with deformed bedrock strata

5.3.2. FLUIDIZED SANDS AT LAST CHANCE BAY AND WARM CREEK BAY, LAKE POWELL

Lake Powell is located at the border of Utah and Arizona and is an artificial water reservoir sourced by the Colorado River. It is the site of several clusters of conical sandstone landforms. These crop out as aeolian sands belonging to the Entrada Formation (Netoff, et al., 2001, Netoff, 2002; Huuse et al., 2005). These landforms are the result of differential erosion between pipe-cores and the surrounding bedrock and are accessible at the north shore of the lake at different locations including Warm Creek Bay, Last Chance Bay and Cookie Jar Butte. The sandstone pipes are the result of fluidization, which occurred in a water-saturated environment (Netoff, 2002). The internal structure of the pipes is down-faulted in comparison to the bedrock (Fig. 5.5a,b; Netoff, 2002). Some of the pipe structures have diameter of up to 75 m (Netoff, 2002).

One of these fluidized pipes is exposed in a cliff at Last Chance Bay (Fig. 5a, b). This structure has a diameter of ~20 m and the exposed section of the pipe has a height of ~80 m. Subsidence and reworking of the strata inside the pipe is clearly visible (Fig. 5.5a, b). Additional fluidization pipes are exposed at Warm Creek

Bay, where they manifest as conical bedforms with diameters of 20 to 30 meter (Fig. 5.5c, d). The contact between intact and fluidized sandstones is associated with different coloration (Fig 5.5c, d).

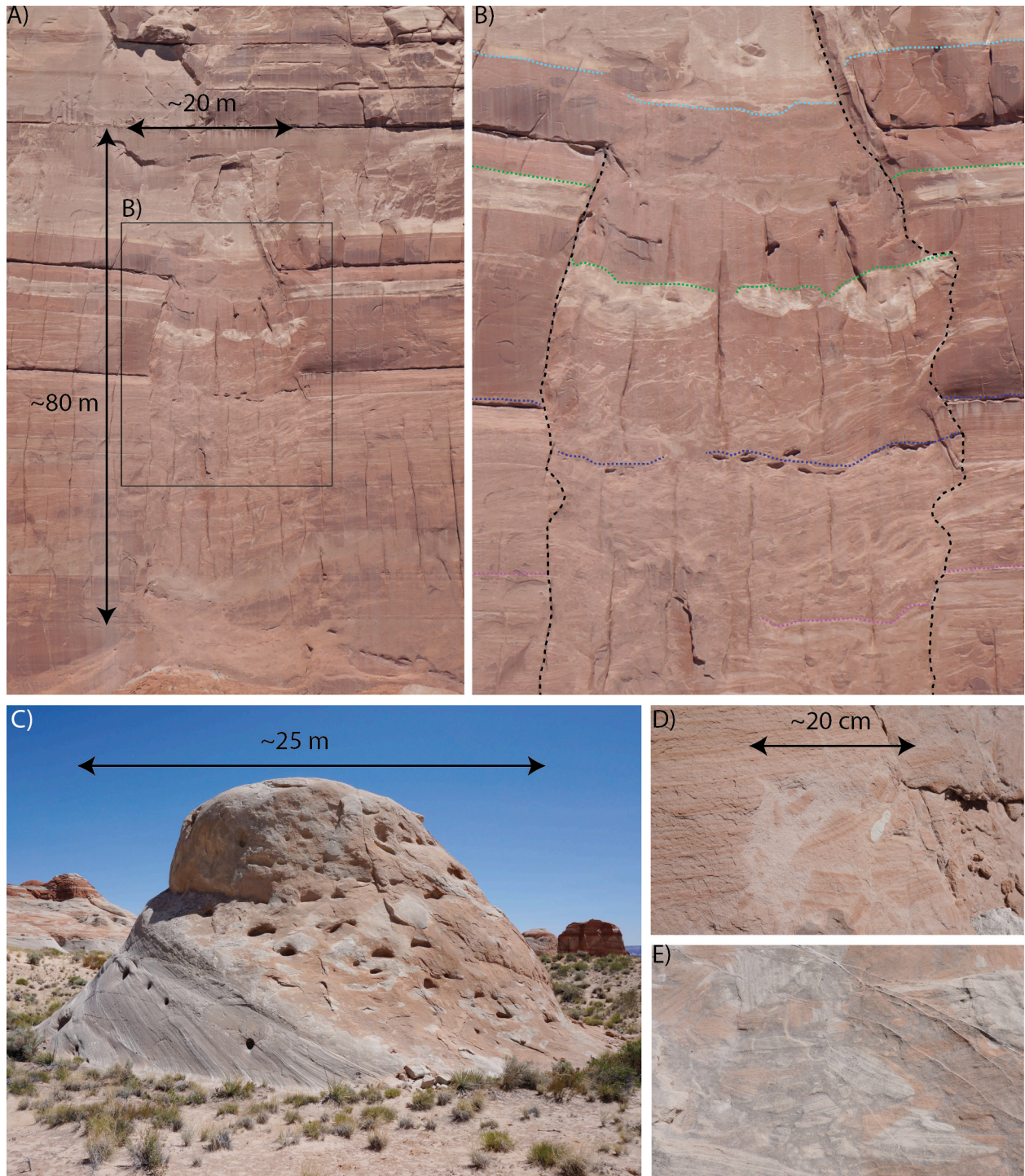


Fig. 5.5: A) Sand fluidization pipe exposed at a cliff at Last Chance bay. B) Enlarged section of the same pipe; subsidence of some layers is highlighted by dashed (mention color) lines. C) Sand fluidization pipe exposed as a conical bedform at Warm Creek Bay. D) The contact between undisturbed and fluidized sandstone. E) Zoom-in showing different coloration of the sandstone.

5.3.3. FRACTURED MOUND AT COOKIE JAR BUTTE, LAKE POWELL

The Cookie Jar Butte site hosts numerous pipe-structures, which have diameters of several meters to several tens of meters (Fig. 5.6b; Netoff, 2002). Most of these structures are very similar to those from Last Chance Bay and Warm Creek Bay. However, one mound-like bedform stands out by having prominent white lineaments, which trace the rim of a crater-like depression in the center of the structure. Lineaments also crosscut the entire mound structures (Fig. 5.6c, d) and correspond to fractures.

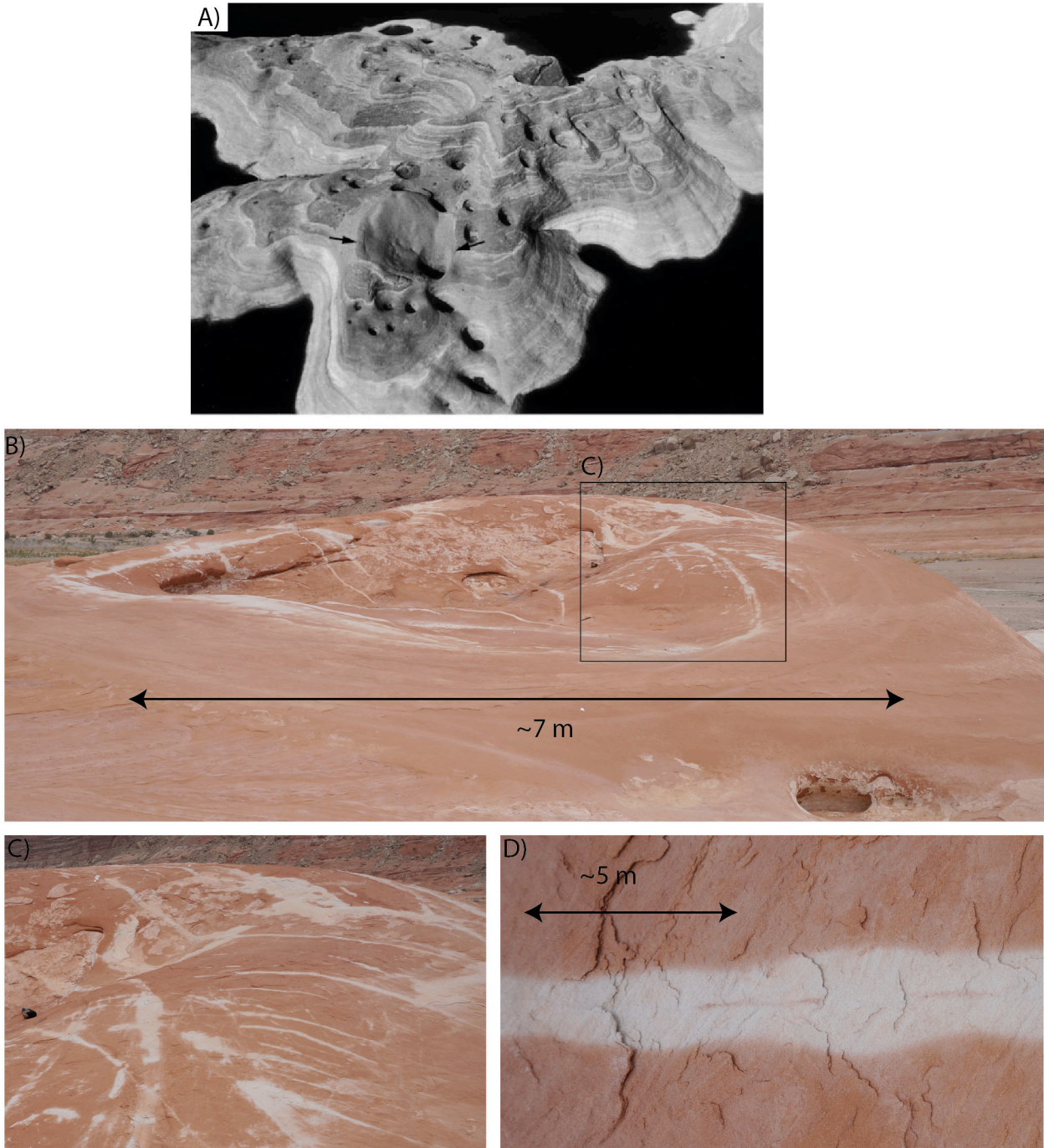


Fig. 5.6: A) Aerial view of Cookie Jar Butte; arrows mark a ~50 m wide pipe from Netoff (2002). B) Fracture mound at Cookie Jar Butte. C) Zoom-in of the same fracture mound. D) Detailed view of a fracture close to the fracture mound (narrow band in the center) and the surrounding leached sandstone.e.

5.4. CORRELATION OF SEISMIC AND FIELD GEOLOGICAL OBSERVATIONS

There are similarities between the seismic signatures of focused fluid conduits commonly seen in 2D and 3D seismic data and the field observations. In a relevant geological context, seismic chimneys and pipes hosting up-bended reflection can be interpreted as the remnants of blowout events. The seismic image of up-bended and broken reflections is very similar to the structural deformation observed at sand injections in the Kodachrome Basin, where pipe structures puncture the host rock. The outcrops show no indications that fluidization of the adjusting bedrock took place (Fig. 5.4). The pipes transported clasts of bedrock (Fig. 4b), which indicates a rapid and highly energetic emplacement. The bedrock around most exposed pipes is entirely eroded and only at one site, it was possible to observe structural deformation of the bedrock, indicated by an upward bending of the strata in the direct vicinity of the injection pipe (Fig. 5.4c). When comparing the sandstone pipes in the Kodachrome Basin with seismic pipe and chimney structures (e.g. Nyegga), it is plausible to interpret up-bended reflections as the seismic image of deformed strata as the result of rapid injection of fluids or fluidized sediments (Fig. 5.7). However, up-bended seismic reflections may also be the result of seismic velocity heterogeneities (Armstrong et al., 2001; Kristensen and Huuse, 2012) and this possibility has to be considered, when interpreting seismic data.

Down-bended reflections within seismic chimneys or pipes are often interpreted as stacks of pockmarks indicating repeated fluid expulsion activity (Fig. 5.7). However, the field observations at Last Chance Bay indicate, that the fluidization of sediments within a fluid conduit may result in subsidence of strata. Subsidence of sediments within a conduit is in agreement with post expulsion plugging of pipe structures, which has been proposed for several chimney and pipe structures (Løseth et al., 2011; Karstens and Berndt, 2015). If the stratification is not completely destroyed during fluidization, specific layers should still be visible as distinct reflections in the seismic data. Therefore, we propose to interpret down-bended reflections as the result of subsidence of fluidized sediments within a fluid conduit, although interpreting them as palaeo pockmarks may in some cases be just as plausible (and validated using 3D seismic data).

The interpretation of zones with chaotic seismic appearance as “gas chimneys”, which represent the seismic image of gas-filled fracture networks, is well constrained by drilling, seismic shear wave experiments and numerical modeling (Granli et al., 2002; Arntsen et al., 2007; Loeseth et al., 2009). The mound structure at Cookie Jar Butte may represent a field analogue for a fracture network that would appear as a gas chimney in seismic data (Fig. 5.7). The white color next to the fractures is most likely the result of leaching of iron from the sandstone due by fluid flow (Fig. 5.6e).

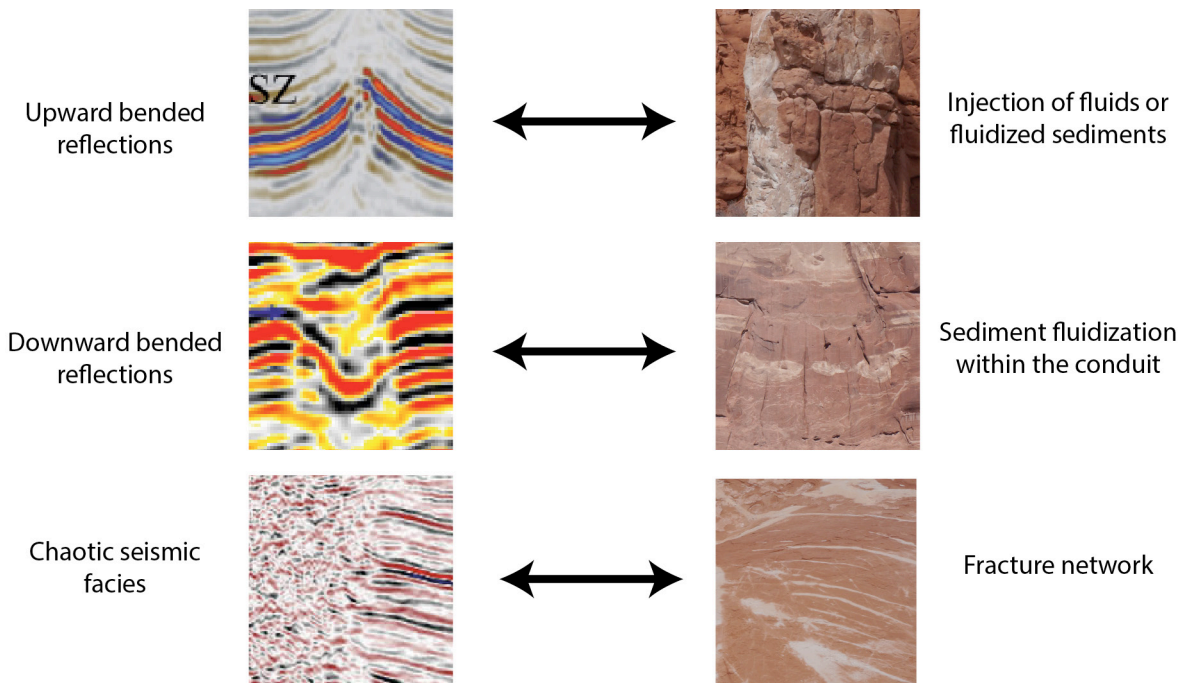


Fig. 5.7: Comparison of seismic signatures related with focused fluid flow and corresponding field analogues

5.5. CONCLUSIONS

It is possible to correlate specific seismic signatures with specific fluid flow manifestations from field observations. This suggests that it will be possible to establish a robust and geologically consistent terminology for seismic interpretations and nomenclature of focused fluid conduits. However, more fieldwork is necessary to support the presented correlations scheme and examples from different geological environments, such as carbonates vs. sandstone and mudstone dominated environments, need to be considered.

There is a discrepancy between dimensions of focused fluid conduits in seismic data and the field, i.e. the observed seismic structures are 10s to 100s of times larger. This is difficult to explain. It may be possible that we just have not recognized the field analogues of large-scale chimney structures, because these structures are not very prominent in the field. Seismic data are extremely sensitive in picking up minor disturbances or fluid infiltration around the conduit itself that affect the seismic properties of the bedrock around a conduit, which escape geological field methods at outcrop scale. Alternatively, it is possible that we have already found these structures, but that we are interpreting them in different ways (e.g. breccia pipes). However, the analysis of field analogues has great potential for providing novel insights into the nature of fluid conduits.

REFERENCES

- Andresen, K.J., 2012. Fluid flow features in hydrocarbon plumbing systems: What do they tell us about the basin evolution? *Marine Geology*, 1–20.
- Armstrong, T., McAteer, J., Connolly, P., 2001. Removal of overburden velocity anomaly effects for depth conversion. *Geophysical Prospecting* 49, 79–99.
- Arntsen, B., Wensaas, L., Løseth, H., Hermanrud, C., 2007. Seismic modeling of gas chimneys. *Geophysics* 72, 251–259.
- Cartwright, J., Huuse, M., Aplin, A., 2007. Seal bypass systems. *AAPG Bulletin* 91, 1141–1166.
- Dumke, I., Berndt, C., Crutchley, G.J., Krause, S., Liebetrau, V., Gay, A., Couillard, M., 2014. *Marine Geology*. *Marine Geology*, 351, 38–52. doi:10.1016/j.margeo.2014.03.006
- Granli, J.R., Arntsen, B., Sollid, A., Hilde, E., 1999. Imaging through gas-filled sediments using marine shear-wave data. *Geophysics* 64, 668–677.
- Ho, S., Cartwright, J.A., Imbert, P., 2012. Vertical evolution of fluid venting structures in relation to gas flux, in the Neogene-Quaternary of the Lower Congo Basin, Offshore Angola. *Marine Geology*, 332-334(C), 40–55. doi:10.1016/j.margeo.2012.08.011
- Huuse, M., Shoulders, S.J., Netoff, D.I., Cartwright, J. A., 2005. Giant sandstone pipes record basin-scale liquefaction of buried dune sands in the Middle Jurassic of SE Utah. *Terra Nova*, 17(1), 80–85. doi:10.1111/j.1365-3121.2004.00587.x
- Karstens, J., Berndt, C., 2015. Seismic chimneys in the Southern Viking Graben – Implications for palaeo fluid migration and overpressure evolution. *Earth and Planetary Science Letters* 412, 88–100. doi:http://dx.doi.org/10.1016/j.epsl.2014.12.017
- Kristensen, T.B., Huuse, M., 2012. Multistage erosion and infill of buried Pleistocene tunnel valleys and associated seismic velocity effects. *Geological Society, London, Special Publications* 368, 159–172. doi:10.1144/SP368.15
- Løseth, H., Gading, M., Wensaas, L., 2009. Hydrocarbon leakage interpreted on seismic data. *Marine and Petroleum Geology* 26, 1304–1319.
- Løseth, H., Wensaas, L., Arntsen, B., Hanken, N.-M., Basire, C., Graue, K., 2011. 1000 m long gas blow-out pipes. *Marine and Petroleum Geology* 28, 1047–1060.
- Moss, J.L., Cartwright, J.A., 2010. The spatial and temporal distribution of pipe formation, offshore Namibia. *Marine and Petroleum Geology*, 27(6), 1216–1234. doi:10.1016/j.marpetgeo.2009.12.013
- Netoff, D. I., & Shroba, R.R., 2001. Conical sandstone landforms cored with clastic pipes in Glen Canyon National Recreation Area, southeastern Utah. *Geomorphology*, 39(3), 99–110. Netoff, D., 2002. Seismogenically induced fluidization of Jurassic erg sands, south-central Utah. *Sedimentology*, 49(1), 65–80.
- Plaza-Faverola, A., Bünz, S., Mienert, J., 2011. Repeated fluid expulsion through sub-seabed chimneys offshore Norway in response to glacial cycles. *Earth and Planetary Science Letters*, 305(3-4), 297–308. doi:10.1016/j.epsl.2011.03.001
- Ross, J. A., Peakall, J., Keevil, G.M., 2014. Facies and flow regimes of sandstone-hosted columnar intrusions: Insights from the pipes of Kodachrome Basin State Park. *Sedimentology*, 61(6), 1764–1792. doi:10.1111/sed.12115

White, J. E., 1975. Computed seismic speeds and attenuation in rocks with partial gas saturation. *Geophysics*, 40(2), 224–232.

CHAPTER 6: QUANTIFICATION OF METHANE EMISSIONS AT ABANDONED GAS WELLS IN THE CENTRAL NORTH SEA

Vielstädte, L., Karstens, J., Haeckel, M., Schmidt, M., Liebetrau, V., Reimann, S., McGinnis, D.F., Linke, P., and Wallmann, K.



Methane bubbles reaching the sea surface at the North Sea blowout site, Block 22/4b, British North Sea

6.1. ABSTRACT

As a result of extensive hydrocarbon exploration, the North Sea hosts several thousand abandoned wells; many believed to be leaking methane. However, how much of this greenhouse gas is emitted into the water column and ultimately reaches the atmosphere is not known. Here, we investigate three abandoned wells at 81-93 m water depth in the Norwegian sector of the North Sea, all of which show gas seepage into the bottom water. The isotopic signature of the emanating gas points towards a biogenic origin and hence to gas pockets in the sedimentary overburden above the gas reservoirs that the wells were drilled into. Video-analysis of the seeping gas bubbles and direct gas flow measurements resolved initial bubble sizes ranging between 3.2 and 7.4 mm in diameter with a total seabed gas flow between 1 and 19 tons of CH₄ per year per well. Estimated total annual seabed emissions from all three wells of ~24 tons are similar to the natural seepage rates at Tommeliten, suggesting that leaky abandoned wells represent a significant source of methane into North Sea bottom waters. However, the bubble-driven direct methane transport into the atmosphere was found to be negligible (< 2%) due to the small bubble sizes and the water depth at which they are released.

6.2. INTRODUCTION

Methane contributes significantly to the atmospheric pool of radiative (greenhouse) gases, suspected to induce global climate change (Crutzen and Zimmermann, 1991; Hartmann et al., 2013; Lelieveld et al., 1993). Marine methane emissions may contribute around 20 Tg yr⁻¹ (Etiope et al., 2008; Kvenvolden and Rogers, 2005; Bange et al., 1994) to the global atmospheric methane budget (i.e. 542±56 Tg yr⁻¹ based on top-down estimates, Ciais et al., 2013), most of it, about 75%, being released from coastal and shelf areas (e.g. Bange et al., 1994). The highest amount of marine methane is produced by methanogenesis in the deeper sediment layers of productive coastal areas (Scranton and McShane 1991; Hovland et al., 1993), which may result in the build-up of free-gas accumulations in the shallow subsurface (Hovland and Judd, 1988; Judd and Hovland, 2007). Such gas pockets constitute a potential risk in connection with drilling operations, because they may be associated with high pore pressures. In 1990, Mobile North LTD created a massive gas blowout in the central UK North Sea (57.922°N, 1.6325°E, WGS84) after drilling into an over-pressurized gas pocket about 360 m below the seafloor. The drilling site had to be abandoned after the incident and methane emissions (“leakage”) from the created seabed depression persisted over several decades (Rehder et al., 1998; Schneider von Deimling et al., 2007; Schneider von Deimling et al., this issue) and represent the strongest gas seepage quantified to date (Leifer, this issue). Smaller methane leaks can result from drilling through less-pressurized gas pockets and the numerous abandoned offshore wells penetrating such gas accumulations may constitute efficient pathways to release gas from the sedimentary strata to the hydrosphere and finally to the atmosphere (Gurevich et al., 1993; Gasda et al., 2004). Although leakage rates are probably orders of magnitude lower compared to a blowout scenario like well 22/4b, leaks along abandoned wells are much more likely to occur. As monitoring generally is not required after proper well abandonment (Gasda et al., 2004), quantitative data on both, the number of leaking wells, and their leakage rates are rare. Most of the available data are related to well integrity surveys that are performed by operating companies and governmental authorities to reduce the risk of major accidents, primarily for the population, environment and economic values, however their focus is mostly on active (production and injection) wells. E.g. on the Norwegian Continental Shelf, 18% of active wells are reported to have integrity issues (Vignes et al., 2006). However, studies in the Gulf of Mexico showed that the majority of integrity issues were related to shut-in or temporarily abandoned wells, rather than to active wells (Wojtanowicz et al., 2001). Thus, even though leakage from abandoned wells poses a lower risk of major accidents for people and economic aspects, it may constitute a relevant source for methane into the ocean.

A large fraction of the released methane will dissolve in the water column, disperse by currents, and is subsequently oxidized by microbes (e.g., Ward et al., 1987; Jones, 1991). Transfer of methane into the atmosphere is possible by both diffusive and turbulent air-sea gas exchange as well as bubble-mediated transport (Leifer and Patro, 2002; Wanninkhof, 1992). The latter is the most efficient way of transferring seabed methane to the atmosphere (McGinnis et al., 2006), which may enhance local sea-air fluxes, particularly in shallow shelf seas. In this study we focus on the North Sea, which acts as a net source for atmospheric methane (Bange et al., 1994). Current flux estimates (Bange et al., 1994; Rehder et al., 1998) seem to be too low, because methane fluxes from estuaries and marine seeps are not adequately represented (Bange et al., 2006) and possible contributions from abandoned wells have not been studied at all.

To our knowledge, this is the first public study aiming to quantify methane leakage from abandoned wells in the North Sea. For this purpose, we investigated three abandoned wells that show continuous bubble release into the water-column during two research cruises in 2012 and 2013. Further, we determine the source of leaking gases and possible migration pathways driving the seabed emissions at leaky wells. Applying a numerical gas bubble dissolution model, we estimate the resulting direct methane flux across the sea surface and finally, methane emissions at the abandoned wells are compared to natural methane seepage as well as other methane sources in the North Sea.

6.2.1. STUDY AREA

The three wells are located on the south-western flank of the Utsira High in the Norwegian sector of the North Sea (Fig. 6.1). The area hosts hydrocarbon-rich Paleocene sediments mainly in the Heimdal Formation, which are charged by Jurassic source rocks (Justwan and Dahl, 2005). The main objectives of the three wells were to delineate hydrocarbon accumulations found in the Heimdal Formation (15/9-13), to prove the presence of a high-risk stratigraphic trap in the Heimdal Formation (16/7-2), and to test a possible small closure at the Top Heimdal Formation (16/4-2). In all cases, the target depths of the wells were deeper than 3000 m below the seafloor (mbsf) corresponding to Jurassic (i.e. 16/4-2) and Permian (i.e. 15/9-13 and 16/7-2) stratigraphic units. Well 16/4-2 was permanently plugged and abandoned as a dry well, while the other two boreholes proved gas in the Heimdal Formation but were subsequently plugged and abandoned. Shallow gas is mostly present within Nordland Group sediments in the upper Cenozoic sequences. The Utsira Formation, the Top Pliocene, and an 11-m thick sand layer above the Top Utsira Formation constitute important sand layers, which are separated by impermeable layers of shale or mudstones (Fig. 6.2), thus creating fairly good conditions for the trapping and accumulation of shallow gas (Karstens and Berndt, 2015). The Utsira Formation overlies marine mudstones at the base of the Nordland Group and is dominated by medium-grained sand intersected with some stringers of clay (Eidvin and Rundberg, 2007, Statoil et al., 1982). While Utsira sands were deposited in a high-energetic shelf environment (Galloway, 2001; 2002), the depositional environment changed from a shallow to a deeper marine environment in the Early Pliocene, which was accompanied by the deposition of finer sediments. The interval from 300 mbsf down to the Utsira Formation thus consist of clay-rich sediments known as Nordland Shales (Fig. 6.2; Horvig, 1982) largely acting as a seal for upward migrating fluids, except for sections with pre-existing or pressure-induced fractures. The uppermost 300 m of the Nordland Group consists mostly of sand with some inter-bedded clay also containing gas in the vicinity of some wells (Horvig, 1982).

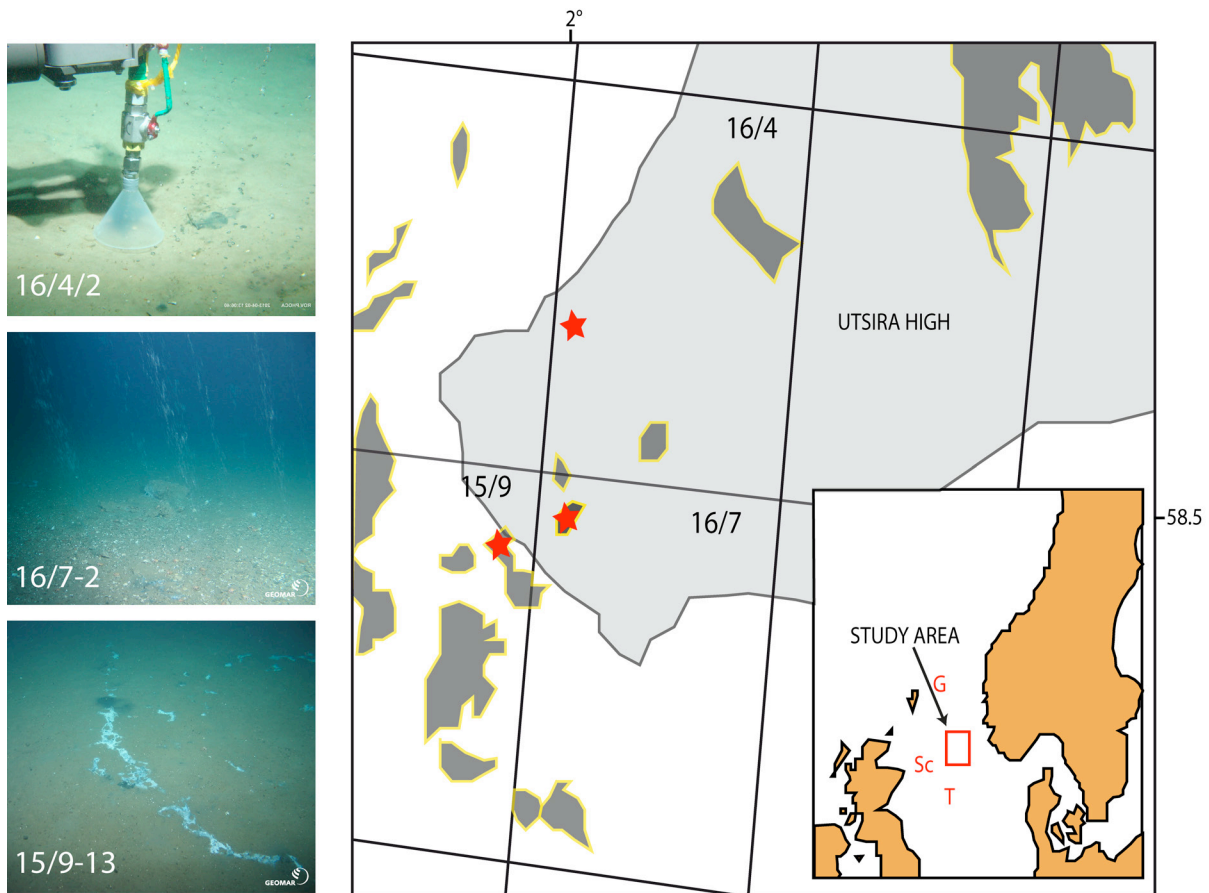


Fig. 6.1: Map of the study area showing the Utsira High as the major structural element, the locations of deep hydrocarbon reservoirs (dark gray; based on Fact Map of the Norwegian Petroleum Directorate), and the locations of the investigated abandoned wells (red stars); Lower right corner: Regional map of the North Sea Basin showing the location of the study area (red box), and natural seep sites discussed in this paper (red letters: T: Tommeliten, Sc, Scanner Pockmark, G: Gullfaks). Left: Pictures showing gas flow measurement at well 16/4-2, the most intensive leakage at well 16/7-2, and bacterial mats related to CH_4 leakage at well 15/9-13.

Age (Ma)	0	2.59	5.33	23	33.9	56	66
Period	Quaternary		Tertiary				Creatc.
Epoch	Pleistocene	Plioc.	Mioc.	Oligocene	Eocene	Paleoc.	Mastr.
Group	Nordland			Hordaland		Rogaland	Chalk
Formation	Nordland Shales		Utsira				Heimdal

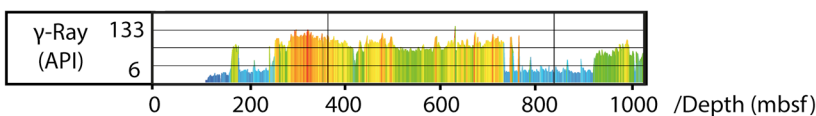


Fig. 6.2: Lithostratigraphic overview of the study area showing the geochronology of groups and formations present in the study area (Creatc. = Cretaceous, Mastr. Maastrichian Fm., Paleoc. = Paleocene, Mioc. = Miocene, Plioc. = Pliocene). Gamma Ray logs (Norwegian Petroleum Directorate) are based on well 15/9-13 and indicate the sedimentology of the Nordland Group, where high values represent clay (yellow to red), intermediate values represent a mixture of clay and sand (green), and low values represent permeable sand layers (blue).

6.3. METHODOLOGY

Geochemical sampling and video investigations were performed at three leaky abandoned wells during cruises on board the research vessels RV Celtic Explorer (CE12010, July-August 2012) and RV Alkor (AL412, March 2013). In addition, an industrial 3D seismic data set (ST98M3, Statoil ASA) covering the area around the three wells of interest was analyzed for gas accumulations and possible vertical migration pathways in the sedimentary strata around the boreholes. Furthermore, well reports and well-logs of the Norwegian Petroleum Directorate (NPD) were investigated for the characterization of the sediments in the uppermost 1200 mbsf.

6.3.1. SEDIMENT AND GAS SAMPLING

During the Celtic Explorer expedition CE12010, surface sediments were collected with ROV-deployed push-cores (PC). For dissolved gas analysis, 3 ml of wet sediment was sub-sampled in 2-cm intervals and filled into 20-ml headspace vials. 6 ml of saturated NaCl solution and an additional 1.5 g of NaCl were added and the vials sealed tight with butyl-rubber stoppers. The samples were stored refrigerated for onshore analyses. Prior to storage in the cold room, the vials were shaken vigorously for half an hour to release dissolved gases into the headspace.

In addition, free gas was sampled directly in the bubble stream with ROV-operated special gas samplers as described by Rehder and Schneider von Deimling (2008) and Pape et al. (2010). The gas sampler consists of a stainless steel cylinder with a PVC funnel attached to it to facilitate gas bubble sampling (Fig. 6.1 and Fig. A.3.1). Onboard, subsamples of pressurized gas were transferred into pre-evacuated headspace glass vials of 20 and 100 ml volume until the pressure in the vials was ~1020 mbar.

In the GEOMAR home laboratory, methane and higher alkane concentrations in the free gas samples and in head space vials were determined with a gas chromatograph GC 8000top (CE instruments) equipped with a FID detector and a capillary column (RT-Alumina Bond-KCl, 50 m, 0.53 mm). Stable carbon isotope composition of methane was determined by using a continuous flow GC-Isotope Ratio Mass Spectrometer combination. Methane was separated from other hydrocarbons in a Thermo Trace GC (isotherm at 60°C, He-carrier gas, ShinCarbon 1.5 m packed column). The subsequent conversion of methane to carbon dioxide was conducted in a Ni/Pt combustion furnace at 1150°C. The $^{13}\text{C}/^{12}\text{C}$ -ratios of the produced CO_2 were determined by a Thermo MAT253 isotope ratio mass spectrometer. All isotope ratios are reported in the δ -notation with respect to Vienna Pee Dee Belemnite (VPDB). Analytical precision of the reported concentrations and isotopic composition is $\pm 3\%$ and $\pm 0.3\%$, respectively.

Sediment porewater was extracted by squeezing wet sediment at low pressure (<5 bar) through 0.45 μm Whatman regenerated cellulose filters. 2 ml aliquots were treated with 10 μL of HgCl_2 to inhibit further microbial degradation and stored cool until analysis. Onshore, the stable carbon isotope composition of dissolved inorganic carbon (DIC), referred to as $\delta^{13}\text{DIC}$ was determined at the University of Bremen using a Finnigan MAT 251 mass spectrometer with an analytical accuracy of <0.07%. Total alkalinity was determined by titration with 0.02 N HCl using a mixture of methyl red and methylene blue as indicator. The titration vessel was bubbled with argon to strip any CO_2 and H_2S produced during the titration. The IAPSO seawater standard was used for calibration; analytical precision and accuracy are both ~2 %.

Carbonate pieces from the sediment surface were sampled with the ROV KIEL 6000 at well 16/7-2 and were cleaned of remaining sediment by washing with site specific seawater. The detailed sub-sampling was conducted after cleaning with MilliQ-water and drying at room temperature. All sub-samples were taken with a hand-held mini-driller from freshly cut or broken surfaces of solid material, after discarding first drill steps as a surface cleaning procedure. Onshore, samples were analyzed for their stable carbon isotope composition using a Thermo Fisher Scientific 253 Mass Spectrometer coupled to a CARBO KIEL online carbonate preparation line. $\delta^{13}\text{C}$ values are reported with respect to the VPDB scale.

6.3.2. VIDEO BASED QUANTIFICATION OF GAS EMISSIONS

ROV videos were analyzed by two approaches to determine the gas flow emitted into the water column at the three abandoned wells: (1) measuring the time for filling up the funnel of the gas sampler and (2) quantifying the gas bubble size spectrum at individual seepage spots.

6.3.2.1. GAS FLOW MEASUREMENTS

The in-situ gas flow was quantified at single bubble streams of well 16/4-2 and well 15/9-13 using the ROV-operated gas sampler with attached funnel (Fig. 6.1 and Tab. A.3.1). Both, the time, t , to fill the funnel with gas and its corresponding volume, V_F , were determined based on video using the software ImageJ (Farreira and Rasband, 2012). The gas volume accumulating in the funnel was calculated from the resulting volume of the cone frustum, $V_F = h \cdot \pi / 3 \cdot (r_B^2 + r_B \cdot r_T + r_T^2)$, where r_B and r_T are the radii of the base plane and top plane, respectively, and h is the distance between both planes, $h = (m^2 - r_T^2 + 2 \cdot r_T \cdot r_B - r_B^2)^{0.5}$ (Fig. A.3.1, Tab. A.3.1). The lateral height of the funnel had a length of $m = 12.5$ cm and was used as scale in the images. The optically-derived gas volume required correction, due to imprecise size measurements of a 3D object in its 2D projection. The ratio between optically-derived and known funnel volume, F_{corr} was used to correct the gas volume (Tab. A.3.1). The resulting gas flow, Q_F , is:

$$Q_F = V_F / t \cdot F_{corr} \quad (\text{Eq. 6.1})$$

The correction factor ranged between 0.88 and 1.33 including optical failures described above and uncertainties in pixel accuracy during measurements with ImageJ (Tab. A.3.1). The error in determining the time for filling the funnel is about 1 s, resulting in an error of the gas flow of < 2.7 cm³/s, i.e. less than 2.5%.

Tab. 6.1: Location, water depth, and bottom water temperature of the abandoned wells and CTD cast 12

Site/Gear	Latitude	Longitude	Water-depth	BW Temperature
	°N	°E	m	°C
16/4-2	58.596	2.028	93	5.1
16/7-2	58.473	2.033	83	7.8*
15/9-13	58.373	1.932	81	7.8*
CTD12	58.406	2.024	80	7.8

*based on measurements of CTD12

6.3.2.2. BUBBLE SIZE SPECTRA

The image editing software ImageJ (Farreira and Rasband, 2012) was applied to the ROV video sequences, which also were used for the funnel measurements, to determine the respective initial (seafloor) gas bubble sizes (e.g. Leifer and MacDonald, 2003; Römer et al., 2012; Sauter et al., 2006). These size spectra are required to calculate the dissolution rate, the bubble rise velocity, and the resulting gas transfer into the atmosphere. For calibration of bubble sizes, the bottom plane of the funnel (diameter = 150 mm) was used as a scale. A video sequence of 5 s, corresponding to 125-150 individual frames, was analyzed frame by frame. The video sequence was first converted to grayscale and was subsequently processed to enhance the contrast. Unfortunately, contrast and pixilation noise remained rather poor making a computer based automatic measurement routine impractical. Hence, ellipses were manually overlaid to individual bubbles leaving the seafloor and were marked as overlays. The overlays were allocated to individual bubbles to track them and analyze their changes in size in subsequent frames. If bubbles had a very irregular shape, they were outlined manually before using the ellipse fitting object of ImageJ (i.e. 10 of 71 measurements at well 16/7-2). For each bubble, the major and minor axes, angle, perimeter, area, circularity, as well as frame number were recorded. The corresponding bubble volume $V_0 = 4/3 * \pi * r_{eq}^2$, was calculated from the equivalent spherical radius, $r_{eq} = (a^2 * b)^{1/3}$ based on the major, a, and the minor axes, b, of the fitted ellipse.

If bubbles were measured in several frames, their average radius was used to level out the trajectory and shape oscillations of the bubble during its ascent (Clift et al., 1978). All determined bubble volumes were added to calculate the total gas volume flow over a period of 5 s.

The methodological error of bubble size measurements was estimated in two ways:

- 1) The volume flow derived from the bubble size spectra was compared to the flow constrained by the funnel measurements. The funnel-derived flow is integrated over much longer time and hence, regarded as more precise. Consequently, the bubble size spectra were corrected to match the funnel-derived flow values.
- 2) Multiple bubble measurements in sequential video frames were used to quantify the error caused by oscillation or wobbling of the gas bubble in the real 3D space, which cannot be correctly represented in a 2D image. The video can only provide a snapshot of current bubble shape and size projected onto a plane.

6.3.2.3. GAS BUBBLE DISSOLUTION MODEL

A numerical model was developed to simulate the shrinking of a gas bubble due to dissolution in the water column, its expansion due to decreasing hydrostatic pressure in the course of its ascent and gas stripping, and the final gas transport into the atmosphere. The model solves a set of coupled ordinary differential equations (ODEs) describing these processes for each of the involved gas species (CH_4 , N_2 , and O_2 ; Eq. 6.2) and the bubble rise velocity (Eq. 6.3), where time solves as the only independent variable. Thermodynamic and transport properties of the gas components, such as molar volume, gas compressibility, and gas solubility in seawater, were calculated from respective equations of state (Duan et al., 1992; Duan and Mao, 2006; Geng and Duan, 2010; Mao and Duan, 2006), and empirical equations for diffusion coefficients (Boudreau, 1997), mass transfer coefficients (Zheng and Yapa, 2002), and bubble rise velocities (Wüest et al., 1992), taking into account local pressure, temperature and salinity conditions as measured by CTD casts. Implemented equations and values are provided in Table 6.2. The ODE system is solved using finite difference methods implemented in the NDSolve object of Mathematica (i.e. LSODA, Sofroniou and Knapp, 2008).

The mass exchange of gas components across the bubble-surface is generally described as (e.g., McGinnis and Little, 2002; Leifer and Patro, 2002; Wüest et al., 1992):

$$dN_i/dt = 4\pi r_{eq}^2 * K_{L,i} * (C_{a,i} - C_{eq,i}) \quad (\text{Eq. 6.2})$$

where i is the i^{th} gas species, N, is the amount of gas in the bubble, $4\pi r_{eq}^2$ is the surface area of the equi-

valent spherical bubble, K_L is the specific mass transfer rate between gas phase and aqueous phase, C_a is the dissolved gas concentration, and C_{eq} is the gas solubility. All of the above variables are functions of the water depth, z , i.e. pressure, temperature and salinity (see Tab. 6.2 for details and references). The change of the vertical bubble position is related to the bubble rise velocity, v_b (Tab. 6.2):

$$d_z/d_t = v_b \quad (\text{Eq. 6.3})$$

Tab 6.2: Parameterization of numerical model

Parameterization	Range	Variance	Reference
Diffusion coeff.: D_i (m^2s^{-1})			
$D_{O_2}=1.05667*10^{-9}+4.24*10^{-11}*T$	T: 0-25°C	$1.00*10^{-21}$	Boudreau, 1997
$D_{N_2}=8.73762*10^{-10}+3.92857*10^{-11}*T$	T: 0-25°C	$2.94*10^{-23}$	Boudreau, 1997
$D_{CH_4}=7.29762*10^{-10}+3.31657*10^{-11}*T$	T: 0-25°C	$5.70*10^{-24}$	Boudreau, 1997
Mass transfer coefficient: $K_{L,i}$ / $m s^{-1}$			
$K_L = 0.013(v_b 10^2/(0.45+0.4r*10^2))^{0.5} D_i^{0.5}$	$r \leq 2.5$ mm		Zheng & Yapa, 2002
$K_L=0.0694 D_i^{0.5}$	$2.5 < r \leq 6.5$ mm		Zheng & Yapa, 2002
$K_L=0.0694 (2r *10^{-2})-0.25 D_i^{0.5}$	$R < 6.5$ mm		Zheng & Yapa, 2002
Fit to CTD data as function of z			
$T(z)=8+7/(1+e^{0.375(-21.7512+z)})$	Z: 0-100 m	$3.99*10^{-2}$	
$S(z)=35.12 - 0.67/(1+e^{0.4125(-20.1595+z)})$	Z: 0-100 m	$4.97*10^{-4}$	
Density of SW: ρ_{SW} / $kg m^{-3}$			
$\rho_{SW}(z)=1027.7 - 2.150/(1+e^{0.279(-21.612+z)})$	Z: 0-100 m	$6.8*10^{-3}$	Unesco, 1981
Bubble rise velocity: v_b ($m s^{-1}$)			
$v_b = 4474 r^{1.357}$	$r < 0.7$ mm		Wüest et al., 1992
$v_b = 0.23$	$0.7 \leq r < 5.1$ mm		Wüest et al., 1992
$v_b = 4.202 r^{0.547}$	$r \geq 5.1$ mm		Wüest et al., 1992
Gas solubility: c_i (mM)			
$c_{N_2} = 0.622+0.0721*z$	Z: 0-100m	$2.5*10^{-3}$	Mao & Duan, 2006
$CO_2=1.08+0.1428*z$	Z: 0-100m	$9.8*10^{-3}$	Geng & Duan, 2010
$c_{CH_4} = 1.44+0.1671*z$	Z: 0-100 m	$2.4*10^{-2}$	Duan & Mao, 2006
CH ₄ molar volume: MV_{CH_4} ($L mol^{-1}$)			
$MV_{CH_4}=1/(0.0418+0.0044+z)$	Z: 0-100 m	$3.0*10^{-2}$	Duan et al., 1992
Hydrostatic Pressure: P_{hydro} (bar)			
$P_{hydro} = 1.013+\rho_{SW}*g*z$			

Model simulations were performed based on boundary conditions obtained from Sea-Bird 9 plus CTD data of August 2012 (Tab. 6.1) and run for 21 different initial bubble sizes (1.7 to 3.7 mm radius, in accordance with the results of the measured bubble spectra), initially containing only methane. The measured initial bubble size distribution is assumed to be representative and the mass transfer of gases other than CH₄, N₂, and O₂, as well as the development of upwelling flows were considered to be negligible. Simulated water depths of 81, 83, and 93 m correspond to those of the investigated wells. The numerical simulation of gas transport by a single rising bubble is justified because only single bubble streams were observed at the wells with very little to no interaction between the bubbles, or plume dynamics.

The bubble-mediated methane flow into the atmosphere was calculated from the remaining amount of CH₄ in the bubble, when it reaches the sea surface, NS, i.e.

$$N_s(r, z) = N_0(r, z) - \int_{t=0}^{tmax} dN(r, z) dt \quad (\text{Eq. 6.4})$$

where N_0 is the initial amount of methane in the bubble and $tmax$ is the time required by the gas bubble to travel to the sea surface and is determined numerically by the bubble dissolution model. The residual methane depends on the bubble size (r) and water depth (z) and was normalized to the corresponding N_0 . The relative amount of methane at the sea surface with respect to the initial bubble methane content, $\Omega(r,z)=N_s(r,z)/N_0(r,z)$, is referred to as the transport efficiency of a single gas bubble. At seep sites, where bubbles are of uniform size, the atmospheric gas flow can be easily quantified by multiplying the bubble transport efficiency with the seabed gas flow. However, if gas bubbles show a size spectrum, $\Omega(r,z)$ has to be calculated for each bubble size and weighted by its volumetric contribution, V_0 , to the total emitted gas bubble volume, V_ψ . Adding-up this weighted bubble transport efficiency over the entire bubble size spectrum and multiplying it by the seabed gas flow at the investigated well, Q_{well} , gives the total gas flow into the atmosphere:

$$F_{Atm}(r, z) = Q_{well} * \sum_{r(min)}^{r(max)} \frac{N_s(r,z)}{N_0(r,z)} * \frac{V_0(r)}{V_\psi} \quad (\text{Eq. 6.5})$$

where, $r(min)$, and $r(max)$ are the minimum and maximum radii of the bubble size spectrum ψ , respectively, and MI is the measurement interval between individual bubble sizes (i.e. 0.1 mm). V_0 and V_ψ refer to optical size measurements at individual gas streams of the investigated wells, which were conducted to determine the combined bubble size spectrum considered to be representative for the three wells. As Eq. 6.5 assumes that there is no change in the weighted volumetric contribution of each bubble size to the total emitted bubble volume (i.e. $V_{\psi_0}(r)/V_\psi=const.$), the relative distribution of bubble sizes is considered to be constant, although the release frequency of bubbles may change due to a variability of the seabed gas flow. This means that an increase in the gas flow increases the rate of bubble formation, but not their size distribution, as generally validated for seeps with a low gas flow (Dewar et al., 2013; Leifer et al., 2004). The numerical accuracy of the model, determined from mass balance errors, was better than 99.9%.

6.4. RESULTS

6.4.1. GAS COMPOSITION AND ISOTOPIC SIGNATURES

The seep gas at the wells consists mainly of methane (85-89 Vol.%) with minor contents of ethane (69-365 ppmV) and propane (2-17 ppmV). Higher hydrocarbons, such as n-butane, n-pentane, and n-hexane, were not present; iso-butane (5.5 ppmV) was only detected at well 16/4-2 (Fig. 6.3a). The remaining gas components making up 11-15 Vol.% are assumed to consist of N_2 and O_2 , which were not determined in our analyses, but were likely stripped from ambient seawater during the time of filling the funnel with gas, i.e. 10 minutes. The volume ratio of methane and higher hydrocarbons, $C1/C2+$ of the expelled gas is 2300 -11100 and the $\delta^{13}C$ value of the methane is -71 to -70 ‰ VPDB (Fig. 6.3a).

The dissolved methane in the surface sediments shows a slightly larger variation in the $\delta^{13}C$ signature of -92.5‰ at well 15/9-13 to -60.3‰ at well 16/7-2. Likewise, DIC in the porewater carries a $\delta^{13}C$ signature ranging between -36.07 and -15.63‰ VPDB at 5 cm sediment depth (Fig. 6.3b) and between -4.76 and -6.07‰ VPDB in the bottom water. Corresponding total alkalinity values at wells 15/9-13 and 16/7-2 are 11.7 and 3.8 meq L^{-1} at 5 cmbsf and 2.5 and 2.4 meq L^{-1} in the bottom water, respectively (Fig. 6.3c).

6.4.2. LEAKAGE SITE CHARACTERISTICS

6.4.2.1. THE NATURE OF SURFACE SEDIMENTS

Surface sediments at the investigated wells were overall sandy with minor admixtures of clay, particularly at wells 15/9-13 and 16/4-2. At well 16/7-2 sediments were generally coarser. Carbonates were found only at well 16/7-2, both in the surface sediments and at the seafloor. Their stable carbon isotopic signature, $\delta^{13}\text{C}$, of -14 to -3‰ VPDB is rather heavy and corresponds well with the observed carbon isotopic signature of the DIC in ambient porewaters (see paragraph 6.4.1).

6.4.2.2. THE NATURE OF METHANE SEEPAGE

Active bubble emissions and patchy bacterial mats were characteristic leakage features at the investigated wells (Fig. 6.1). The total seepage area was roughly estimated to cover ~10 m² of seabed at each well, thus significantly exceeding the actual well diameter of ~76 cm (Horvig, 1982; Statoil et al., 1982). Bubbles generally pinched-off as single bubble streams from tiny depressions in the sandy sediments. Seepage activity varied substantially between the studied wells, evident by the significantly different numbers of total vents per well: 39 individual bubble streams were observed at well 16/7-2, whereas only 2 and 8 seep spots were found at wells 15/9-13 and 16/4-2, respectively (Tab. 6.3).

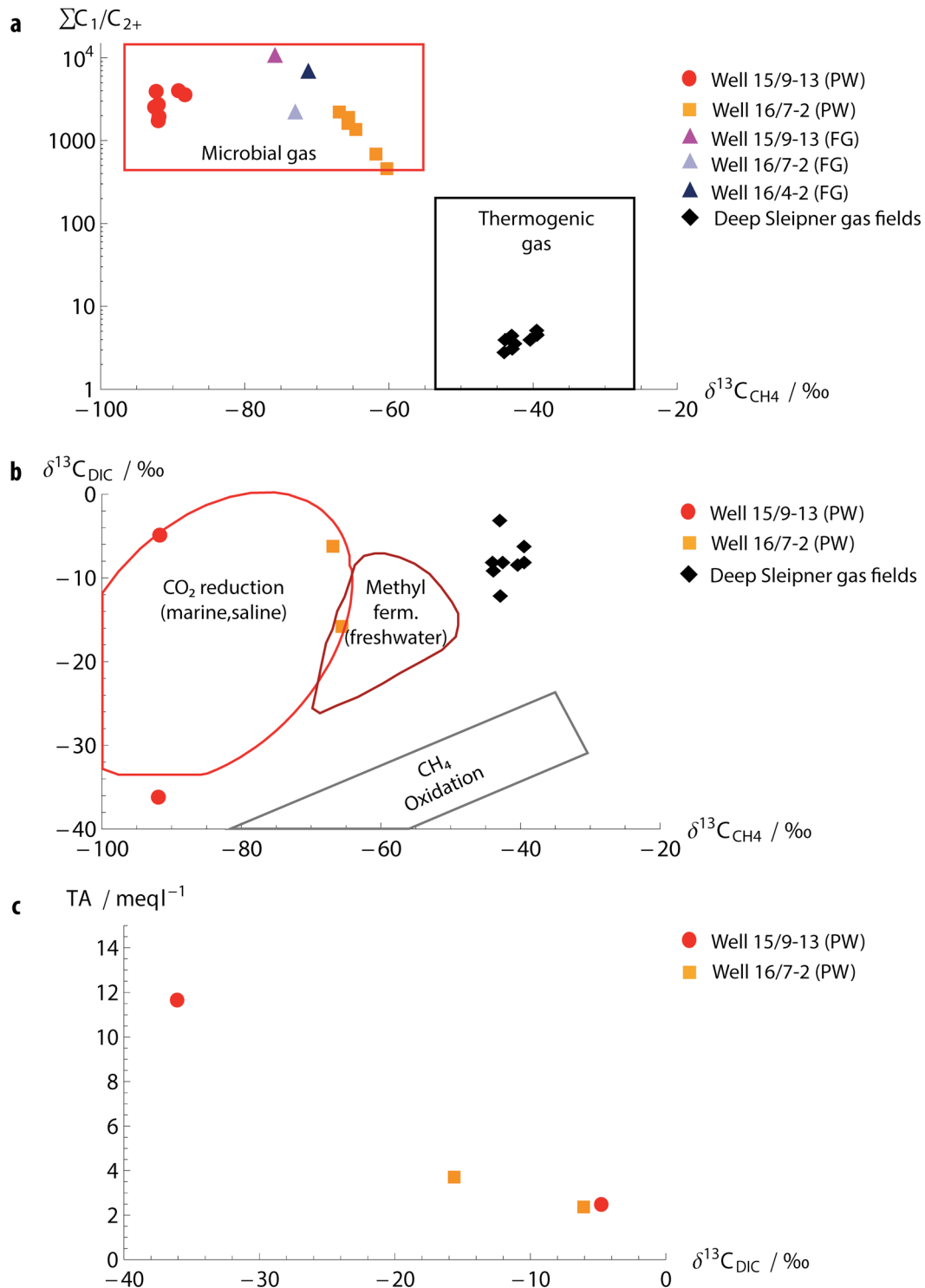


Fig. 6.3: a) Bernard diagram of the molecular and isotopic gas composition (after Bernard et al., 1978) indicating the gas source of the gas at abandoned wells (red dots: porewater (PW) at well 15/9-13, orange rectangle: porewater at well 16/7-2, triangles: free seep gas (FG) at wells 15/9-13, 16/7-2, and 16/4-2) and the deep hydrocarbon reservoirs in the area (black diamonds; James, 1990). (b) Cross-plot of $\delta^{13}\text{C}$ of DIC versus $\delta^{13}\text{C}$ of CH_4 in the porewater at well 16/7-2 (orange rectangles), well 15/9-13 (red dots), and the deep hydrocarbon reservoirs (black diamonds; James, 1990). (c) Cross-plot of total alkalinity (TA) and $\delta^{13}\text{C}$ of DIC indicating microbial anaerobic oxidation of methane.

Tab. 6.3: Quantification of seabed and atmospheric gas emissions at abandoned wells

Well	Seabed				Atmosphere	
	In situ Q per vent (L min ⁻¹)	Q (STP) per vent (L min ⁻¹)	Number of vents	Q per well ^a (t CH ₄ yr ⁻¹)	F _{Atm} per well (%)	F _{Atm} per well (kg CH ₄ yr ⁻¹)
16/4-2	0.15 /0.17 ^b	1.6/1.8 ^{b,e}	8	3.8	0.40	15.3
16/7-2	0.15 ^c	1.4 ^f	39	18.5	1.31	241.3
15/9-13	0.09	0.9 ^g	2	1	1.52	14.3
Total			49	23.3	1.2	270.9
Abs. error (2σ)	0.03	0.4		6.3 ^d		73.4 ^d
Rel. error (2σ)	24.74	27.1	121.6			

^a based on the average gas flow of 1.4 L min⁻¹ at STP

^b based on replicate gas flux measurements at well 16/4-2

^c derived from bubble size, due to lack of direct funnel measurements

^d based on a spatial variability of 27.1%

^e measured at high tide

^f measured at low tide

^g measured 2 h after low tide

6.4.3. SEABED METHANE EMISSIONS

Results of the funnel-derived gas flow measurements at individual bubble streams of well 16/4-2 and well 15/9-13 are shown in Table 6.3. At well 16/7-2 the gas flow was derived from bubble size measurements (see section 6.5.4, and Tab. 6.3). To allow comparison of the gas emissions, measured at different locations (i.e. 58.373° N and 1.932° E; 58.473° N and 2.033° E; and 58.596° N and 2.028° E, see Tab. 6.1) and at variable water-depths (i.e. 81, 83, and 93 m at well 15/9-13, 16/7-2, and 16/4-2, respectively), in-situ gas flows measured at 7.8 °C and 5.1 °C were expressed in standard conditions, referred as STP (p = 1 bar; T = 298.15 K). The standard gas flows, Q, ranged from 0.9 to 1.8 L min⁻¹ (STP) with an average gas flow of 1.4 (±0.4) L min⁻¹ (STP) at the sampled bubble streams (Tab. 6.3). This corresponds to a relative variability of 27%, which was (due to lack of information) also assumed to be equivalent to the spatial variability at a single well. Thus, based on the average Q and the number of individual bubble streams at the wells, the total seabed methane gas flow was estimated to range between 2.8 L min⁻¹ and 55 L min⁻¹ (STP), corresponding to an annual methane release of 1.0-19 t yr⁻¹ well⁻¹ assuming no larger variability over prolonged times. Estimates of the methane release were highly variable and were controlled clearly by the number of seep spots per well. Based on the relative variability of 27%, the total annual methane release of all three wells was estimated to be 24 (±6) tons.

Uncertainties in the estimation of the seabed methane flow arise from five different factors: (1) uncertainty in estimating the total number of vents, (2) error in funnel-based flow measurements (<2.5 %), (3) uncertainty due to variability in methane emission rates at individual gas streams (27%), (4) unknown temporal variability of the gas flux on time scales larger than hours, and (5) uncertainty based on the initial assumption that expelled gas consists only of methane. The latter may result in an overestimation of seabed methane emissions, because measured compositional CH₄ data were lower (85-89 Vol.%). Nevertheless, we propose that it is acceptable to assume that seep gases consist only of methane, because N₂ and O₂ uptake as well as methane dissolution during the time for filling-up the funnel (i.e. 10 minutes) likely reduced the methane content in our

gas samples. The uncertainty in the quantified number of vents is expected to be small because the counting of individual seep spots in the video material was repeated several times. However, single vents, particularly at well 16/7-2, where gas bubbling was most active, could have been missed due to the low contrast and resolution of the videos, or simply because vents were outside the area covered during the ROV dives.

5.4.4. BUBBLE SIZE MEASUREMENTS

Bubble sizes measured from video ranged from 3.2 to 16 mm in diameter (Fig. 5.4). Except for the measurements at well 16/7-2, where bubbles were observed to escape from below a carbonate rock, bubbles were emitted from sandy sediments with an average release frequency of 27 Hz. At well 16/7-2, larger bubbles were expelled into the water column because gas accumulated below a carbonate rock, thus forming significantly larger bubbles of 7.2 -16 mm in diameter compared to those directly released from the sandy sediments into the water column, i.e. 3.2- 7.4 mm in diameter.

According to the rather low gas flow, bubble emissions were classified as minor bubble plumes, typically showing narrow size distributions with peaks for radii of 2.4 and 2.7 mm at wells 15/9-13 and 16/4-2, respectively. These can be described by a simple Gaussian function, as suggested by Leifer and Culling (2010) (Fig. 5.4). The combined bubble size distribution, ψ , was determined from 274 size measurements, combining bubble size measurements at well 16/4-2 and well 15/9-13 (Fig. 5.4d). Bubble measurements at well 16/7-2 were excluded for the determination of the combined size spectrum because bubble sizes were strongly affected by gas accumulating below a carbonate rock. Given that gas flow at individual seeps is low and assuming that initial bubble formation is controlled by the mechanical properties of the surface sediments (Dewar et al., 2013), ψ is proposed to be representative for bubbles released from the fine to medium-grained clayey sand found at the investigated wells.

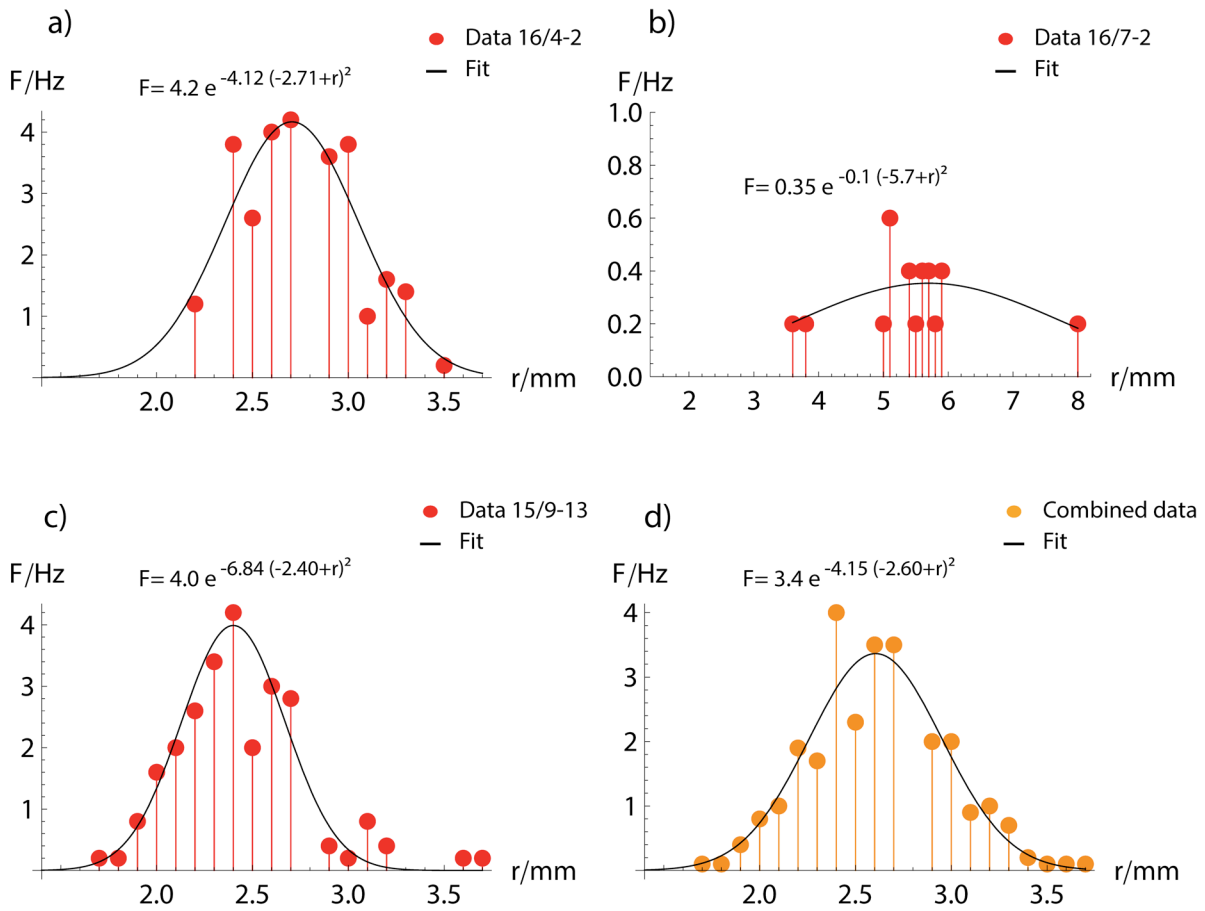


Fig. 6.4: Measured bubble release frequency (F) versus bubble radius (r), and Gaussian fits for the bubble size distribution of single streams at the investigated wells (a-c). d) Combined bubble size distribution based on measurements at wells 15/9-13 and 16/4-2. Gaussian functions were fitted to the data using the non-linear least-squares fitting algorithm "NonlinearModelFit" of Mathematica. The variance, s^2 , of the fits is 0.53, 0.002, 0.31, and 0.18 for the bubble size distributions at wells 16/4-2, 16/7-2, 15/9-13, and the combined spectrum, respectively.

The averaged uncertainty in optical size measurements arising from the 2-D projection of a 3-D oscillating volume was estimated to be 12.4%, based on multiple measurements of the same bubbles in subsequent video frames. The error significantly increased with an increasing amount of large bubbles, which is in agreement with enhanced shape oscillations (wobbling) as bubbles become larger. Furthermore, bubble size measurements at wells 15/9-13 and 16/4-2 both resulted in an in-situ gas flow of 0.10 L min^{-1} , which differed from funnel-derived gas flows of 0.09 and 0.17 L min^{-1} , respectively. Thus, bubble sizes were corrected by 1 – 14% to match direct gas flow measurements, indicating that small bubbles might have been missed, and/or that the scale was in front of the measured bubbles, both of which resulting in an under-estimation of bubble size-derived gas emissions. At well 16/7-2 video-data of funnel-derived gas flow measurements were not available. However, due to the lower release frequency, the tracking of bubbles in following frames was easier, and allowed measuring each bubble several times, which reduced the error in the bubble size-derived gas flow at this particular well.

6.4.5. CONTRIBUTION TO ATMOSPHERIC METHANE

The bubble-driven methane transport to the sea-surface strongly depends on the initial bubble size and the leakage depth. Numerical simulations show that the largest bubble of the size spectrum ($r_{eq} = 3.7$ mm) that is released from the shallowest well (i.e. well 15/9-13 at 81 mbsl) has the highest methane transport efficiency, nonetheless losing about 93% of its initial methane content on its way from the seafloor towards the sea-surface. Hence, the majority of the methane leaking from the seabed will dissolve in seawater before bubbles reach the atmosphere. Based on the determined bubble size distribution ψ , which was found to be characteristic for the investigated abandoned wells, we calculated the direct seabed methane contribution to the atmosphere for each investigated well using equation 6.5. Any additional contributions to (or from) the atmosphere arising from the diffusive air-sea gas exchange have not been quantified in this study.

Our results show that the transport efficiency, $\Omega(\psi)$, decreases with increasing water depth, but is always below 2 % (Tab. 6.3): i.e. 1.5 %, 1.3%, and 0.4% for the water depths of 81, 83, and 93 m of the respective three abandoned wells. Assuming that the observed seepage activity and the bubble size distribution are representative, this corresponds to an atmospheric methane emission of 15, 250, and 16 kg yr⁻¹, at wells 15/9-13, 16/7-2 and 16/4-2, respectively. Hence, at all three wells, combined bubbles were estimated to transport around 280 kg of seabed methane to the atmosphere each year, most of it being emitted at well 16/7-2.

Uncertainties in atmospheric emission estimates arise from two different factors: (1) spatial and temporal variability in seabed emissions, and (2) seasonal changes of sea water conditions. Based on CTD casts obtained in March 2013, the latter was found to be negligible for the investigated wells, enhancing the CH₄ transport efficiency of bubbles by less than 0.2% in winter, as determined by numerical modeling. Based on the relative spatial variability of seep emissions of 27%, the respective uncertainty in the total atmospheric methane release was estimated to be 280 (± 76) kg yr⁻¹. Some uncertainties due to the unknown temporal variability of leakage rates on time scales longer than hours and related changes of the bubble-chain dynamics remain. However, enhanced bubble rise velocities have not been observed at the investigated seeps, neither at low nor at high tide, suggesting that the atmospheric gas transport from the three wells is probably not affected by upwelling.

6.5. DISCUSSION

6.5.1. GAS ORIGIN

The methane leaking at the investigated abandoned wells is clearly of biogenic origin, as indicated by a $\delta^{13}\text{C}$ of CH₄ lighter than -70‰ VPDB and a C1/C2+ ratio larger than 1000 (Fig. 6.3a). Hence, the source depth is shallower than 2 km, considering a regional geothermal gradient of $\sim 30^\circ\text{C km}^{-1}$ and an upper temperature limit of microbial methanogenesis of 55-60°C (Rice, 1992). This interpretation is corroborated by literature values of the gases in the deep hydrocarbon reservoirs in the area showing significantly lower C1/C2+ ratios of 2.9 - 5.3 and heavier stable isotopic values, i.e. $\delta^{13}\text{C}_{\text{CH}_4} = -39$ to -44 ‰ VPDB, clearly identifying their thermogenic origin (James, 1990) (Fig. 6.3a).

The slightly larger variation in the $\delta^{13}\text{C}$ signature of the dissolved methane in the surface sediments at wells 15/9-13 and 16/7-2 suggests two different carbon pools of the seeping methane. While the $\delta^{13}\text{C}_{\text{CH}_4}$ values measured at well 15/9-13 ($\delta^{13}\text{C}_{\text{CH}_4} \approx -90$ ‰ VPDB) are produced by microbial CO₂ reduction related to a marine carbon pool, less negative values at well 16/7-2 (i.e. $\delta^{13}\text{C}_{\text{CH}_4} > -67$ ‰ VPDB) point towards microbial fermentation of methylated substrates of a fresh-water carbon pool (Fig. 6.3b). The latter may originate from fluvial or glacial sediment deposits, both common in the North Sea. The corresponding $\delta^{13}\text{C}_{\text{DIC}}$ of -15.6 ‰ VPDB and a slightly increased TA value of 3.8 meq L⁻¹ at well 16/7-2 and even more so the $\delta^{13}\text{C}_{\text{DIC}}$ of -36.07‰ VPDB and the elevated TA value of 11.7 meq L⁻¹ at well 15/9-13, both indicate that methane is oxidized by anaerobic microbial consortia in the ambient surface sediments (Fig. 6.3b, c).

In order to further constrain the origin of the leaking gas, we correlate the well paths of the three boreholes with geological information described in Well-Reports (Horvig, 1982; Statoil et al., 1982; Hydro, 1990) and with the locations of gas pockets in the subsurface sediment. The latter have been mapped as high-amplitude anomalies in the seismic data (Fig. 6.5; Karstens and Berndt, 2015).

The well-paths of 15/9-13 and 16/7-2 both penetrate sand-dominated layers with a high density of seismic bright spots, indicating a focused gas distribution forming distinct gas pockets in ~600 and ~750 mbsf (Fig. 6.5a, b). The seismic indications of free gas are in good agreement with observations in the well completion report of well 16/7-2 (Horvig, 1982). In particular, Lower Pliocene sediments at a depth of 750 m were described to contain thin gas-bearing sand stringers. However, evidence for gas was found also in shallower sediment depths, such as 715 mbsf, 687 mbsf, 539 mbsf, and 242 mbsf (Horvig, 1982). Thus, leaking gases might originate from different shallow source areas, with a biogenic signature in common. For well 16/4-2, the seismic data do not reveal prominent bright spots in the direct vicinity of the well-path, but the near-surface sediments (Fig. 6.5c, 0.1 – 0.4 s two-way-travel time TWT) show seismic turbidity, which might indicate an unfocussed distribution of gas (Judd and Hovland, 1992). Hence, the presence of free gas in the pore space is less constrained by the seismic data at well 16/4-2 than at 15/9-13 and 16/7-2. Well 16/4-2 further penetrates a topographic high at the Top Pliocene (Fig 6.5c; 0.5 s TWT), which may facilitate buoyancy-controlled gas migration towards the well.

6.5.2. THE NATURE OF GAS MIGRATION ALONG AN ABANDONED WELL

In the absence of high overpressures, gas migration along an abandoned well can be best described by buoyancy-driven capillary invasion of well-induced pathways where the gas has to exceed the capillary pressure to enter an initially water-saturated conduit (Clayton et al., 1994; Gurevich et al., 1993). The capillary resistance that needs to be overcome generally decreases with increasing pore-space (sediments) or width (fracture), making a water-saturated clay totally impermeable for non-overpressured gas (i.e. due to the very large capillary pressure of ~300 kPa, Wheeler et al., 1990; Judd and Hovland, 2007), unless there are pre-existing cracks and fractures.

Thus, leakage problems often are compounded by geotechnical fracturing of sediment around the wellbore and by insufficient filling of these fractures with cement, resulting in a fracture system along the well (Gurevich et al., 1993). The upward migration of gas can occur along any of several pathways associated with the abandoned well: a) between casing and cement; b) between cement plug and casing; c) through the cement pore space as a result of cement degradation; d) through the casing as a result of corrosion; e) through fractures in the cement; and f) between cement and sediment (Gasda et al., 2004). Because all investigated wells have plugs and casing, each of these possible migration conduits is conceivable and would be associated to enhanced effective permeability providing the key to the initiation of gas migration, drawing gas from the surrounding sediment because of lower capillary pressure in the fracture (Bethke et al., 1991; Judd and Hovland, 2007). Nordland Group sediments from ~300 mbsf down to the Utsira Formation primarily consist of clay as indicated by high gamma ray values in the well-logs (Fig. 6.2). Therefore, they provide an efficient barrier for capillary gas invasion holding gas at a higher pressure than sand. Hence, strata-crossing upward migration of gas should only be possible along secondary, either natural or well-induced, pathways.

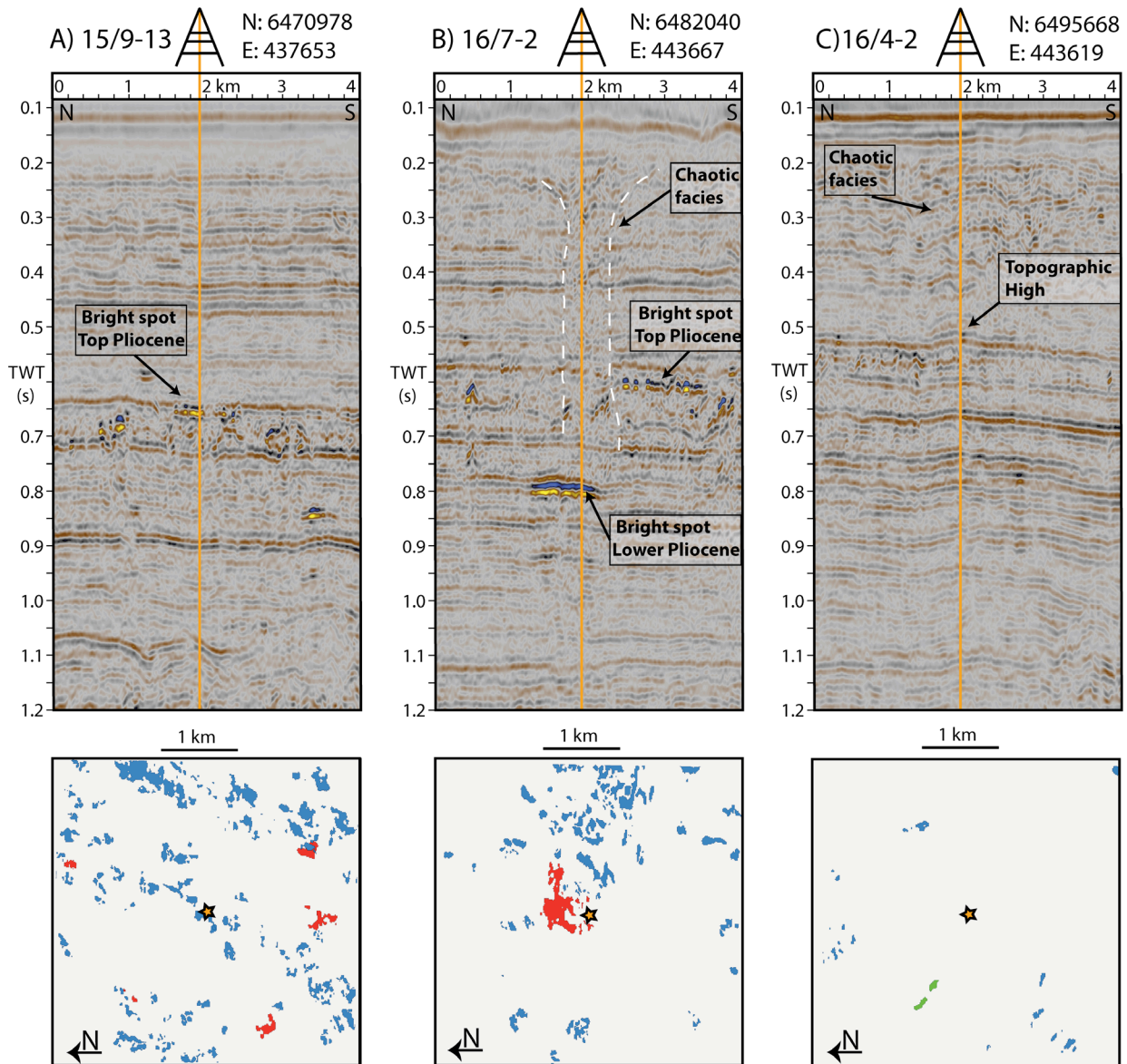


Fig. 6.5: (Top panel) Seismic profiles indicating shallow gas pockets in the subsurface and the well paths of the 3 abandoned wells (orange line). At well 16/7-2 the outline of the seismic chimney and chaotic reflections is depicted. (Bottom pane) Areal distribution of shallow gas pockets (green= Pleistocene, blue = Top Pliocene, and red= Lower Pliocene) above the deep hydrocarbon reservoirs (orange stars: seafloor location of the abandoned wells).

6.5.3. GEOLOGICAL CONTROL OF LEAKAGE

Leaky Leaky wells showed continuous gas bubble release into the water-column. However, total seabed emissions at the wells were highly variable (ranging from 1 to 19 t yr⁻¹ of CH₄), being ultimately controlled by differences in the number of bubble streams per well (2, 8, and 39). In order to understand the mechanisms that might control leakage activity at abandoned wells, we correlate the bubble emissions of the three boreholes with properties of the subsurface sediments. The most remarkable observation is the presence of a seismic chimney at well 16/7-2 (Fig. 6.5b), indicated by disturbed and chaotic reflections in Upper Cenozoic sequences, coinciding with the highest leakage activity being observed here. The chimney apparently provides additional pathways and appears to facilitate gas migration towards the seabed. However, it is not obvious from our data if and to what extent the migrating gas appears to separate from the borehole fracture and uses

pre-existing conduits created by the chimney sometime in the geological past. Seismic modelling and S-wave experiments conducted on chimneys above the Tommeliten reservoirs proved that seismic chimneys represent gas-filled fracture networks within impermeable bedrock (Granli et al., 1999; Arntsen et al., 2007; Løseth et al., 2009). Hence, the chimney at well 16/7-2 also might represent a potential source and pathway for leaking gas. The seismic feature is also in good agreement with the evidence of carbonates found at the seafloor that may indicate a longer history of gas seepage in the area of the seismic chimney. However, with the current carbonate isotopic data it is not possible to constrain the seepage history for well 16/7-2 any further.

Considering permanent well plugging and abandonment procedures, final (upper) gas migration and bubble formation are controlled by surface sediments unless there are very high gas flows affecting bubble sizes (Dewar et al., 2013). The required sediment depth for cutting of the wellhead and the following casings typically is at least 5 mbsf to minimize the risk of parts of the well protruding the seabed (NORSOK D010, 2004). A comparison of the three wells with natural seepage systems shows that the initial bubble size distribution at leaky wells is in good agreement to bubble diameters found at Tommeliten (Schneider von Deimling et al., 2011) and the Scanner Pockmark field (Judd and Hovland, 2007) (Tab. 6.4). Thus, the bubble formation mechanisms are supposed to be quite similar, regardless if seepage is of anthropogenic or natural origin. Analogous to natural seep sites, local changes in lithology (i.e. clays), and biogeochemical boundaries (i.e. carbonate cementation) might cause lateral diversion or re-trapping of migrating gas bubbles along surfaces in the sedimentary overburden (Judd and Hovland, 2007). Clay inter-beddings in retrieved push cores are in good agreement with reduced leakage activity. With increasing amounts of clay in the upper sediment, vertical movement of the gas likely is restricted and lateral movement encouraged, thus favoring diversion of seepage paths, as indicated by the presence of large bacterial mats at well 15/9-13 and 16/4-2. By contrast, the relatively coarse sediments at well 16/7-2 facilitate gas migration to the sediment-surface, due to higher permeability (Judd and Hovland, 2007).

Unfortunately, we were unable to measure any longer temporal variability of seabed gas emissions. Hence, we are unable to report on the dependency of tidal pressure fluctuations or release and re-filling of near-surface gas pockets, which are commonly believed to control the rate of bubble emissions at the seabed (e.g., Leifer and Wilson, 2007; Linke et al., 1994; Tryon et al., 1999; Wiggins et al., this issue).

We conclude that intense gas leakage at well 16/7-2 is related to relatively coarse surface sediments and a gas chimney in the subsurface, which provides additional pathways for gas migration. Thus, sediment properties appear to control bubble emissions at leaky wells, as previously observed at natural seep sites (Judd and Hovland, 2007). Nevertheless, we cannot exclude further mechanisms that may drive gas migration in the subsurface and leakage activity at the seafloor, such as overpressure in the shallow gas reservoir or fluctuations and differences in gas supply.

Tab. 6.4: Comparison of natural and anthropogenic gas emissions in the North Sea

Location	Nr. of vents	Bubble radius (mm)	Area (m ²)	Q per vent (kg/a)	Q per area (t/yr)	Reference
Scanner Pockmark	3	2.5	-	36	-	Hovland et al., 2012; Judd and Hovland, 2007; Hovland, 1985, Clayton and Dando, 1996
UK Block 15/25	-	-	22,825	-	6.8	Judd, 2004; Clayton and Dando, 1996
Anvil Point, Dorset UK	-	-	-	-	68	Judd, 2004; Hinchcliffe, 1978
Torre Bay, Firth of Forth, Scotl.	-	-	2400	-	1.25-1.8	Judd et al., 2002
Tommeliten	550	2.2	-	37.1	26	Schneider von Deimling et al., 2011
Gulfaks-Heincke seeps	1-2 every 5 m ²	-	1000	-	-	Wegener et al., 2008, Hovland et al., 2012
Blowout well 22/4b	176	-	360	-	32x103	Leifer et al., this issue
3 abandoned wells	49	2.55*	10	470	23.3	This study

* based on the peak radius of the global size distribution determined in this study

6.5.4. METHANE EMISSIONS IN A NORTH SEA CONTEXT

In order to place the methane release from the three investigated wells in context to other North Sea methane emissions, we compare them with natural seabed methane fluxes. Although many natural seep locations are known, only few North Sea methane flux calculations have been reported in the literature so far: Tommeliten (Schneider von Deimling et al., 2011), the Scanner Pockmark field within UK Block 15/25 (Hovland, 1985; Judd and Hovland, 2007; Clayton and Dando, 1996; Hovland et al., 2012), Anvil Point (UK, Judd, 2004; Hinchcliffe, 1978), Torre Bay (Scotland, Judd et al., 2002) and the Gulfaks seeps (Hovland, 2007; Wegener et al., 2008). All of them occur as long-lasting-macro-seep systems, associated with continuous gentle methane venting in the central and northern North Sea (Hovland et al., 2012). Due to their large seepage area, these sites are supposed to contribute considerable amounts of methane to North Sea bottom waters (Bange, 2006) (Tab. 6.4). Annual methane emissions vary between 1.25, 26 and 68 t at Torre Bay, Tommeliten, and Anvil Point, respectively, demonstrating the high spatial variability of natural seep sites, apparently in response to variations in the geological setting (Judd and Hovland, 2007). Active venting has been reported at Tommeliten, where around 550 bubble streams emanate at the seafloor (Schneider von Deimling et al., 2011). Despite

the much smaller source area and smaller number of vents at the three leaky abandoned wells, their emission rates were estimated to be similar to Tommeliten, due to a source strength exceeding that at Tommeliten by one order of magnitude, i.e. the bubble release rate at individual vents was 27 Hz at each abandoned well and 7 Hz at Tommeliten (Schneider von Deimling et al., 2011). Together with a slightly larger bubble peak radius (i.e. 0.4 mm larger), the three abandoned wells are estimated to emit a comparable seabed flow of $\sim 24 \text{ t CH}_4 \text{ yr}^{-1}$, mainly driven by the large seabed emissions from well 16/7-2.

Compared to the overpressure-driven gas blowout at well 22/4b, which is shown to be a significant source for methane into the seawater (Leifer, this issue) and the atmosphere (Judd, this issue, Rehder et al., 1998), the leakage from the three abandoned wells indicates an additional and potentially significant anthropogenic methane source in the North Sea. Considering the extensive drilling activity over the past 40 years and given that overall emissions from only three abandoned wells appear to be comparable to natural emissions at Tommeliten, leaky abandoned wells, depending on the overall number and the magnitude of their emissions, should provide a significant input to the North Sea methane budget.

6.5.5. METHANE CONTRIBUTION TO THE ATMOSPHERE

To assess the direct release of seabed methane to the atmosphere, we simulated the bubble-driven methane transport towards the sea-surface with a numerical bubble dissolution model. The vertical transport efficiency of bubbles strongly depends on initial/seabed parameters, in particular bubble size and water depth. Hence, the bubble size distribution and the leakage depth are crucial initial parameters to simulate the fate of methane bubbles. Based on the combined bubble size distribution of wells 15/9-13 and 16/4-2, the model results suggest that the three investigated wells contribute less than 2 % of seabed methane directly to the atmosphere (Tab. 6.3). The transport efficiency thus slightly exceeds that of bubbles released at the blowout well 22/4b (i.e. $\sim 1 \%$; Leifer et al., this issue) where plume-induced turbulences likely enhance the mass transfer at the bubble-water-interface compensating high rise velocities. In the absence of any plume-induced advection, the critical parameter is the release frequency of large bubbles, which manage to reach the sea surface and still contain methane. At the investigated wells, the major volume fraction (60%) consists of bubbles with radii smaller than 2.7 mm, transporting less than 1% of seabed methane to the sea surface. Bubbles with radii smaller than 2 mm completely lose their methane by the time they have reached the sea surface.

We conclude that the three wells represent no significant source for direct methane emissions by bubble transport to the atmosphere. However, methane bubble dissolution in the water-column, particularly in the surface mixed layer, could contribute additional methane to the atmosphere via diffusive gas exchange (Wanninkhof, 1992). The seasonal deepening and breakdown of the thermocline during fall to spring (Nauw et al., this issue; Sommer et al., this issue) and even more so, frequent fall and winter storms (Shakhova et al., 2013) will aid the ventilation of the water column and hence, diffusive outgassing of methane to the atmosphere may slightly enhance emission rates.

Possible leaky wells at shallower depths will be more important for direct atmospheric fluxes, underscoring the importance for leaky well surveys in shallower depths. Although our results indicate the potential for a significant impact of these leaking abandoned wells on the regional CH_4 budget of the North Sea, more data on the number of leaking wells, bubble size spectra and longer time-series of leakage rates will be necessary to constrain their actual role.

6.6. CONCLUSIONS

A well, analogous to a fracture, provides the key for the initiation of vertical gas migration in the subsurface. Boreholes surrounded by mechanically disturbed and fractured sediments with enhanced permeability, may guide gas directly to the wellhead, and serve to focus gas migration into a single pathway. To what extent and when gas migration pathways tend to separate from the borehole cannot be clarified in this study, although it seems that sediments which provide additional conduits for migrating gases, such as gas chimneys, tend to facilitate gas migration and increase seepage activity at the seafloor. The generally light isotopic signature of methane and the minor constituents of higher hydrocarbons in seep gases point towards a microbial origin. Shallow gas pockets overlying the deep hydrocarbon reservoirs are likely sources for the gas emanating at the wells, which is supported by bright spots and zones with chaotic signatures in the seismic data. Comparing properties that are equivalent to natural seep sites, such as bubble size, release frequency, and sediment characteristics, we conclude that geology provides the ultimate control for bubble venting at the seafloor, for both anthropogenic and natural seeps. Our first measurements of methane gas fluxes at abandoned wells indicate that numerous leaky wells may contribute significantly to the North Sea methane budget because estimated annual emissions at the studied wells ($\sim 24 \text{ t CH}_4 \text{ yr}^{-1}$) are comparable to those at major natural seepage sites such as Tommeliten. Direct bubble-driven methane fluxes to the atmosphere remain small at the studied wells since more than 98% of the gas released at the seabed is dissolved in the 81 to 93 m deep water column before reaching the atmosphere. However, the diffusive sea/air gas exchange may provide an additional pathway of methane release to the atmosphere at these sites. Long-term monitoring campaigns are needed to better constrain the total (annual) methane release into the atmosphere derived from abandoned offshore wells.

ACKNOWLEDGEMENTS

We would like to thank the crew and master of RV Celtic Explorer and RV Alkor as well as the Kiel ROV6000 team for their invaluable support during the cruises CE12010 and AL412. We would also like to acknowledge the high-quality support for geochemical analyses by Andrea Bodenbinder and Meike Dibbern as well as Monika Segl at MARUM/University Bremen for the DIC isotope measurements. We thank Statoil ASA for permission to use the 3D seismic data. Special thanks to Martin Hovland for making us aware of the gas seepage at the three wells. The cruises and scientific work received funding through the European Community's 7th Framework Program (FP7/2007-2013) in the EUROFLEETS program, the ECO2 project (grant agreement no. 265847) and the DFG funded Cluster of Excellence "Future Ocean".

REFERENCES

- Arntsen, B., Wensaas, L., Løseth, H., Hermanrud, C., 2007. Seismic modeling of gas chimneys. *Geophysics* 72, SM251–SM259.
- Bange, H.W., Bartell, U.H., Rapsomanikis, S., Andreae, M.O., 1994. Methane in the Baltic and North Seas and a reassessment of the marine emissions of methane. *Global Biogeochemical Cycles* 8, 465–480.
- Bange, H.W., 2006. Nitrous oxide and methane in European coastal waters. *Est.Coast.Shelf Sci.* 70, 361-374
- Behtke, C. M., Reed, J.D., Olzt, D.F., 1991. Long –range petroleum migration in the Illinois Basin. *American Association of Petroleum Geologists (Bulletin)*, 75, 925-45.
- Bernard, B.B., Brooks, J.M., Sackett, W.M., 1987. Light hydro-carbons in recent Texas continental shelf and slope sediments. *J. Geophy. Res.* 83, 4053-4061.
- Boudreau, B.P., 1997. Diagenetic models and their implementation: modelling transport and reactions in aquatic sediments. Berlin, Heidelberg, New York, London, Paris, Tokyo, Hong Kong: Springer, 414 pp.
- Ciais, P., Sabine, C., Bala, G., Bopp, L., Brovkin, V., Canadell, J., Chhabra, A., DeFries, R., Galloway, J., Heimann, M., Jones, C., Le Quéré, C., Myneni, R.B., Piao, S., Thornton, P., 2013. *Climate Change 2013: The Physical Science Basis. Contribution of Working Group I to the Fifth Assessment Report of the Intergovernmental Panel on Climate Change*, in: Stocker, T.F., Qin, D., Plattner, G.-K., Tignor, M., Allen, S.K., Boschung, J., Nauels, A., Xia, Y., Bex, V., Midgley, P.M. (Eds.). IPCC, Cambridge, UK, pp. 465-570.
- Clayton, C.J., Hay, J., 1994. Gas migration mechanisms from accumulation to surface. *Bulletin of the Geological Society of Denmark*, Vol. 41, 12-23.
- Clayton, C.J., Dando, R.D., 1996. Comparison of seepage and seep leakage rates. In: Schumacher, D., Abrams, M.A. (Eds.), *Hydrocarbon Migration and its Near-Surface Expression*. American Association of Petroleum Geologists Memoir, 66, pp. 169–171.
- Clayton, C.J., Hay, S.J., Baylis, S.A., Dipper, B., 1997. Alteration of natural gas during leakage from a North Sea salt diapir field. *Marine Geology* 137, 69-80.
- Clift, R., Grace, J.R., Weber, M.E., 1978. *Bubbles, Drops, and Particles*. Academic Press, London p. 380.
- Crutzen, P.J., Zimmermann, P.H., 1991. The changing photochemistry of the troposphere. *Tellus Series A – Dynamic Meteorology and Oceanography* 43, 136–151.
- Dewar, M., Wei, W., Chen, B., 2013. Small-scale modelling of the physicochemical impacts of CO₂ leaked from sub-seabed reservoirs or pipelines within the North Sea and surrounding waters. *Marine Pollution Bulletin*, 73, 504-515.
- Duan, Z., Moller N., Weare, J.H., 1992. An equation of state for the CH₄-CO₂-H₂O system: I. Pure systems from 0-1000°C and from 0 to 8000 bar. *Geochimica et Cosmochimica Acta* Vol. 56. 2605-2617.
- Duan, Z.H., Mao, S., 2006. A thermodynamic model for calculating methane solubility, density and gas phase composition of methane-bearing aqueous fluids from 273 to 523 K and from 1 to 2000 bar. *Geochimica et Cosmochimica Acta* 70, 3369-3386.
- Eidvin, T., Rundberg, Y., 2007. Post-Eocene strata of the southern Viking Graben, northern North Sea; integrated biostratigraphic, strontium isotopic and lithostratigraphic study. *Norwegian Journal of Geology* 87, 391–450.
- Etioppe, G., Lassey, K.R., Klusmann, R.W., Boschi, E., 2008. Reappraisal of the fossil methane budget and related emissions from geologic sources. *Geophysical Research Letters*, Vol. 35 (9), L09307, doi:10.1029/2008GL033623.

- Farreira, T., Rasband, W., 2012. ImageJ User Guide IJ 1.46r. 185p. <http://imagej.nih.gov/ij/docs/guide/index.html>
- Galloway, W.E., 2001. Seismic expressions of deep-shelf depositional and erosional morphologies, Miocene Utsira Formation, North Sea Basin. *Marine Geophysical Research* 22, 309–321.
- Galloway, W.E., 2002. Paleogeographic setting and depositional architecture of a sand-dominated shelf depositional system, Miocene Utsira Formation, North Sea Basin. *Journal of Sedimentary Research* 72, 476–490.
- Gasda, S.E., Bachu, S., Celia, M.A., 2004. Spatial characterization of the location of potentially leaky wells penetrating a deep saline aquifer in a mature sedimentary basin. *Environmental Geology* 46, 707-720
- Gautier, D.L., 2005. Kimmeridgian Shales Total Petroleum System of the North Sea Graben Province: U.S. Geological Survey Bulletin 2204-C, 24 p.
- Geng, M., Duan, Z.H., 2010. Prediction of oxygen solubility in pure water and brines up to high temperatures and pressures. *Geochimica et Cosmochimica Acta* 74, 5631-5640.
- Granli, J.R., Arntsen, B., Sollid, A., Hilde, E., 1999. Imaging through gas-filled sediments using marine shear-wave data. *Geophysics* 64, 668–677.
- Grunwald, M., Dellwig, O., Liebezeit, G., Schnetger, B., Reuter, R., Brumsack, H.J., 2007. A novel time-series station in the Wadden Sea (NW Germany): first results on continuous nutrient and methane measurements. *Marine Chemistry* 107, 411–421.
- Grunwald, M., Dellwig, O., Beck, M., Dippner, J.W., Freund, J.A., Kohlmeier, C., Schnetger, B., Brumsack, H.J., 2009. Methane in the southern North Sea, spatial distribution and budgets. *Est.Coast.Shelf Sci.* 81, 445-456.
- Gurevich, A.E., Endres, B.L., Robertson Jr, J.O., Chilingar, G.V., 1993. Gas migration from oil and gas fields and associated hazards. *J. Petr. Sci. Eng.* 9, 233-238.
- Haeckel, M., Boudreau, B.P., Wallmann, K., 2007. Bubble induced porewater mixing: A 3-D model for deep porewater irrigation. *Geochimica et Cosmochimica Acta*, Vol. 71, Nr. 21, 5135-5154.
- Hartmann, D.L., A.M.G. Klein Tank, M. Rusticucci, L.V. Alexander, S. Brönnimann, Y. Charabi, F.J. Dentener, E.J. Dlugokencky, D.R. Easterling, A. Kaplan, B.J. Soden, P.W. Thorne, M. Wild and P.M. Zhai, 2013: Observations: Atmosphere and Surface. In: *Climate Change 2013: The Physical Science Basis. Contribution of Working Group I to the Fifth Assessment Report of the Intergovernmental Panel on Climate Change* [Stocker, T.F., D. Qin, G.-K. Plattner, M. Tignor, S.K. Allen, J. Boschung, A. Nauels, Y. Xia, V. Bex and P.M. Midgley (eds.)]. Cambridge University Press, Cambridge, United Kingdom and New York, NY, USA.
- Heggland, R., 1997. Detection of gas migration from a deep source by the use of exploration 3D seismic data. *Marine Geology* 137, 41–47.
- Hinchcliffe, J.C., 1978. Death stalks the secret coast. *Triton* 23:56–57
- Hoefs J., 1997. *Stable Isotope Geochemistry*. Berlin, Heidelberg, New York, London, Paris, Tokyo, Hong Kong: Springer-Verlag, 4th edition, 201 pp.
- Horvig, S., 1982. WDSS 40 01 16 7 2: Geological Completion Report Well 16/7-2. Esso Exploration and production Norway Inc.
- Hovland, M., Sommerville, J.H., 1985. Characteristics of two natural gas seepages in the North Sea. *Marine and Petroleum Geology* 2, 319–326.
- Hovland, M., Judd, A.G., 1988. *Seabed Pockmarks and Seepages. Impact on Geology, Biology and Marine Environment*. London, Dordrecht, Boston: Graham & Trotman (Kluwer), 293 pp.

- Hovland, M., Judd, A.G., Burke Jr., R.A., 1993. The global flux of methane from shallow submarine sediments. *Chemosphere* 26 (1–4), 559–578.
- Hovland, M., 2007. Discovery of prolific natural methane seeps at Gullfaks, northern North Sea. *Geo-Marine Letters*, 27 (2-4), 197-201.
- Hovland, M., Jensen, S., Fichler, C., 2012. Methane and minor oil macro-seep systems- Their complexity and environmental significance. *Marine Geology*, 332-334, 163-173.
- Hydro, 1990. WDSS 15 60 01: General Information Well 16/4-2. http://www.npd.no/engelsk/cwi/pbl/wdss_old/1560_01_WDSS_General_Information.pdf
- Jones, R.D., 1991. Carbon-monoxide and methane distribution and consumption in the Photic Zone of the Sargasso Sea. *Deep-Sea Research Part A – Oceanographic Research Papers* 38, 625–635.
- Judd, A.G., Hovland, M., 1992. The evidence of shallow gas in marine sediments. *Cont. Shelf Res.* 12: 1081-1095
- Judd, A.G., Sim, R., Kingston, P., McNally, J., 2002. Gas seepage on an intertidal site: Torry Bay, Firth of Forth, Scotland. *Cont. Shelf Res.* 22:2317–2331
- Judd, A.G., 2004. Natural seabed gas seeps as sources of atmospheric methane. *Environmental Geology* 46, 988-996.
- Judd, A.G., Hovland, M., 2007. *Seabed Fluid Flow- The impact on geology, biology and marine environment.* Cambridge University Press, 475 pp.
- Judd, A.G., this issue. Title: The significance of the 22/4b blow-out site methane emissions in the context of the North Sea. *Journal of Marine and Petroleum Geology*, this issue.
- Justwan, H., Dahl, B., 2005. Quantitative hydrocarbon potential mapping and organofacies study in the Greater Balder Area, Norwegian North Sea 6, 1317–1329.
- Karstens, J., Berndt, C., 2015. Seismic chimneys in the Southern Viking Graben - Implications for palaeo fluid migration and overpressure evolution. *Earth and Planetary Science Letters*, 412, pp. 88-100
- Kvenvolden, K.A., Rogers, B.W., 2005. Gaia's breath-global methane exhalations. *Marine and Petroleum Geology* 22, 579-590.
- Leifer, I., Patro, R., Bowyer, P., 2000. A study on the temperature variation of rise velocity for large clean bubbles. *J. Atm. Ocean Tech.* 17, 1392–1402.
- Leifer, I., and Patro, R.K., 2002. The bubble mechanism for methane transport from the shallow sea bed to the surface: A review and sensitivity study, *Cont. Shelf Res.*, 22, 2409–2428, doi:10.1016/S0278-4343(02)00065-1.
- Leifer, I., MacDonald, I.R., 2003. Dynamics of the gas flux from shallow gas hydrate deposits: Interaction between oily hydrate bubbles and the oceanic environment. *Earth and Planetary Science Letters* 210, 411-424.
- Leifer, I., Boles, J.R., Luyendyk, B.P., Clark, J.F., 2004. Transient discharges from marine hydrocarbon seeps: Spatial and temporal variability. *Environmental Geology*, 46, 1038-1052.
- Leifer, I., Wilson, K., 2007. The tidal influence on oil and gas emissions from an abandoned oil well: Nearshore Summerland, California, *Marine Pollution Bulletin*, Vol. 54, 9, 1495-1506.
- Leifer, I., Culling, D., 2010. Formation of seep bubble plumes in the Coal Oil Point seep field. *Geo-Mar Lett.* 30, 339-353, DOI 10.1007/s00367-010-0187-x.

Leifer, I., this issue. Seabed bubble flux estimation by calibrated video survey for a large blowout seep in the North Sea. *Journal of Marine and Petroleum Geology*, this issue.

Leifer, I., Solomon, E., Schneider von Deimling, J., Rehder, G., Coffin, R., Linke, P., this issue. The Fate of Bubbles in a Large, Intense Megaplume for Stratified and Unstratified Water: Numerical Simulations of 22/4b Expedition Field Data. *Journal of Marine and Petroleum Geology*, this issue.

Lelieveld, J., Crutzen, P.J., Bruhl, C., 1993. Climate effects of atmospheric methane. *Chemosphere* 26, 739–768.

Linke, P., Suess, E., Torres, M., Martens, V., Rugh, W. D., Ziebis, W., and Kulm, L. D., 1994. In situ measurement of fluid flow from cold seeps at active continental margins. *Deep-Sea Research I* 41, 721-739.

Løseth, H., Gading, M., Wensaas, L., 2009. Hydrocarbon leakage interpreted on seismic data. *Marine and Petroleum Geology* 26, 1304–1319.

McGinnis, D. F., Greinert, J., Artemov, Y., Beaubien, S.E., Wüest, A., 2006. Fate of rising methane bubbles in stratified waters: How much methane reaches the atmosphere? *J. Geophys. Res.*, 111, C09007, doi:10.1029/2005JC003183.

McGinnis, D. F., Little J.C., 2002. Predicting diffused-bubble oxygen transfer rate using the discrete-bubble model. *Water Res.*, 36, 4627–4635, doi:10.1016/S0043-1354(02)00175-6.

Nauuw, J., de Haas, H., Leifer, I., Rehder, G., this issue. A review of oceanographic and meteorologic controls on the fate of North Sea methane from a seabed source. *Journal of Marine and Petroleum Geology*, this issue.

Norbotten, J.M., Celia, M.A., Bachu, S., Dahle, H.K., 2005. Semianalytical Solution for CO₂ Leakage through an Abandoned Well. *Environ. Sci. Technol.* 39, 602-611

NORSOK Standard D-010, 2004. <http://www.standard.no/PageFiles/1315/D-010r3.pdf>

Mao, S., Duan, Z.H., 2006. A thermodynamic model for calculating nitrogen solubility, gas phase composition and density of the N₂-H₂O-NaCl-system. *Fluid Phase Equilibria* 248, 103-114.

Pape, T., Bahr, A., Rethemeyer, J., Kessler, J.D., Sahling, H., Hinrichs, K.U., Klapp, S.A., Reeburgh, W.S., Bohrmann, G., 2010. Molecular and isotopic partitioning of low-molecular-weight hydrocarbons during migration and gas hydrate precipitation in deposits of a high-flux seepage site. *Chemical Geology* 269, 350–363.

Rehder, G., Schneider von Deimling, J., 2008. RV Sonne Cruise Report SO 196, SUMSUN 2008, Suva Guam Okinawa Trough Manila. February 19- March 26 2008. PANGAEA, hdl: 10013/epic.35734.

Rice D.D., 1992. Controls, habitat, and resource potential of ancient bacterial gas. Vially R (Ed.) *Bacterial Gas*, Editions Technip, Paris, 91–118

Römer, M., Sahling, H., Pape, T., Bohrmann, G., Spieß, V., 2012. Quantification of gas bubble emissions from submarine hydrocarbon seeps at the Makran continental margin (offshore Pakistan). *Journal of Geophysical Research: Oceans* 117, C10015.

Sauter, E.J., Muyakshin, S.I., Charlou, J.-L., Schlüter, M., Boetius, A., Jerosch, K., Damm, E., Foucher, J.-P., Klages, M., 2006. Methane discharge from a deep-sea submarine mud volcano into the upper water column by gas hydrate-coated methane bubbles. *Earth and Planetary Science Letters* 243, 354-365.

Schneider v. Deimling J, Brockhoff J, Greinert J (2007) Flare imaging with multibeam systems: Data processing for bubble detection at seeps. *Geochemistry, Geophysics, Geosystems* 8

Schneider von Deimling, J., Rehder, G., Greinert, J., McGinnis, D.F., Boetius, A., Linke, P., 2011. Quantification of seep-related methane gas emissions at Tommeliten, North Sea. *Continental Shelf Res.* 31, 867-878.

Schneider von Deimling, J., Linke, P., Schmidt, M., Rehder, G., this issue. A mega methane gas plume with spiral vortex motion- rediscovery of and insights about the abandoned Blowout site in the North Sea since 2005. *Journal of Marine and Petroleum Geology*, this issue.

Scranton, M.I., McShane, K., 1991. Methane fluxes in the southern North-Sea – the role of European rivers. *Continental Shelf Research* 11, 37–52.

Shakhova, N., Semiletov Igor P., Leifer, I., Sergienko, V., Salyuk, A., Kosmach, D., Chernikh, D., Stubbs, C., Nicolsky, D., Tumskoy, V., Alexeev, V., Gustafsson, O., 2013. Ebullition and storm-induced methane release from the East Siberian Arctic Shelf. *Nature Geoscience* 7, 64-70.

Sofroniou, M., Knapp, R., 2008. Wolfram Mathematica Tutorial Collection- Advanced numerical differential equation solving in Mathematica. Wolfram Research, Inc. <http://www.wolfram.com/learningcenter/tutorialcollection/AdvancedNumericalDifferentialEquationSolvingInMathematica/AdvancedNumericalDifferentialEquationSolvingInMathematica.pdf>

Sommer, S., Schmidt, M., Linke, P., this issue. Continuous inline tracking of dissolved methane plume at a blow out site in the North Sea UK – water column stratification impedes immediate methane release into the atmosphere. *Journal of Marine and Petroleum Geology*, this issue.

Statoil, ESSO, NORSK Hydro, 1982. 45 01 WDSS General Information: Completion Report Well 15/9-13 PL 046.

Tryon, M. D., Brown, K. M., Torres, M. E., Trehu, A. M., McManus, J., and Collier, R. W., 1999. Measurements of transience and downward fluid flow near episodic gas vents, Hydrate Ridge, Cascadia. *Geology* 27, 1075-1078.

UNESCO. 1981a. The Practical Salinity Scale 1978 and the International Equation of State of Seawater 1980. UNESCO Technical Papers in Marine Science 36, 25 pp.

Upstill-Goddard, R.C., Barnes, J., Frost, T., Punshon, S., Owens, N.J.P., 2000. Methane in the southern North Sea: low-salinity inputs, estuarine removal, and atmospheric flux. *Global Biogeochemical Cycles* 14, 1205–1217.

Vignes, B., Andreassen, J., Tønning, S.A., 2006. PSA Well Integrity Survey, Phase 1 summary report. Petroleum Safety Authority. Chapter 3a.docx

Wanninkhof, R., 1992. Relationship between wind speed and gas exchange over the ocean. *Journal of Geophysical Research* 97: doi: 10.1029/92JC00188.

Ward, B.B., Kilpatrick, K.A., Novelli, P.C., Scranton, M.I., 1987. Methane oxidation and methane fluxes in the ocean surface-layer and deep anoxic waters. *Nature* 327, 226–229.

Wegener, G., Shovitri, M., Niemann, H., Hovland, M., Boetius, A., 2008. Biogeochemical processes and microbial diversity of the Gullfaks and Tommeliten methane seeps (Northern North Sea). *Biogeoscience* 5, 1127-1144.

Wheeler, S.J., Sham, W.K., Thomas, S.D., 1990. Gas pressure in undersaturated offshore soils. *Canada Geotechnical Journal*, 27, 79-89.

Wiggins, S., Hildebrand, J., Leifer, I., this issue. Long-term acoustic monitoring at North Sea well site 22/4b. *Journal of Marine and Petroleum Geology* this issue

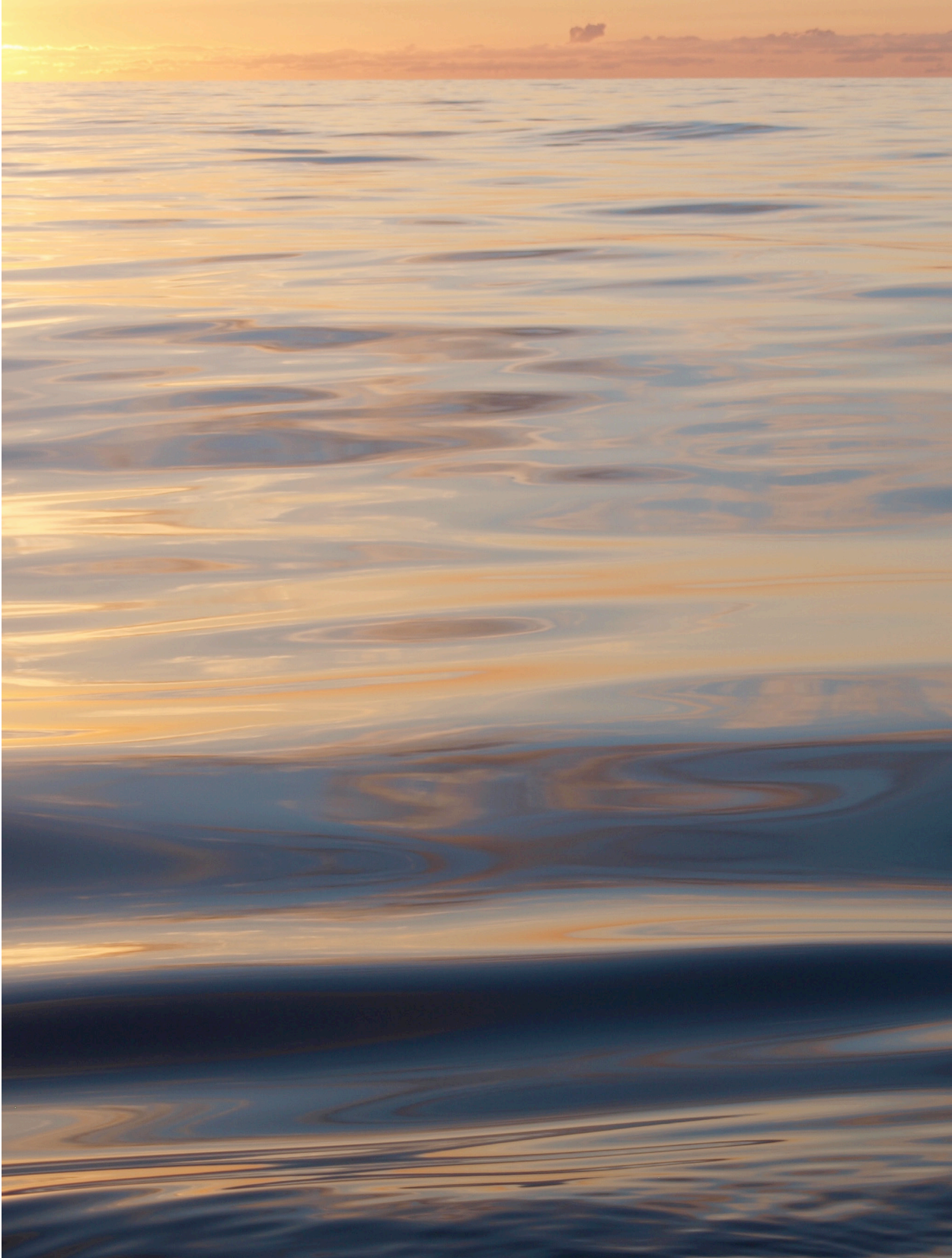
Wojtanowicz, A.K., Nishikiwa, S., Rong, X., 2001. Diagnosis and Remediation of sustained casing pressure in wells. Mineral Management Service. <http://www.wellintegrity.net/Documents/MMS%20-%20Diagnosis%20of%20SCP%20-%202001-07-31.pdf>

Wüest, A., N. H. Brooks, and D. M. Imboden (1992), Bubble plume modeling for lake restoration, *Water Resour. Res.*, 28(12), 3235–3250, doi:10.1029/92WR01681.

Zheng, L., Yapa, P.D., 2002. Modeling gas dissolution in deepwater oil/gas spills. *J. of Marine Systems* 31, 299-309.

CHAPTER 7: GREATER FOCUS NEEDED ON BIOGENIC METHANE LEAKAGE FROM OIL AND GAS WELLS IN THE NORTH SEA

Vielstädte, L., Haeckel, M., Karstens, J., Linke, P., Schmidt, M., Steinle, L., and Wallmann, K.



Sundown during calm weather conditions in the Sleipner area, Norwegian North Sea

7.1. INTRODUCTORY PARAGRAPH

Gas leakage induced by industrial hydrocarbon activities is a concern because the primary fugitive component of petroleum and natural gas is methane (CH_4), which has a significant global warming potential (Ciais et al., 2013). However, regular testing and monitoring of wells is only mandatory throughout the active life time of the well and is targeted on the leakage of thermogenic gas and formation fluids from the unlocked hydrocarbon reservoir (Davies et al., 2014; NORSOK, 2004). Here, we present a unique geochemical- and seismic data set of methane leaking abandoned wells in the Central North Sea (CNS) showing that hydrocarbon wells constitute important conduits for the release of biogenic methane sourced from shallow gas accumulations in the overburden of deep reservoirs. The 3D seismic data reveals that about one third of the wells in the study area of the CNS have been drilled through shallow gas (i.e. in the upper 1,000 m of sediment) and may thus leak CH_4 . Extrapolating our findings (i.e. the leakage potential and measured leakage rates) on a North Sea scale, we hypothesize that the existing large well inventory could release $19 (\pm 10)$ kt $\text{CH}_4 \text{ yr}^{-1}$ into the North Sea, significantly contributing to the North Sea CH_4 budget. Some of this gas, i.e. ~ 8 kt, may reach the atmosphere via direct bubble transport (2 kt) and diffusive outgassing of CH_4 dissolving in the surface mixed layer (6 kt), as indicated by numerical modeling. These unexpected findings clearly advance our understanding of greenhouse gas emissions from the petroleum industry that might alter regional CH_4 budgets in hydrocarbon provinces all over the world. It indicates that the conventional approach of well integrity studies to focus on the gas flow from deep-seated hydrocarbon reservoirs through leaky wells is not sufficient.

7.2. LETTER

There is increasing evidence that boreholes provide a focused pathway for shallow gas to migrate from the geosphere to the hydrosphere, and atmosphere (Gasda et al., 2004; Darrah et al., 2014; Nordbotten et al., 2005; Watson and Bachu, 2009). The initiation of shallow gas migration along the borehole is associated to the enhanced effective permeability resulting from the hydraulic fracturing or mechanical disturbance of the sediment during drilling operations and by insufficient filling of these fractures with cement (Watson and Bachu, 2009; Gurevich et al., 1993). This draws gas from the surrounding sediment because of the lower capillary pressure in the disturbed sediments (Behtke et al., 1991; Judd and Hovland, 2007). Although generally considered as an important pathway in the CCS (Carbon Capture and Storage) community (Gasda et al., 2004; Nordbotten et al., 2005; Phelps et al., 2014), leakage of shallow gas along the outside of the well is still unrecognized in the petroleum industry where well integrity surveys focus exclusively on the leakage of deep, thermogenic gas caused by the failure of the well material itself (Davies et al., 2014; Vignes et al., 2006; Vignes, 2011), i.e. casing, plug, or cement. On the Norwegian Continental Shelf 18% of the active wells (Vignes et al., 2006) and 38% of the temporarily abandoned wells (Vignes, 2011) have this type of well integrity issues. Therefore, human-induced subsea-leakages of shallow gas and their potential impact on regional oceanic- and atmospheric greenhouse gas budgets have so far been ignored.

In the North Sea, Pleistocene and Pliocene organic-rich sediments are the most prominent biogenic gas bearing stratigraphic units (Judd et al., 1997), which are widespread in ~ 300 -750 m sediment depths and correlate to the distribution of boreholes that have been drilled in the North Sea (Judd et al., 1997; Schroot et al., 2005; DANS, V.09; Trape et al., 2014). Here, we identify these units as a potential source for biogenic CH_4 emitted from three investigated leaky abandoned wells in the Norwegian Sector of the CNS. These wells release similar CH_4 emissions to the water column as a major natural seepage site in that area (Schneider von Deimling et al., 2009; Tab. 7.1; Fig. 7.1). The generally light isotopic signature of CH_4 ($\delta^{13}\text{C}_{\text{CH}_4} < -70\text{‰}$) and the minor contents of higher hydrocarbons ($\Sigma\text{C}_1/\text{C}_{2+} > 1000 \text{ ppmV}$) in the seep gases clearly point towards a microbial origin in the shallow subsurface overlying the deep hydrocarbon reservoirs (Tab.

7.1; Fig. A.4.2). The shallow origin of the gas is supported by bright spots (e.g. reverse polarity high amplitude anomalies) and zones of chaotic signatures in the seismic data surrounding the well paths of the three wells (Fig. 1b).

Tab. 7.1: Summary of data obtained at three leaking abandoned wells in the Central North Sea. Stable carbon isotope ($\delta^{13}\text{C}_{\text{CH}_4}$) and hydrocarbon composition ($\Sigma\text{C1}/\text{C2}+$) in the free gas, methane oxidation rates (MOx) and peak concentrations of dissolved methane (CH_4_{max}) in the bottom water, and results of video-derived analysis of active gas bubble venting, i.e. the peak radius of the bubble size distribution (peak r_e), the number of seep spots per well (seeps), and the per-well leakage rate from the seabed (Q_{SF}).

Well ID	$\delta^{13}\text{C}_{\text{CH}_4}$	$\Sigma\text{C1}/\text{C2}+$	MOx	CH_4_{max}	Peak r_e	Seeps	Q_{SF}^c
%o VPDB	%o VPDB	ppmV	nM day ⁻¹	nM	mm		t CH ₄ yr ⁻¹
15/9-13	-75.9	11,131.5	0a	1,014a	2.4	2	1
16/4-2	-71.2	7,254.5	n.d.	n.d.	2.7	8	3.8
16/7-2	-73.1	2,320.0	0.19-1.4b	10,579- 17,294b	5.7*	39	19
Error (1 σ)							

* Larger bubbles were only expelled into the water-column where gas accumulated below a carbonate rock (i.e. well 16/7-2), thus forming significantly larger bubble diameters compared to those directly released from the sandy sediments

a Data from CE12010 1 ROV1 and CTD7

b Data from CE12010 20 ROV6

c based on an average gas flow of 1.4 l min⁻¹ seep⁻¹ at STP

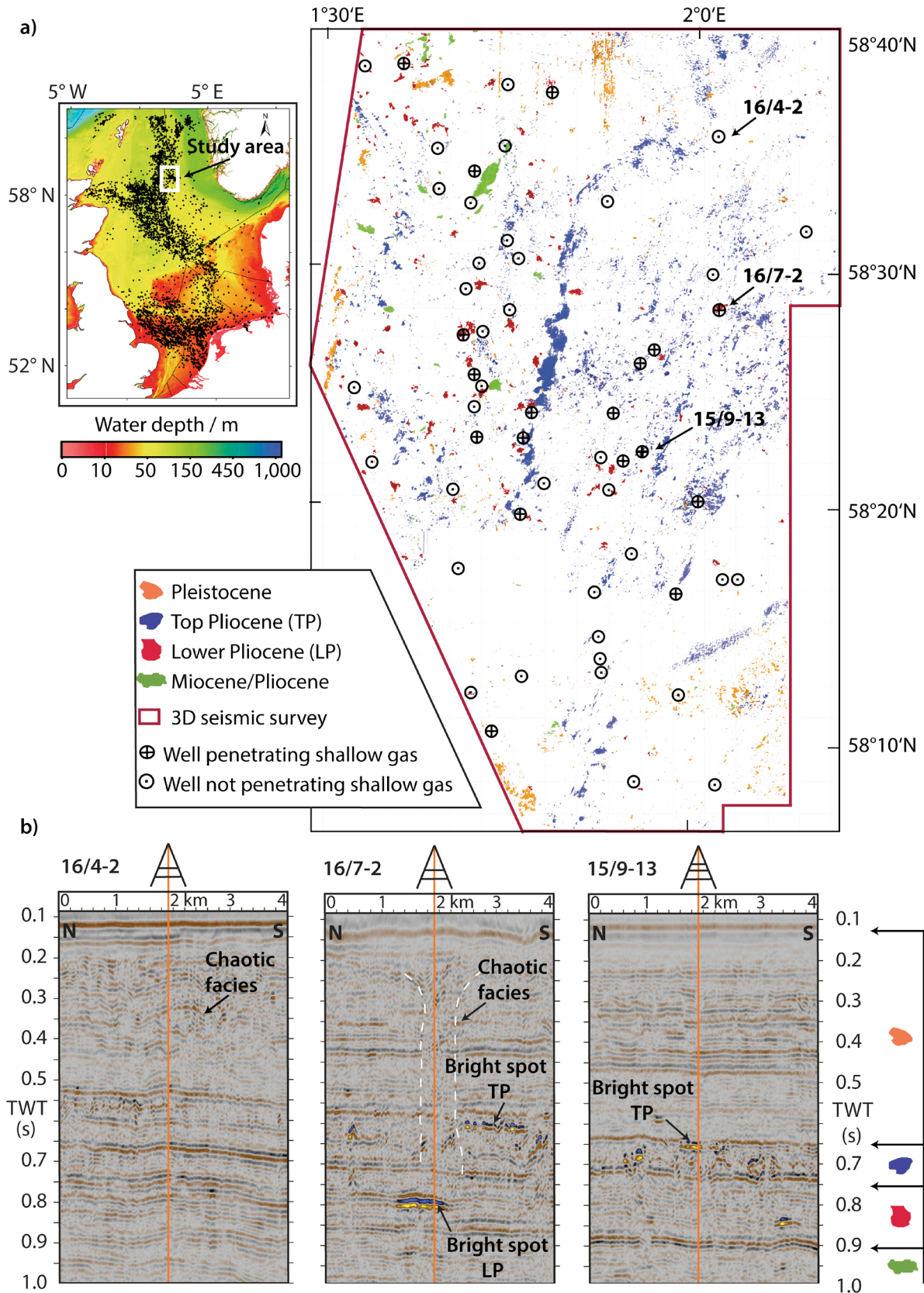
n.d.: not determined

We further hypothesize that leakage from existing North Sea wells is likely to constitute an important part of the respective regional CH₄ budget due to the large well inventory (i.e. ~11,122 wells excluding sidetracked and multilateral wells) and the ubiquitous gas accumulations in the shallow subsurface (Fig. 7.1; Judd et al., 1997; Schroot et al., 2005; DANS, V.09; Trape et al., 2014). In the following, we will thus, assess methane leakage from North Sea wells and estimate their emissions into the atmosphere. To examine the probability of wells to leak, we mapped indications for shallow gas accumulation (e.g. reverse polarity high amplitude anomalies) in an industrial 3D seismic dataset covering 2,000 km² of the Norwegian CNS and compared them with the well paths of 55 boreholes (Fig. 7.1). This comparison revealed that about one third of the investigated wells were drilled through shallow gas and are thus supposed to leak CH₄ (Fig. 7.1). Measurements of per-well leakage rates were highly variable between the three investigated wells (ranging between 1-19 CH₄ yr⁻¹). The highest emissions were measured at site 16/7-2 where the well was drilled through a seismic chimney (Fig. 7.1b). Furthermore, uncertainty in our estimates is related to the temporal variability of per-well leakage rates. To address these uncertainties in the flux assignment we distinguish between a conservative- (2.4 ± 1.4 t CH₄ yr⁻¹ well⁻¹) and a maximum (7.8 ± 7.7 t CH₄ yr⁻¹ well⁻¹) leakage estimate taking the average of available flow data, either excluding or including the high emissions from well 16/7-2, respectively.

Extrapolating our results on a North Sea scale, we estimate that leaky wells may release around 19 (±10) thousand tons of CH₄ from the North Sea seafloor each year, assuming a probability to leak for 33% of the 11,122 North Sea wells with an average per-well leakage rate of 2.4 and 7.8 kt CH₄ yr⁻¹ for the conservative- and maximum estimate, respectively. In comparison to other major North Sea CH₄ sources, i.e. rivers

(0.5 kt yr⁻¹; Uppstill-Goddard et al., 2000; Grunwald et al., 2009; Scranton et al., 1991; Rehder et al., 1998), the Wadden Sea area (1.6 ± 0.5 kt yr⁻¹; Grunwald et al., 2009), and known natural seep sites (0.2 kt yr⁻¹; Judd and Hovland, 2007; Schneider von Deimling et al., 2011; Hovland and Summerville, 1985; Clayton and Dando, 1996; Judd, 2004; Judd et al., 2002; Hinchcliffe, 1978), leaky wells may constitute a significant proportion of the total methane budget of the North Sea (Fig. 7.2 and Fig. 7.3). It should, however, be noted that numerous additional gas seeps have been observed at the North Sea seabed. Their abundance and the CCH₄ emission through these natural seabed features have not been determined but may be comparable to those of leaky wells (Judd et al., 1997). Despite the poor characterization of North Sea CH₄ sources, the patchiness and high spatial variability of methane super-saturations with respect to atmospheric partial pressure in the surface mixed layer (SML) of the open North Sea, i.e. 103 - 50,000% (Rehder et al., 1998; Bange et al., 1994) indicate that point sources at the seabed (wells and natural seeps) dominate the regional CH₄ budget.

Fig. 7.1: Distribution of wells and shallow gas in the North Sea. a) Areal distribution of shallow gas pockets that have been mapped by high amplitude anomalies in an industrial 3D seismic data set (ST98M3, Statoil ASA) and the seafloor location of wells in the Norwegian CNS. The seismic correlation of 55 well paths revealed that one third of the wells were drilled through shallow gas accumulations in Miocene/Pliocene (green), Lower Pliocene (red), Top Pliocene (blue), and Pleistocene (orange) stratigraphic units. Upper left corner: Bathymetric map of the North Sea showing the location of the study area (white rectangle) and the distribution of wells (black dots). b) Seismic profiles indicating shallow gas pockets in the subsurface around the well paths of three investigated leaky abandoned wells (orange line). At well 16/7-2 the outline of a seismic chimney and chaotic reflections are depicted (dashed white line).



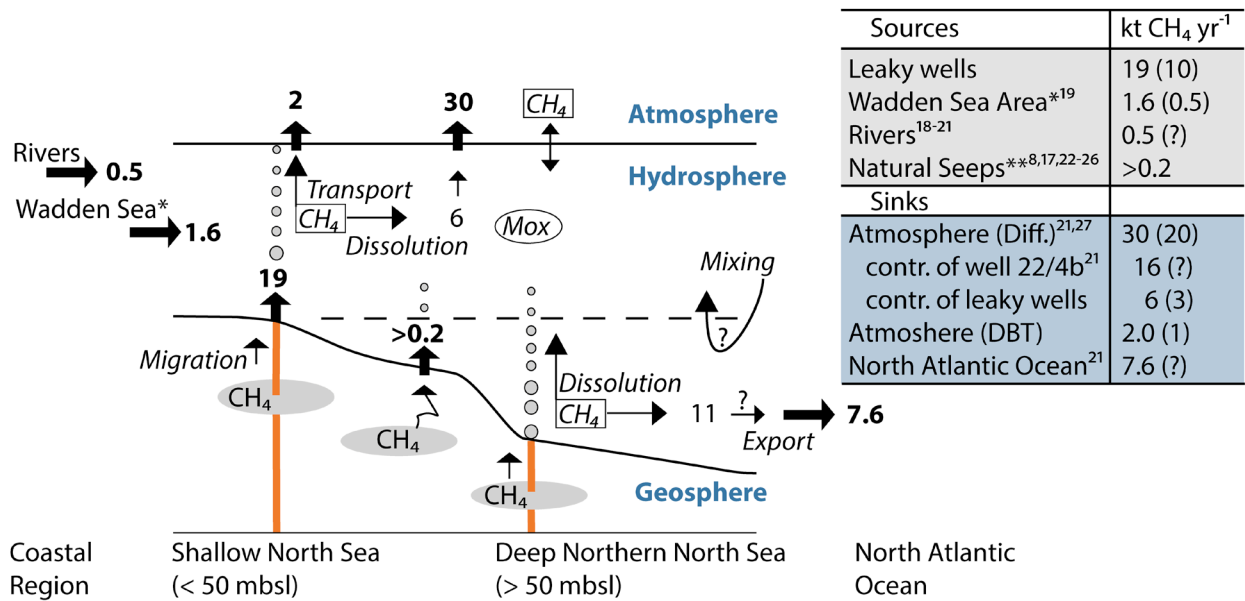


Fig. 7.2: Sketch of the CH₄ cycle and budget of the North Sea. CH₄ sources and sinks are depicted as bold black arrows and expressed in kilo tones (kt) of CH₄ per year. Atmospheric methane emissions comprise direct emissions from leaky wells via bubble transport (DBT), predominantly in the shallower coastal and southern regions, and the diffusive outgassing of methane from the surface mixed layer (SML). The curved black arrow illustrates the mixing of dissolved methane from the deep layer (11 ± 6 kt CH₄ yr⁻¹) to the SML by the seasonal deepening and breakdown of the thermocline (dashed line). Leaky hydrocarbon wells (orange line) may constitute up-to 50% of the total diffusive emissions, comprising the release of shallow buried gas (gray ellipse) investigated in this study and from the single blowout well 22/4b. Note, the imbalance of the North Sea methane budget suggests that an additional input of methane (i.e. $\sim 19 \pm 11$ kt yr⁻¹) is required, either by natural or anthropogenic sources.

To examine the extent to which CH₄ emissions from leaky wells may contribute to the high diffusive flux of methane from the North Sea to the atmosphere, i.e. 10-50 kt yr⁻¹ (Rehder et al., 1998; Bange et al., 1994; Fig. 7.2), we extrapolate results of a numerical bubble dissolution model on a North Sea scale. The model calculates each of the three key fates of leaky CH₄: 1) dissolution in the deep stratified layer (i.e. > 50 m below seafloor (mbsl); Thomas et al., 2005), 2) dissolution in the surface mixed layer (SML, <50 mbsl; Thomas et al., 2005) probably outgassing to the atmosphere, and 3) direct bubble transport to the atmosphere. According to the numerical model, leakage depths and initial bubble sizes play a critical role in transporting CH₄ from the seafloor to the atmosphere, significantly influencing the magnitude of diffusive- and direct atmospheric CH₄ emissions. Bubble sizes measured at wells (peak radius=2.7 mm, Fig. A.4.3) were predominantly controlled by the mechanical properties of the surface sediments (Dewar et al., 2013) (i.e. fine- to medium grained clayey sand) and comparable to those at natural seep sites (i.e. $r_e=2.2$ at Tommeliten; Schneider von Deimling et al., 2011) and $r_e=2.5$ mm at the Scanner Pockmark field (Judd and Hovland, 2007), suggesting that bubble formation processes are similar in wide areas of the North Sea. Extrapolating numerical results on a North Sea scale, we estimate that leaky wells could emit a non-negligible $8 (\pm 4)$ thousand tons of CH₄ into the atmosphere each year, assuming no variation of initial bubble sizes over the extended area of the North Sea. This is a significant proportion (~ 24 -40%) of the total diffusive CH₄ flux from the North Sea into the atmosphere (30 ± 20 kt yr⁻¹; Rehder et al., 1998; Bange et al., 1994). It is predominantly driven by the diffusive outgassing of CH₄ dissolving in the SML (i.e. 6 ± 3 kt), rather than by direct bubble transport (i.e. 2 ± 1 kt). The biological sink for CH₄ in the water-column is expected to be negligible because methane oxidation at the investigated leaky wells was slow (i.e. < 1.4 nM day⁻¹, Tab. 7.1) compared to the fast ventilation of CH₄ in the SML (i.e. days to weeks; Bange et al., 1994) and the turnover time of North Sea water masses (0.75 years; Thomas et al., 2005), suggesting that most of the methane in

the SML reaches the atmosphere. The large proportion of methane dissolving in the deep layer of the North Sea (11 ± 6 kt) supports the lateral methane export into the North Atlantic (7.6 kt; Rehder et al., 1998) and contributes to annual diffusive emissions in the North Sea due to the seasonal deepening and breakdown of the thermocline (Schneider von Deimling et al., 2011; Rehder et al., 1998; Thomas et al., 2005) and the efficient ventilation of the entire water column during frequent fall and winter storms (Shakhova et al., 2013). Thus, if validated in future studies, anthropogenic CH_4 emissions sourced from shallow buried gas may constitute a significant part of the regional CH_4 budget, which could at least partly explain the high diffusive flux of CH_4 from the North Sea into the atmosphere (Fig. 7.2) and the patchiness of CH_4 super-saturation in the surface waters with respect to atmospheric partial pressure (Fig. 7.3). Including other anthropogenic CH_4 sources, such as a single leaky blowout well in the British Sector of the North Sea (Rehder et al., 1998), and the numerous leaky wells with well integrity issues (Vignes et al., 2006; Vignes, 2011), subsea emissions from the hydrocarbon industry very likely play an important role for the North Sea CH_4 budget.

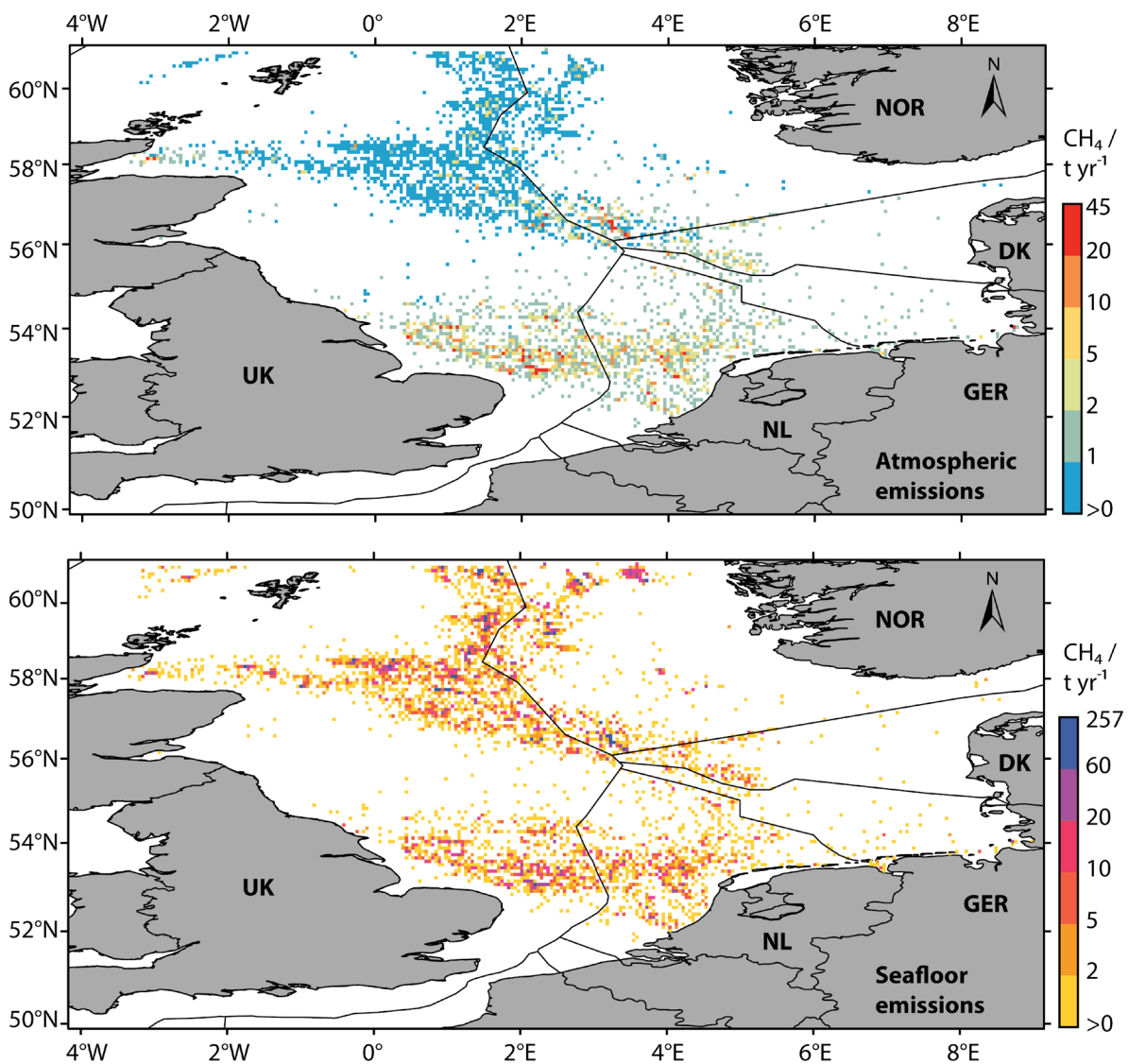


Fig. 7.3: CH_4 emissions from leaky wells into the North Sea and the atmosphere. CH_4 emissions were estimated in 25 km^2 cells assuming that 33% of the 11,122 selected wells leak methane at a rate of $5.1 (\pm 2.7) \text{ t CH}_4 \text{ yr}^{-1} \text{ well}^{-1}$. Emission rates are expressed in tons of methane per year per cell. Total annual seabed emissions of $19 (\pm 10) \text{ kt CH}_4$ are estimated for the North Sea (bottom), only about $8 (\pm 4) \text{ kt}$ of CH_4 may reach the atmosphere with highest emissions occurring in the Southern North Sea where the water-depths are shallower (top). (The coordinate system of the map refers to WGS84 displayed as Cylindrical Equal Area Projection).

In our conservative estimate, we assume that the average of the two lower emission rates, which have been measured at the three investigated wells in the Norwegian Sector, are representative for all leaky wells and that leakage only occurs where the seismic data revealed prominent gas indications in the direct vicinity of the well. However, leakage was also found where the presence of free gas was not imaged by seismic data, either, because the extent of the gas pocket or the gas saturation, were beyond the resolution of the seismic method (Fig. 7.1b, well 16/4-2). The lower emission estimate is thus definitely conservative, because per-well leakage rates and the number of leaky wells might have been underestimated. More knowledge on the abundance of leaky wells, their emission rates, and bubble size spectra, and the dynamics of leakage from the shallow gas reservoir is needed in order to better constrain the regional significance of leaky oil and gas wells for the oceanic and atmospheric methane budget.

The demonstration of the large leakage potential, arising from boreholes poking through gas accumulations in the shallow subsurface, reveals that the conventional approach to offshore well integrity studies focused on the gas flow from deep-seated hydrocarbon reservoirs through leaky wells is not sufficient. It needs to be augmented by additional studies targeting the leakage of shallow gas through the sedimentary overburden in the direct vicinity of the well disturbed by the drilling operation. CH₄ released via this pathway may affect the CH₄ budget of continental margins and enhance greenhouse gas emissions from the surface ocean into the atmosphere.

7.4. METHODS SUMMARY

Data analysis in the Central North Sea (CNS). Three leaky abandoned wells (15/9-13, 16/4-2, and 16/7-2) in 81-93 m water-depths in the CNS were investigated to characterize the origin of emanating seep gases, leakage rates, CH₄ oxidation rates in the water-column, and initial gas bubble sizes during research cruises on board the research vessels RV Celtic Explorer (CE12010, July-August 2012) and RV Alkor (AL412, March 2013). Emanating seep gases were sampled with ROV-operated special gas samplers and were analyzed for their chemical and isotopic composition. The stable carbon isotope composition of CH₄ was measured by using a continuous flow Gas Chromatograph (GC) Isotope Ratio Mass Spectrometer combination. CH₄ and higher alkane concentrations in the free gas samples were determined with a GC 8000top (CE instruments) equipped with a FID detector and a capillary column (RT-Alumina Bon-KCl, 50 m, 0.53 mm). To assess methane concentrations and methane oxidation rates in the water column, seawater samples were collected with ROV- and CTD-operated Niskin bottles. CH₄ oxidation rates in the water-column were determined from ex-situ incubations with trace amounts of ¹⁴C labeled methane (¹⁴C-CH₄). Gas ebullition from the seabed and initial bubble sizes at the seabed were determined from visual measurements of ROV-video using the image editing software ImageJ; details and extended data are provided in the Supplementary Methods. An industrial 3D seismic data set (ST98M3, Statoil ASA) covering an area of more than 2,000 km² and including 55 wells was analyzed for gas accumulations in the sedimentary strata to identify the potential gas source in the subsurface and to examine the probability of wells to leak shallow gas.

Extrapolation of CH₄ leakage on a North Sea scale. To assess CH₄ ebullition from the North Sea seabed and into the atmosphere, we extrapolate leakage data obtained in the CNS and results of a numerical bubble dissolution model on a North Sea scale, using ArcGIS 10.1 and publicly available data of the North Sea bathymetry (EMODnet) and well inventory sourced from online datasets populated by governmental energy departments or regulation agencies in 2012 to 2013. In total, 11,122 operating and non-operating wells were selected for analysis excluding sidetracked- and multilateral wells. The North Sea was subdivided into equally-sized polygons of 25 km² area and the seabed methane flow (OSF) was calculated for each of these

polygons multiplying the seismically determined leakage potential of wells (i.e. 33%), the number of wells that fall inside each polygon, and the per-well leakage rate, i.e. 2.4 and 7.8 t CH₄ yr⁻¹ for the conservative and maximum flow estimate, respectively. For each polygon, the resultant CH₄ flow from the North Sea into the atmosphere was then estimated applying a transfer function describing the methane bubble transport efficiency to the sea-surface and to the SML of the North Sea as a function of the seabed methane flow and water-depth. All determined flow estimates were added to calculate lower- and upper bounds of the total CH₄ ebullition from the seafloor and into the atmosphere. Full methodology details are in the Supplementary Methods (Appendix; A.4).

REFERENCES

- Bange, H.W., Bartell, U.H., Rapsomanikis, S., Andreae, M.O., 1994. Methane in the Baltic and North Seas and a reassessment of the marine emissions of methane. *Glob. Biogeochem. Cycles* 8, 465–480.
- Behrke, C. M., Reed, J.D., Olzt, D.F., 1991. Long-range petroleum migration in the Illinois Basin. *Am. Assoc. Petr. Geol. B.* 75, 925-45.
- Ciais, P., et al., 2013. Climate Change 2013: The Physical Science Basis. Contribution of Working Group I to the Fifth Assessment Report of the Intergovernmental Panel on Climate Change, in: Stocker, T.F., Qin, D., Plattner, G.-K., Tignor, M., Allen, S.K., Boschung, J., Nauels, A., Xia, Y., Bex, V., Midgley, P.M. (Eds.). IPCC, Cambridge, UK, pp. 465-570.
- Clayton, C.J., Dando, P.R., 1996. Comparison of seepage and seep leakage rates. In: Schumacher D, Abrams MA (Eds), *Hydrocarbon migration and its near-surface expression*. *Am. Assoc. Petr. Geol. B.* 66, 169–171.
- Darrah, T.H., Vengosh, A., Jackson, R.B., Warner, N.R., Porda, R.J., 2014. Noble gases identify the mechanisms of fugitive gas contamination in drinking-water wells overlying the Marcellus and Barnett Shales. *Proc. Natl. Acad. Sci. U.S.A.* 111 (39), 14076-14081. www.pnas.org/cgi/doi/10.1073/pnas.1322107111
- Davies, R.J., et al., 2014. Oil and gas wells and their integrity: Implications for shale and unconventional resource exploitation. *Mar. Petrol. Geol.* 56, 239-154.
- Dewar, M., Wei, W., Chen, B., 2013. Small-scale modelling of the physicochemical impacts of CO₂ leaked from sub-seabed reservoirs or pipelines within the North Sea and surrounding waters. *Mar. Pollut. Bull.* 73, 504-515.
- Gasda, S.E., Bachu, S., Celia, M.A., 2004. Spatial characterization of the location of potentially leaky wells penetrating a deep saline aquifer in a mature sedimentary basin. *Environ. Geol.* 46, 707-720
- Grunwald, M., Dellwig, O., Beck, M., Dippner, J.W., Freund, J.A., Kohlmeier, C., Schnetger, B., Brumsack, H.J., 2009. Methane in the southern North Sea, spatial distribution and budgets. *Est. Coast. Shelf Sci.* 81, 445-456.
- Gurevich A.E., Endres, B.L., Robertson, J.O., Chilingar, G.V., 1993. Gas migration from oil and gas fields and associated hazards. *J. Petrol. Sci. Eng.* 9, 223-238.
- Hinchcliffe, J.C., 1978. Death stalks the secret coast. *Triton* 23, 56–57.
- Hovland, M., Sommerville, J.H., 1985. Characteristics of two natural gas seepages in the North Sea. *Mar. Petrol. Geol.* 2, 319–326.
- Judd, A., Davies, G., Wilson, J., Holmes, R., Baron, G., Bryden, I., 1997. Contributions to atmospheric methane by natural seepage on the U.K. continental shelf. *Mar. Geol.* 140, 427-455.
- Judd, A.G., 2004. Natural seabed gas seeps as sources of atmospheric methane. *Environ. Geol.* 46, 988-996. DOI 10.1007/s00254-004-1083-3.
- Judd, A.G., Hovland, M., 2007. *Seabed Fluid Flow- The Impact on Geology, Biology and Marine Environment*. Cambridge University Press, New York, 475 pp.
- Judd, A.G., Sim, R., Kingston, P., McNally, J., 2002. Gas seepage on an intertidal site: Torry Bay, Firth of Forth, Scotland. *Cont. Shelf Res.* 22, 2317–2331.
- Nordbotten, J.M., Celia, M.A., Bachu, S., Dahle, H.K., 2005. Semianalytical solution for CO₂ leakage

through an abandoned well. *Environ. Sci. Technol.* 39, 602-611

NORSOK Standard D-010, 2004. <http://www.standard.no/PageFiles/1315/D-010r3.pdf>

Phelps, J.J.C., Blackford, J.C., Holt, J.T., Polton, J.A., 2014. Modelling large-scale CO₂ leakage in the North Sea. *Int. J. Greenh. Gas Control* 1337.

Rehder, G., Keir, R.S., Suess, E., Pohlmann, T., 1998. The multiple sources and patterns of methane in North Sea waters. *Aquat. Geochem.* 4, 403-427.

Schneider von Deimling, J., Rehder, G., Greinert, J., McGinnis, D.F., Boetius, A., Linke, P., 2011. Quantification of seep-related methane gas emissions at Tommeliten, North Sea. *Cont. Shelf Res.* 31, 867-878.

Schroot, B.M., Klaver, G.T., Schüttenhelm, R.T.E., 2005. Surface and subsurface expressions of gas seepage to the seabed- examples from the Southern North Sea. *Mar. Petrol. Geol.* 22, 499-515.

Scranton, M.I., McShane, K., 1991. Methane fluxes in the southern North-Sea – the role of European rivers. *Cont. Shelf Res.* 11, 37–52.

Shakhova, N., Semiletov Igor P., Leifer, I., Sergienko, V., Salyuk, A., Kosmach, D., Chernikh, D., Stubbs, C., Nicolsky, D., Tumskoy, V., Alexeev, V., Gustafsson, O., 2013. Ebullition and storm-induced methane release from the East Siberian Arctic Shelf. *Nat. Geosci.* 7, 64-70.

The Digital Atlas of the North Sea- An overview about geo-information considering the sea floor and the bottom water column, V.0.9. http://www.awi.de/en/research/research_divisions/geosciences/marine_geochemistry/marine_gis/digital_atlas_of_the_north_sea/

Thomas, H., Bozec, Y., de Baar, H.J.W., Elkalay, K., Frankignoulle, M., Schiettecatte, L.S., Kattner, G., Borges, A.V., 2005. The carbon budget of the North Sea. *Biogeosciences* 2, 87-96.

Trape, A.F., Lutz, R., Franke, D., Bücker, C.H.R., 2014. Oberflächennahes Erdgas in der deutschen Nordsee- Aktuelle Untersuchungen anhand seismischer Daten. *Erdöl Erdgas Kohle* 130, Heft 1.

Upstill-Goddard, R.C., Barnes, J., Frost, T., Punshon, S., Owens, N.J.P., 2000. Methane in the southern North Sea: Low-salinity inputs, estuarine removal, and atmospheric flux. *Glob. Biogeochem. Cycles* 14 (4), 1205-1217.

Vignes, B., 2011. Contribution to Well Integrity and Increased Focus on Well Barriers from a Life Cycle Aspect (PhD thesis). University of Stavanger.

Vignes, B., Andreassen, J., Tønning, S.A., 2006. PSA Well Integrity Survey, Phase 1 Summary Report. Petroleum Safety Authority. <http://www.ptil.no/getfile.php/z%20Konvertert/Helse,%20miljø%20og%20sikkerhet/Sikkerhet%20og%20arbeidsmiljø/Dokumenter/nettpsawellintegritysurveyphase1reportrevision3006.pdf>

CHAPTER 8: SYNTHESIS, RECOMMENDATIONS AND OUTLOOK



Horseshoe Bend, Arizona, USA

8.1. SUMMARY OF MAIN RESULTS

The formation of focused fluid conduits significantly affects fluid flow systems by altering the integrity of sealing caprocks and by transferring fluids as well as pressure between previously unconnected reservoirs of the system. These processes persistently alter the hydraulic properties of fluid flow systems and have important implications on sub-seafloor operations, such as the exploitation of hydrocarbons and the geological storage of CO₂. Our understanding of large-scale geological processes in the subsurface made tremendous progress during the last decade due to the availability of 3D seismic technology for the geoscientific community. The advances in seismic technology and its availability in academia enable the scientific community to conduct seismic analysis, which a decade back would have only been possible for the petroleum industry. While the scientific community benefits from the access to industrial high-resolution 3D seismic datasets, the hydrocarbon industry may profit from the scientific results allowing a critical assessment of environmental and economic risks. However, scientific results may raise previously unforeseen concerns from regulators or the public and, therefore, may not always be favored by the industry. As a consequence, studies like my PhD thesis develop between conflicting priorities of industry and academia. In consequence, it is necessary to maintain a balance between cooperation with an industry partner and critical questioning of their information, interpretations and risk assessment.

8.1.1. THE EVOLUTION OF THE FLUID FLOW SYSTEM IN THE SOUTHERN VIKING GRABEN

The fluid flow system in the Southern Viking Graben is characterized by the interplay between deep hydrocarbon reservoirs, the Utsira Formation as a temporary hydrocarbon storage formation and the focused fluid flow dominated overburden. The focused fluid flow manifestations in the overburden of the Utsira Formation include gas accumulations at the top of the Utsira Formation and the Pliocene section, which appear to be (or at least have been) connected by comparably small and narrow pipe structures in the Pliocene section. Therefore, it is likely that these gas accumulations are not only the result of biogenic gas production within the Pliocene section itself, but were also at least partly charged by the upward migration of fluids from depth.

The most prominent fluid flow associated seismic anomalies in the study area are at least 46 hundreds of meter long and hundreds of meter wide chimney structures, which can be categorized into three types (A–C) of seismic anomalies based on their seismic appearance. Type-A-chimney shows similarities to “blowout pipes”, which are known from different sedimentary basins around the world and generally associated with rapid expulsion of fluids. Type B is very similar to large “gas chimney” structures, which have been identified above several leaking hydrocarbon reservoirs and which is interpreted as a gas filled fracture network crosscutting a low permeable seal. Type C chimneys cause seismic disturbances in bands of up to 6 km length and correlate with overlying tunnel valleys, which densely populate the study area. This correlation may suggest that type-C-chimneys are only seismic artifacts as the result of poor imaging due to seismic velocity heterogeneities caused by the tunnel valley infill, but there are several observations pointing towards a geological, fluid flow related origin. Based on the available data, it is not possible to conclusively exclude one of both options.

The vast majority of the identified chimneys root in the Upper Pliocene section or the Utsira Formation indicating that the chimney structures were sourced by fluids from sandy, high permeable layers. The Utsira Formation itself is not likely to be the source of the probably large gas volumes, which was most likely in place before the formation of the seal cross-cutting chimney structures as well as the narrow pipe structures. This indicates that the leakage from deeper hydrocarbon sources, most likely the very productive oil, gas and condensate reservoirs of the study area, played an important role in the evolution of the present fluid flow system. The chimney structures crosscut very shallow glacial sediments affected by deglaciation associated with tunnel valleys, while some chimneys have even an effect on the seismic reflection of the seafloor. These

observations indicate a comparably recent formation age or latest phase of activity, which is very likely to be related with loading and unloading of the Fennoscandian ice-sheet in the study area.

8.1.2. THE FORMATION OF LARGE-SCALE FOCUSED FLUID CONDUITS IN THE SOUTHERN VIKING GRABEN

The formation of the focused fluid conduits is generally associated with seal breaching due to overpressure. In the Sleipner case, it is possible to quantify the required threshold pressure to the availability of core samples of the caprock. Rock physical experiments on mudstone samples from the lower seal of the Utsira Formation suggest that a comparably high overpressure (~1.5 MPa) is required to breach the seal.

It is a very difficult task to reconstruct palaeo-pressure conditions based on seismic data. However, there are several seismic observations, which help to understand the formation mechanism of the chimney structures in the study area:

1. The interpretation of the fluid flow system revealed that large amount of hydrocarbons have migrated from the deep reservoirs into the shallow subsurface (Utsira Formation and overlying Nordland Shales). The availability of unbound and mobile fluids, especially gas, has the potential to create overpressure just by their buoyancy. However, this effect is not sufficient for generating the required overpressure.
2. The intrusion of liquefied sands into mudstone layers form pronounced mound structures at the base of the Utsira Formation. This deformation has an imprint on the overlying strata for several hundred meters affecting the lower caprock and the Pliocene section. The deformation is not present in the glacially affected sediments, which indicates that the deformation took place earlier than their deposition and way earlier than the formation of the chimney structures, which crosscut these strata. However, it may be possible that the strength of the caprock has been enduringly lowered in areas with pronounced deformation.
3. The observed chimney structures crosscut sediments affected by glacial bedforms like tunnel valleys, which are generally associated with melt water discharge during deglaciation. Therefore, their formation or at least their latest phase of activity appears to be associated with deglaciation as well.

There are different concepts, how loading and unloading by ice-sheets may affect or initiate focused fluid flow including gas hydrate dissociation or dewatering of shale layers. However, the timing of formation, the chimney rooting in two separate, high permeable layers (Upper Pliocene section or the Utsira Formation) cannot be explained by gas hydrate destabilization or dewatering of shale gas hydrate destabilization or dewatering of shale layers and require a novel explanation.

The presented concept of gas compression compensated compaction assumes that the volume loss of gas pockets during increasing loading allows an undrained system to compact without expelling fluids. During unloading, the gas cannot expand to its pre-compression volume due to the compaction and affected layers retain the acquired pore pressure, while unaffected layers return to hydrostatic pressure condition. This pressure difference may then have the potential to initiate breaching of a seal and thereby the formation of focused fluid conduits.

8.1.3. THE IMPACT OF CHIMNEY STRUCTURES ON THE SLEIPNER CO₂ STORAGE OPERATION

The Sleipner area hosts a multitude of seismic chimneys, which root as deep as the Utsira Formation. Some of these chimneys are as close as 7 km from the CO₂ injection point and time-lapse seismic data indicate that the growing CO₂ plume successively migrates towards these structures. By comparing the shape of the CO₂ plume with results from numerical modeling performed with the multiphase fluid flow simulator DuMux, it is possible to constrain the permeability field of the Utsira Formation in order to predict the future plume evolution. The Utsira Formation shows a pronounced permeability anisotropy of 10:1 between NNE-SSW and WNW-ESE, which may be attributed to the orientation of its depositional system controlled by the spreading axis of the Viking Graben.

The simulation of the CO₂ plume evolution for CO₂ injection over a duration of 30 years and simulation time of 200 years revealed that it is not likely that the CO₂ plume will ever reach the chimney structures. These are conservative estimations, since they are performed with a continuous injection rate of 1 Mt/a (while the actual injection rate is gradually declining, Statoil, personal communication) and the simulation does not include the dissolution of CO₂, which would further decrease the volume of the plume. By simulating a continuous CO₂ injection over the entire simulation time of 200 years, it was possible to model the interaction of CO₂ and the chimney structures. These simulations revealed that CO₂ would reach the chimney structures after ~90 years of continuous injection. The simulation assumed different chimney permeabilities between 10 and 2000 mD, which resulted in all the leakage of CO₂ at seafloor. The chimney permeability affects the onset of leakage at the seafloor, but does not change the general shape of the leakage rate curve, which is the result of the large dimension of the modeled chimney structures. The peak leakage rates are by several magnitudes higher than those leakage rates known from natural seep sites (e.g. Tommeliten), but are in the same magnitude as those estimated for blowout sites in the North Sea. There are no indications in the time-lapse seismic data that the injection of CO₂ has caused any overpressure-related seal-breaching and the formation of chimney structures as the result of the injection of CO₂ at Sleipner appears unlikely, because the resulting pressure increase is comparably small.

8.1.4. IMPLICATIONS OF SHALLOW FLUID FLOW ON WELLBORE ACTIVITIES

The integrated analysis of seafloor methane emission quantifications, geochemical measurements and 3D seismic mapping of shallow fluid flow features revealed that abandoned wells may act as pathways for vertical gas migration. The light isotopic signature of the leaking methane points towards a shallow microbial origin of the leaking gas and coincides with seismic observations of gas related seismic anomalies including bright spots and zones with chaotic seismic appearance.

Leakage parameters like bubble size and frequency as well as microbial colonies on the seafloor are comparable to natural seep sites. The leakage rates measured at three wells vary between 1, 3.8 and 18 t/a and are most likely controlled by the availability of mobile methane and the well with highest leakage rate penetrates a comparably large gas pocket overlain by the zones with chaotic seismic facies (gas chimneys). This indicates that the presence of fluid flow manifestations controls the leakage of shallow methane.

One third of all wells in the Sleipner area crosscuts shallow gas accumulations and are, therefore, prone to act as pathways for shallow methane. By assuming that these observations are representative for other hydrocarbon provinces in the North Sea Basin, it is possible to extrapolate basin-scale methane emission from abandoned wells resulting in a yearly emission estimate of 19,000 (±10,000) t.

The analysis of leakage of methane from abandoned wells has additionally important implications for the storage of CO₂:

1. The methane from the analyzed wells has a shallow origin and there is no indication for upward migration of thermogenic gas from the deep reservoirs through the well itself.
2. The leaking gas migrates outside of the well indicating that drilling operation has caused hydraulic fracturing or mechanical disturbance of the sediments around the well, which may act as a seal-bypass for upward migrating fluids.
3. The measured methane leakage rates are comparably low. Methane has significantly higher buoyancy than CO₂, which implies leaking CO₂ would require longer time to migrate from the storage formation to the seafloor.

8.2. RECOMMENDATIONS FOR SITE SELECTION OF FUTURE SUB-SEABED CO₂ STORAGE OPERATIONS

The process of site selection and the evaluation of potential storage systems focuses on the reservoir quality of the storage formation and the availability of thick impermeable caprocks, which are undoubtedly the most important and primary requirements for site selection. However, the results of PhD thesis highlight that the presence of focused fluid flow conduits within the caprock may affect the long-term performance of CO₂ storage operations and need to be considered during site selection as well.

The presence of seismic chimneys and other manifestations of seal-bypassing focused fluid conduits in the caprock of a potential CO₂ storage site does not per se imply that this site is not suitable for CCS. If these conduits are proved to be inactive and impermeable, if they will not be reached by the CO₂ or if they root way above the storage formation, they do not necessarily affect the integrity of the caprock and the storage operation. However, to be able to constrain these requirements, it is necessary to perform detailed geological and geophysical investigations as well as fluid flow simulations. For such surveys, it is possible to perform a top to bottom strategy, which focuses on the detection of fluid flow manifestations at the seafloor and can be implemented by multi-instrument, high-resolution AUV surveying. If such a survey detects a seafloor structure (e.g. the Hugin fracture in the Sleipner area), it is then required to investigate its origin, source depth and evaluate its impact on the caprock integrity by using additional techniques like echosounding or high-resolution seismics as well as geochemical sampling. The evaluation of seafloor seepage structures should focus on the origin of the venting fluids. The seepage of higher hydrocarbons or thermogenic methane points towards deep rooted, permeable fluid pathways and should be a contraindicator for CO₂ storage, while the seepage of shallow, biogenic gas or pore water (e.g. at the Hugin fracture) may be no concern at all.

Alternative to top to bottom approach, an operator could choose a bottom to top surveying strategy and analyze deep fluid flow structures using conventional (industrial) 3D seismic data. If there are indications for focused fluid flow (seismic chimneys or pipes, buried pockmarks, fractures, fault or pronounced bright spots), a detailed fluid flow analyses with the aim to reconstruct the evolution of the fluid flow system is required. In addition, it is necessary to perform seafloor surveying to understand if the detected fluid flow structures are still active. If surveying reveals that a potential storage site hosts vertical fluid conduits, which reach down to or crosscut the storage formation, a general precaution would be to avoid the regions bearing these structures.

However, if subseabed CCS is implemented on a scale that would have a relevant impact on CO₂ emissions (2 to 3Gt/a; IEA, 2012), hundreds of CCS operations with higher injection rates than Sleipner would need to be installed. Considering the commonness of focused fluid flow manifestations in sedimentary basin, it is not possible to implement CCS on an emissions-relevant-scale and on the same time to avoid areas hosting

chimney structures. Only very little is known about the hydraulic properties of active or inactive chimney structures and these properties may be very different between one and the other chimney structure. Therefore, if avoiding chimney structures is not possible, they need to be closely monitored by time-lapse 3D seismic and high-resolution seafloor surveys.

8.3. OUTLOOK ON PLANNED PROJECTS AND RECOMMENDATIONS FOR FUTURE RESEARCH

This thesis highlights, how little is actually known about the nature of focused fluid conduits including their formation, their internal architecture and their hydraulic properties. To provide reliable guidance for cost- and time-efficient site surveying for future CO₂ storage sites, it is necessary to learn more about the formation and long-term properties of focused fluid conduits. The most important parameter for risk assessment of geotechnical operations is the permeability of a chimney structure. The only reliable method to constrain the permeability of a chimney structure is drilling into it, which is one of the main actions planned within the framework of the follow-up project STEMM-CCS. However, direct probing can only provide information about the present-day hydraulic properties, which may be very site-specific and have been very different in the past.

Therefore, it is crucial to learn more about the underlying geological processes, which affect the discharge of fluids along focused fluid conduits and how these may change the hydraulic parameter of a conduit over time (e.g. opening and closing of fractures, consolidation of sediments, cementation). These processes can be constrained by the geological, geochemical and geophysical investigations of field analogues. The integration of field geological and 3D seismic observations has a great potential for improving the basin-scale analysis fluid flow systems. There are several well-established field analogues for fluid conduits and sand injections. These structures have diameters of meter to tens of meters and are by an order of magnitude narrower than the fluid flow features visible in seismic data, which have diameters of several hundred meters. This discrepancy in dimensions is hard to explain. It may be possible that we just have not recognized the field analogues of large-scale chimney structures, because these structures are not very prominent in the field. Alternatively, it is possible that we have already found these structures, but we are just interpreting them differently (e.g. breccia pipes). Or seismic data are just extremely sensitive in picking up minor disturbances or fluid infiltration around the conduit itself that affect the seismic properties the bedrock around a conduit, which are not visible with the human eye at outcrops. All the same, the analysis of field analogues has great potential for providing novel insights into the nature of fluid conduits.

The analysis of field analogues and wellbores are site specific and the information gathered with these techniques should feed into numerical modeling of the formation of chimney structures and the flow of fluids along these structures. The numerical simulations presented in this thesis are only first estimates of the migration of fluids along chimneys and represent an end member of possible hydraulic behavior by integrating the chimneys as homogeneous cylindrical structures. Future simulations should try to evaluate the properties of different types of fluid conduits (e.g. fracture networks, fluidization, sand injection). Such simulations are planned for the chimney structures and the Hugin Fracture in the Sleipner area and will be performed in cooperation with the GFZ Potsdam as part of the Helmholtz OCEAN initiative.

Another, possibility to study focused fluid conduits is the geophysical analysis of blowout sites like in sector 22/4b of the British sector of the North Sea and at Tordis, offshore Norway. These structures are particularly valuable for the analysis of focused fluid conduits, because they are very young, the fluids responsible for the blowout formation are known and it is even possible to constrain pressure condition during their formation (at least for Tordis). By surveying using seismic and multi-frequency hydroacoustic techniques, it would even be possible to compare gas-driven (22/4b) and water-driven (Tordis) conduit formation. For such a survey,

I would suggest the acquisition of high-resolution 3D seismic cubes to get detailed information about the internal structure of the conduits as well as 2D lines using a long streamer to acquire far-offset data in order to be able to undershoot gas pockets, which may seismically mask underlying strata, and to acquire velocity information.

The integrated analysis of focused fluid conduits by drilling, analyzing of field analogues, numerical modeling and seismic surveying will provide new insights into the formation and properties of focused fluid flow conduits as well as the general understanding of fluid flow systems in marine sediments. A better understanding of focused fluid flow in marine sediments will make seabed and sub-seafloor operations much safer, help us to reconstruct marine sediment-related geological and climatic processes in the past and allows us to predict the feedback of the marine geosphere on the global changes estimate related to global warming and its consequences.

APPENDIX



Hand prints carved into sandstone, Kodachrome Basin, Utah, USA

A.1 LIST OF RESEARCH ARTICLES PUBLISHED IN THE PERIOD OF MY PHD

SEISMIC CHIMNEYS IN THE SOUTHERN VIKING GRABEN – IMPLICATIONS FOR PALAEO FLUID MIGRATION AND OVERPRESSURE EVOLUTION

Karstens, J., and Berndt, C., 2015. Seismic chimneys in the Southern Viking Graben – Implications for palaeo fluid migration and overpressure evolution. **Earth and Planetary Science Letters**, Volume. 412, pages 88-100. doi:10.1016/j.epsl.2014.12.017

Detailed understanding of natural fluid migration systems is essential to minimize risks during hydrocarbon exploration and to evaluate the long-term efficiency of the subsurface storage of waste water and gas from hydrocarbon production as well as CO₂. The Southern Viking Graben (SVG) hosts numerous focused fluid flow structures in the shallow (< 1000 m) subsurface. The seismic expressions of vertical fluid conduits are variously known as seismic chimneys or pipes. Seismic pipes are known to form large clusters. Seismic chimneys have so far been described as solitary structures. Here, we show that the study area in the SVG hosts more than 46 large-scale vertical chimney structures, which can be divided in three categories implying different formation processes. Our analysis reveals that seal-weakening, formation-wide overpressure and the presence of free gas are required to initiate the formation of vertical fluid conduits in the SVG. The presence of numerous vertical fluid conduits implies inter-stratigraphic hydraulic connectivity, which significantly affects the migration of fluids in the subsurface. Chimney structures are important for understanding the transfer of pore pressure anomalies to the shallow parts of the basin.

HEAT FLOW IN THE SOUTHERN CHILE FOREARC CONTROLLED BY LARGE-SCALE TECTONIC PROCESSES

Villar-Muñoz, L., Behrmann, J.H., Diaz-Naveas, J., Klaeschen, D., and **Karstens, J.**, 2014. Heat flow in the southern Chile forearc controlled by large-scale tectonic processes. **Geo-Marine Letters**, v. 34, pp. 185-188. doi: 10.1007/s00367-013-0353-z

Between 33°S and 47°S, the southern Chile forearc is affected by the subduction of the aseismic Juan Fernandez Ridge, several major oceanic fracture zones on the subducting Nazca Plate, the active Chile Ridge spreading centre, and the underthrusting Antarctic Plate. The heat flow through the forearc was estimated using the depth of the bottom simulating reflector obtained from a comprehensive database of reflection seismic profiles. On the upper and middle continental slope along the whole forearc, heat flow is about 30–60 mW m⁻², a range of values common for the continental basement and overlying slope sediments. The actively deforming accretionary wedge on the lower slope, however, in places shows heat flow reaching about 90 mW m⁻². This indicates that advecting pore fluids from deeper in the subduction zone may transport a substantial part of the heat there. The large size of the anomalies suggests that fluid advection and outflow at the seafloor is overall diffuse, rather than being restricted to individual fault structures or mud volcanoes and mud mounds. One large area with very high heat flow is associated with a major tectonic feature. Thus, above the subducting Chile Ridge at 46°S, values of up to 280 mW m⁻² indicate that the overriding South American Plate is effectively heated by subjacent zero-age oceanic plate material.

EMPLACEMENT OF PYROCLASTIC DEPOSITS OFFSHORE MONTSEERRAT: INSIGHTS FROM 3D SEISMIC DATA

Karstens, J., Crutchley, G.J., Berndt, C., Talling, P.J., Watt, S.F.L., Hühnerbach, V., Le Friant, A.L., Lebas, E., Trofimovs, J., and Watt, S.F.L., 2013. Emplacement of pyroclastic deposits offshore Montserrat: Insights from 3D seismic data. **Journal of Volcanology and Geothermal Research**, v. 257, pp. 1-11. doi: 10.1016/j.jvolgeores.2013.03.004.

During the current (1995–present) eruptive phase of the Soufrière Hills volcano on Montserrat, voluminous pyroclastic flows entered the sea off the eastern flank of the island, resulting in the deposition of well-defined submarine pyroclastic lobes. Previously reported bathymetric surveys documented the sequential construction of these deposits, but could not image their internal structure, the morphology or extent of their base, or interaction with the underlying sediments. We show, by combining these bathymetric data with new high-resolution three dimensional (3D) seismic data, that the sequence of previously detected pyroclastic deposits from different phases of the ongoing eruptive activity is still well preserved. A detailed interpretation of the 3D seismic data reveals the absence of significant (>3 m) basal erosion in the distal extent of submarine pyroclastic deposits. We also identify a previously unrecognized seismic unit directly beneath the stack of recent lobes. We propose three hypotheses for the origin of this seismic unit, but prefer an interpretation that the deposit is the result of the subaerial flank collapse that formed the English's Crater scarp on the Soufrière Hills volcano. The 1995–recent volcanic activity on Montserrat accounts for a significant portion of the sediments on the southeast slope of Montserrat, in places forming deposits that are more than 60 m thick, which implies that the potential for pyroclastic flows to build volcanic island edifices is significant.

INSIGHTS INTO THE EMPLACEMENT DYNAMICS OF VOLCANIC LANDSLIDES FROM HIGH-RESOLUTION 3D SEISMIC DATA ACQUIRED OFFSHORE MONTSEERRAT, LESSER ANTILLES

Crutchley, G.J., **Karstens, J.**, Berndt, C., Talling, P.J., Watt, S.F.L., Vardy, M.E., Hühnerbach, V., Urlaub, M., Sarkar, S., Klaeschen, D., Paulatto, M., Le Friant, A., Lebas, E., and Maeno, F., 2013. Insights into the emplacement dynamics of volcanic landslides from high-resolution 3D seismic data acquired offshore Montserrat, Lesser Antilles. **Marine Geology**, v. 335, pp. 1–15. doi:10.1016/j.margeo.2012.10.004.

We present results from the first three-dimensional (3D) marine seismic dataset ever collected over volcanic landslide deposits, acquired offshore of the Soufrière Hills volcano on the island of Montserrat in the Lesser Antilles. The 3D data enable detailed analysis of various features in and around these mass wasting deposits, such as surface deformation fabrics, the distribution and size of transported blocks, change of emplacement direction and erosion into seafloor strata. Deformational features preserved on the surface of the most recent debris avalanche deposit (Deposit 1) reveal evidence for spatially-variant deceleration as the mass failure came to rest on the seafloor. Block distributions suggest that the failure spread out very rapidly, with no tendency to develop longitudinal ridges. An older volcanic flank collapse deposit (Deposit 2) appears to be intrinsically related to large-scale secondary failure of seafloor sediments. We observe pronounced erosion directly down-slope of a prominent headwall, where translational sliding of well-stratified sediments was initiated. Deep-reaching faults controlled the form and location of the headwall, and stratigraphic relationships suggest that sliding was concurrent with volcanic flank collapse emplacement. We also identified a very different mass wasting unit between Deposit 1 and Deposit 2 that was likely emplaced as a series of particle-laden mass flows derived from pyroclastic flows, much like the recent (since 1995) phase of deposition offshore Montserrat but at a much larger scale. This study highlights the power of 3D seismic data in understanding landslide emplacement processes offshore of volcanic islands.

COMBINATIONS OF VOLCANIC-FLANK AND SEAFLOOR-SEDIMENT FAILURE OFFSHORE MONTSERRAT, AND THEIR IMPLICATIONS FOR TSUNAMI GENERATION

Watt, S.F.L., Talling, P.J., Vardy, M.E., Heller, V., Hühnerbach, V., Urlaub, M., Sarkar, S., Masson, D.G., Henstock, T.J., Minshull, T.A., Paulatto, M., Le Friant, A., Lebas, E., Berndt, C., Crutchley, G.J., **Karstens, J.**, Stinton, A.J., and Maeno, F., 2012. Combinations of volcanic-flank and seafloor-sediment failure offshore Montserrat, and their implications for tsunami generation. **Earth and Planetary Science Letters**, Vol. 319-320, pp. 228–240. doi:10.1016/j.epsl.2011.11.032.

Recent seafloor mapping around volcanic islands shows that submarine landslide deposits are common and widespread. Such landslides may cause devastating tsunamis, but accurate assessment of tsunami hazard relies on understanding failure processes and sources. Here we use high-resolution geophysical data offshore from Montserrat, in the Lesser Antilles, to show that landslides around volcanic islands may involve two fundamentally different sources of sediment (island-flank and larger seafloor-sediment failures), and can occur in multiple stages. A combination of these processes produces elongate deposits, with a blocky centre (associated with island-flank collapse), surrounded by a smoother-surfaced deposit that is dominated by failed seafloor sediment. The failure of seafloor sediment is associated with little marginal accumulation, and involves only limited downslope motion. Submarine landslide deposits with similar blocky and smooth surfaced associations are observed in several locations worldwide, but the complex emplacement processes implied by this morphological relationship can only be revealed by high-resolution geophysical data. Such complexity shows that the volume of landslide deposits offshore of volcanic islands cannot simply be used in tsunami models to reflect a single-stage collapse of primary volcanic material. By applying predictive equations for tsunami amplitude to investigate general scenarios of volcanic island landslide generation, we show that the tsunami hazard associated with volcanic island collapse remains highly significant. Volcanic flank failures, even if relatively small, may generate large local tsunamis, but associated seafloor sediment failures, even if they have a much greater volume, have a substantially lower potential for tsunami generation.

WIDESPREAD AND PROGRESSIVE SEAFLOOR-SEDIMENT FAILURE FOLLOWING VOLCANIC DEBRIS AVALANCHE EMPLACEMENT: LANDSLIDE DYNAMICS AND TIMING OFFSHORE MONTSERRAT, LESSER ANTILLES

Watt, S.F.L., Talling, P.J., Vardy, M.E., Masson, D.G., Henstock, T.J., Hühnerbach, V., Minshull, T.A., Urlaub, M., Lebas, E., Le Friant, A., Berndt, C., Crutchley, G.J., and **Karstens, J.**, 2012. Widespread and progressive seafloor-sediment failure following volcanic debris avalanche emplacement: Landslide dynamics and timing offshore Montserrat, Lesser Antilles. **Marine Geology**, v. 323-325, pp. 69-94. doi:10.1016/j.margeo.2012.08.002.

Landslides associated with flank collapse are volumetrically the most significant sediment transport process around volcanic islands. Around Montserrat, in the Lesser Antilles, individual landslide deposits have volumes (1 to 20 km³) that are up to two orders of magnitude larger than recent volcanic dome collapses (up to 0.2 km³). The largest landslide deposits were emplaced in at least two stages, initiated by the emplacement of volcanic debris avalanches which then triggered larger-scale failure of seafloor sediment, with deformation propagating progressively downslope for up to 30 km on gradients of 1°. An unusually detailed seismic, side-scan sonar and bathymetric dataset shows that the largest landslide off Montserrat (forming Deposit 8) incorporated ~70 m of in-situ sediment stratigraphy, and comprises ~80% seafloor sediment by volume. Well-preserved internal bedding and a lack of shortening at the frontally-confined toe of the landslide, shows that sediment failure involved only limited downslope transport. We discuss a range of models for progressively-driven failure of in-situ bedded seafloor sediment. For Deposit 8 and for comparable deposits elsewhere in the Lesser Antilles, we suggest that failure was driven by an over-running surface load that generated excess pore pressures in a weak and deforming undrained package of underlying stratigraphy. A propagating basal shear rupture may have also enhanced the downslope extent of sediment failure. Extensive seafloor-sediment failure

may commonly follow debris avalanche emplacement around volcanic islands if the avalanche is emplaced onto a fine-grained parallel-bedded substrate. The timing of landslides off Montserrat is clustered, and associated with the deposition of thick submarine pyroclastic fans. These episodes of enhanced marine volcanoclastic input are separated by relatively quiescent periods of several 100 ka, and correspond to periods of volcanic edifice maturity when destructive processes dominate over constructive processes.

A.2 LIST OF PRESENTATIONS DURING MY PHD

Karstens, J., and Berndt, C. 2014. Insights into focused fluid conduit formation from comparing seismic chimneys and pipes with field observations of fluid flow manifestations in the Colorado Plateau. **AGU Fall Meeting**, San Francisco, 15-19 December, 2014.

Flach, T., Solomon, S., Cavanagh, A., Schelland, M., Wildenborg, T., Buenz, S., **Karstens, J.**, Ahmed, N., Chadwick, A., and Holloway, S., 2014. Evaluating propensity of leakage with Bayesian Belief Nets (BN). **International Conference on Greenhouse Gas Technology (GHGT)**, 5 – 9 October 2014.

Karstens, J., and Berndt, C., 2014. Seismic chimneys in the Southern Viking Graben. **Gas in Marine Sediments (GIMS 12)**, 1 – 4 September 2014.

Vielstädte, L., **Karstens, J.**, Haeckel, M., Schmidt, M., Linke, P., Reimann, S., Liebetau, V., and Wallmann, K., 2014. Anthropogenic Methane Emissions from Abandoned Oil and Gas Wells in the North Sea- How much Methane is Leaking into the Ocean and finally into the Atmosphere? **Gas in Marine Sediments (GIMS 12)**, 1 – 4 September 2014.

Karstens, J., Berndt, C., and Crutchley, G., 2014. 3D seismic investigation of volcanic landslide deposits offshore Montserrat. **P-Cable 3D Seismic Annual Workshop 2014**, 3 – 4 February, 2014.

Haeckel, M., Wallmann, K., Schmidt, M., Liebetau, V., Sommer, S., Schroller, D., Schönfeld, J., **Karstens, J.**, and Berndt, C., 2013. Fluid expulsion at a 3-km long fracture system in the Northern North Sea – geochemical constraints on the origin of gas and water. **AGU Fall Meeting**, San Francisco, 9 -13 December, 2013.

Karstens, J., Berndt, C., Crutchley, G.J., 2013. Why every dimension matters: Interpretation of volcanic landslide deposits from 3D seismic and time-lapse bathymetric data from offshore Montserrat. **International Symposium on Submarine Mass Movements and Their Consequences (ISSMMTC)**, Kiel, 23 - 25 September, 2013.

Karstens, J., and Berndt, C., 2013. Analysis of seismic chimneys in the Southern Viking Graben. **ECO2 Annual Meeting**, Bergen, 13 – 16 May, 2013.

Karstens, J., and Berndt, C., 2013. Implications of palaeo fluid flow for the storage of CO₂ at Sleipner. **ECO2 Post cruise meeting**, Brussels, 6. March, 2013.

Berndt, C., Crutchley, G.J., Krastel, S., **Karstens, J.**, Dumke, I., and Dünnbier, K., 2012. Recent slope mobilizations in the Storegga Slide area. Invited talk at the **AGU Fall Meeting**, San Francisco, 3-7 December, 2012.

Talling, P.J., Kataoka, K., Endo, D., Watt, S.F., Le Friant, A., Ishizuka, O. IODP Expedition 340 Scientific Party, Berndt, C., Crutchley, G., and **Karstens, J.**, 2012. New insights into composition and source, single or multistage emplacement, and relationship to eruption cycles from first drilling of volcanic island landslides, offshore Montserrat. **AGU Fall Meeting**, San Francisco, 3-7 December, 2012.

Karstens, J., Berndt, C., and Crutchley, G., 2012. Insights into pyroclastic flow emplacement from high-resolution 3D seismic data from Montserrat, Lesser Antilles. **DGG Annual Assembly**, Hamburg, 5 – 8 March, 2012.

A.3. APPENDIX OF “QUANTIFICATION OF METHANE EMISSIONS AT ABANDONED GAS WELLS IN THE CENTRAL NORTH SEA“

Tab. A.3.1: Quantification of gas emissions from funnel measurements based on video material. Left columns: gas volume estimations; Right columns: funnel volume estimation. The optically derived funnel volume was compared to the known funnel volume to calculate a correction factor, F_{corr} , and corrected gas flows, Q_{corr} . The error of the gas flows is estimated from the uncertainty in fill time of 1 s.

Gas Volume				Funnel Volume			
Measures	15/9-13	16/4-2	16/4-2	True funnel dimensions	15/9-13	16/4-2	16/4-2
m (mm)	98.30	52.23	15.01	125	120.3	124.471	125.5
r_T (mm)	37.70	33.22	85.30	30	37.7	33.224	27.8
r_B (mm)	142.66	86.91	96.46	150	166.8	155.620	129.9
h (mm)	83.12	44.80	13.93	109.66	101.5	108.390	114.7
V (L)	0.59	0.14	0.09	0.8	0.9	0.87	0.6
Gas Flow				Correction			
Start Time	00:00:43	00:01:08	00:00:00	Offset/ L	0.14	0.006	-0.16
End Time	00:05:14	00:01:59	00:00:42	F_{corr}	0.88	0.92	1.33
Fill time (s)	331	51	42				
Q (L min ⁻¹)	0.11	0.16	0.13				
Q_{corr} (L min ⁻¹)	0.09	0.15	0.17				
Error (cm ³ s ⁻¹)	0.01	0.05	0.05				

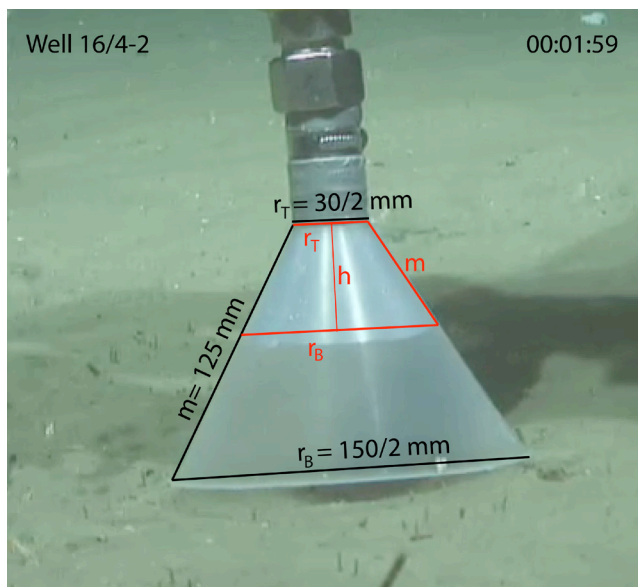


Fig. A.3.1: Exemplary visualization of optically derived gas flow measurement at well 16/4-2 using the funnel attached to the gas sampler. The known dimensions of the funnel are given in black: lateral funnel height, m , and radii of the top plane, r_T , and bottom plane, r_B , respectively. The gas volume was determined by measuring the corresponding h and m .

A.4. SUPPLEMENTARY METHODS FOR “GREATER FOCUS NEEDED ON BIOGENIC METHANE LEAKAGE FROM OIL AND GAS WELLS IN THE NORTH SEA”

A.4.1. DATA ANALYSIS IN THE CENTRAL NORTH SEA

A.4.1.1. DETERMINING THE ORIGIN OF LEAKING GASES

The origin of leaking gases was analyzed by a combination of geochemical- and seismic investigations at three leaky abandoned wells, i.e. 15/9-13, 16/4-2, and 16/7-2, in the Norwegian Sector of the CNS (Fig. 7.1). During the Celtic Explorer expedition CE12010, surface sediments were collected with ROV- (Remotely Operated Vehicle) deployed push-cores (PC). For dissolved gas analysis, 3 ml of wet sediment was sub-sampled in 2 cm intervals and filled into 20 ml headspace vials. 6 ml of saturated NaCl solution and an additional 1.5 g of NaCl were added and the vials sealed tight with butyl-rubber stoppers. The samples were stored refrigerated for onshore analyses. Prior to storage in the cold room, the vials were shaken vigorously for half an hour to release dissolved gases into the headspace.

In addition, free gas was sampled directly in the bubble stream with ROV-operated special gas samplers as described by Rehder and Schneider von Deimling (2008) and Pape et al. (2010). The gas sampler consists of a stainless steel cylinder with a PVC funnel attached to it to facilitate gas bubble sampling (Fig. A.4.1). Onboard, subsamples of pressurized gas were transferred into pre-evacuated headspace glass vials of 20 and 100 ml volume until the pressure in the vials was ~1020 mbar. In the GEOMAR home laboratory, methane and higher alkane concentrations in the free gas samples and in head-space vials were determined with a gas chromatograph GC 8000top (CE instruments) equipped with a FID detector and a capillary column (RT-Alumina Bond-KCl, 50 m, 0.53 mm). Stable carbon isotope composition of methane was determined by using a continuous flow GC-Isotope Ratio Mass Spectrometer combination. Methane was separated from other hydrocarbons in a Thermo Trace GC (isotherm at 60°C, He-carrier gas, ShinCarbon 1.5 m packed column). The subsequent conversion of methane to carbon dioxide was conducted in a Ni/Pt combustion furnace at 1150°C. The ¹³C/¹²C-ratios of the produced CO₂ were determined by a Thermo MAT253 isotope ratio mass spectrometer. All isotope ratios are reported in the δ-notation with respect to Vienna Pee Dee Belemnite (VPDB). Analytical precision of the reported concentrations and isotopic composition is ± 3% and ± 0.3 ‰, respectively. Results of stable carbon isotope- and hydrocarbon composition at the three wells are given in Table 7.1 and Figure A.4.2.

Sediment porewater was extracted by squeezing wet sediment at low pressure (<5 bar) through 0.45 μm Whatman regenerated cellulose filters. 2 ml aliquots were treated with 10 μL of HgCl₂ to inhibit further microbial degradation and stored cool until analysis. Onshore, the stable carbon isotope composition of dissolved inorganic carbon (DIC), referred to as δ¹³DIC was determined at the University of Bremen using a Finnigan MAT 251 mass spectrometer with an analytical accuracy of <0.07‰. Total alkalinity was determined by titration with 0.02 N HCl using a mixture of methyl red and methylene blue as indicator. The titration vessel was bubbled with argon to strip any CO₂ and H₂S produced during the titration. The IAPSO seawater standard was used for calibration; analytical precision and accuracy are both ~2 %.

In addition, an industrial 3D seismic data set (ST98M3, Statoil ASA) was analyzed for shallow gas pockets in the area around the three wells by mapping high amplitude anomalies (Loeseth et al., 2009) in the upper 1000 m of sediment using Petrel. The locations of identified gas pockets were assigned to stratigraphic units (Karstens and Berndt, 2015) and correlated with the well-paths of the three leaky wells. Two of the wells (i.e. 15/9.13 and 16/7-2) have been drilled through shallow gas in Lower Pliocene (LP) and Top Pliocene (TP) stratigraphic units (Fig. 1). For well 16/4-2, the seismic data do not reveal prominent bright spots (i.e. reverse polarity high amplitude anomalies) in the direct vicinity of the well-path, but the near-surface sediments (Fig. 7.1b, 0.1 – 0.4 s two-way-travel time TWT) show seismic turbidity, which might indicate an

unfocussed distribution of gas (Judd and Hovland, 1992).

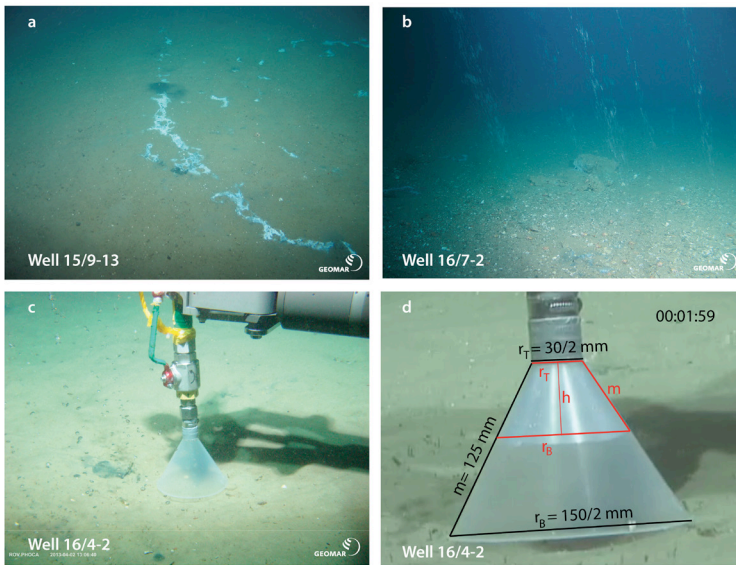


Fig. A.4.1: Gas leakage and gas flow measurements at the investigated wells. Pictures showing a) bacterial mats related to CH₄ leakage at well 15/9-13, b) the most intense leakage at well 16/7-2, c) gas flow measurement at well 16/4-2, and d) exemplary visualization of optically derived gas flow measurement at well 16/4-2 using the funnel attached to the gas sampler. The known dimensions of the funnel are given in black: lateral funnel height, *m*, and radii of the top plane, *r_T*, and bottom plane, *r_B*, respectively. The gas volume was determined by measuring the corresponding dimensions of the gas filled frustum of a cone and calculating the height, *h* (red letters).

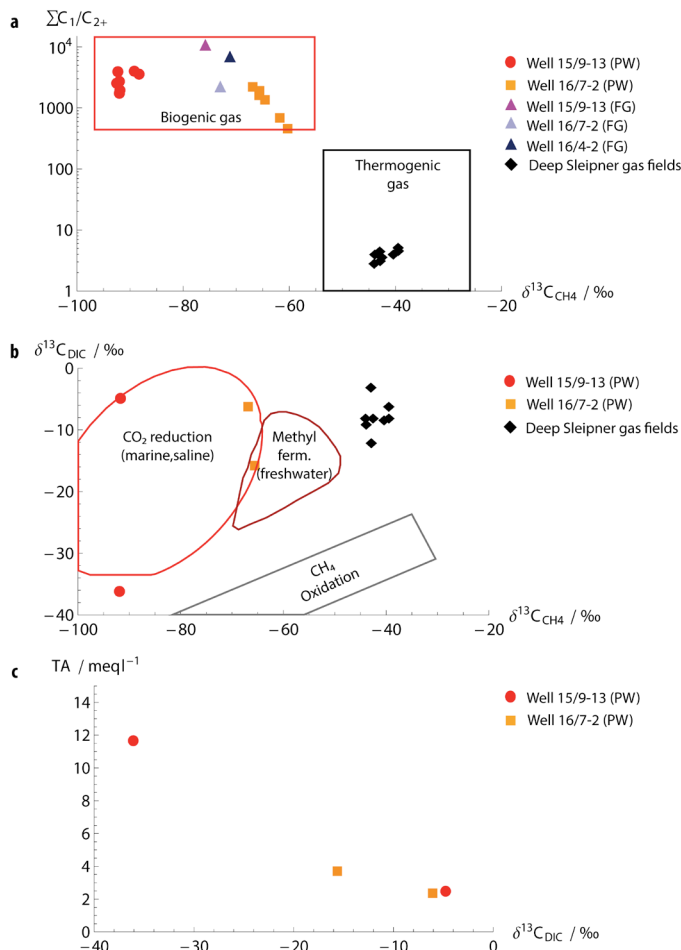


Fig. A.4.2: Results of geochemical analysis of free seep gases and porewaters at the three investigated wells. a) Bernard diagram of the molecular and isotopic gas composition (after Bernard et al., 1978) indicating the gas source of the gas at the abandoned wells (red dots: porewater (PW) at well 15/9-13, orange rectangle: porewater at well 16/7-2, triangles: free seep gas (FG) at wells 15/9-13, 16/7-2, and 16/4-2) and the deep hydrocarbon reservoirs in the area (black diamonds; James, 1990). (b) Cross-plot of $\delta^{13}C$ of DIC versus $\delta^{13}C$ of CH₄ in the porewater at well 16/7-2 (orange rectangles), well 15/9-13 (red dots), and the deep hydrocarbon reservoirs (black diamonds; James, 1990). (c) Cross-plot of total alkalinity (TA) and $\delta^{13}C$ of DIC indicating microbial anaerobic oxidation of methane.

A.4.1.2. QUANTIFYING PER-WELL LEAKAGE RATES

The in-situ gas flow was quantified at single bubble streams of well 16/4-2 and well 15/9-13 using the ROV-operated gas sampler with attached funnel (Fig. A.4.1). Both, the time, t , to fill the funnel with gas and its corresponding volume, V_F , were determined based on video footage using the software ImageJ (Farreira and Rasband, 2012)38. The gas volume accumulating in the funnel was calculated from the resulting volume of the cone frustum, $V_F = h \cdot \pi / 3 \cdot (r_B^2 + r_B \cdot r_T + r_T^2)$, where r_B and r_T are the radii of the base plane and top plane, respectively, and h is the distance between both planes, $h = (m^2 - r_T^2 + 2 \cdot r_T \cdot r_B \cdot r_B^2)^{0.5}$ (Fig. A.4.1). The lateral height of the funnel had a length of $m = 12.5$ cm and was used as scale in the images. The optically-derived gas volume required correction, due to imprecise size measurements of a 3D object in its 2D projection. The ratio between optically-derived and known funnel volume, F_{corr} was used to correct the gas volume. The resulting gas flow at a single gas stream, Q_F is:

$$Q_F = V_F / t \cdot F_{corr} \quad (\text{Eq. S.1})$$

The correction factor ranged between 0.88 and 1.33 including optical failures described above and uncertainties in pixel accuracy during measurements with ImageJ. The error in determining the time for filling the funnel is about 1 s, resulting in an error of the gas flow of < 2.7 cm³/s, i.e. less than 2.5 %.

At well 16/7-2, the in-situ gas flow was derived from bubble size measurements described in Section A.4.1.3. To allow comparison of the gas emissions, measured at different locations (i.e. 58.373° N and 1.932° E; 58.473° N and 2.033° E; and 58.596° N and 2.028° E) and at variable water-depths (i.e. 81, 83, and 93 m at well 15/9-13, 16/7-2, and 16/4-2, respectively), in-situ gas flows measured at 7.8 °C and 5.1 °C were expressed in standard conditions, referred to as STP ($P = 1$ bar; $T = 298.15$ K). The standard gas flows, Q , ranged from 0.9 to 1.8 L min⁻¹ (STP) with an average gas flow of 1.4 (± 0.4) L min⁻¹ (STP) at the sampled bubble streams (Tab. A.4.1). This corresponds to a relative variability of 27 %, which was (due to lack of information) also assumed to be equivalent to the spatial variability at a single well. Thus, based on the average Q and the number of individual bubble streams at the wells, the total seabed methane gas flow was estimated to range between 2.8 L min⁻¹ and 55 L min⁻¹ (STP), corresponding to an annual methane release of 1.0 - 19 t yr⁻¹ well⁻¹ assuming no larger variability over prolonged times (Tab. A.4.1).

Tab. A.4.1. Quantification of seabed- and atmospheric gas emissions (via direct bubble transport and diffusive outgassing of methane from the surface mixed layer) at the investigated abandoned wells in the Central North Sea

Well	Seabed				Atmosphere	
	In situ Q per vent (L min ⁻¹)	Q (STP) per vent (L min ⁻¹)	Number of vents	Q per well ^a (t CH ₄ yr ⁻¹)	F _{Atm} per well (%)	F _{Atm} per well (t CH ₄ yr ⁻¹)
16/4-2	0.15 / 0.17 ^b	1.6 / 1.8 ^{b,e}	8	3.8	21	0.8
16/7-2	0.15 ^c	1.4 ^f	39	18.5	36	6.8
15/9-13	0.09	0.9 ^g	2	1	40	0.4
Total			49	24		8
Abs. error (1 σ)	0.03	0.4		7 ^d		2 ^d
Rel. error (1 σ)	24.74	27.1	121.6			

^a based on the average gas flow of 1.4 L min⁻¹ at STP

^b based on replicate gas flux measurements at well 16/4-2

^c derived from bubble size, due to lack of direct funnel measurements

^d based on a spatial variability of 27.1%

^e measured at high tide

^f measured at low tide

^g measured 2 h after low tide

A.4.1.3. MEASURING INITIAL BUBBLE SIZES

The image editing software ImageJ (Farreira and Rasband, 2012) was applied to the ROV video sequences, which also were used for the funnel measurements, to determine the respective initial (seafloor) gas bubble sizes. These size spectra are required to calculate the fate of leaking methane from the seafloor to the atmosphere using a numerical bubble dissolution model (Section A.4.1.6). For calibration of bubble sizes, the bottom plane of the funnel (diameter = 150 mm) was used as a scale. A video sequence of 5 s, corresponding to 125-150 individual frames, was analyzed frame by frame. The video sequence was first converted to grayscale and was subsequently processed to enhance the contrast. Unfortunately, contrast and pixilation noise remained rather poor making a computer based automatic measurement routine impractical. Hence, ellipses were manually overlaid to individual bubbles leaving the seafloor and were marked as overlays. The overlays were allocated to individual bubbles to track them and analyze their changes in size in subsequent frames. If bubbles had a very irregular shape, they were outlined manually before using the ellipse fitting object of ImageJ (i.e. 10 of 71 measurements at well 16/7-2). For each bubble, the major and minor axes, angle, perimeter, area, circularity, as well as frame number were recorded. The corresponding bubble volume, $V_0 = 4/3 \times \pi \times req^2$, was calculated from the equivalent spherical radius, $req = (a^2 \times b)^{1/3}$ based on the major, a , and the minor axes, b , of the fitted ellipse. If bubbles were measured in several frames, their average radius was used to level out the trajectory and shape oscillations of the bubble during its ascent (Clift et al., 1978). All determined bubble volumes were added to calculate the total gas volume flow over a period of 5 s.

The methodological error of bubble size measurements was estimated in two ways: (1) The volume flow derived from the bubble size spectra was compared to the flow constrained by the funnel measurements. The funnel-derived flow is integrated over a much longer time scale and hence, regarded as more precise. Consequently, the bubble size spectra were corrected to match the funnel-derived flow values. (2) Multiple bubble measurements in sequential video frames were used to quantify the error caused by oscillation or wobbling of the gas bubble in the real 3D space which cannot be correctly represented in a 2D image. The video can only provide a snapshot of current bubble shape and size projected onto a plane.

Bubble size measurements at well 15/9-13 and 16/4-2 were combined resulting in a combined bubble size distribution (ψ) (Fig. A.4.3). Measurements at well 16/7-2 were excluded for the determination of the combined bubble size distribution because bubbles escaped from below a carbonate rock, which expelled significantly larger bubbles into the water column than bubbles directly released from the sandy sediments (i.e. at well 15/9-13 and 16/4-2, Fig. A.4.3). Given that the gas flow at individual seeps of the three wells was low such that initial bubble formation processes were mainly controlled by the mechanical properties of the surface sediments (Dewar et al., 2013), ψ is proposed to be representative for bubbles released from the fine to medium-grained clayey sand found at the investigated wells.

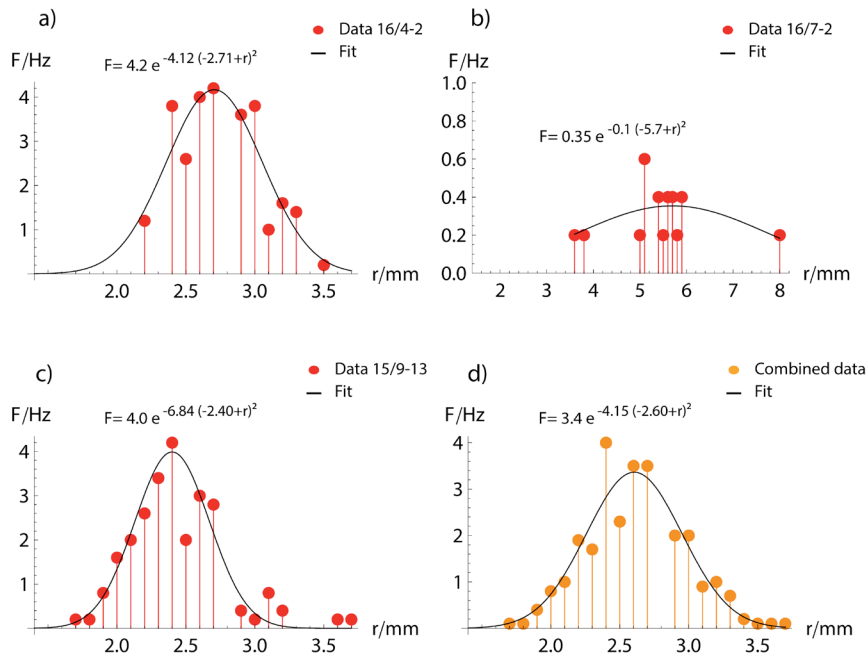


Fig. A.4.3: Results of bubble size measurements. Measured bubble release frequency (F) versus bubble radius (r), and Gaussian fits for the bubble size distribution of single streams at the investigated wells (a-c). d) Combined bubble size distribution based on measurements at wells 15/9-13 and 16/4-2 which was considered to be representative for gas leakage in the North Sea and used for extrapolation. Gaussian functions were fitted to the data using the non-linear least-squares fitting algorithm “NonlinearModelFit” of Mathematica. The variance, s^2 , of the fits is 0.53, 0.002, 0.31, and 0.18 for the bubble size distributions at wells 16/4-2, 16/7-2, 15/9-13, and the combined spectrum, respectively.

A.4.1.4. QUANTIFYING DISSOLVED METHANE AND METHANE OXIDATION RATES IN THE WATER COLUMN.

During cruise CE12010, seawater samples were taken with Niskin bottles attached to a video-guided CTD or operated by ROV Kiel 6000 (Linke et al., 2015). At wells 15/9-13 and 16/7-2 seawater was sampled near the seafloor and additionally through the water column at well 15/9-13. No water samples were recovered at well 16/4-2. For dissolved gas analysis, subsamples were transferred bubble-free into 100 ml headspace vials immediately after recovery of the Niskin Water Sampler Rosette. Dissolved gases were released from the seawater samples by headspace technique (headspace of 10 ml of Ar 4.5). After adding 50 μ l of saturated HgCl₂-solution the vials were stored at 4°C. Concentration determination of methane released into the headspace was conducted by using onboard gas chromatography (Shimadzu, 2010; for results see Tab. 7.1 and Fig. A.4.4).

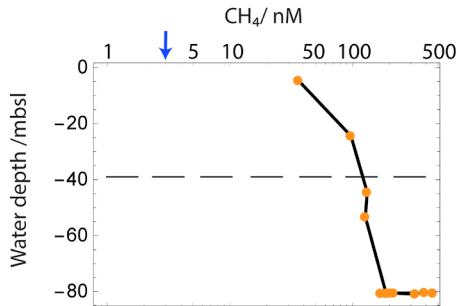


Fig. A.4.4: : Depth profile showing the concentration of dissolved methane in the water column (orange bullets) based on measurements during CE12010 CTD7 at well 15/9-13. The dashed line indicates the depth of the thermocline and the blue arrow represents the equilibrium concentration of methane in the surface mixed layer (i.e. 3 nM)21 with respect to the atmospheric partial pressure of methane

To assess methane oxidation rates (rMOx) in the water column, subsamples were transferred bubble-free into ~23 ml headspace vials and closed with grey bromo-butyl stoppers (Helvoet Pharma, Belgium), immediately after recovery of the Niskin bottles. Shortly after sampling, a 6 µl gas bubble of ¹⁴C-CH₄:N₂ gas (70 – 250 Bq) was added to the subsamples, which were then incubated for 2 days in the dark at in-situ temperature (~8°C). After 2 days, samples were fixed in 4 pellets of NaOH and stored at 4°C until rate measurements were performed in the home laboratory. Radioactive substrate and product pools were quantified as described by Blees and colleagues (Blees et al. 2014, Treude et al. 2003) to determine the first order rate constant. Rates were then calculated according to:

$$rMOx = k \times [CH_4] / t \quad (\text{Eq. S.2})$$

, where k is the first order rate constant and $[CH_4]$ denotes the concentration of CH_4 at t_0 of the incubation, and t the incubation time (for results see Tab. 1). All rates were determined in quadruplicates. Killed controls (addition of 200 µl saturated HgCl₂ at the start of the incubation) were analyzed for each incubation period. Recovery of the radioactive tracer was >95 %. The detection limit of the rate depends on the amount of radioactive methane added and the initial methane concentration and varied between 0.01 and 6.45 nM day⁻¹ depending on the sample. Above well 15/9-13, all rates were below detection limit. Above well 16/7-2, one out of three sampling location showed rates below detection limit. For the other two locations above well 16/7-2, rates were 0.19 ± 0.07 and 1.40 ± 0.83 nM day⁻¹ (σ_n/SE , $n=4$).

A.4.1.5 SEISMIC MAPPING OF SHALLOW GAS AND THE PROBABILITY OF WELLS TO LEAK

The examination of the probability of wells to leak shallow gas is based on the analysis of the three-dimensional (3D) seismic data set ST98M3, which is the result of merging seven independently acquired and processed sub-datasets. Detailed information regarding processing parameters of the specific subsets are not available, while the processing sequence for merging the data included resampling, filtering, phase rotation and amplitude adjustments. The final 3D seismic cube shows positive acoustic impedance contrasts as positive amplitude (blue) followed by negative amplitude (yellow). The bin-size is 12.5 m and the vertical resolution is 10 m (dominant frequency 45Hz, seismic velocity of ~1,800 m/s). The dataset extends 62 km from North to South and 46 km East to West covering an area of more than 2,000 km² (Fig. 7.1a).

The localizations of shallow gas pockets, indicated by high amplitude anomalies (Løseth et al., 2009)35, were mapped for the upper 1,000 m of sediment and assigned to stratigraphic units (Karstens and Bernd,

2015)36 using the seismic analysis software Petrel. Assuming that leakage of shallow gas can potentially occur along any type of well (producing, injecting, or abandoned), as long as there is a shallow gas source in its direct vicinity, an increased permeability induced by the drilling operation, and a driving force for gas movement, which could be buoyancy or excess pore pressure, we correlated the well paths of 55 operating- and non-operating wells in the seismic study area with locations of shallow gas pockets. 50 sidetracked- and multilateral wells were excluded for the correlation analysis because they separate from the main well in the deeper subsurface, which was not the scope of this study. Further, 55 platform wells were deselected because the seismic data set does not cover sediments located directly below platforms. The probability of wells to leak shallow gas was then determined by the fraction of wells which penetrate high amplitude anomalies in the shallow subsurface (i.e. 18 of 55 selected wells, Fig. 7.1) and is required for further extrapolation of methane leakage on a North Sea scale.

A.4.1.6. MODELING THE FATE OF LEAKING METHANE

A numerical bubble dissolution model was used to calculate the bubble-mediated methane flow to the atmosphere by a single rising gas bubble. The simulation of a single rising bubble seems to be justified because only single bubble streams were observed at the investigated wells with very little to no interaction between the bubbles, or plume dynamics (upwelling). Assuming that the release of single bubble streams is representative for leaky wells in the North Sea, the model simulates the shrinking of a gas bubble due to dissolution in the water column, its expansion due to decreasing hydrostatic pressure in the course of its ascent and gas stripping, and the final gas transport to the atmosphere. A set of coupled ordinary differential equations (ODEs) was solved numerically describing these processes for each of the involved gas species (Ch₄, N₂, and O₂; Eq. S3) and the bubble rise velocity (Eq. S4), where time solves as the only independent variable. Thermodynamic and transport properties of the gas components, such as molar volume, gas compressibility, and gas solubility in seawater, were calculated from respective equations of state (Duan et al., 1992; Duan and Mao, 2006; Geng and Duan, 2010; Mao and Duan, 2006)4, and empirical equations for diffusion coefficients (Boudreau, 1997), mass transfer coefficients (Zheng and Yapa, 2002), and bubble rise velocities (Wüest et al., 1992), taking into account local pressure, temperature and salinity conditions as measured by CTD casts. Implemented equations and values are provided in Table A.4.2. The ODE system is solved using finite difference methods implemented in the NDSolve object of Mathematica (i.e. LSODA, Sofroniou and Knapp, 2008).

The mass exchange of gas components across the bubble surface is generally described as (e.g., Wüest et al., 1992; McGinnis and Little, 2002; Leifer and Patro, 2002).

$$dN_i/dt = 4\pi r_{eq}^2 K_{L,i} (C_{a,i} - C_{eq,i}) \quad (\text{Eq. S.3})$$

, where i is the i th gas species, N , is the amount of gas in the bubble, $4\pi r_{eq}^2$ is the surface area of the equivalent spherical bubble, K_L is the specific mass transfer rate between gas phase and aqueous phase, C_a is the dissolved gas concentration, and C_{eq} is the gas solubility. All of the above variables are functions of the water depth, z , i.e. pressure, temperature and salinity (see Tab. A.4.5 for details and references). The change of the vertical bubble position is related to the bubble rise velocity, v_b (Tab. A.4.5):

$$dz/dt = v_b \quad (\text{Eq. S.4})$$

Model simulations were performed based on boundary conditions obtained in the CNS from Sea-Bird 9 plus CTD data of August 2012 (Tab. A.4.2) and run for different initial bubble sizes (ranging between 1.0 to 4.0 mm radius, in accordance to radii of the combined bubble size distribution, Section 1.1.3), initially containing only methane. Simulated water depths ranged between 20 and 150 m in accordance to those

important for the methane bubble transport to the SML of the North Sea. Larger water depths were not considered because additional model runs revealed that the combined bubble size distribution completely loses its initial methane content in the deep layer of the North Sea when released from more than 150 m depths, Fig. A.4.6.

Tab A.4.3. Parameterization of numerical model

Parameterization	Range	Variance	Reference
Diffusion coeff.: D_i (m^2s^{-1})			
$D_{O_2}=1.05667*10^{-9}+4.24*10^{-11}*T$	T: 0-25°C	$1.00*10^{-21}$	Boudreau, 1997
$D_{N_2}=8.73762*10^{-10}+3.92857*10^{-11}*T$	T: 0-25°C	$2.94*10^{-23}$	Boudreau, 1997
$D_{CH_4}=7.29762*10^{-10}+3.31657*10^{-11}*T$	T: 0-25°C	$5.70*10^{-24}$	Boudreau, 1997
Mass transfer coefficient: $K_{L,i}$ / $m s^{-1}$			
$K_L = 0.013(v_b 10^2/(0.45+0.4r*10^2))^{0.5} D_i^{0.5}$	$r \leq 2.5$ mm		Zheng & Yapa, 2002
$K_L=0.0694 D_i^{0.5}$	$2.5 < r \leq 6.5$ mm		Zheng & Yapa, 2002
$K_L=0.0694 (2r * 10^{-2})-0.25 D_i^{0.5}$	$R < 6.5$ mm		Zheng & Yapa, 2002
Fit to CTD data as function of z			
$T(z)=8+7/(1+e^{0.375(-21.7512+z)})$	Z: 0-100 m	$3.99*10^{-2}$	
$S(z)=35.12 - 0.67/(1+e^{0.4125(-20.1595+z)})$	Z: 0-100 m	$4.97*10^{-4}$	
Density of SW: ρ_{SW} / $kg m^{-3}$			
$\rho_{SW}(z)=1027.7 - 2.150/(1+e^{0.279(-21.612+z)})$	Z: 0-100 m	$6.8*10^{-3}$	Unesco,1981
Bubble rise velocity: v_b ($m s^{-1}$)			
$v_b = 4474 r^{1.357}$	$r < 0.7$ mm		Wüest et al., 1992
$v_b = 0.23$	$0.7 \leq r < 5.1$ mm		Wüest et al., 1992
$v_b= 4.202 r^{0.547}$	$r \geq 5.1$ mm		Wüest et al., 1992
Gas solubility: c_i (mM)			
$c_{N_2} = 0.622+0.0721*z$	Z: 0-100m	$2.5*10^{-3}$	Mao & Duan, 2006
$CO_2=1.08+0.1428*z$	Z: 0-100m	$9.8*10^{-3}$	Geng & Duan, 2010
$c_{CH_4} = 1.44+0.1671*z$	Z: 0-100 m	$2.4*10^{-2}$	Duan & Mao, 2006
CH ₄ molar volume: MV_{CH_4} ($L mol^{-1}$)			
$MV_{CH_4}=1/(0.0418+0.0044+z)$	Z: 0-100 m	$3.0*10^{-2}$	Duan et al., 1992
Hydrostatic Pressure: P_{hydro} (bar)			
$P_{hydro} = 1.013+\rho_{SW} * g * z$			

The potential methane emissions from leaky wells to the atmosphere were calculated distinguishing between direct emissions via bubble transport and indirect emissions via the diffusive outgassing of methane dissolving in the surface mixed layer (SML, i.e. the upper 50 m of the North Sea water column; Thomas et al., 2005)29. The direct bubble methane transport to the atmosphere was calculated from the remaining/residual amount of CH₄ in the bubble, when it reaches the sea surface, NS, i.e.

$$N_S(r, z) = N_0(r, z) - \int_{t=0}^{t^{max}} dN(r, z) dt \quad (\text{Eq. S.5})$$

,where N_0 is the initial amount of methane in the bubble and t^{max} is the time required by the gas bubble to travel to the sea surface and is determined numerically by the bubble dissolution model. The amount of methane dissolving in the SML of the North Sea (NSML) was calculated by integrating the rate of methane bubble dissolution over the time which is needed by the bubble to travel through the upper 50 m of the

water column (i.e. t_{50} to t_{max} , both determined numerically by the bubble dissolution model):

$$N_{SML}(r, z) = \int_{t_{50}}^{t_{max}} dN(r, z) dt \quad (\text{Eq. S.6})$$

Both, the residual methane and the methane dissolving in the SML depend on the bubble size (r) and water depth (z) and were normalized to the corresponding N_0 . The relative amount of methane at the sea surface and in the SML with respect to the initial bubble methane content, i.e. $\Omega_S(r, z) = N_S(r, z) / N_0(r, z)$ and $\Omega_{SML}(r, z) = N_{SML}(r, z) / N_0(r, z)$, are referred to as the transport efficiencies of a single gas bubble to the sea surface and to the SML, respectively.

A transfer function was fitted to numerical results using the non-linear least-square fit algorithm of Matlab. The fit describes the methane transport efficiency of a single bubble to the sea surface as a function of the initial bubble size (r) and the leakage depth (z):

$$\Omega_S = e^{-0.156/r^{1.26} \cdot z} \quad (\text{Eq. S.7})$$

The variance, s^2 of the residuals is better than 0.00013 and the linear correlation coefficient of the fit-curve to the numerical data is better than 0.99. The fit function is valid for initial bubble radii ranging between 1 and 4 mm initially containing only methane and for the given physicochemical properties of the water column obtained in the CNS from Sea-Bird 9 plus CTD data of August 2012 (Tab. A.4.2). By applying Eq. 7, the mass transfer of gases other than CH_4 , N_2 , and O_2 , as well as the development of upwelling flows are considered to be negligible for the methane transport to the sea surface.

Because leaky wells expelled a range of initial bubble sizes, the transport efficiencies $\Omega_S(r, z)$ and $\Omega_{SML}(r, z)$ were calculated for each bubble size and weighted by its volumetric contribution, V_0 , to the total emitted gas bubble volume, V_ψ . Integrating this weighted bubble transport efficiencies over the entire bubble size spectrum (ψ) gives the total methane transport efficiency to the SML (Ω_{SML}) and to the sea surface (Ω_S) with respect to the initial methane release at the seafloor, respectively:

$$\Omega_S(\psi, z) = \int_{r(min)}^{r(max)} \Omega_S(r, z) \times \frac{V_0(r)}{V_\psi} \times \frac{1}{MI} dr \quad (\text{Eq. S.8})$$

$$\Omega_{SML}(\psi, z) = \int_{r(min)}^{r(max)} \frac{N_{SML}(r, z)}{N_0(r, z)} \times \frac{V_0(r)}{V_\psi} \times \frac{1}{MI} dr \quad (\text{Eq. S.9})$$

where, $r(min)$, and $r(max)$ are the minimum and maximum radii of the bubble size spectrum ψ , respectively, and MI is the measurement interval between individual bubble sizes (i.e. 0.1 mm). V_0 and V_ψ refer to optical size measurements at individual gas streams of the investigated wells, which were conducted to determine the combined bubble size spectrum. Applying Supplement Eq. 8 and Eq. 9, we assume that there is no change in the weighted volumetric contribution of each bubble size to the total emitted bubble volume (i.e. $V_0(r) / V_\psi = \text{const.}$), so that the relative distribution of bubble sizes is considered to be constant, although the release frequency of bubbles may change due to a variability of the seabed gas flow. This means that at a constant mass flow (i.e. per-well leakage rate) a decrease in the hydrostatic pressure (i.e. leakage depth) increases the rate of bubble formation but not their size distribution, as generally validated for seeps with a low gas flow (Dewar et al., 2013)30. Transfer functions were fitted to numerical results of Equation 8 and 9, respectively using the non-linear least-squares fitting algorithm “NonlinearModelFit” of Mathematica (Fig. A.4.5). The fit-curves describe the transport efficiency of the bubble size distribution to the sea surface (Eq. S10) and to the SML (Eq. S11) with respect to the seabed methane flow and as a function of the leakage depth (z), respectively:

$$\Omega_{S(\psi, z)} = e^{-0.043 \times z} \quad (\text{Eq. S.10})$$

$$\Omega_{S(\psi,z)} = 1/(1+e^{z-50}) \times 0.127 \times z^{0.5} + 1/(1+e^{50-z}) \times 1/(0.73 \times 6.1 \times 10^{-9} \times z^{4.6}) \quad (\text{Eq. S.11})$$

The variance, s^2 , of the fits is 0.0001 and 0.0005 for the transport efficiency to the sea surface and to the SML, respectively. The numerical accuracy of the model, determined from mass balance errors, was overall better than 99.9%. Supplementary equation 10 and 11 are required for the extrapolation analysis to calculate the potential methane emissions from the seafloor into the atmosphere (Section 1.2.2).

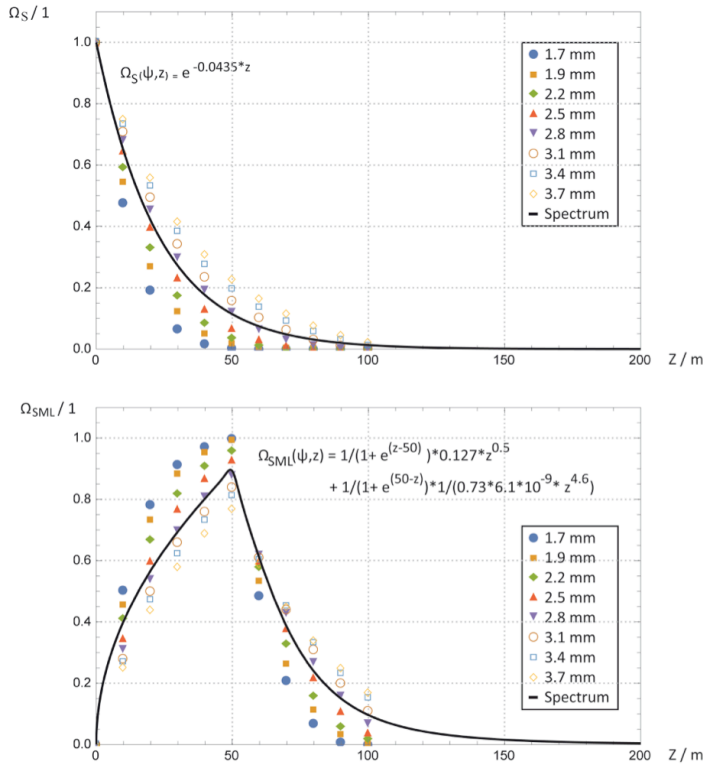


Fig. A.4.5: Numerical results of the bubble dissolution model. Model results show the methane bubble transport efficiency to the surface mixed layer (Ω_{SML}) and to the sea surface (Ω_S) of the North Sea, respectively as a function of the leakage depth (z) and for initial bubble radii ranging between 1.7 to 3.7 mm (in accordance to bubble sizes of the combined bubble size distribution). The methane transport efficiency of the combined bubble size distribution (black curve) was determined by fit curves to the data using the non-linear least-squares fitting algorithm “NonlinearModelFit” of Mathematica. The variance, s^2 , of the fit-curves is better than 0.001 and 0.005 for $\Omega_{S(\psi,z)}$ and $\Omega_{SML(\psi,z)}$, respectively.

A.4.2. EXTRAPOLATION ANALYSIS OF LEAKAGE ON A NORTH SEA SCALE

A.4.2.1. DEVELOPMENT OF AN ARCGIS DATABASE (NORTH SEA WELL INVENTORY)

To extrapolate methane leakage on a North Sea scale, about 15,800 offshore wellbore data (including the well identification, location, status, and type) were incorporated to an ArcGIS database (10.1; WGS84), sourced from online datasets populated by governmental energy departments and regulation agencies in 2012 to 2013 (Tab. A.4.3). Filters (queries) were applied to categorize and identify the wells for analysis. As leakage of shallow gas can potentially occur along any type of well, whether it is being producing hydrocarbons, injecting fluid into a reservoir, or has been abandoned, we selected all types of wells (i.e. 11,122 wells, see Tab. A.4.4), excluding sidetracked and multilateral wells which tend to separate from the main well in the deeper subsurface (i.e. < 1,000 m). Sidetracked and multilateral wells were deselected manually from the database following the guidelines for designation of wells and wellbores³². In addition,

bathymetric metadata with a spatial resolution of 5 minutes were incorporated to the ArcGIS database, derived from the EMODnet Bathymetry portal, i.e. <http://www.emodnet-bathymetry.eu>. Bathymetric data were required for the estimation of methane emissions to the atmosphere, which are depth-dependent.

Tab. A.4.3: Source data of the North Sea well inventory

Country	Data Source	Description (Date)
Norway ^a	Norwegian Petroleum Directorate	(Sept. 2013)
United Kingdom ^b	Department of Energy and Climate Change	All wells (Aug. 2013)
Germany ^c	Landesamt für Bergbau, Energie und Geologie	KWBORUNG (Jul. 2013)
Denmark ^d	Danish Energy Agency	DeepWells (Jan. 2012)
Netherlands ^e	Netherlands Oil and Gas Portal	NLOG Boreholes (Jun. 2013)

^ahttp://factpages.npd.no/ReportServer?/FactPages/geography/geography_all&rs:Command=Render&rc:ToOlbar=false&rc:Parameters=f&IpAddress=1&CultureCode=en

^b <https://www.gov.uk/oil-and-gas-offshore-maps-and-gis-shapefiles>

^c <http://nibis.lbeg.de/cardomap3/?TH=BOHRKW>

^d <http://www.ens.dk/en/oil-gas/oil-gas-related-data/wells>

^e <http://www.nlog.nl/en/activity/activity.html>

Tab. A.4.4: Classification of the North Sea well inventory and selection of wells used for the extrapolation analysis

Well Status	Main Wells/Wellheads	Sidetracked & Multilateral wells	Offshore wells
Operating ^a	1,301	1,365	2,666
Non-operating ^b	9,821	3,294	13,115
P&A ^{c,d}	1,847	343	2,190
Total	11,122 ^e	4,659	15,781

^a including injection, production, and open wells, and UK wells for which no completion date was specified

^b including plugged and abandoned, plugged, closed, junked, plugged back, plugged back and sidetracked, closed-in, completed to well, suspended at TD., and suspended wells

^c permanently plugged and abandoned wells (P&A)

^d excluding wells in the Danish- (DK) and British (UK) Sector because the well status was not specified in UK and DK source data

^e selected for analysis

A.4.2.2 ESTIMATING POTENTIAL METHANE EMISSIONS FROM LEAKY WELLS IN THE NORTH SEA

The potential methane emissions from leaky wells in the North Sea were estimated based on the North Sea well inventory (Section 1.2.1) and the extrapolation of leakage data obtained in the CNS, i.e. leakage rates (Section 1.1.2), initial bubble sizes (Section 1.1.3), and the potential fraction of leaky wells (Section 1.2.4), using ArcGIS. We distinguished between a conservative- ($2.4 \pm 1.4 \text{ t Ch}_4 \text{ yr}^{-1} \text{ well}^{-1}$) and a maximum (7.8

$\pm 7.1 \text{ t Ch}_4 \text{ yr}^{-1} \text{ well}^{-1}$) leakage estimate taking the average of available per-well flux data, either excluding or including the high emissions from well 16/7-2, respectively. Flow distribution maps (Fig. 3) were constructed by subdividing the North Sea into equally-sized polygons of 25 km² area using the “Cylindrical Equal Area Projection” and the “Fishnet” tool of ArcGIS 10.1. Spatial joining of the selected wells and bathymetric data gives each polygon a summary of numeric attributes that fall inside it, i.e. the average water depth (z) and a count field showing how many points fall inside it, i.e. the number of wells (NW). For each polygon the seabed flow (QSF) was calculated multiplying the seismically determined leakage potential (LP, i.e. 33%), the number of wells that fall inside each polygon (AF activity factor), and the per-well leakage rate (LR), i.e. 2.4 and 7.8 for the conservative and maximum flow estimate, respectively

$$Q_{SF} = AF \times LP \times LR \quad (\text{Eq. S.12})$$

The resultant methane emissions from the North Sea into the atmosphere were estimated using the same ArcGIS project, which previously was used to estimate the rate of methane leaky from the seabed. Atmospheric emission estimates encompass the direct bubble transport of methane from the seafloor to the sea surface and the diffusive emissions of methane bubble dissolution in the SML of the North Sea. The latter assumes the complete ventilation of methane dissolving in the upper 50 m of the water column, which is generally well-mixed throughout the year (Thomas et al., 2005). For each polygon of the ArcGIS project, direct and indirect emissions to the atmosphere (Q_{Atm}) were calculated using best-fit curves to numerical results, i.e. Eq. S10 and Eq. S11 describing the methane bubble transport efficiency to the sea surface ($\Omega_{S(\psi,z)}$) and to the SML ($\Omega_{SML(\psi,z)}$) with respect to the seabed gas flow (QSF), assuming no variation of initial bubble sizes over the extended area of the North Sea:

$$Q_{Atm,i} = Q_{SF,i} \times \Omega_{SML,i/S,i(\psi,z)} \quad (\text{Eq. S.13})$$

, where i is the leakage scenario, i.e. the conservative or maximum leakage estimate, and z is the average water-depth of the polygon derived from the spatial joining of bathymetric data to each cell of 25 km² area.

The flow estimates of individual polygons, both from the seabed and into the atmosphere and each for the conservative and maximum leakage estimates, were added to calculate the lower- and upper bounds of the total methane release from the seafloor into the North Sea and the atmosphere. All estimates are reported as arithmetic means of lower-and upper bounds plus minus the standard deviation (1σ).

A.4.2.3 SOURCES OF UNCERTAINTY IN OUR ESTIMATES

The uncertainty ranges on shallow gas leakage in the North Sea are large, as might be expected from the current state of knowledge of leaky wells, mainly depending on the representativeness of data obtained in the Norwegian CNS. There is a large uncertainty in our estimates related to the temporal and spatial variability of per-well leakage rates that might, in addition to sediment properties and tidal pressure fluctuations, be driven by overpressure in the shallow gas reservoir, or by differences in the gas supply. Further uncertainty is associated to the probability of wells to leak shallow gas. Leakage was only assumed to occur where the seismic data revealed prominent bright spots in the direct vicinity of the well, but leakage was also found where the presence of free gas was less constrained by the seismic data, either because the extent of the gas pocket or the gas saturation where beyond the resolution of the seismic method (Fig. 7.1, well 16/4-2). The lower emission estimate is thus definitely conservative, because per-well leakage rates and the number of leaky wells might have been underestimated. More data on the abundance of leaky wells, their leakage rates, and geochemical and isotopic composition of free seep gases including longer time series should be generated in order to better constrain the significance of leaky oil and gas wells for the North Sea methane budget.

Atmospheric emission estimates bear further uncertainty arising from three additional factors: (1) temporal and spatial variability of the bubble chain dynamics (upwelling), (2) variability of initial bubble sizes, and (3) seasonal changes of seawater conditions. Uncertainties related to inter-annual changes may significantly affect the diffusive outgassing of methane due to the seasonal deepening and breakdown of the thermocline (Schneider von Deimling et al., 2011; Rehder et al., 1998; Thomas et al., 2005) and the efficient ventilation of the entire water column during frequent fall and winter storms (Shakhova et al., 2013), which should aid annual diffusive methane emissions. No significant inter-annual variability is expected in the rate of direct methane releases to the atmosphere because the bubble methane transport is independent of the water column stratification and also nearly temperature-independent. This is because the increase in gas transfer velocity (K_L) compensates the decrease in gas solubility at elevated temperature. The lower atmospheric emission estimate is thus definitely conservative because the gas transport to the atmosphere might have been underestimated due to the seasonal increase in the ventilation of the water column or the evidence of upwelling flows at high-emitting seeps. Uncertainties related to initial bubble sizes remain, which might, in addition to spatial heterogeneities in the sediment properties, be driven by variations in the seabed gas flow or bottom current intensity or changes in the hydrostatic pressure (Dewar et al., 2013).

REFERENCES

- Blees, J., et al., 2014. Micro-aerobic bacterial methane oxidation in the chemocline and anoxic water column of deep south-Alpine Lake Lugano (Switzerland). *Limnol. Oceanogr.* 59 (2), 311–324.
- Boudreau, B.P., 1997. *Diagenetic Models and their Implementation: Modelling Transport and Reactions in Aquatic Sediments*. Berlin, Heidelberg, New York, London, Paris, Tokyo, Hong Kong: Springer, 414 pp.
- Clift, R., Grace, J.R., Weber, M.E., 1978. *Bubbles, Drops, and Particles*. Academic Press, London p. 380.
- Duan, Z., Moller N., Weare, J.H., 1992. An equation of state for the CH₄-CO₂-H₂O system: I. Pure systems from 0-1000°C and from 0 to 8000 bar. *Geochim. Cosmochim. Acta* 56. 2605-2617.
- Duan, Z.H., Mao, S., 2006. A thermodynamic model for calculating methane solubility, density and gas phase composition of methane-bearing aqueous fluids from 273 to 523 K and from 1 to 2000 bar. *Geochim. Cosmochim. Acta* 70, 3369-3386.
- Farreira, T., Rasband, W., 2012. ImageJ User Guide IJ 1.46r. 185p. <http://imagej.nih.gov/ij/docs/guide/index.html>
- Geng, M., Duan, Z.H., 2010. Prediction of oxygen solubility in pure water and brines up to high temperatures and pressures. *Geochim. Cosmochim. Acta* 74, 5631-5640.
- Judd, A.G., Hovland, M., 1992. The evidence of shallow gas in marine sediments. *Cont. Shelf Res.* 12, 1081-1095
- Karstens, J., Berndt, C., 2015. Seismic chimneys in the Southern Viking Graben- Implications for paleo fluid migration and overpressure evolution. *Earth Planet. Sc. Lett.* 412, 88-100.
- Leifer, I., and Patro, R.K., 2002. The bubble mechanism for methane transport from the shallow sea bed to the surface: A review and sensitivity study, *Cont. Shelf Res.* 22, 2409–2428, doi:10.1016/S0278-4343(02)00065-1.
- Linke, P., Schmidt, M., Rohleder, M., Al-Barakati, A., Al-Farawati, R., 2015. Novel online digital video and high-speed data broadcasting via standard coaxial cable onboard marine operating vessels. *Mar. Technol. Soc. J.* 49 (1), 7-18.
- Løseth H., Gading, M., Wensaas, L., 2009. Hydrocarbon leakage interpreted on seismic data. *Mar. Petrol. Geol.* 26, 1304-1319.
- Mao, S., Duan, Z.H., 2006. A thermodynamic model for calculating nitrogen solubility, gas phase composition and density of the N₂-H₂O-NaCl-system. *Fluid Phase Equilib.* 248, 103-114.
- McGinnis, D. F., Little J.C., 2002. Predicting diffused-bubble oxygen transfer rate using the discrete bubble model. *Water Res.* 36, 4627–4635, doi:10.1016/S0043-1354(02)00175-6.
- NPD Guidelines for Designation of Wells and Wellbores, 2014. http://www.npd.no/Global/Norsk/5Regelverk/Tematiskeveiledninger/Bronner_betegnelser_og_klassifisering_e.pdf
- Pape, T., Bahr, A., Rethemeyer, J., Kessler, J.D., Sahling, H., Hinrichs, K.U., Klapp, S.A., Reeburgh, W.S., Bohrmann, G., 2010. Molecular and isotopic partitioning of low-molecular-weight hydrocarbons during migration and gas hydrate precipitation in deposits of a high-flux seepage site. *Chemical Geology* 269, 350–363
- Rehder, G., Schneider von Deimling, J., 2008. RV Sonne Cruise Report SO 196, SUMSUN 2008, Suva

Guam Okinawa Trough Manila. February 19- March 26 2008. PANGAEA, hdl: 10013/epic.35734.

Sofroniou, M., Knapp, R., 2008. Wolfram Mathematica Tutorial Collection- Advanced numerical differential equation solving in Mathematica. Wolfram Research, Inc. <http://www.wolfram.com/learningcenter/tutorialcollection/AdvancedNumericalDifferentialEquationSolvingInMathematica/AdvancedNumericalDifferentialEquationSolvingInMathematica.pdf>

Treude, T., Boetius, A., Knittel, K., Wallmann, K., Jørgensen, B.B., 2003. Anaerobic oxidation of methane above gas hydrates at Hydrate Ridge, NE Pacific Ocean. *Mar. Ecol. Prog. Ser.* 264, 1–14, doi:10.3354/meps264001

Vielstädte, L., Karstens, J., Haeckel, M., Schmidt, M., Liebetrau, V., Reimann, S., McGinnis, D.F., Linke, P., and Wallmann, K., revised. Quantification of methane emissions at abandoned gas wells in the Central North Sea. *Mar. Petrol. Geol.*

Wüest, A., N. H. Brooks, and D. M. Imboden , 1992. Bubble plume modeling for lake restoration, *Water Resour. Res.* 28(12), 3235–3250, doi:10.1029/92WR01681.

Zheng, L., Yapa, P.D., 2002. Modeling gas dissolution in deepwater oil/gas spills. *J. Marine Syst.* 31, 299-309.

A.5. CURRICULUM VITAE

Jens Karstens

Date of birth: 05.06.1985
Place of birth: Flensburg
Nationality: German
Adresse: Holtenauer Straße 85
24105 Kiel, Germany

Education

Since 07/2011: PhD student, GEOMAR and Christian-Albrechts-Universität, Kiel
06/2011: Master of Science in Geophysics
10/2009 - 06/2011: student in Geophysics, Christian-Albrechts-Universität, Kiel
09/2009: Bachelor of Science, Applied Geophysics
10/2006 - 09/2009: student in Geophysics, Christian-Albrechts-Universität, Kiel
05/2005: Abitur, Altes Gymnasium, Flensburg
07/1996 - 05/2005: Altes Gymnasium, Flensburg